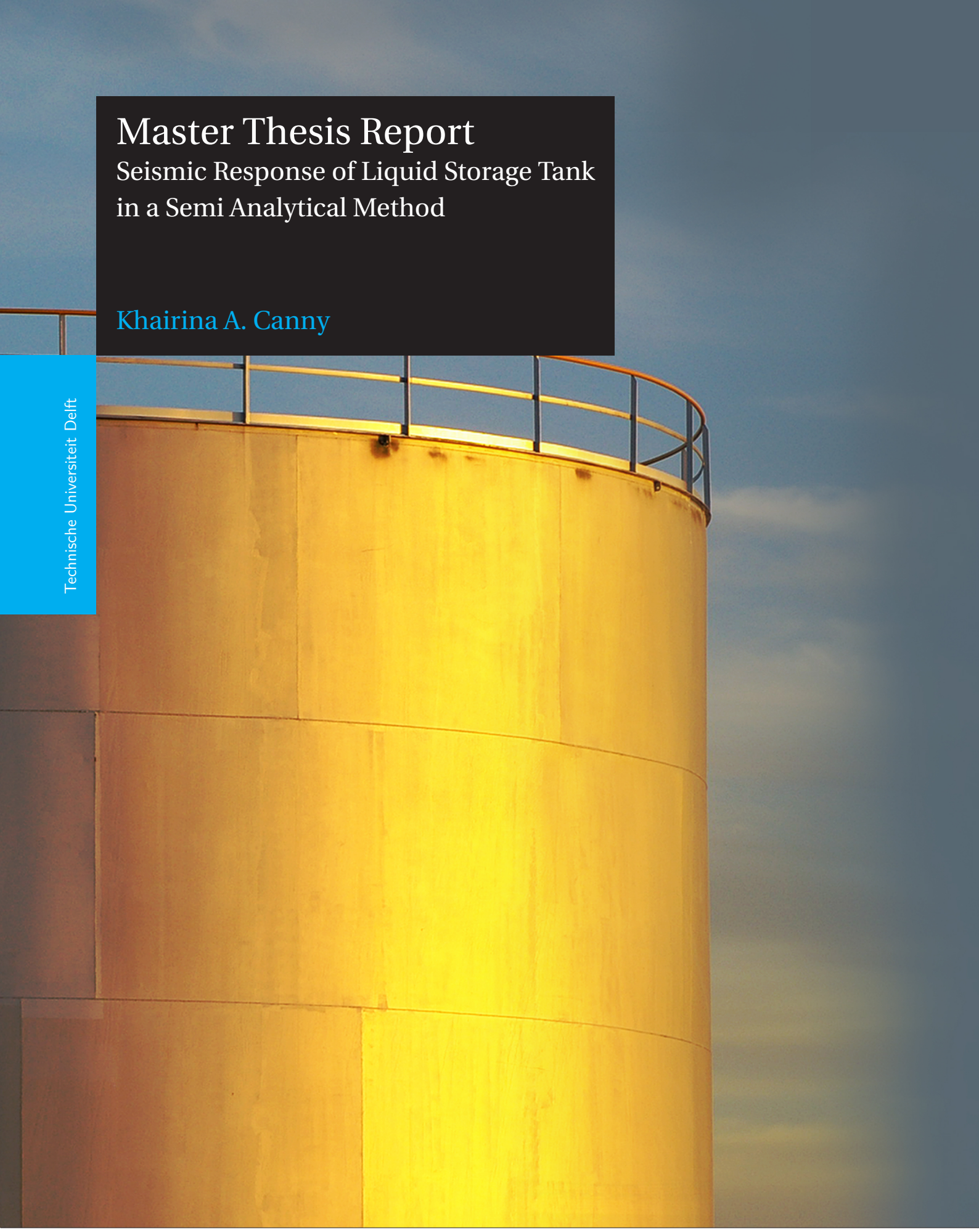

Master Thesis Report

Seismic Response of Liquid Storage Tank in a Semi Analytical Method

Khairina A. Canny

Technische Universiteit Delft

TU Delft Delft University of Technology

Challenge the future

Cover photo:
Fuel storage tank, North Fremanlte in the jointly operated Caltex, Shell Terminal. Approxiamate capacity is 2,000,000 litres.

Photograph by:
Gnangarra (https://commons.wikimedia.org)

MASTER THESIS REPORT

SEISMIC RESPONSE OF LIQUID STORAGE TANK IN A SEMI ANALYTICAL METHOD

by

Khairina A. Canny

in partial fulfillment of the requirements for the degree of

Master of Science
in Civil Engineering

Thesis committee: Chairman:	Prof. dr. ir. A. V. Metrikine	
Committee Member:	Dr. ir. A. Tsouvalas,	TU Delft, Offshore Engineering
	Ir. M. Versluis,	Witteveen+Bos
	Dr. ir. drs. C.R. Braam,	TU Delft, Structural Engineering
	Ir. J.M. Houben,	TU Delft, Structural Engineering

TU Delft Delft University of Technology

Witteveen + Bos

We can know only that we know nothing. And that is the highest degree of human wisdom
Leo Tolstoy

ABSTRACT

The demand for liquid storage tanks increases as the economy grows. Due to this increasing demand, a large number of tanks needs to be analyzed for both static and dynamic load cases. One of the most relevant dynamic load cases is the seismic excitation. There are numerous cases of tanks that have been damage during earthquakes; one typical example is the collapsed tank at Haba's plant in Turkey during the catastrophic Kocaeli earthquake of 1999. Additionally to tectonic earthquakes, induced seismicity can cause damage to liquid storage tanks. An example of induced earthquakes is the Groningen region in the north of the Netherlands known for its significant amount of hydrocarbons located onshore. Liquid storage tanks in that region should therefore also be able to withstand induced earthquakes on top of other standard operational loads.

This thesis focuses on the dynamic analysis of liquid storage tanks subjected to seismic excitation with its primary aim being the development of a semi-analytical model able to predict this dynamic response accurately. In engineering practice, there are two primary methods to solve this problem. Numerical models based primarily on the finite element (FE) method, can treat the dynamics of the tank-liquid system with high accuracy. However, this comes at the cost of low computational speed; these models are slow and sophisticated finite element packages are required that can deal with both the structure and the liquid with equal rigor. On the other hand, analytical methods exist to solve the tank-liquid interaction problem. The latter, although computationally fast, lack of accuracy and can treat only the most simplistic configurations regarding the structural type. In this thesis, we aim to develop a semi-analytical model that combines the strong elements of both approaches, i.e. it is computationally fast and accurate.

In the first part of the thesis, a two-dimensional case is analyzed in which the tank is composed out of three beams representing the plate and the wall of the tank, while the liquid is assumed two-dimensional. With this model, the semi-analytical solution method is established. The method is very straightforward and is based on the principle of dynamic sub-structuring which is valid for linear systems. The response of the structure, i.e., the three interconnected beams, is expressed in terms of the in-vacuo beam modes; a modal basis that is convenient since different modes are orthogonal to each other. The liquid motion is expressed as a superposition of two or three potentials each of which, in turn, is also shown in terms of modes. By representing the response of each sub-structure in terms of an orthonormal set of modes, the behavior of the system is spatially fixed, and the remaining unknowns are only the modal coefficients representing the multipliers of the various modal shapes. The latter is obtained by enforcing displacement compatibility conditions at the liquid-tank interface and by satisfying the forced equations of motion of the structure. The results of the adopted solution approach are compared against known results in the literature for validation purposes.

In the second part of the thesis, the solution method is extended to the case of a cylindrical tank in which the problem is tackled in the same way. The only complication arises from the need to solve a three-dimensional configuration but other than that the solution approach remains essentially unchanged. The thesis includes a thorough parametric study of the effect of soil flexibility. The soil in the model is described by distributed springs (Winkler foundation) attached to the bottom of the tank and subjected to the seismic excitation at the base. Amongst others, the model allows the representation of the seismic action in the form of a propagating wave at the ground surface, i.e. a Rayleigh wave, the effect of which can be significant for tanks of large dimensions.

With the developed three-dimensional model a parametric study is conducted in order to determine the influence of tanks dimensions, soil flexibility and wave speed on the structural response. Results are compared with others available in the literature in order to validate the model. The present model can be easily extended to include more complicated structures, e.g. horizontal tanks and tanks of different geometry. Finally, the model can be amended by a more accurate representation of the soil in terms of a three-dimensional layered continuum by merely adding an extra sub-structure to the system (the layered soil) while keeping the same solution approach.

PREFACE

This master thesis is worked in order to obtain the degree of Master of Sciences in Civil Engineering at Delft University of Technology. This works is carried out with the cooperation of Faculty of Civil Engineering and Witteveen+Bos.

This thesis could not be set apart from the help and contribution of several people. Firstly, I would like to thank God, for His grace throughout my life, especially during my study. I would like to express my deep and sincere gratitude to my committee: Prof.dr.ir. A.V. Metrikine, Dr.ir.A. Tsouvalas, Ir. Marco Versluis, Dr.ir.drs.C.R. Braam; for their time, patience, guidance and feedback. It is a very beautiful and intangible learning experience for me. I will make use this experience to improve myself in the future. I would also like to give gratitude to Ir. J. M. Houben and the Anneke Meijer for helping the ceremonial and administrative affairs regarding my graduation.

I would like also to give thank to my boyfriend, Yosua Djapara and best friends, Danisa W. Zulhendri and Riandita Amanda for their love and kind support. I am also grateful for the friends in both Delft University of Technology and Witteveen+Bos especially for Niels, Thijs, Alex, Juliette, Gerrit and Teddy that help me by giving their feedbacks for this thesis. I would also like to give my gratitude to my family for always supporting, accepting, and loving me regardless my flaws.

Last but not least, I would like to thank the Indonesian government and the rest of the citizens for giving me the scholarship to study in the Netherlands.

Khairina Anindya Canny
Delft, January 2018

CONTENTS

NOMENCLATURE

η	Oscillatory liquid displacement
$\mathscr{L}$	Lagrangian Function
Φ	Liquid potential velocity
ρ_s	Structure density
ρ_{liq}	Liquid density
a_e	Earthquake Acceleration
a_e	Earthquakes Acceleration
A_p	Plate cross section area
A_w	Wall cross section area
c	Frequency independent damping
E_p	Plate Young's Modulus
E_w	Wall Young's Modulus
g	Gravitational acceleration
H	Height of the tank
H_l	Liquid Height
I_m	Modified Bessel functions of the first kind for integer $m^{th} order$
I_p	Plate cross section inertia
I_w	Wall cross section inertia
J_m	Bessel functions of the first kind for integer $m^{th} order$
K	Kinetic energy
k	Soil Stiffness
K_m	Modified Bessel functions of the second kind for integer $m^{th} order$
L	Width of the tank
L'	Half width of the Tank
m_c	Convective Mas
m_i	Impulsive Mass
P	Potential energy
p_c	Convective Pressure
p_i	Impulsive Pressure
P_{liq}	Liquid Pressure

R Radius of the tank

$u_{earthquake}$ Horizontal earthquake displacement

$w_{earthquake}$ Vertical earthquake displacement

Y_m Bessel functions of the second kind for integer $m^{th} order$

1

INTRODUCTION

There are various types of storage tanks. These tanks can be filled with water, or any liquid, or bulk of cokes, coals, and much more. However, in this thesis, it is only focused on liquid. These tanks are also used in various fields of industry. As the growth of the economy keeps increasing, the industry's demand for the tank facility is also growing. The trend in the recent years is for a larger-sized tank (source : ANSON storage tank manufacturer). Due to the increasing need for storage tanks, the safety of the tank become more critical aspect to be ensured. These safety aspects must consist of both static and dynamic requirements. The dynamic requirements for the storage tank is the tank resistance against time dependent loads such as earthquake and wind.

One of the leading cause of the dynamic movement of the tank is the seismic excitation. The earthquakes are the natural disaster that almost unpredictable and may cause some severe damages in infrastructures. The damages to the liquid storage tank may cause spilling of toxic and flammable liquid or by the loss of containment. These incidents may result in the resource shortage that give adverse financial, social or environmental impacts. Unlike buildings, tanks have different mechanisms to dissipate any amount of seismic energy. Knowing how important the treat of the failure, in this thesis the dynamic behavior of the tank is analyzed.

1.1. PROBLEM STATEMENT

Filled Liquid storage tank subjected to earthquakes is in the scope of *fluid-structure interaction* (FSI). The fluid-structure interaction itself is a multiphysics of coupling system that combines the law of fluid and structure dynamics. One or more solid structure which are in this thesis is the plate and the wall, interact with surrounding liquid flow. These two materials interaction can be seen in the cross-section of the tank in figure 1.1.

From the definition of the fluid-structure interaction, one can know that the problem of the structural vibration and fluid motion is a coupled problem. The solution to the coupled problem can be obtained with some approaches. It can be solved entirely numerical which is using the Finite Element Method (FEM) or analytical approach. This thesis address the fluid-structure interaction in the later method. However, due to two reasons which are the mathematical complexity of the three-dimensional model and efficient computing time, the modeling is using the semi-analytical approach. For solving the coupled problem, this thesis uses the *modal analysis*.

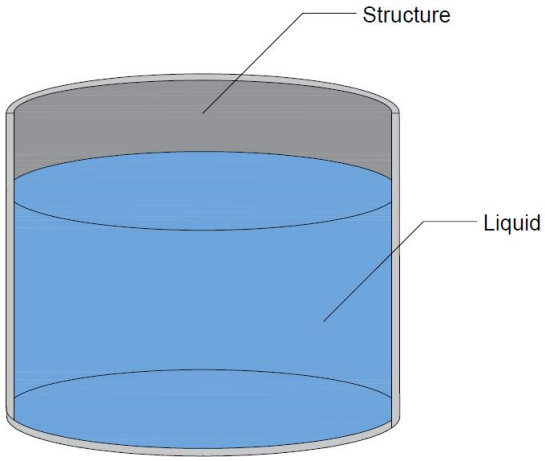

Figure 1.1: Cross section of the tank

1.2. SCOPE

In this thesis, the focus is on the liquid and structure interaction of the storage tank. The assumption is that both of the liquid and the structure are considered in the linear phase. The soil structure interaction is also described in a simple Winkler model. The damping that is modeled in this thesis is the frequency independent damping. The effect of soil layers, non-linearity and other types of damping are disregard in this thesis. In reality, there are a number of failure modes due to seismic excitation such as : overturning, elastic buckling, elasto-plastic buckling (elephant foot), and roof damage. However in this thesis, buckling failure modes are disregard. Moreover due to the absence of the roof for the sake of simplification, the roof damage due to the sloshing is also not considered in this thesis.

1.3. AIM OF THE PROJECT

The project aims to build a program of a storage tank that incorporates liquid and subjected to the earthquakes. Where from this program the dynamic behaviors of the whole system can be analyzed. The output of the dynamic analyses are the liquid pressure, the forces, free vibration of the tank and the sloshing modes of liquid.

1.4. RESEARCH QUESTIONS

In expectation of breaking down the project output, it is necessary to assemble research questions. The research questions are divided into two classifications which are the main question and the sub-questions.

1.4.1. MAIN QUESTION

The project's main question that is formulated from the aim of the project which is:

How does the tank behave under the dynamic loading and how does the liquid influence the dynamic behavior of the tank by using the semi analytic model?

To be more specific, the dynamic behaviors of the tank that are analyzed in the thesis are:

1. **Hydrodynamic Pressure**.
   The hydrodynamic pressure is derived from the liquid potential flow. The liquid is assumed *incompressible*,*inviscid*, and *linear*. The main difference between the hydrodynamic pressure and hydrostatic pressure is the dynamic pressure depends on time variable while static does not.

2. **Free Surface Water Elevation**.
   The free surface water can be simply defined as the surface of the fluid. If the free surface of a liquid

is disturbed by dynamic loading, it might produce waves on the surface. These waves have certain elevation and cause pressure in the total structure of the system.

1.4.2. THE SUB-QUESTIONS

To follow the main question, let the formulation of sub-questions for other objectives in this project, be:

1. *What are the effects of flexibility and geometry of tank structure to the whole dynamic motion of the tank?*

   This question focuses on studying the effect of dimension and geometrical properties of the tank structure. The geometry of the tank is closely related to the liquid volume in the tank. By answering this question, the sensitivity of the tank geometry and properties for liquid and structure interaction can be analyzed.

2. *What are the differences between other available methods?*

   The dynamic analysis of the tank container is already formulated since the 50s. Due to the limitation of technology at that time and also practical reasons, the structure and the liquid interaction was simplified and represent as the discrete systems. Therefore for this specific topic is available analysis with various methods and assumptions. This sub-question answer comprehends the differences between other available methods.

1.5. CHAPTER OUTLINE

The needed sections of the study to complete the objectives are expressed in 6 structured chapters below:

In the *Chapter 2*, the summaries from the literature study are presented here. The theories are divided into four sections. The first section is the theory of *earthquakes and seismic analysis*. After the first section, the *dynamic system* theories are explained in this chapter. Afterwards, the approach on how to model a simple *soil-structure interaction* is explained in this chapter. Last but not least, in this section, the *flow potential of the liquid* is derived to obtain the governing equation for the liquid. The theories from the literature study are the basic principles for the modeling of the structure in both two-dimensional model and three-dimensional model.

In the *Chapter 3*, the modeling of the two-dimensional structure is performed. The main purpose of this chapter is as an introduction before entering the three-dimensional model. Since the three dimensional model has a higher complexity than two dimensional model, this chapter is dedicated to building the basic foundation of the liquid and the structure interaction. This chapter mainly focuses on three points which are the derivation, result, parameter study and validation.

In the *Chapter 4*, the analytic derivation of the three-dimensional model is written. After modeling the two-dimensional model, one can already have the basic knowledge how the liquid-structure interaction works. The procedures of the three-dimensional model have slight differences and higher complexity than the two-dimensional model. The analytical derivation for both liquid and the structure is no longer in the Cartesian coordinates but in the cylindrical coordinates. This chapter is dedicated only for the three-dimensional analytic derivations. For the modeling, result and parameter study are discussed separately in the next chapter.

In the *Chapter 5*, real case study, parametric studies, and validations for the three-dimensional model is presented here. Three parameters are be studied to answer the first point of the subquestions which are the volume of the liquid, geometry of the tank, and the structure thickness. Through the validation, the second subquestion is answered as well, since the present results are compared to the available methods.

In the *Chapter 6*, conclusions and recommendations are described. The conclusions have to answer the project's main question and the subquestions. Lastly, since the model has assumptions and simplifications, the recommendations are written here. From the recommendations, a better and representative future model development is hope to be achieved.

2

LITERATURE STUDY

This second chapter consists of the summaries from literature study that are relevant to find the solution of the liquid container tank under seismic excitation. This section can be classified with the four of essential items which are:

- *the earthquakes and seismic analysis;*
- *dynamic of the structure;*
- *liquid potential flow;*
- *available standard and frequently used method.*

Each of these essential parts is further discussed in the subsequent subchapters.

2.1. EARTHQUAKES

Since the main loading in the thesis is the seismic loading, this subsection is dedicated for introductions on earthquakes and seismic engineering. Earthquakes have occurred for million years and brought significant risks to the lives and properties of the people. During these phenomena, the ground shakings can be sensed. This ground shakings are resulted by the sudden release of energy in the earth's lithosphere. From the reference [11], it is explained that the point at where the earthquakes originate is called the focus or hypo-center, and the node on the earth's surface directly above hypo-center is the epicenter. These two locations are depicted in the figure below:

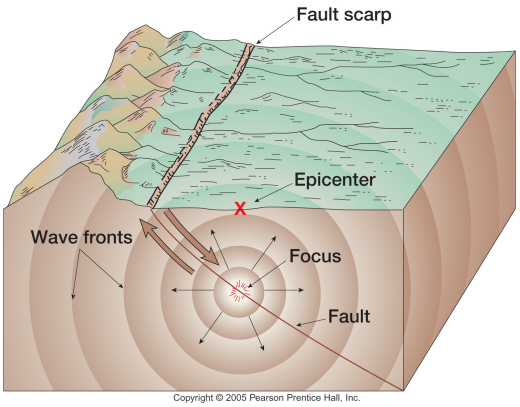

Figure 2.1: Focus and epicentrum in earthquakes occurance
Source : Pearson Prentice Hall

2.1.1. CAUSE OF EARTHQUAKES

Based on how they formed, earthquakes are divided into two main characterizations. These classifications are *tectonic earthquakes* and *induced earthquakes*. The causes of the seismic occurrences are discussed in this section and referred to [11],[19].

TECTONIC EARTHQUAKES

For the naturally occurring earthquakes, there are two leading causes that responsible for the majority earthquakes occurrences in the world. The first cause is due to **the movement of the tectonic plate boundaries in the edges** which cause the interplate earthquake. This tectonic plate motion is branched into three directions which are:

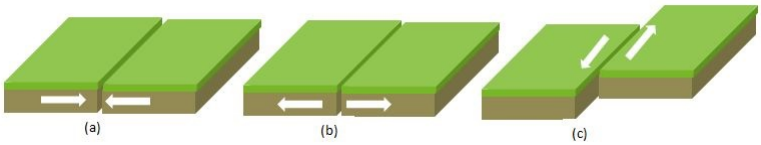

Figure 2.2: Tectonic plate motion: (a) convergent boundaries; (b) divergent boundaries; (c) transform boundaries

1. **Convergent boundaries or compressional movement:** This boundary depicts where the two plates are coming together and colliding plate. The two plates movement can be seen in the first picture of Figure 2.2. This phenomenon is resulting in powerful earthquakes with ranging in depth from very near to the surface to hundreds of kilometers depth. The largest earthquakes in the world, the 1960 Great Chilean earthquakes with a magnitude of 9.6 on the Richter scale is due to such plate movement.

2. **Divergent boundaries or extensional movement:** Divergent boundaries are the contrary to the compressional movement. Instead of colliding each other, the two plates are moving apart and eventually open up and create ocean basins or rifts. The earthquakes that this phenomenon produces are shallow and tend to be smaller than a magnitude of 8 on the Richter scale. The second of Figure 2.2 depicts the compressional movement.

3. **Transform boundaries:** The motion of the plates is horizontal. Because the plates have friction, they can not glide past each other and build up stress within plates. This stress is eventually released earthquakes. The earthquakes are shallow with the depth of 25 kilometers and smaller than a magnitude 8.5 on the Richter scale. One of the earthquakes example due to transform boundaries is the 1906 San Francisco earthquakes with a magnitude of 7.8 on the Richter scale. The transform boundaries movement can be seen in the last picture of Figure 2.2

The other cause of the tectonic earthquakes is **local fault line**. The earthquakes that it produced is away from the plate boundary. This condition is why it is called the intraplate earthquakes. Intraplate earthquake is considered rare and has a smaller magnitude compared to the previous classification.

HUMAN INDUCED EARTHQUAKE

Unlike the occurring tectonic earthquakes, these induced earthquakes are caused by human activities. The difference between the tectonic earthquakes and the human-induced earthquakes is the human-induced earthquakes have a smaller magnitude compare to the tectonic earthquakes (Source : Earth Magazine August 2014, Jennifer Georgek). Some human activities can alter the stresses and the strains of the earth's crust. One of the examples of human activities that can induce such earthquakes is oil and gas extraction in the Dutch province of Groningen. This area is known for hydrocarbons since the early sixties. In Figure 2.3, it can be seen how closely related the location of earthquakes with the gas extraction activities are. Compare to the tectonic earthquakes, the Groningen earthquakes can be considered a light magnitude. However, the point of interest of the Groningen Earthquakes is not in the scale of magnitude but how close the focus of the earthquakes to the surface. The focus of the Groningen earthquakes is located near the surface with only 3 km distance from the source. Even small tremors within such a close distance to the surface may cause damage to buildings and infrastructure.

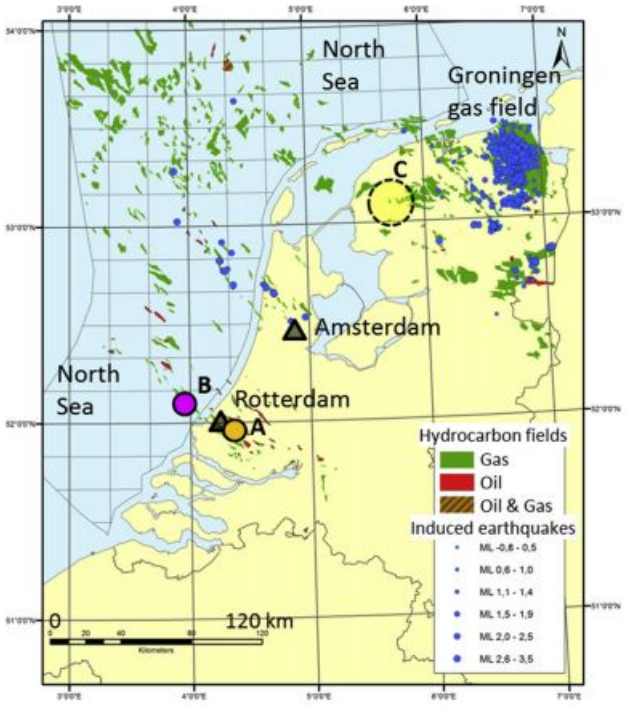

Figure 2.3: The Netherlands earthquake and gas extraction
(Source : Geomechanical effects of CO2 storage in depleted gas reservoirs in the
Netherlands: Inferences from feasibility studies and comparison with aquifer storage (Bogdan Orlic)[13])

2.1.2. THE SEISMIC WAVES

When the earthquakes occur, they produce different types of seismic waves. The following explanation of the seismic wave is referred from [11]. There are two main branches of the seismic waves which are the body and surface waves. The body waves can travel through the interior of the earth and also consists of two types of waves which are P-waves and S-waves. The travel speed of body waves varies with the type of soil material they propagate through. As the geologic materials are stiffest in compression, therefore p-waves travel faster than other seismic waves. The surface waves are the product of the interaction between the body waves and the surface and surficial layer of the earth. All types of surface waves share one common characteristic which is the exponentially decreasing amplitude to the depth of the earthquake. How these types of seismic wave travel can be seen in Figure 2.4 and Figure 2.5.

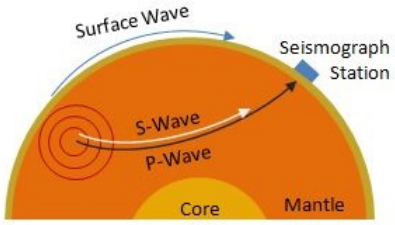

Figure 2.4: Body Wave and surface wave propagation
(Source: Incorporated Research Institutions for Seismology (IRIS))

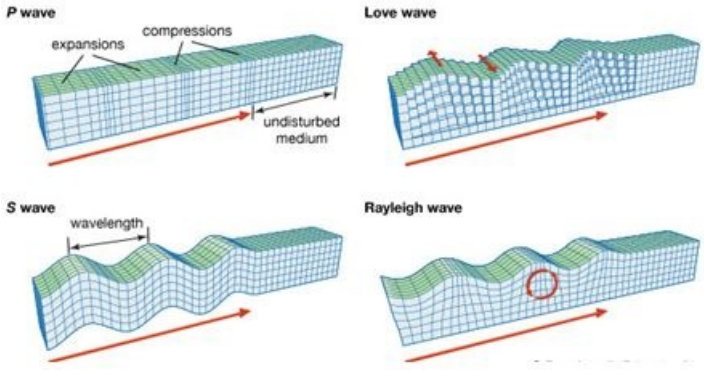

Figure 2.5: Type of wave propagation
Source: Encyclopedia Britanica

P-WAVES

P waves or primary waves are the fastest and the first waves to arrive. These body waves travel at speed between 1 to the 14 km/sec. The lowest speed corresponds to the traveling P-waves through the water. Meanwhile, the highest velocity is due to the speed of the traveling P-waves near the base of the earth's mantle. From these two speeds, one can say that the stiffer the material that the waves are passing through, the higher the velocity of the waves. P-waves are sound waves, and the vibration that they cause are the changes in volume. These volume changes are the change between compression and expansion in the direction that the waves are traveling. How the P-waves travel can be seen in Figure 2.5. The increasing speed causes the P-waves to travel in the curved paths that are concave upwards. This curved paths are depicted in Figure 2.4.

S-WAVES

The other type of body waves are the S-waves or the secondary waves or the shear waves. Since these waves do not change in volume, they travel by shear deformation. Between the two body waves, the shear waves travel slower than the p-waves. Nevertheless, they propagate relative fast at speed 1 to 8 km/sec. The other difference that distinguishes p-waves and s-waves is, s-waves inability to travel through fluid or gas. This inability is because of the fluids and gasses are unable to transmit shear stress. S-waves themselves are divided into two movements which are SV (vertical pane movement) and SH (Horizontal movement). Similarly, with P-waves, S-waves also traveled the same concave upward path as it can be seen in Figure 2.4. Figure 2.5 depicts how the shear waves travel.

RAYLEIGH WAVES

Rayleigh waves are produced from the interaction of p-waves and SV-waves with the earth's surface, involving both vertical and horizontal particle motion. Rayleigh waves are the slowest wave compared to the other seismic waves. These waves are also dispersive. Therefore the particular speed at which they travel depends on the period of the wave and the near-surface geologic structure. How the Rayleigh waves propagate can be seen in the Figure 2.5

LOVE WAVES

Love waves are transverse waves that vibrate to the horizontal direction perpendicular to the direction of the propagating waves. The Love waves are the product of the interaction of SH-waves with a soft surficial layer and have no vertical component of the particle motion. These waves are the horizontally polarized surface waves and can be seen in Figure 2.5.

2.1.3. SEISMIC ANALYSIS

Ground motion from earthquakes can be measured with a particular instrument. However, the movement of the instrument may look very complicated since there are many reflected seismic waves subjected to on the way. Most ground motion is the expressed in the acceleration and recorded by an instrument called accelerogram. One of the example of a recorded ground acceleration is shown in the following figure :

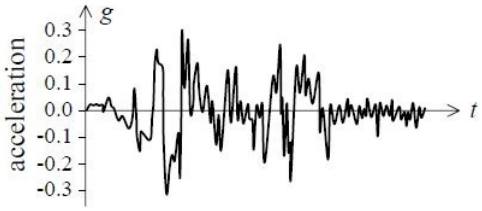

Figure 2.6: Reccorded acceleration in accelerogram
Source : Random Vibration Lecture Notes CIE5145, Prof.ir. A.C.W.M. Vrouwenvelder[20]

There are several approaches for seismic analysis from references: [11],[19],[20] in which is explained in the following:

TIME HISTORY ANALYSIS

Time history analysis provides both linear (LTHA) and nonlinear (NLTHA) evaluation of structural dynamic response under loading. Instead of taking a few peak values, in this analysis, all values are inputted. Therefore, this method gives highly accurate interpretation of the structural behavior. Time history analysis can be done in both time domain and frequency domain. Solving in the frequency domain using Fourier or Laplace transform is preferable than time domain analysis due to its simplicity. The only disadvantage of the time history analysis is its sophistication compare to any other method which might result in a more expensive computing time.

RESPONSE SPECTRUM

The response spectrum is one of the most useful and applied tools in the seismic analysis. This method is using a response of a linear one-degree of freedom system to a set of earthquakes. The idea behind the response spectrum method is the relation between the maximum of structural acceleration of a single degree of freedom system and an earthquake with the unit of peak acceleration of 1 m/s^2. The accuracy of this seismic analysis depends on the amount of the considered modes. If the structure is irregular or tall the response spectrum is no longer can be applied.

QUASI STATIC METHOD

The quasi-static or more commonly known as the seismic coefficient method has been one of the most simplified and the oldest way to evaluate seismic loading on structures. Different with the other methods, this method considered the earthquake load as static forces. The idea behind the seismic analysis is the seismic force can be combined with other static forces while still considering dynamic factor by using multiplication of seismic coefficient(horizontal acceleration).

2.2. WINKLER MODEL

The most well-known and used foundation model for the soil-structure interaction is the Winkler model. Winkler theory was derived in 1867 by Emil Winkler. Other approaches are more refined on describing soil structure interaction (SSI) such as elastic continuum, multi-parameter model, and a hybrid model (Kerr model), according to the reference [3]. However, for this thesis project, Winkler model is used for the sake of simplification. The main advantage of the Winkler model is easy to implement in a structural system.

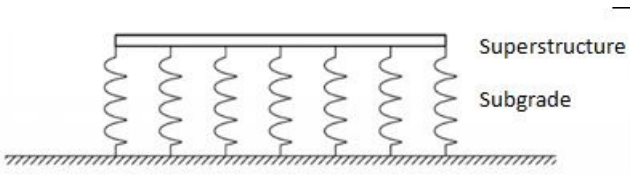

Figure 2.7: Visualization of a structural Winkler Model
Source : Structural Element Approaches for Soil Structure Interaction, Aron Caselunghe and Jonas Eriksson [3]

In the Winkler model [3], the springs are only affecting the structure in its degree of freedom. It considers that the reaction force equals to the displacement at each point of the structure. Subsequently, the reaction forces that are obtained is converted into springs which dependent on the soil parameter. Therefore the reaction force relationship with the deflection can be described in the following manner:

$$k_i = F_i / \delta_i \tag{2.1}$$

Where the force from the foundation is

$$F = -k \times \Delta u \tag{2.2}$$

F_i = the reaction force in every point of i;
k_i = the Winkler spring stiffness in every point of i;
δ = the relative difference of the displacement;
k_i = the Winkler spring stiffness in every point of i;
Δu = the relative displacement.

2.3. DYNAMIC SYSTEMS

The dynamic system derivations are ascribed to the following references [12],[21], and [9]. From the Chapter 1, it is stated in the problem statement that this thesis is in the scope of fluid-structure interaction. This section is dedicated to the explanation on how to derive the governing equations of the structural vibration. To analyze the dynamic behavior, one has to derive the equation motion which is different compared to static equations. The figure below visualize the derivation of the governing equations for both statics and dynamics:

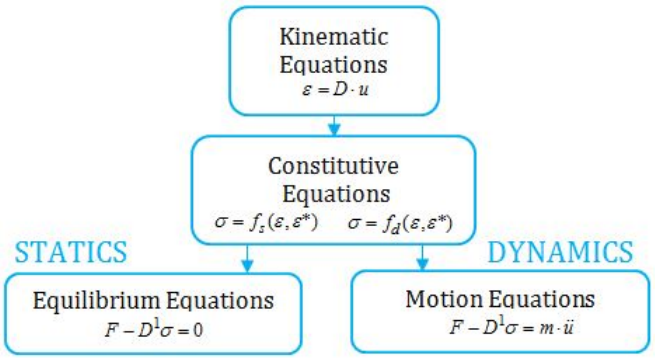

Figure 2.8: The Basic Equation of Statistics and Dynamics

Two methods that mostly used for the equations of motion of the system are *the displacement method* and *the Lagrangian formalism.*

1. ***The Displacement Method***
   The displacement method is derivation of equations of motion by prescribing displacement in all the degree of freedoms to achieve the result of acting forces. Subsequently, by applying Newton's second law with the respect of the degree of freedom, the whole equation motion can be calculated.

$$\begin{aligned} m_1(\ddot{x_1}) &= \sum F(x_1, \ddot{x}_1, \dot{x}_1, x_1', x_1''..) \\ m_2(\ddot{x_2}) &= \sum F(x_2, \ddot{x}_2, \dot{x}_2, x_2', x_2''..) \\ m_3(\ddot{x_3}) &= \sum F(x_3, \ddot{x}_3, \dot{x}_3, x_3', x_3''..) \end{aligned} \tag{2.3}$$

   m_i = the lumped mass for each degree of freedom i;
   F = the force in the system;
   $\ddot{x}_i$ = the lumped mass acceleration for each degree of freedom i.

2. ***Lagrangian Method***
   The other method is Lagrange's method. This method is an alternate approach by placing Newton's law into a solution that particularly convenient for a complex coordinate system. The Lagrange's equation based upon conservation of energy which is a fundamental law of physics that governs the motion of particles and rigid bodies. The basic equation of this method is:

$$\frac{d}{t}\frac{\partial \mathscr{L}}{\partial \dot{u}} - \frac{d}{t}\frac{\partial \mathscr{L}}{\partial u} \tag{2.4}$$

   Where the Lagrange function is consisted of:

$$\mathscr{L} = K - P \tag{2.5}$$

   Another form of the Lagrangian equation is *Hamilton's principle* [16]. This law is based on principle stationary action. This principle achieved from integration of differences in energy is equal to 0 as in the following equation:

$$\delta \int_{t_1}^{t_2} (K - U - W_{nc})\, dt = 0 \tag{2.6}$$

   The parameters of the Lagrangian method is written in the following:

   $\mathscr{L}$ = the Lagrangian function;
   K = the kinetic energy;
   P = the potential energy;
   U = the strain energy, obtained from Appendix B, Section B.6.1;
   W_{nc} = the input energy, obtained from Appendix B, Section B.6.3.

2.3.1. SINGLE DEGREE OF FREEDOM

The most basic dynamic system consists of a single lumped mass and a spring and/or a dashpot. This structure indicates that there is only one possible direction of the lumped mass movement. This system is mostly used as an idealization of a complex structure by lumping the mass in particular points. The use of this system is an approximation, since in reality structure can move in more than one direction. The following figure depicts the spring and dashpot system:

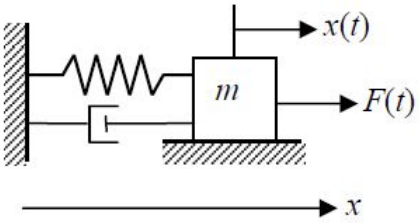

Figure 2.9: Spring and dashpot system
Source: Dynamics,Slender Strucutures and an Introduction to Continuum Mechanics CT 4145, A.V. Metrikine [12]

The derivation using Newton's second law results in the following equation:

$$F(t) + F_{spring}(t) + F_{dashpot}(t) = m\ddot{x} \tag{2.7}$$

Where for each forces is given by:

$$F_{spring}(t) = -k\Delta x \tag{2.8}$$

$$F_{dashpot}(t) = -c\Delta\dot{x} \tag{2.9}$$

Afterwards these equation are substituted back to equation 2.7, which results in:

$$m\ddot{x} + c\dot{x} + kx = 0 \tag{2.10}$$

As for the free vibration response where the external force is excluded the general solution is for this ordinary differential equation is:

$$x(t) = A_o \exp(-\zeta\omega_n t)\cos(\omega_n t) \tag{2.11}$$

with the component in the following:

$$\omega_n = \sqrt{\frac{k}{m}} \tag{2.12}$$

$$\frac{c}{m} = 2n \tag{2.13}$$

$$\varsigma = \frac{c}{2\sqrt{km}} \tag{2.14}$$

$$\omega_1 = \omega_n\sqrt{1-\varsigma^2} \tag{2.15}$$

$$A_o = \sqrt{(x_o^2 + (\frac{v_o}{\omega_1} + \varsigma x_o\frac{\omega_n}{\omega_1})^2} \tag{2.16}$$

The variables from above equations can be defined in the following list:

ω_n	= the undammped natural frequency corresponding to c=0;
n	= measure for the viscous damping in the system;
$\frac{c}{m}$	=the damping factor;
ζ	= the damping ratio;
k	= the spring stiffness;
m	= the mass;
v_o	= the initial velocity;
x_o	= the initial displacement;
A_o	= the amplitude.

The earthquakes loading for SDOF system is written as moving boundary conditions in the ground. The system is depicted in the following figure:

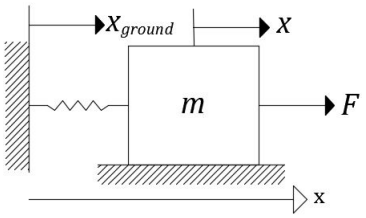

Figure 2.10: The earthquake loading in Single Degree of Freedom

Applying equation 2.8 to 2.10, the equation of motion can be written in the following:

$$m\ddot{x}_{total} + kx_{relative} = 0 \tag{2.17}$$

Where:
x_{total} = the total displacement ($x_{ground} + x$);
$x_{relative}$ = the relative displacement (x).

From the definitions above, equation 2.17 can be expanded as the following expression:

$$m\ddot{x} + c\dot{x} + kx = -m\ddot{x}_{ground} \tag{2.18}$$

2.3.2. MULTI DEGREE OF FREEDOM

Another idealization of a structure else than SDOF is *the Multi Degree of Freedom* (MDOF) system. This system regards movement not only in one direction but in multiple (N) number of directions. It can be described as more than one masses system or a structure that moves in a few directions. The general description is defined in matrix and vectors:

$$\underline{\underline{\mathbf{M}}}\ddot{x} + \underline{\underline{\mathbf{C}}}\dot{x} + \underline{\underline{\mathbf{K}}}x = \underline{\mathbf{F}} \tag{2.19}$$

Where:
$\underline{\underline{\mathbf{M}}}$ = the mass matrix;
$\underline{\underline{\mathbf{C}}}$ = the damping matrix;
$\underline{\underline{\mathbf{K}}}$ = the stiffness matrix;
$\underline{\mathbf{F}}$ = the force matrix;
$\ddot{x}$ = the acceleration vector
$\dot{x}$ = the velocity vector
x = the displacement vector

The following figure delineates an example of the multi degree of freedom system:

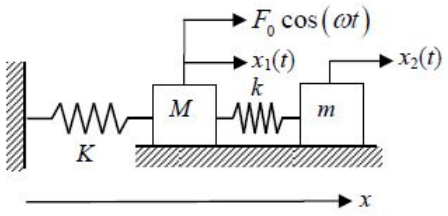

Figure 2.11: The example of multi degree of freedom system
Source: Dynamics,Slender Strucutures and an Introduction to Continuum Mechanics CT 4145, A.V. Metrikine [12]

From the above figures, one can understand that there are two masses that move in two different directions (x_1 and x_2).

The equation motion for each degree of freedom can be derived by using displacement method or Lagrangian method. However, the problem arises that the damping matrix **C** in most cases cannot be quantified as it is not a diagonal matrix. Consequently, the equation of motion cannot be decoupled. One can use the pragmatic approach to solve it by assuming the matrix **C** is diagonal. However, this method is not the best approach to address this equation. Another refined approach that available is using the Fourier analysis or Rayleigh method but these approaches are not addressed in this thesis.

2.3.3. THE CONTINUOUS SYSTEM

The multi-degree of freedom system only compromises a particular number of degree of freedoms of the lumped masses. This MDOF system can be classified as a *discrete system or lumped mass systems.* With the continuous system, the mass is continuously distributed along a line, on a plane or in a volume element. The examples of type elements that the continous system can be applied are the bending beam, shear beam, the torsion shaft, the cable and the bar. This method is more detailed than the discrete system

This section solely focuses on bending beam (*classic Euler Bernoulli theory*) and disregarding the other components such as torsion and shear beam. This assumption is used for the two-dimensional model analysis in Chapter 3. The bending beam system is defined in the following figure:

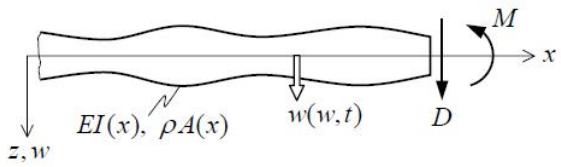

Figure 2.12: The bending beam system
Source : Structural Dynamics CT 4140 : Structural Vibration, J.M.J. Spijkers [9]

The full derivation of continuous system is explained in the Appendix B. For the sake of reading convenience, the equation of motion is rewritten in the expressions below:

$$a^2 \frac{d^4 w}{dx^4} + \frac{\partial^2 w}{\partial t^2} = 0 \qquad a^2 = \frac{EI}{\rho A} \tag{2.20}$$

Where the variables of equation 2.20 can be defined in the following list:

E	= beam Young's Modulus;
I	= area moment of inertia;
ρ	= beam density;
A	= cross section area.

THE SOLUTION

The solution of dynamic systems consists out of three solutions. These solutions are the *harmonic free vibration, steady-state,* and *transient solutions.* The free vibration is the condition of the system with disregard of the external load. The steady state or the forced vibration is the contrary of the free vibration. In the forced vibration, the external load is taken into account throughout the calculation. As the name suggests, the steady state is when the variables that define the system's behavior are unchanging (*steady*) in time. The transient phase is in contrast with the previous term, steady state. The transient solution is the solution to the sudden change of system from equilibrium or steady state. It occurs in the two conditions. The first condition is when the system is objected to an input signal or loading for the first time. The second condition is after any abnormal load conditions, for instance, a sudden load change in a steady state system. Unlike the steady-state solution, the transient response is gradually diminished in time. Whenever there is a loading, the total solutions consist of the two solutions which are the steady state and the transient. The total solution (*combined motion*) and the difference between the two solutions are summarized in the following figure:

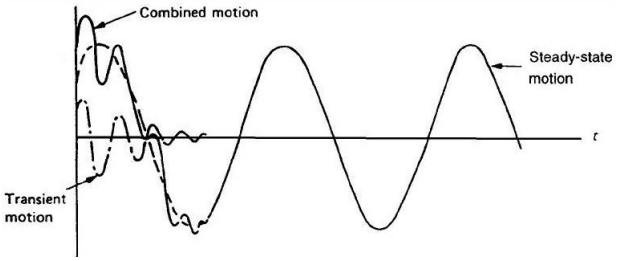

Figure 2.13: The total, steady-state, and transient solution of the system
Source : SCIA Engineering: theoretical dynamic system

In this subsection, only the free vibration solution that is discussed as an example. However, there are differences between solving the equation for total solutions and the harmonic free vibration. The derivation for the total solutions is discussed in references: [12] and [15].

From the equations of motion in equation 2.20, one can see that it consists of two functions. These two functions are the derivation in time and space. In this thesis, all the systems are assumed in the *linear phase*. Based on this assumption, one can use the separation method of the variable. This method assumes that the solution consists of multiplication between displacement dependent and time-dependent partial solutions. The solution is written in the following equation:

$$w(x,t) = W(x)\Psi(t) \tag{2.21}$$

Where W is an unknown space-dependent and Ψ is an unknown time-dependent function. Therefore from substituting equation 2.21 to the equation of motion in expression 2.20, it results to:

$$\frac{1}{\Psi}\frac{d^2\Psi}{dt^2} + \frac{a^2}{W}\frac{\partial^4 W}{\partial x^4} = 0 \tag{2.22}$$

In order to solve equation 2.22, these terms has to be equal to a separation constant (ω). The introduction of the separation constant is written in the expressions bellow:

$$\begin{aligned} \frac{1}{\Psi}\frac{d^2\Psi}{dt^2} &= -\omega^2 \\ \frac{a^2}{W}\frac{\partial^4 W}{\partial x^4} &= \omega^2 \end{aligned} \tag{2.23}$$

Where ω is a real value that describes the frequency vibration. The general solution for the time dependent term in equation 2.23 is derived using Euler derivations that resulting to :

$$\Psi(t) = A\sin(\omega t) + B\cos(\omega t) \tag{2.24}$$

The space dependent term in equation 2.23 can also be described into this following equation:

$$\frac{d^4 W}{dx^4} - \frac{\omega^2}{a^2}W = 0 \tag{2.25}$$

Again, using the Euler derivation the solution of the fourth order differential equation can be written in cosine form as the following :

$$W(x) = C_1\sin(\beta x) + C_2\cos(\beta x) + C_3\sinh(\beta x) + C_4\cosh(\beta x) \tag{2.26}$$

where:

$$\beta^4 = \frac{\omega^2}{a^2} \tag{2.27}$$

After both of the solutions that depend on both space and time are obtained, the constants $(A, B, C_1, C_2, C_3, C_4)$ are needed to be solved. These constants are solved by using the interface and boundary conditions.

2.3.4. VIBRATION OF THE SHELLS AND PLATES

For this thesis, the structural elements of the tank are described as the cylindrical shell and the circular plate (see Figure 2.14). This section and the Appendix B are dedicated for deriving the governing equations for these two systems. The complete derivations are explained in Appendix B and referred to *Soedel* in his book [16]. From the Appendix, one can understand that the shell equations are described as a set of generic expressions where each type of structures has their own unique *Lamé parameters*. The derivation of the Lame parameter is explained also in the Appendix B. The solutions for both of the structures are considered as **thin shell structures** *(Love's Theory)*, where shear deformation and rotational inertia are neglected throughout the process. This assumption can be fully justified since most of the time tank structure elements are considered to have thin structures where these two terms barely contribute to the system. The outline of the derivation is depicted in Figure 2.15.

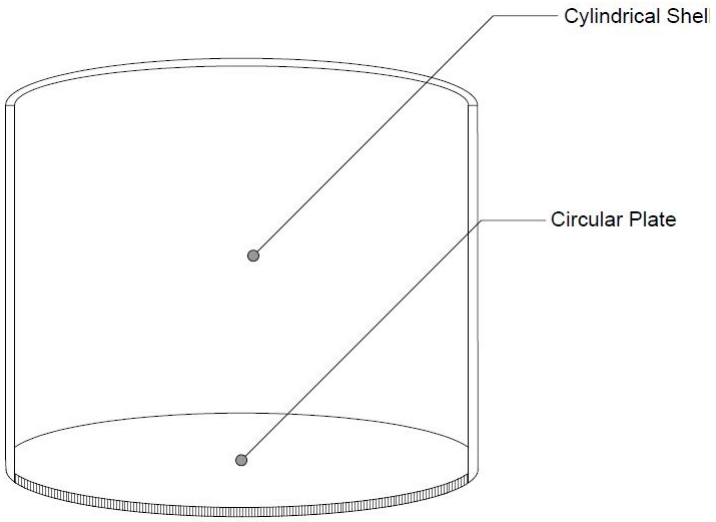

Figure 2.14: Cylindrical shell and circular plate

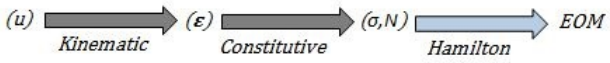

Figure 2.15: Vibration Shells and Plate Outline

CIRCULAR SLAB

The slab can be defined as a zero curvature shell. Since the slab does not have curvature, one can simply write these following expressions:

$$\frac{1}{R_1} = \frac{1}{R_2} = 0 \tag{2.28}$$

After substituting equation 2.28 to the *Love's equations* B.83 to B.87, the governing expressions can be written as:

$$-\frac{\partial(N_{11}A_2)}{\partial\alpha_1} - \frac{\partial(N_{21}A_1)}{\partial\alpha_2} - N_{12}\frac{\partial A_1}{\partial\alpha_2} + N_{22}\frac{\partial A_2}{\partial\alpha_1} + \rho h A_1 A_2 \ddot{u}_1 = A_1 A_2 q_1 \tag{2.29}$$

$$-\frac{\partial(N_{12}A_2)}{\partial\alpha_1} - \frac{\partial(N_{22}A_1)}{\partial\alpha_2} - N_{21}\frac{\partial A_2}{\partial\alpha_1} + N_{11}\frac{A_1}{\partial\alpha_2} + \rho h A_1 A_2 \ddot{u}_2 = A_1 A_2 q_2 \tag{2.30}$$

These two equations are equation motion of the slab **in plane motion**. While for the uncoupled equation from the two above:

$$-\frac{\partial(Q_{13}A_2)}{\partial\alpha_1} - \frac{\partial(Q_{23}A_1)}{\partial\alpha_2} + A_1 A_2 \rho h \ddot{u}_3 = A_1 A_2 q_3 \tag{2.31}$$

The equation above is used for the slab **out of plane motion**. In order to have a clear understanding between the two motions, these figures bellow describe the loading between the two motion in the Cartesian coordinate:

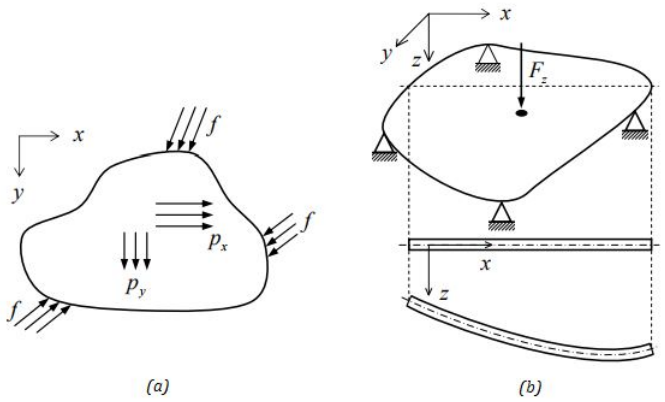

Figure 2.16: In-plane and out of plane loading of a plate: (a) in-plane loading; (b) out of plane loading
Source : Plate analysis, theory and application, Prof.dr.ir. J. Blaauwendraad

The unique *Lamé parameters* for the circular plate is following the polar coordinate and written in the following definitions:

$$\begin{aligned} A_1 &= 1 \quad \text{and} d \quad A_2 = r \\ \alpha_1 &= r \quad \text{and} \quad \alpha_2 = \theta \end{aligned} \tag{2.32}$$

1. ***In Plane Motion***
   The circular plate's *Lamé Parameters* in equation 2.32 are substituted to the in-plane motion expressions in the equations 2.30. This substitution yield into these two equations:

$$-\frac{\partial(N_{rr}r)}{\partial r} - \frac{\partial(N_{\theta r})}{\partial \theta} + N_{\theta\theta} + r\rho h\ddot{w}_r = rq_r \tag{2.33}$$

$$-\frac{\partial(N_{r\theta}r)}{\partial r} - \frac{\partial(N_{\theta\theta})}{\partial \theta} - N_{\theta r} + r\rho h\ddot{w}_\theta = rq_\theta \tag{2.34}$$

2. ***Out of Plane Motion***
   Firstly the transverse shear can be defined into the term of the moment, this is referred to equation B.86 and equation B.87. Then input the strains which satisfy the condition of zero curvature. Therefore it would result into the following equations :

$$D\nabla^4(r,\theta,t) + \rho h\ddot{w}_z = 0 \tag{2.35}$$

   Where the Laplace operator for a circular coordinate is:

$$\nabla^2 = \frac{\partial^2}{\partial r^2} + \frac{1}{r}\frac{\partial}{\partial r} + \frac{1}{r}\frac{\partial^2}{\partial \theta^2} \tag{2.36}$$

The three degree of freedoms and reference axes are derived from the Figure B.7 and depicted in the following figure:

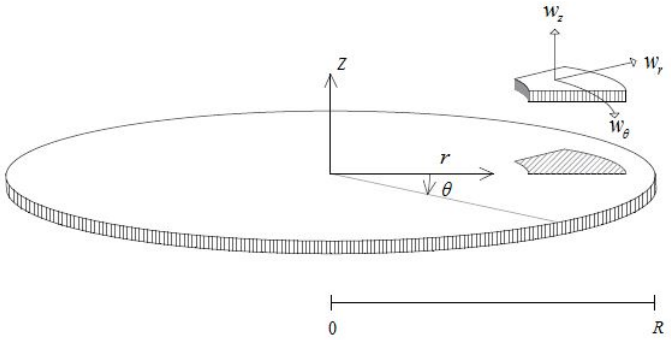

Figure 2.17: Circular slab coordinate

CYLINDRICAL SHELL

From Figure 2.18, the form equation for cylindrical shell can be written as:

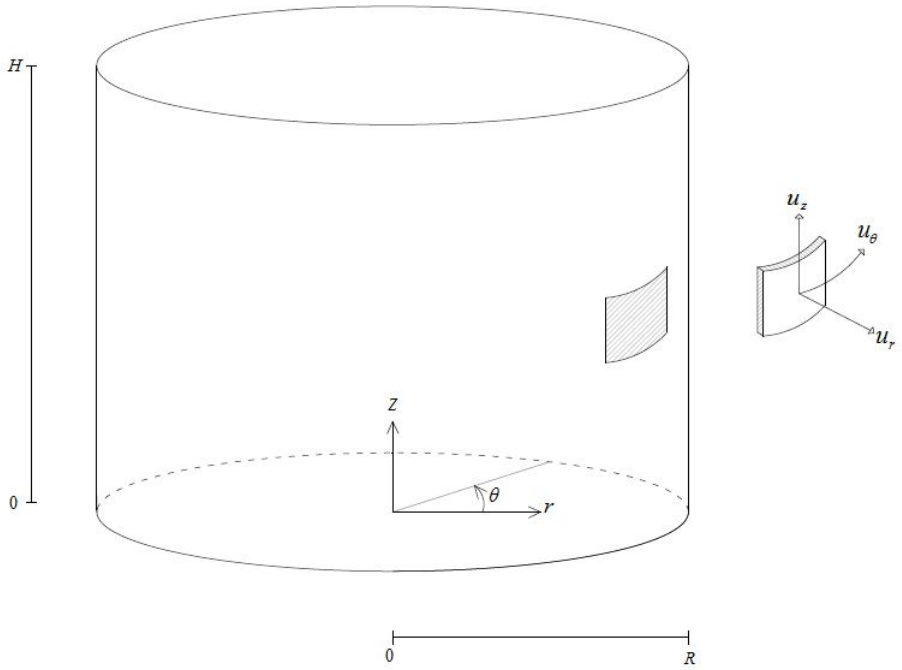

Figure 2.18: Cylindrical shell coordinate

$$(ds)^2 = (dz)^2 + R^2(d\theta)^2 \tag{2.37}$$

From the equation above, *Lamé Parameters* can be written in these components:

$$\begin{aligned} A_1 &= 1 \quad and \quad A_2 = R \\ \alpha_1 &= z \quad and \quad \alpha_\theta = \theta \end{aligned} \tag{2.38}$$

With the same procedural as plate, the equation of motion for a cylindrical shell are:

$$\frac{\partial(N_{zz})}{\partial z} + \frac{1}{R}\frac{\partial(N_{\theta z})}{\partial \theta} - \rho h \ddot{u}_z = 0 \tag{2.39}$$

$$\frac{\partial(N_{z\theta})}{\partial z} + \frac{1}{R}\frac{\partial(N_{\theta\theta})}{\partial \theta} - \frac{1}{R}Q_{\theta r} - \rho h \ddot{u}_\theta = 0 \tag{2.40}$$

$$\frac{\partial(Q_{zr})}{\partial z} + \frac{1}{R}\frac{\partial(Q_{\theta r})}{\partial \theta} - \rho h \ddot{u}_r = 0 \tag{2.41}$$

From these expressions one can see that the three displacements are coupled together.

2.4. FLUID POTENTIAL FLOW

Since the tank contains liquid, the analysis includes how it behaves dynamically. The fluid potential flow can be used to describe fluid motion. Based on the scope of this thesis, the liquid is derived as *linear*, *inviscous*, and *incompressible*. Linear motion means neglecting the rotational flow. Assuming liquid as an inviscous material means that the effect of viscosity is neglected. Lastly, the incompressible liquid means that one assumes that the density does not change in time. The equation for the fluid potential flow is derived in the Appendix C and referred to [16] and [19].The final derivations are rewritten in the following equations 2.42 to 2.44 for the sake of better readability.

$$\begin{aligned} v_x &= -\frac{\partial \phi}{\partial x} \\ v_y &= -\frac{\partial \phi}{\partial y} \\ v_z &= -\frac{\partial \phi}{\partial z} \end{aligned} \tag{2.42}$$

The governing equation of motion is:

$$\frac{\partial^2 \phi}{\partial x^2} + \frac{\partial^2 \phi}{\partial y^2} + \frac{\partial^2 \phi}{\partial z^2} = 0 \tag{2.43}$$

The equation of motion can also be expressed in term of pressure

$$\frac{\partial^2 p}{\partial x^2} + \frac{\partial^2 p}{\partial y^2} + \frac{\partial^2 p}{\partial z^2} = 0 \tag{2.44}$$

p = the liquid pressure;
ϕ = the liquid potential velocity;

2.5. COMMONLY USED PROCEDURE FOR RESERVOIR TANK UNDER SEISMIC LOADS

There are many methods available for dynamic analysis of the reservoir tank under seismic load. In the engineering practice there are three commonly used methods which are the Housner [7], Velestos and Yang [18], and also Eurocode 8: 1998-4:2006 [5] that can be found in the European countries.

2.5.1. PRELIMINARY SEISMIC TANK DESIGN FROM EUROCODE 8: 1998-4:2006

For preliminary design, the most simplified method is described in [5]. For a rigid case, Eurocode 8 discretized the system as two single-degree-of-freedom. The discretization system is also derived by Housner and depicted in Figure 2.21. The *impulsive pressure* is the component that satisfies the boundary conditions liquid with the wall and/or the bottom of the tank. The boundary condition that the impulsive pressure component satisfies is the kinematic equilibrium between the liquid potential and the structure velocity or acceleration. However, this component does not consider the free surface wave.

The other component is the *convective response*. This component is the counterpart of the *impulsive response*. This response only regards the surface waves, yet it neglects the boundary condition of the wall and the tank bottom. For a better understanding, the following figure is presented to describe the boundary conditions of the convective and the impulsive responses:

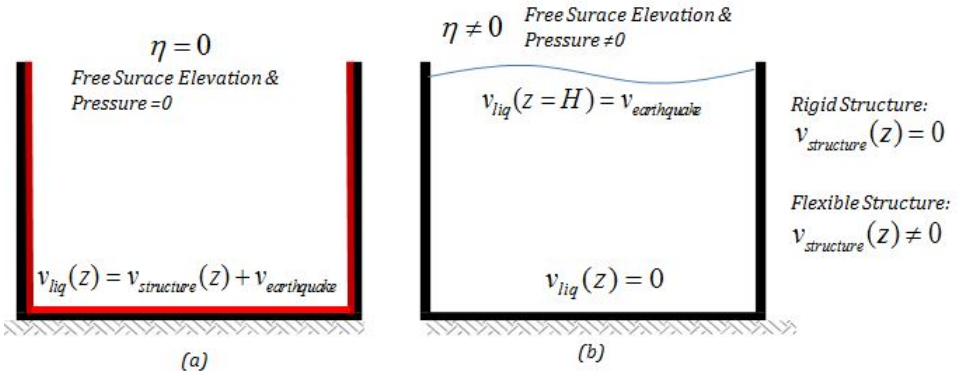

Figure 2.19: The boundary conditions of the impulsive response (a); the boundary conditions of the convective respons (b).

Together the two responses complete the total condition of the seismic liquid tank.The simplified method that is presented in the Eurocode 8 takes into account the flexibility of the structures in the impulsive response. The difference between the rigid and flexible tank can also be seen in Figure 2.19. In this code, only the structure fundamental period that is regarded. The other structure higher periods are neglected. The natural periods of the impulsive and the convective response in seconds are in the following:

$$T_{imp} = C_i \frac{\sqrt{\rho_{liq}} \cdot H}{\sqrt{s/R} \cdot \sqrt{E}}$$
$$T_{con} = C_c \sqrt{R} \tag{2.45}$$

Where the variables are defined in the following:

T_{imp}	= the impulsive period;
T_{con}	= the convective period;
H	= the liquid height;
R	= the tank's radius
s	= the equivalent uniform wall thickness;
ρ_{liq}	= the mass density of liquid;
E	=the modulus of elasiticity of the tank wall;
C_i	= the coefficient for impulsive fundamental natural period, as shown in Table 2.1;
C_c	= the coefficient for convective fundamental natural period, as shown in Table 2.1.

For practical purpose, the Eurocode 8 simplifies Velestos and Yang derivation [18] into the following table for different tank geometries:

Table 2.1: Coefficients C_i and C_c for the natural periods, masses m_i and m_c and heights h_i and h_c from the base of the point of application of the wall pressure, for the impulsive and convective components
Source : Eurocode 8: EN 1998-4:2006 [5]

H/R	C_i	C_c $(s/m^{0.5})$	m_i/m	m_c/m	h_i/H	h_c/H	h_i'/H	h_c'/H
0.3	9.28	2.09	0.176	0.824	0.400	0.521	2.640	3.414
0.5	7.74	1.74	0.300	0.700	0.400	0.543	1.460	1.517
0.7	6.97	1.60	0.414	0.586	0.401	0.571	1.009	1.011
1.0	6.36	1.52	0.548	0.452	0.419	0.616	0.721	0.785
1.5	6.06	1.48	0.686	0.314	0.439	0.690	0.555	0.734
2.0	6.21	1.48	0.763	0.237	0.448	0.751	0.500	0.764
2.5	6.56	1.48	0.810	0.190	0.452	0.794	0.480	0.796
3.0	7.03	1.48	0.842	0.158	0.453	0.825	0.472	0.825

The impulsive mass is written as m_i, and the convective mass is defined as m_c. The two masses is derived from the division of the integration of the pressure response with the respect to the height with the acceleration. The total liquid mass m which is defined as $m_i + m_c$. The heights from the base to the centroid of the impulsive and the convective hydrodynamic wall pressure are defined as h_i and h_c. The accented heights (h_i' and h_c') are the heights of the centroid of the impulsive and convective pressures to the base by taking into account both hydrodynamic pressure in the tank's wall and base plate. For a better understanding, the difference between the two types of height (with and without accents) can be seen the figures below:

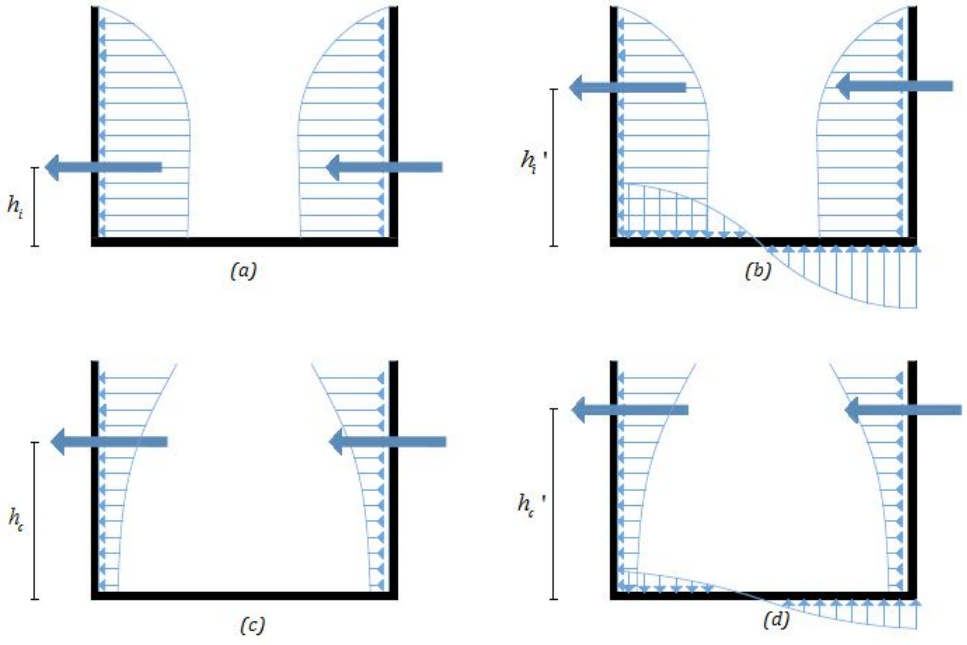

Figure 2.20: The distribution and centroidal heights of impulsive (a,b) and convective (c,d) pressures.
(a) Impulsive pressure on the wall;(b) Impulsive pressure on the wall and the base;
(c) Convective pressure on the wall (d) Convective pressure on the wall and the base

According to Eurocode 8: EN 1998-4:2006, base shear can be calculated in the following manner:

$$Q = (m_i + m_w + m_r)S_d(T_{imp}) + m_c S_e(T_{con}) \tag{2.46}$$

Q = the base shear;
m_w = mass of the tank wall;
m_t = mass of the tank roof;
m_i = impulsive mass;
m_c = convective mass;
m_t = mass of the tank roof;
$S_d(T_{imp})$ = Impulsive spectral acceleration, obtained from design response spectra;
$S_e(T_{conv})$ = Convective spectral acceleration, obtained from elastic response spectra.

The overturning moment immediately above the base slab which excludes of bottom pressure is written in the following expressions:

$$M = (m_i \cdot h_i + m_w \cdot h_w + m_r \cdot h_r)S_d(T_{imp}) + m_c h_c S_e(T_{conv}) \tag{2.47}$$

M = the overturning moment immediately above the base slab;
h_r = the height of the centre of gravity roof;
h_w = the height of the centre of gravity tank;
h_i = the height of the impulsive pressure that excludes bottom pressure, as shown in Figure 2.20 (a);
h_c = the height of the convective pressure that excludes bottom pressure, as shown in Figure 2.20 (c);

The overturning moment immediately below the base plate that includes bottom pressure is expressed as:

$$M' = (m_i \cdot h'_i + m_w \cdot h_w + m_r \cdot h_r)S_d(T_{imp}) + m_c h'_c S_e(T_{conv}) \tag{2.48}$$

M' = the overturning moment immediately bellow the base slab;
h'_i = the height of the impulsive pressure that includes bottom pressure, as shown in Figure 2.20 (b);
h'_c = the height of the convective pressure that includes bottom pressure, as shown in Figure 2.20 (d).

The difference between the two moments is: the moment above base slab does not consider the plate pressure. Therefore the moment level arms that the equation use are the heights without the accent. These level arms refer to Figure (a) and (c) of Figure 2.20. Meanwhile, the moment below the slab considers the pressure on the plate. Therefore, this moment use the accented heights as its level arms, that refer to the Figure (b) and (d) in the Figure 2.20

For a complete solution of the hydrodynamic pressure and response under seismic loading, Eurocode refers to Velestos and Yang [18].

2.5.2. HYDRODYNAMIC PRESSURE BY HOUSNER

The hydrodynamic pressure that is derived by Housner [7] is proposed in the 50s. The formulation that Housner developed is a simplification of liquid and structure interaction by using lumped mass. The liquid mass is divided into two parts which are the free mass that causing sloshing and the fixed mass that contributing to the inertial force. These terms can also be described as *the impulsive mass* (inertial force) and *the convective mass* (sloshing force) that satisfy the boundary condition in the Figure 2.19. The discretization of the two masses are shown in the figure below:

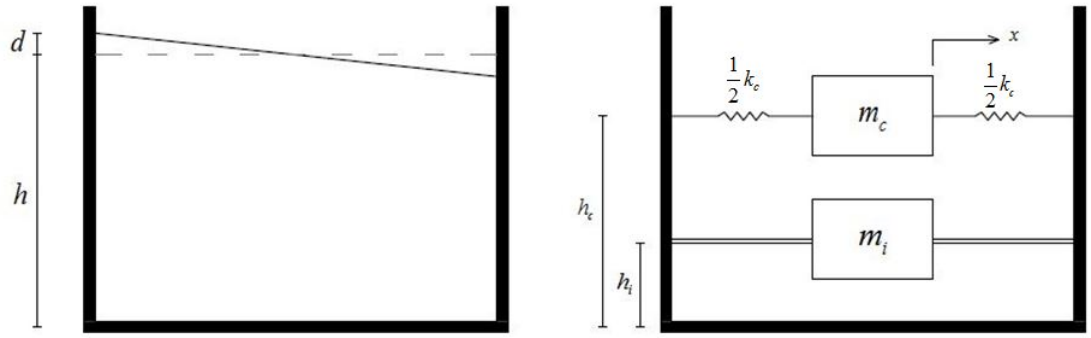

Figure 2.21: Equivalent of a dynamic system of the tank from Housner. The discrete lumped mass can be seen in the right. The impulsive mass (m_i) and the compulsive mass (m_c) equivalent to the forces that are produced by the water. (Source : The dynamic behaviour of Water Tanks, George W, Housner[7])

Housner derives both the rigid pressure for both cylindrical tank and rectangular tank. The cross section of the tanks can be seen in the following:

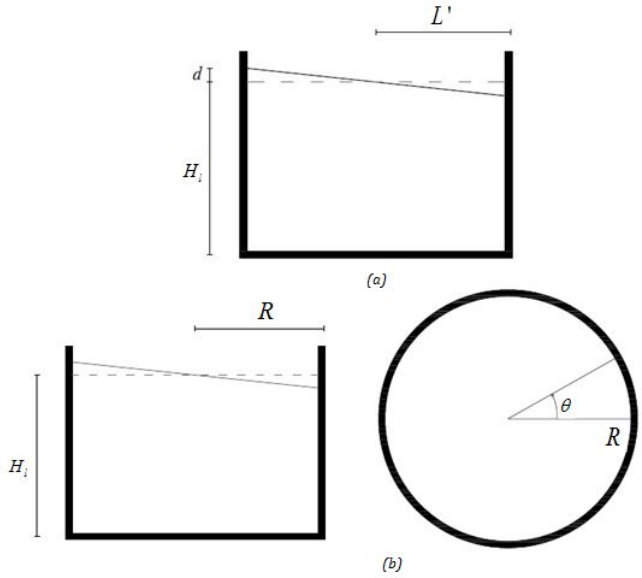

Figure 2.22: (a) The cross section of rectangular tank; (b) The cross section of cylindrical tank. (Source : The dynamic behaviour of Water Tanks, George W, Housner[7])

The Housner's expressions below is specifically written for rigid tanks.

RIGID PRESSURE COMPONENTS OF THE RECTANGULAR TANK

For rectangular tank the equation for the impulsive and convective masses are:

The impulsive components:

$$\begin{aligned} m_i &= m\frac{\tanh(1.7\times L'/H_l)}{1.7\times L'/H_l} \\ h_i &= \frac{3}{8}H_l\left\{1+\alpha\left[\frac{m}{m_i}\left(\frac{L'}{H_l}^2\right)-1\right]\right\} \\ p_i(z) &= \rho_{liq}H_l\left(\frac{z}{H_l}-0.5\left(\frac{z}{H_l}\right)^2\right)\sqrt{3}\tanh(\sqrt{3}L'/H_l)a_e(t) \end{aligned} \tag{2.49}$$

The convective components:

$$\begin{aligned} m_c &= m\frac{0.83\tanh(1.6\times H_l/L')}{1.6\times H_l/L'} \\ k_c &= 3\frac{m_i^2}{m}\frac{gH_l}{L'^2} \\ h_c &= H_l\left[1-\frac{m}{3m_c}\left(\frac{L'}{H_l}\right)^2-0.63\beta\frac{L'}{H_l}\sqrt{0.28\left(\frac{mL'}{m_cH_l}\right)^2-1}\right] \\ T_{conv} &= 2\pi\sqrt{m_c/k_c} \end{aligned} \tag{2.50}$$

Most of the variables is already described in the previous Section 2.5.1. However, there are extra terms for Housner derivations which are:

$p_i(z)$ = the impulsive pressure;
H_l = the liquid height, shown in Figure 2.22;
g = gravitational acceleration ($9.81 m/s^2$);
L' = half width of the tank, shown in Figure 2.22;
α = the coefficient for impulsive centroid height for rectangular tank. If the bottom pressure is included the value $\alpha = 1.33$. However, if the bottom pressure is not included $\alpha = 0$;
β = the coefficient for convective centroid height for rectangular tank. If the bottom pressure is included the value $\beta = 2.0$. However, if the bottom pressure is not included $\beta = 1$.
a_e = the ground acceleration in the function of time

RIGID PRESSURE COMPONENTS OF THE CYLINDRICAL TANK

The impulsive and the convective components for cylindrical tank is defined in the following:
The impulsive components:

$$\begin{aligned} m_i &= m\frac{\tanh(1.7\times R/H_l)}{1.7\times R/H_l} \\ h_i &= \frac{3}{8}H_l\left\{1+\alpha\left[\frac{m}{m_i}\left(\frac{R}{H_l}^2\right)-1\right]\right\} \\ p_i(z) &= \rho_{liq}H_l\left(\frac{z}{H_l}-0.5\left(\frac{z}{H_l}\right)^2\right)\sqrt{3}\tanh(\sqrt{3}R/H_l)\cos(\theta)a_e(t) \end{aligned} \tag{2.51}$$

The convective components:

$$\begin{aligned} m_c &= m\frac{0.6\tanh(1.8\times H_l/R)}{1.8\times H_l/R} \\ k_c &= 5.4\frac{m_i^2}{m}\frac{gH_l}{R^2} \\ h_c &= H_l\left[1-0.85\frac{m}{m_c}\left(\frac{R}{H_l}\right)^2-0.56\beta\frac{R}{H_l}\sqrt{\left(\frac{mR}{3}m_cH_l\right)^2-1}\right] \\ T_{conv} &= 2\pi\sqrt{m_c/k_c} \end{aligned} \tag{2.52}$$

Likewise the rectangular tank, most of the variables are already defined in the Section 2.5.1. However, the α and β are exclusively defined for cylindrical tank, which are:

$p_i(z)$ = the impulsive pressure;
H_l = the liquid height, shown in Figure 2.22;
R = the radius of the tank, shown in Figure 2.22;
θ = the angle plane of the tank, shown in Figure 2.22;
α = The coefficient for impulsive centroid height for cylindrical tank. If the bottom pressure is included the value $\alpha = 1.33$. However, if the bottom pressure is not included $\alpha = 0$
β = The coefficient for convective centroid height for cylindrical tank. If the bottom pressure is included the value $\beta = 2.0$. However, if the bottom pressure is not included $\beta = 1$

The equation above are specifically derived by Housner for fluid containers with geometry ratio of $H_l/L \leq 1.6$. For narrower tank with geometry ratio of $H_l/L > 1.6$, there is a correction from Housner. The correction is written in the following forms:
for rectangular tank:

$$p_i(z) = \begin{cases} \rho_{liq} H_l \left(\frac{z}{H_l} - 0.5\left(\frac{z}{H_l}\right)^2\right)\sqrt{3}\tanh\left(\sqrt{3}L'/H_l\right)a_e(t), & z \leq 1.6L \\ \rho_{liq} H_l a_e(t), & z > 1.6L \end{cases} \tag{2.53}$$

for cylindrical tank:

$$p_i(z) = \begin{cases} \rho_{liq} H_l \left(\frac{z}{H_l} - 0.5\left(\frac{z}{H_l}\right)^2\right)\sqrt{3}\tanh\left(\sqrt{3}R/H_l\right)\cos(\theta)a_e(t), & z \leq 1.6L \\ \rho_{liq} H_l a_e(t), & z > 1.6L \end{cases} \tag{2.54}$$

The correction of the narrow tanks are also depicted in the following figures:

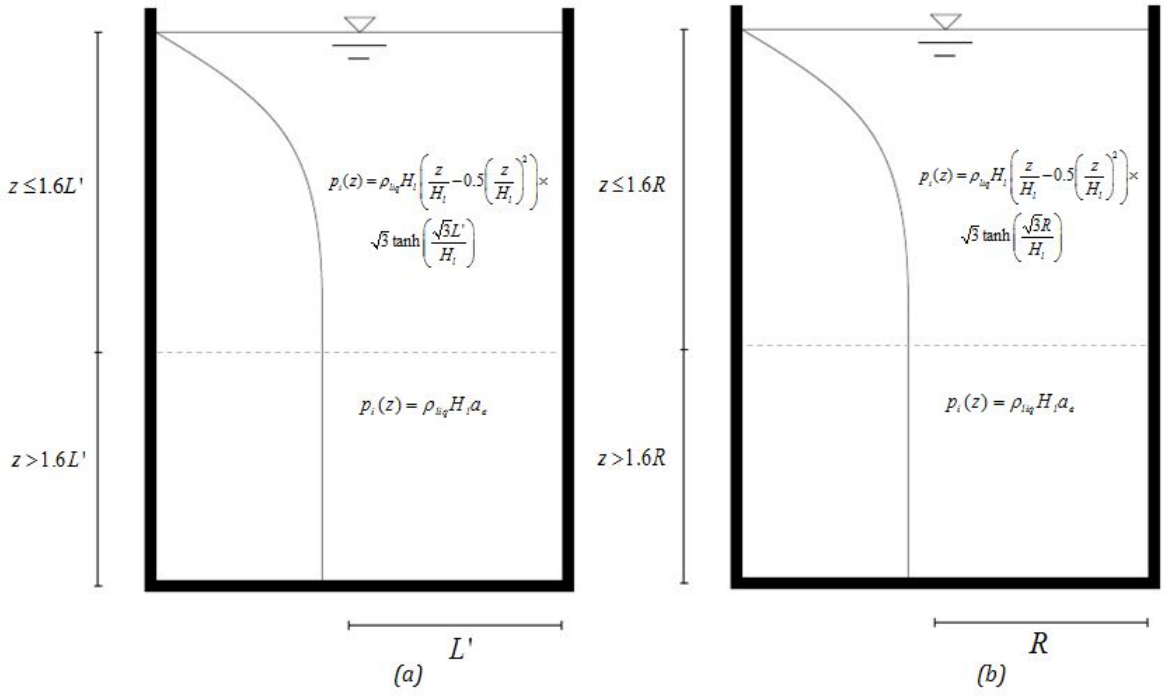

Figure 2.23: Housner correction for tanks with tank geometry ratio $H/R > 1.6$ or $H/L' > 1.6$. (a) Rectangular tank; (b) Cylindrical tank. (Source : The dynamic behaviour of Water Tanks, George W, Housner[7])

2.5.3. HYDRODYNAMIC PRESSURE BY A.S. VELESTOS AND YANG

The tank fluid system that is investigated by Velestos [18] is a cylindrical tank with the radius of a and the structural height of H_s. The tank is water filled with the height of H. The following figures depict the parameters that Velestos and Yang define on his derivations:

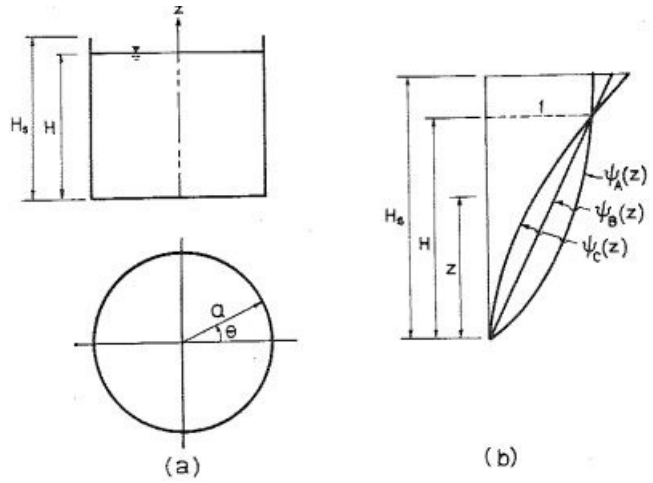

Figure 2.24: The tank system (a) ; example vibration mode shapes (b)
Source : Dynamic of fixed-base liquid storage tank, A.S. Velestos and Jong Y. Yang [18]

RIGID TANKS (SIMILIAR TO HOUSNER)

The hydrodynamic pressure against the wall for a rigid wall according to Velestos and Yang is:

$$p(z,\theta,t) = \Big(\underbrace{c_o(z)\cdot\ddot{x}(t)}_{\text{the impulsive component}} + \underbrace{\sum_{k=1}^{\infty} c_k(z)A_k(t)}_{\text{the convective component}} \Big) \rho_{liq} H \cos\theta \tag{2.55}$$

Where the parameters are defined in the following description:

$p(z)$	=	the total pressure varies with respect to the height;
ρ_{liq}	=	the liquid mass density;
θ	=	the plane angle in tank geometry, shown in Figure 2.24;
c_o	=	dimensionless function that varies along the height, described in equation 2.59;
$\ddot{x}$	=	the ground acceleration;
$A_k(t)$	=	the pseudo acceleration for SDOF system with natural frequency; from equation 2.56.

The sloshing frequencies (f_k), are given by:

$$f_k = \frac{1}{2\pi}\sqrt{\lambda_k \frac{g}{a}\tanh(\lambda_k \frac{H}{a})} \tag{2.56}$$

Where the g is the gravitational acceleration, and λ_k are the zeros that is first order of the Bessel first kind function (J_1) [1] in following equation:

$$\frac{\partial J_1(\lambda_k \zeta)}{\partial \zeta}\Big|_{\zeta=1} \tag{2.57}$$

From the equation 2.57, the first four values of λ_k are:

$$\begin{aligned} \lambda_1 &= 1.8412 \\ \lambda_2 &= 5.3314 \\ \lambda_3 &= 8.5363 \\ \lambda_4 &= 11.7060 \end{aligned} \tag{2.58}$$

The function of $c_o(z)$ is a dimensionless function along that varies with respect to the liquid height. This function is one of the impulsive components and described as the following:

$$c_o(z) = \frac{8}{\pi^2} \sum_{i=1}^{\infty} \frac{(-1)^{(i+1)}}{(2i-1)^2} \epsilon_i \cos((2i-1)\frac{\pi z}{2H}) \tag{2.59}$$

$$\epsilon_i = \frac{I_1\left[(2i-1)\frac{\pi a}{2H}\right]}{I_1'\left[(2i-1)\frac{\pi a}{2H}\right]} \tag{2.60}$$

a = the radius of the tank;
I_1 = the modified Bessel function of the first order;
I_1' = the first derivation relative of I_1.

The impulsive pressure that acts on the wall yields to:

$$p_o(z,\theta,t) = c_o(z)\rho H \cdot \ddot{x}(t)\cos\theta \tag{2.61}$$

The distribution function $c_o(z)$ is also defined by Velestos and Yang for different tank geometry and depicted in the following figure :

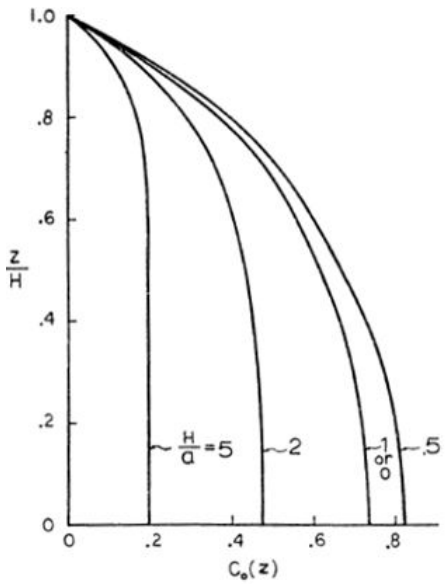

Figure 2.25: Impulsive pressure distribution in rigid tanks
Source : Dynamic of fixed-base liquid storage tank, A.S. Velestos and Jong Y. Yang [18]

The distribution function for the convective pressure c_k is defined in the following expression:

$$c_k(z) = \frac{2}{\lambda_k^2 - 1} \frac{a}{H} \frac{\cosh(\lambda_k z/a)}{\cosh(\lambda_k H/a)} \tag{2.62}$$

The first two sloshing modes are defined by Velestos and Yang for different tank geometries in the two figures below:

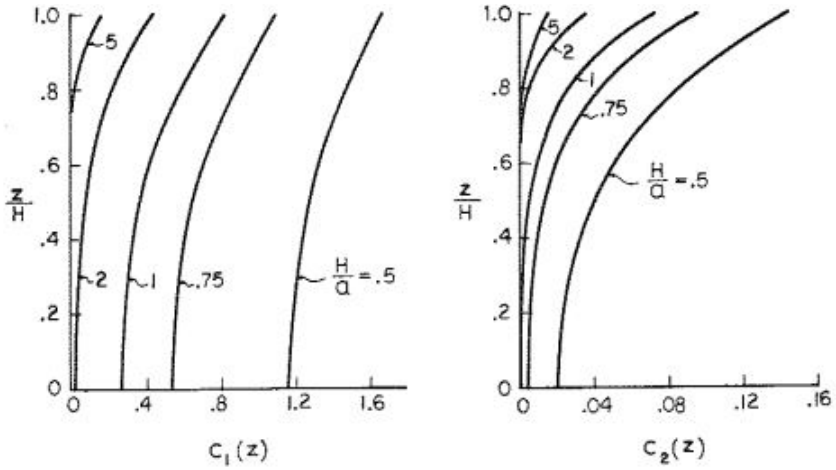

Figure 2.26: Coefficient $c_k(z)$ for convective preassure in rigid Tanks
Source : Dynamic of fixed-base liquid storage tank, A.S. Velestos and Jong Y. Yang [18]

SIMPLIFIED METHOD FOR FLEXIBLE TANKS

The calculation for the impulsive pressure is derived by assuming that it vibrates in fixed configurations $\psi(z)$ of modes that is obtained from the fundamental mode instead of using infinite modes. This analysis does not consider the distortion of the cross-section and the effect of the higher modes. The mode shape configurations that are derived by Velestos and Yang are based on assumption and simplification. The three possible example of mode shape can also be seen in Figure 2.24 (b). The three configurations are expressed in the following equations:

$$\begin{aligned} \psi_A(z) &= \sin\left(\frac{\pi}{2}\frac{z}{H}\right) \\ \psi_B(z) &= \frac{z}{H} \\ \psi_C(z) &= 1-\cos\left(\frac{\pi}{2}\frac{z}{H}\right) \end{aligned} \tag{2.63}$$

However, this method also holds for any arbitrary mode shape(s).

In the analysis, the impulsive component of the hydrodynamic pressure (p_o) that acts on the flexible wall changed into the following form:

$$p_o(z,\theta,t) = C \cdot b_o(z)\rho_{liq} H \cdot A_o(t)\cos\theta \tag{2.64}$$

In which that the C is a dimensionless coefficient that depends on the liquid and structure mass and represent the modal participation factor. The newly introduced constant b_o also a dimensionless function that varies along the liquid height. The above-explained constants can be expanded in these expressions:

$$b_o(z) = \frac{4}{\pi}\sum_{i=1}^{\infty}\frac{\delta_i}{2i-1}\epsilon_i \cos\left(\frac{(2i-1)\pi z}{2H}\right) \tag{2.65}$$

While the expression for δ_i is:

$$\delta_i = \frac{1}{H}\int_0^H \psi(z)\cos\left(\frac{(2i-1)\pi z}{2H}\right) \tag{2.66}$$

Meanwhile, for the calculation of C is derived from the mass ratio, or more specifically it is defined by the following equation:

$$C = \frac{m_x}{m_w} = \frac{m_{x,s}+m_{x,l}}{m_{w,s}+m_{w,l}} \tag{2.67}$$

m_x = mass of the structure fluid system for a rigid body motion of the tank ($m_{x,l}$ for liquid contribution to the mass and $m_{x,s}$ for structure contribution to mass), obtained from equation 2.68 and 2.69;

m_w = the effective mass of the system when it vibrates from the mode shape configuration in equation 2.63 ($m_{w,l}$ for liquid contribution to the mass and $m_{w,s}$ for structure contribution to mass), obtained from equation 2.68 and 2.69.

These mass quantities are depicted by the following expressions:

$$\begin{aligned} m_{x,s} &= \int_0^{H_s} \mu_s(z) \cdot \psi(z) dz + m_r \cdot \psi(H_s) \\ m_{w,s} &= \int_0^{H_s} \mu_s(z) \cdot \psi^2(z) dz + m_r \cdot \psi^2(H_s) \end{aligned} \tag{2.68}$$

Where the constant $\mu_s(z)$ is the mass per unit of the height of the structure **without the liquid**. The coefficient m_r is the roof mass concentrated in the wall.

The other component which are $m_{x,l}$ and $m_{w,l}$ is expressed in these equation below:

$$\begin{aligned} m_{x,l} &= \frac{1}{a} \int_0^{H} c_o(z) \cdot \psi(z) dz \\ m_{w,l} &= \frac{1}{a} \int_0^{H} b_o(z) \cdot \psi(z) dz \end{aligned} \tag{2.69}$$

The new equation for the flexible tank is also different in the previous equation which instead of the ground acceleration it involves to the **pseudo acceleration** $A_o(t)$. Using the pseudo acceleration by means is including the structure acceleration also *(ground acceleration*$(z = 0)$ + *relative structure acceleration*(z)*)*. The figure bellow demonstrated the differences between the flexible and rigid tank hydrodynamic pressure.

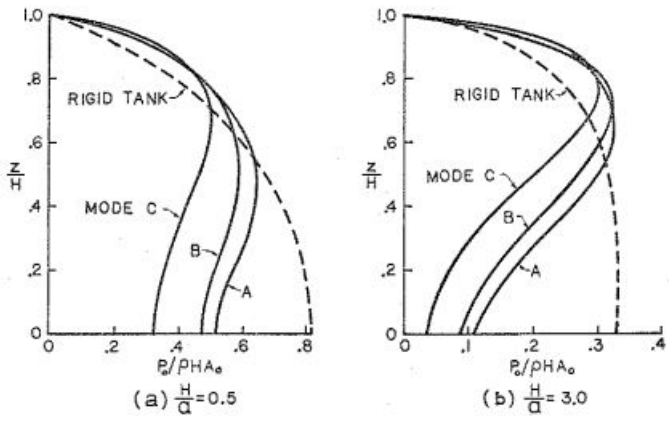

Figure 2.27: Flexible and Rigid Tanks pressure
Source : Dynamic of fixed-base liquid storage tank, A.S. Velestos and Jong Y. Yang [18]

In the case of **rigid tank**, the configuration mode shapes in equation 2.63 (ψ) **equals to one** and **the relative structure acceleration equals to zero** (see Figure 2.19). These two conditions reduces equation 2.64 to equation 2.61.

2.5.4. SIGNAL PROCESSING

From the previous section, one can understand that the seismic analysis can be done in multiply ways. The seismic acceleration input can be either time domain or frequency domain. However, for thid thesis, the analytic calculation is done in frequency domain because of the main advantage of its simplicity and its straightforward manner. The input can be still in the time domain. However, an additional step is necessary which is the conversion of the time domain to the frequency domain. Where then the time domain input can be still analyzed. This conversion is using the Fourier transform in the following expression:

$$a(\omega) = \int_0^{\infty} a(t) \exp(-i\omega t) \tag{2.70}$$

The advantage of using the Fourier transform is its versatility to express the result into time domain by utilizing the inverse Fourier transform which is :

$$a(\omega) = \frac{1}{\pi} \int_0^{\infty} F(\omega) \exp(i\omega t d\omega \tag{2.71}$$

3

TWO DIMENSIONAL MODEL

This chapter is meant as an introduction of knowledge about liquid-structure interaction in a liquid filled tank structure. This fundamental knowledge is essential to have a clear picture how liquid-structure interaction works. The initial derivations for the two-dimensional model are referred in Chapter 2. The structural vibration is discussed more detail in Subsection 2.3.3. For the liquid, the derivations are written in the Section 2.4. This third chapter includes derivations, results, and parameter studies.

3.1. GENERAL PROCEDURE

The plate and the walls are described with *the Euler Bernoulli beam theory* with specific stiffness properties. These stiffness properties depend on the material and the cross-sectional properties. Both the walls and the plate are considered as inextensible beams that solely have the bending stiffness. The liquid is defined as the potential flow in the two-dimensional plane, i.e. x and z. The following figure depicts the two-dimensional model:

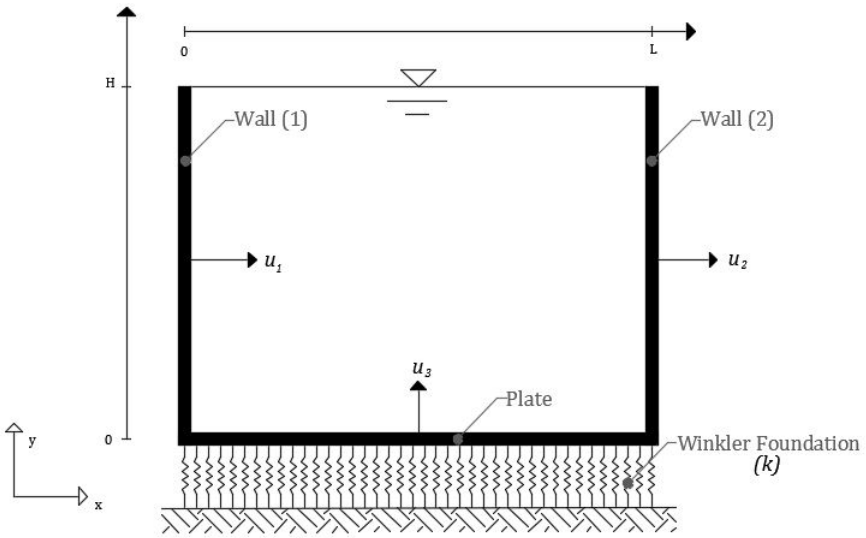

Figure 3.1: Two dimensional Model of the tank

3.1.1. THE PROCESS FLOWCHART

This section discusses the structure of the performed two-dimensional model. The flowchart in Figure 3.2 visualizes the followed strategy

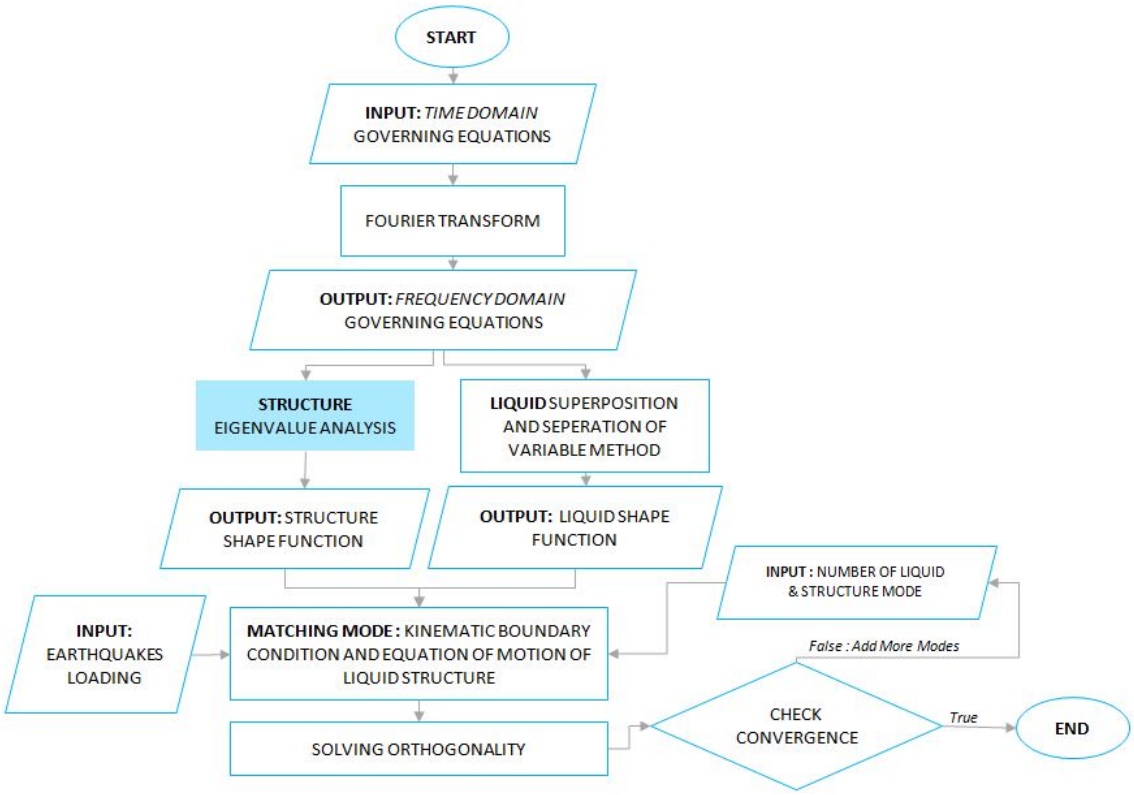

Figure 3.2: The Process Flowchart of the Two-Dimensional Model

Most of the processes in this model are analytically performed. However, the structural eigenvalue analysis is performed numerically. The reasons behind the decision of using numerical solver for the structure eigenvalue analysis are the reduced computation time and its simplicity. Since the modeling is not entirely analytical nor numerical, the method of solving this two-dimensional model is a "*semi-analytical approach.*"

3.1.2. THE ASSUMPTIONS

In the previous chapter, the assumptions are written in different sections. Therefore for the sake of legibility, the assumptions for the two-dimensional model are rewritten in this subsection. Since the total systems consist of two coupled systems which are the liquid and the structure, the re-explanation of the assumptions are also divided into two sections.

LIQUID ASSUMPTIONS

In the list bellow, the liquid assumptions for the two dimensional model is defined:

- **Two-dimensional plane flow motion**.
  Since the derivation is performed in the two-dimensional model, the potential flow of liquid is written in the two-dimensional form. From the Figure 3.1, one can realize that the modeling is in the Cartesian coordinates. Based on these two statements the potential flow is described in term of x and z coordinates.

- **Inviscous**.
  The liquid is considered as a non-viscous material. This assumption simplifies the potential flow motion. Since the liquid viscosity is considered zero, there is no friction term in the equation. Note that this assumption may only be applied for the fluid with low viscosity and not to solid-like fluid.

- **Incompressible**
  The assumption of incompressibility in liquid means that the material density is constant within the fluid volume. The simplification resulting to the divergence of the flow velocity equals to zero (see equation C.13).

- **Linear**
  Linear or irrotational liquid is used in this thesis to simplify the model. When the liquid is considered linear, the superposition solution of potential flow can be performed. The application is highly convenient, for liquid-structure interaction of the tank. The reason why it is convenient is explained in Section 3.4.

STRUCTURAL ASSUMPTIONS

For modeling the structure, the following assumptions are used in this two dimensional-model:

- **Linear Material**.
  For the structural materials that are used in the section 3.7 are considered linear, meaning that materials are always in the elastic regime.

- **Euler Bernoulli Beam Theory**.
  In the modeling of the plate and the walls,*Euler Bernoulli beam theory* is used. The reason of using this theory instead of other available theories is due to its simplicity. Using Euler Bernoulli theory means that the two-beams have infinitesimal strains and small rotations. Furthermore, the Euler Bernoulli's theory considers that the shear stiffness is rigid and negligible the effect of inertial rotation. In case where the deformation is high, this theory cannot be applied any longer. Instead, the extended form of Euler Bernoulli beam theory for this specific problem (*von Kármán strains*) is more applicable. If the shear stiffness is flexible and the effect of inertia rotation is prominent, *the Timoshenko Beam theory* is more applicable.

- **Inextensible Beams**
  This assumptions does not allow axial deformation which is perpendicular to the beam. This assumption results to zero axial strain and force.

3.2. GOVERNING EQUATIONS IN TIME DOMAIN

The governing equation is divided into four subsections which are:

- the seismic excitation;
- the structural equation of motion;
- the boundary conditions.

3.2.1. SEISMIC GROUND EXCITATION

From Chapter 2 and Subsection 2.1.2, it is stated that the seismic load can be described as the harmonic waves. These harmonic waves propagate along the free surface of the soil. Due to the linearity of the model, one can treat the vertical and the horizontal excitation separately and then superimpose the responses to obtain the final result. The wave characteristic is dependent on both time and space variables. In general, the harmonic wave can be described as shown in the next figure:

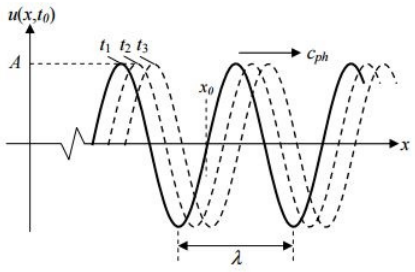

Figure 3.3: Harmonic Wave

The harmonic wave is given by the following mathematical expression:

$$u_{(x,t)} = A \cdot \exp(\omega t - \gamma x) \tag{3.1}$$

The three components in equation 3.1 which are A, ω and γ are known as the amplitude, frequency and wave number of the harmonic wave, respectively. The amplitude is the maximum value of displacement of the harmonic wave. The earthquake itself can be described in two directions which are: the horizontal and vertical loading.

Vertical ground motion of the earthquakes as surface waves

$$w_{earthquake(x,\omega)} = w(x) \cdot \exp(i\omega t) = w_e \exp(i\omega t) \exp(-i \cdot \gamma x) \tag{3.2}$$

Horizontal ground motion of the earthquakes as surface waves

$$u_{earthquake(x,\omega)} = u(x) \cdot \exp(i\omega t) = u_e \exp(i\omega t) \exp(-i \cdot \gamma x) \tag{3.3}$$

However in this thesis the phase difference is neglected since the plate is considered inextensible. This assumption lead to no effect of the soil stiffness in the transverse direction (see Figure 3.1) and equal motion in horizontal direction. Therefore the variable γ is equals to 0. Which result in the following seismic motion:

Vertical ground motion of the earthquakes

$$w_{earthquake(x,\omega)} = w(x) \cdot \exp(i\omega t) = w_e \exp(i\omega t) \tag{3.4}$$

Horizontal ground motion of the earthquakes

$$u_{earthquake(x,\omega)} = u(x) \cdot \exp(i\omega t) = u_o \exp(i\omega t) \tag{3.5}$$

The application of the seismic loading is depicted in the following figure:

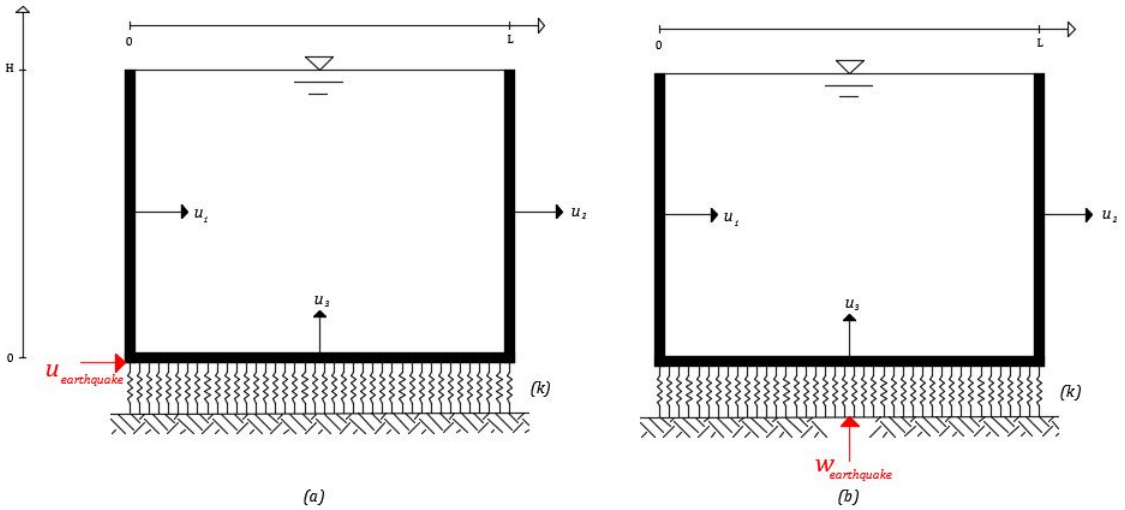

Figure 3.4: Seismic application in the structure. (a) Horizontal seismic loading. (b) Vertical seismic loading

From Figure 3.4, it can be seen that the horizontal and the vertical seismic loading are applied at the different level. This placement is due to the statement that the soil stiffness in the transverse direction is disregarded. Neglecting the soil spring in transverse direction also means neglecting the soil-structure interaction in the horizontal direction. In contrast to the horizontal loading, the application of the vertical loading is on the tip of the soil spring. This location indicates that the soil structure interaction is taken into account in the vertical direction.

3.2.2. SEISMIC ANALYSIS IN VERTICAL DIRECTION

The equation of motion of the structure can be divided into two substructures which are the walls and the plate. The first wall and second wall are indexed respectively (1) and (2). The plate is indexed (3) (Figure 3.1). The pressure of the liquid *acts on the normal surface* of the container. One can also state that the pressure exerts the force in the perpendicular direction to the surface. The positive direction of the liquid pressure is shown in the following figure:

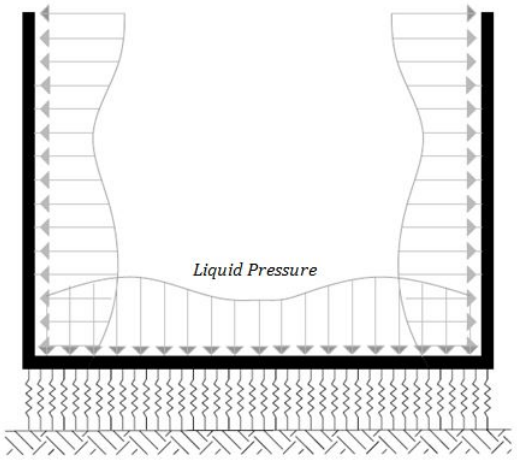

Figure 3.5: The positive direction of the liquid pressure

The governing equation (as given in the previous equattion 2.20) can be rewritten to:

WALL 1 EQUATION OF MOTION

$$E_w \cdot I_w \cdot \frac{\partial^4 u_{1(z,t)}}{\partial z^4} + \rho_s A_w \frac{\partial^2 u_{1(z,t)}}{\partial t^2} = -P_{liq(x=0,z,t)} \tag{3.6}$$

By substituting to equation 3.13, the solution can be expanded into the following equation:

$$E_w \cdot I_w \cdot \frac{\partial^4 u_{1(z,t)}}{\partial z^4} + \rho_s A_w \frac{\partial^2 u_{1(z,t)}}{\partial t^2} = -\rho_{liq}\left(\frac{\partial \phi_{(x=0,z,t)}}{\partial t}\right) \tag{3.7}$$

WALL 2 EQUATION OF MOTION

$$E_w \cdot I_w \cdot \frac{\partial^4 u_{2(z,t)}}{\partial z^4} + \rho_s A_w \frac{\partial^2 u_{2(z,t)}}{\partial t^2} = P_{liq(x=L,z,t)} \tag{3.8}$$

Within the similar steps, the equation of motion for the first wall can be expanded in the following manner:

$$E_w \cdot I_w \cdot \frac{\partial^4 u_{2(z,t)}}{\partial z^4} + \rho_s A_w \frac{\partial^2 u_{2(z,t)}}{\partial t^2} = \rho_{liq}\left(\frac{\partial \phi_{(x=0,z,t)}}{\partial t}\right) \tag{3.9}$$

PLATE EQUATION OF MOTION

Since the application of the earthquake loading is in the tip of the soil springs (see Figure 3.4), the equation results in the following:

$$E_p \cdot I_p \cdot \frac{\partial^4 u_{3(x,t)}}{\partial x^4} + \rho_s A_p \frac{\partial^2 u_{3(x,t)}}{\partial t^2} + k(u_{3(x,t)} - w_{earthquake(t)}) = -P_{liq(x,z=0,t)} \tag{3.10}$$

By substituting the pressure regarding potential flow, the plate equation result in the following:

$$E_p \cdot I_p \cdot \frac{\partial^4 u_{3(x,t)}}{\partial x^4} + \rho_s A_p \frac{\partial^2 u_{3(x,t)}}{\partial t^2} + k(u_{3(x,t)} - w_{earthquake(t)}) = -\rho_{liq}\left(\frac{\partial \phi_{(x,z=0,t)}}{\partial t}\right) \tag{3.11}$$

From previous subsection 2.3.3, it is known that the fourth order derivation will result into **four unknown constants**. In the case where there are three beams, the number of unknown constants is **twelve** (4×3).

LIQUID POTENTIAL FLOW

For the liquid equation motion, it can be referred to equation (2.43). However for this case, instead of using three directions, the potential flow is described in the two-dimensional plane. Therefore, the expressions are redefined as:

$$\frac{\partial^2 \phi_{(x,z,t)}}{\partial x^2} + \frac{\partial^2 \phi_{(x,z,t)}}{\partial z^2} = 0 \tag{3.12}$$

Pressure :

$$P_{liq(x,z,t)} = \left(\frac{\rho_{liq} \cdot \partial \phi_{(x,z,t)}}{\partial t}\right) + \rho_{liq} \times g(z - H) \tag{3.13}$$

Velocities:

$$\begin{aligned} V_{f,x(x,z,t)} &= -\frac{\partial \phi_{x,z,t}}{\partial x} \\ V_{f,z(x,z,t)} &= -\frac{\partial \phi_{x,z,t}}{\partial z} \end{aligned} \tag{3.14}$$

THE STRUCTURE BOUNDARY AND INTERFACE CONDITIONS

The boundary conditions and the interface conditions are divided into two terms. These two terms are *the internal structure boundary conditions and interface conditions* and *liquid-structure interaction boundary conditions*.These conditions are split into two forms which are kinematic and dynamic conditions. The kinematic conditions are related to motions such as displacement and rotation. Meanwhile, the dynamic condition is associated with the forces such as moment and shear forces. Boundary conditions include either kinematic part or dynamic part. Different with boundary conditions, interface conditions consist of both kinematic and dynamic conditions. In the above figure, the locations where the boundary conditions and interface conditions are explained:

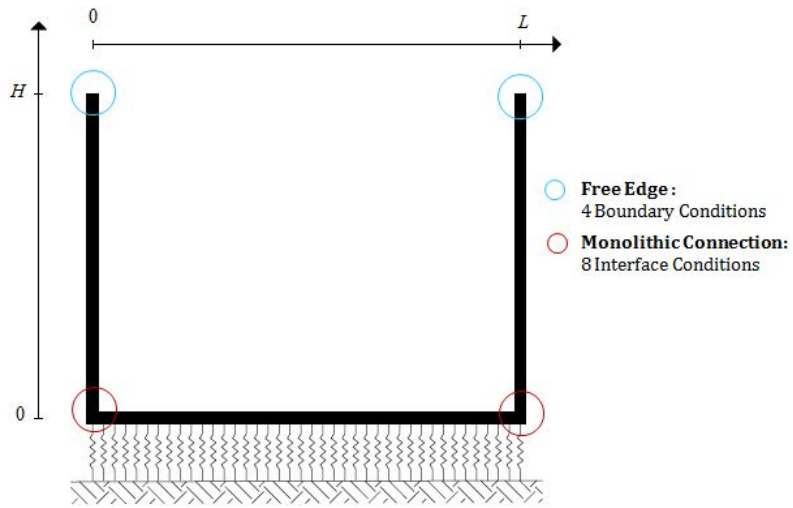

Figure 3.6: Boundary and interface conditions of the structure

The edges on top of the tank $z = H$ are **free edges** (see Figure 3.6), which implies that the first 4 boundary conditions for both walls are:

1. **Moment force of the wall 1 at** $z = H$**,** $(x = 0)$**:**

$$\frac{\partial^2 u_{1(z,t)}}{\partial z^2}\Big|_{z=H} = 0 \tag{3.15}$$

2. **Moment force of the wall 2 at** $z = H$**,** $(x = L)$**:**

$$\frac{\partial^2 u_{2(z,t)}}{\partial z^2}\Big|_{z=H} = 0 \tag{3.16}$$

3. **Shear force of the wall 1 at** $z = H$**,** $(x = 0)$**:**

$$\frac{\partial^3 u_{1(z,t)}}{\partial z^2}\Big|_{z=H} = 0 \tag{3.17}$$

4. **Shear force of the wall 1 at** $z = H$**,** $(x = L)$**:**

$$\frac{\partial^3 u_{2(z,t)}}{\partial z^2}\Big|_{z=H} = 0 \tag{3.18}$$

For the corners where the plate and the walls are meet, the connections are **monolithic**. The beam structures are inextensible for both plate and walls. The displacement of the first wall and the second wall are equal at $z = 0$ due to the in-extensibility of the plate. The assumption of inextensibility of the plate also determines how the shear forces act in the wall. One can understand that the movements of the two walls are included in the force equilibrium for the shear force. All in all, the interface conditions for monolithic connection are written in the following:

5. **Wall displacement due to the in-extensibility of the plate at** $z = 0$**,** $(x = 0, L)$**:**

$$u_{1(z=0,t)} = u_{2(z=0,t)} = 0 \tag{3.19}$$

6. **Shear force equilibrium due to the in-extensibility of the plate at** $z = 0$**,** $(x = 0, L)$**:**

$$\rho AH \frac{\partial^2 u_{1(z,t)}}{\partial t^2}\Big|_{z=0} = E_w \cdot I_w \cdot \Big(-\frac{\partial^3 u_{1(z,t)}}{\partial z^3} + \frac{\partial^3 u_{2(z,t)}}{\partial z^3} \Big)\Big|_{z=0} \tag{3.20}$$

7. **Rotation of the plate and the wall 1 at** $z = 0$**,** $(x = 0)$**:**

$$\frac{\partial u_{1(z,t)}}{\partial z}\Big|_{z=0} = -\frac{\partial u_{3(x,t)}}{\partial x}\Big|_{x=0} \tag{3.21}$$

8. **Rotation of the plate and the wall 2 at** $z = 0$**,** $x = L$**:**

$$\frac{\partial u_{2(z,t)}}{\partial z}\Big|_{z=0} = -\frac{\partial u_{3(x,t)}}{\partial x}\Big|_{x=L} \tag{3.22}$$

9. **Moment force of the plate and the wall 1 at** $z = 0$ **and** $x = L$**:**

$$E_w \cdot I_w \frac{\partial^2 u_{1(z,t)}}{\partial z^2}\Big|_{z=0} = E_p \cdot I_p \frac{\partial^2 u_{3(z,t)}}{\partial x^2}\Big|_{z=0} \tag{3.23}$$

10. **Moment force of the plate and the wall 2 at** $x = L$ **and** $z = 0$**:**

$$E_w \cdot I_w \frac{\partial^2 u_{2(z,t)}}{\partial z^2}\Big|_{z=0} = -E_p \cdot I_p \frac{\partial^2 u_{3(x,t)}}{\partial x^2}\Big|_{x=L} \tag{3.24}$$

Subsequently, the motion of the first wall as the rigid body in plane causes inertia force $\rho_w A_w \frac{\partial u_{(x=0,t)}}{\partial t}$ at the position of the connection with the plate. The same holds for $x = L$ which is to the second wall.

11. **Shear force of the plate at** $x = 0$**:**

$$\rho_w \cdot A_w \cdot H \frac{\partial^2 u_{3(x,t)}}{\partial t^2}\Big|_{x=0} = -E_w \cdot I_w \cdot \frac{\partial^3 u_{3(x=0,t)}}{\partial x^2}\Big|_{x=0} \tag{3.25}$$

12. **Shear force of the plate at** $x = L$**:**

$$\rho_w \cdot A_w \cdot H \frac{\partial^2 u_{3(x,t)}}{\partial t^2}\Big|_{x=L} = E_w \cdot I_w \cdot \frac{\partial^3 u_{3(x,t)}}{\partial x^2}\Big|_{x=L} \tag{3.26}$$

THE LIQUID-STRUCTURE INTERACTIONS

The structure and the liquid are coupled in the velocity equilibrium between these two components. The first kinematic condition is the equilibrium of the first wall velocity and of the liquid velocity in the x-direction at $x = 0$ along the height. Subsequently, this same principle applies on the second wall velocity and the liquid velocity. For the bottom plate, the velocity of the liquid in the z-direction at $z = 0$ equals to the plate velocity. Unlike pressure, the positive directions of the velocity are the Cartesian coordinates in Figure 3.1.

The last boundary condition is the free surface waves condition. This final condition is mostly neglected for static analysis which means the pressure at the liquid surface is equal to zero. In this case, the dynamic calculation is the key point in which the liquid surface can also be included in the equation. However the pressure that is exerted from the free surface condition is relatively small when is compared to the impulsive pressure on the wall, in some practices, it can be disregard once again to the equation. Nonetheless, this thesis will take the free surface condition into account. This following figure explains the kinematic boundary condition between the liquid and the structure:

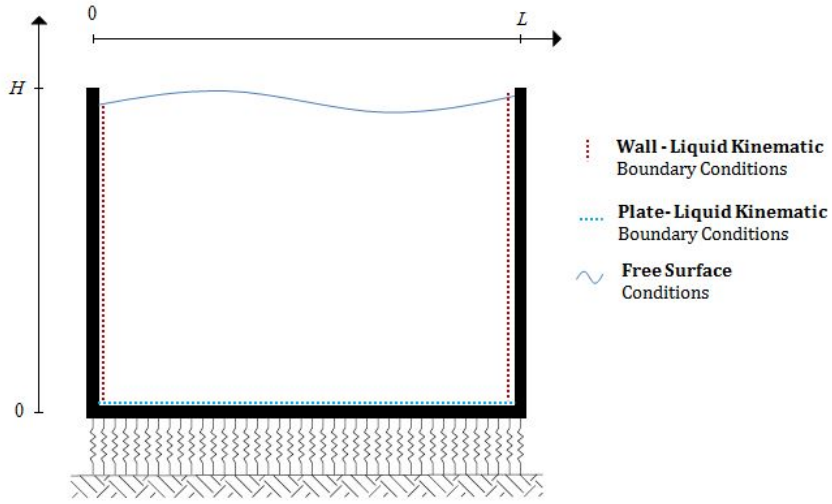

Figure 3.7: Kinematic boundary conditions of the structure with the liquid

From Figure 3.7, the kinematic boundary conditions can be defined as bellow:

1. **Wall 1 and liquid interaction at** $x = 0$:

$$\dot{u}_{1(z,t)} = -\frac{d\phi_{(x,z,t)}}{dx}\Big|_{x=0} \tag{3.27}$$

2. **Wall 2 and liquid interaction at** $x = L$:

$$\dot{u}_{(2(z,t)} = -\frac{d\phi_{(x,z,t)}}{dx}\Big|_{x=L} \tag{3.28}$$

3. **Plate and liquid interaction at** $z = 0$:

$$\dot{u}_{3(x,t)} = -\frac{d\phi_{(x,z,t)}}{dz}\Big|_{z=0} \tag{3.29}$$

4. **Free surface water at** $z = H$:

$$P = \rho \cdot g \cdot \eta(z,t) \quad \text{at } z = H \tag{3.30}$$

$$\frac{d^2\eta_{(z,t)}}{dt} = \frac{dv_{(z,t)}}{dt} \tag{3.31}$$

Therefore through the substitution, in term of velocity flow the calculation would result in the following:

$$-\frac{\rho}{\rho(g)}\frac{\partial^3\phi_{(x,z,t)}}{\partial t^3}\Big|_{z=H} = \frac{\partial^2\phi_{(x,z,t)}}{\partial z\partial t}\Big|_{z=H} \tag{3.32}$$

Through simplification, the equation for the free surface waves can be redefined into:

$$-\frac{1}{(g)}\frac{\partial^2\phi_{(x,z,t)}}{\partial t^2}\Big|_{z=H} = \frac{\partial\phi_{(x,z,t)}}{\partial z}\Big|_{z=H} \tag{3.33}$$

3.2.3. SEISMIC ANALYSIS IN HORIZONTAL DIRECTION

The difference between the horizontal and the vertical seismic analysis is found in the bottom plate equation of motion. Whereas the vertical and the horizontal earthquakes motion are orthogonal to each other, the vertical seismic movement vanishes in the plate equation of motion (see Figure 3.4). The vertical However, there is no change for the wall equation of motion. The explanation of the differences between the horizontal and vertical loading is written in Section 3.2.1.

PLATE EQUATION OF MOTION

$$E_p \cdot I_p \cdot \frac{\partial^4 u_{3(x,t)}}{\partial x^4} + \rho_s A_p \ddot{u}_{3(x,t)} + k(u_{3(x,t)}) = P_{liq(x,z=0,t)} \tag{3.34}$$

For the horizontal seismic loading, most of the boundary and interface conditions stay the same. However, only the boundary condition (5), is different. The change in this interface condition is due to on the wall deformation is input the seismic wave in the x-direction.

5. **Wall deformation due to the in-extensible plate at** $x = 0, L$ **and** $z = 0$ (see Figure 3.4):

$$u_{1(z=0,t)} = u_{2(z=0,t)} = u_{earthquake(t)} \tag{3.35}$$

3.3. SOLUTION IN FREQUENCY DOMAIN

Before entering the frequency domain, one can realize that the liquid load consists both dynamic and static pressure. In this thesis, the analysis of the static load cases are carried out separately from the dynamic equation. Subsequently, the static load is superimposed to the dynamic response to obtain the total response of the tank liquid system. This superimposed principle can only be applied based on the linear condition, and in case the static stress does not affect the dynamic stresses. Therefore the static and dynamic load can be analyzed separately. This explanation is depicted in the following diagram.

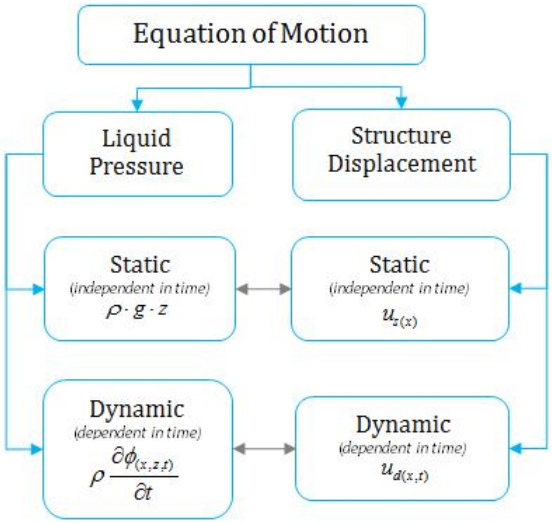

Figure 3.8: Separate analyzing between dynamic and static conditions

The main reason to analyze the response in the frequency domain is due to the simplicity of the analytic derivations. The method to convert from the time domain to the frequency domain is the Fourier transform. Nonetheless, the Fourier transform has its restriction which is neglecting the transient phase. The transient phase can be solved using the Laplace transform. However in this thesis, the Fourier transform is considered sufficient. As a consequence, this thesis only analyzes the steady-state and disregard the effect of transient phase.

In seismic loading, most of the data are recorded in the time domain. However, this condition is not a hindrance, as by using the inverse Fourier transform, time domain analysis can also be performed.

The damping inclusion allows the response to damps out through time along the disappearance of the seismic loading. The Fourier transform solution is given in the section 2.5.4. Specifically for this case the Fourier transform for both beam and the liquid are:

SOLUTION FOR BEAM EQUATION OF MOTION

$$u_{(x \text{ or } z,t)} = u_{s(x \text{ or } z)} + \frac{1}{2\pi}\int_{-\infty}^{\infty} \tilde{u}_{d(x \text{ or } z,t)} \exp(i\omega t) d\omega \tag{3.36}$$

SOLUTION FOR LIQUID EQUATION OF MOTION

$$\phi_{(x,z,t)} = \int_{-\infty}^{\infty} \frac{1}{2\pi} \tilde{\phi}_{(x,z,\omega)} \cdot \exp(i\omega t) d\omega \tag{3.37}$$

After the general solutions for the liquid and the beam are obtained, the solutions are substituted in the equation of motion and boundary conditions. These substitutions are fully derived in Appendix D.1.

3.4. LIQUID SUPERPOSITION

From the all the expressions in Appendix D.1.1, one can see that the liquid constants are unbalanced with the number of boundary conditions of the liquid. This implies that the kinematic liquid and structure boundary conditions are not enough to satisfy all the equations.

In order to solve such problem, the superposition method is introduced in this thesis. The superposition can only be applied if the liquid is irrotational. The irrotational liquid result to the $\nabla\phi = 0$, if the liquid is rotational where $\nabla\phi \neq 0$ the superposition cannot be applied. This explanation explains why assuming the liquid as irrotational is convenient for the analytical derivations. The figure below shows how the liquid is superpositioned:

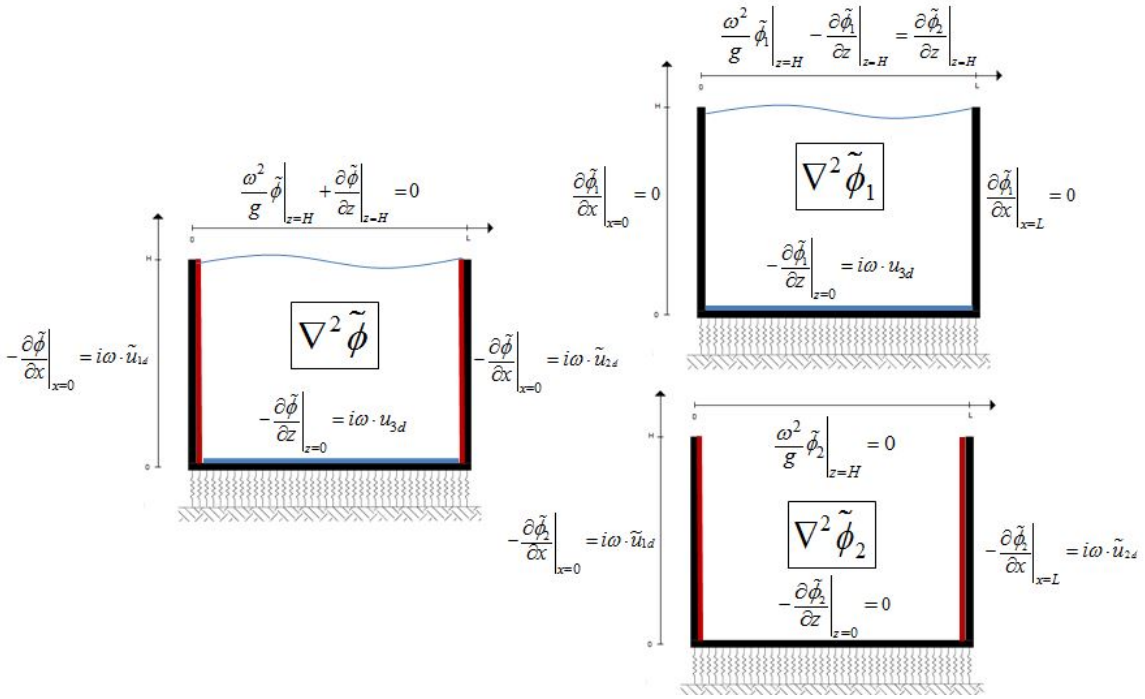

Figure 3.9: Superposition of the fluid potentials

From the figure above, one can see the similarity with what the Eurocode 8 defines (see Figure 2.19). However, in figure 2.19, the flexibility of the plate is neglected. The superposition of the two potentials can be formulated into the following equations:

$$\tilde{\phi}_{(x,z,\omega)} = \tilde{\phi}_{1(x,z,\omega)} + \tilde{\phi}_{2(x,z,\omega)} \tag{3.38}$$

The first potential is only considering the velocity in the z-direction which is the plate and the free surface condition. However, this potential regards the two walls are rigid. For the second potential is the other way around. This second component considers the velocity in the x-direction which is the two walls, yet regards the plate is stiff and no free surface waves can occur at the top. Each component of the liquid is dependent on both x and z-coordinates. The method of separation variable are used to solve the coupled variable which is described in the following expression of:

$$\tilde{\phi}_{(x,z,\omega)} = \tilde{\phi}_{x(x,\omega)} \times \tilde{\phi}_{z(z,\omega)} \tag{3.39}$$

In the appendix D section D.2 , the liquid derivation, the superposition and separation of variables methods are fully written down. The result are summarized in the following equations.

THE FIRST LIQUID POTENTIAL MODE

$$\tilde{\phi}_{1(x,z,\omega)} = \sum_{n=0}^{\infty} \left(C_{1n} \cdot \cosh\left(a_n \cdot z\right) + D_{1n} \sinh\left(a_n \cdot z\right)\right)\left(\cos\left(a_n \cdot x\right)\right)$$
$$a_n = \frac{n\pi}{L} \tag{3.40}$$

THE SECOND LIQUID POTENTIAL MODE

$$\tilde{\phi}_{2(x,z,\omega)} = \sum_{n=1}^{\infty} \left(A_{2n} \cdot \cosh\left(b_n \cdot x\right) + B_{2n} \cdot \sinh\left(b_n \cdot x\right)\right) \cos\left(b_n \cdot z\right)$$
$$b_n = \frac{\pi \cdot (2n-1)}{2H} \tag{3.41}$$

The fundamental mode for the second liquid potential starts at the wave number of $\pi/2$ which result to the n starts from one for the summation instead of 0.

THE TOTAL LIQUID POTENTIAL MODE

$$\tilde{\phi}_{(x,z,\omega)} = \sum_{n=0}^{\infty} \left(C_{1n} \cdot \cosh\left(a_n \cdot z\right) + D_{1n} \sinh\left(a_n \cdot z\right)\right)\left(\cos\left(a_n \cdot x\right)\right) + \sum_{n=1}^{\infty} \left(A_{2n} \cdot \cosh\left(b_n \cdot x\right) + B_{2n} \cdot \sinh\left(b_n \cdot x\right)\right) \cos\left(b_n \cdot z\right) \tag{3.42}$$

In principle the index n in a_n can be chosen differently from the index n in b_n for example a_n and b_m. However here it is assumed that summation can be merged in the same n order.

3.5. ALTERNATIVE SOLUTION FOR LIQUID SUPERPOSITION

Another method to derive the liquid superposition is by separating the liquid into three parts instead of two. In this procedure, the free surface waves are separated from the plate kinematic boundary condition. The alternative superposition of the potential liquid is depicted as the following figure:

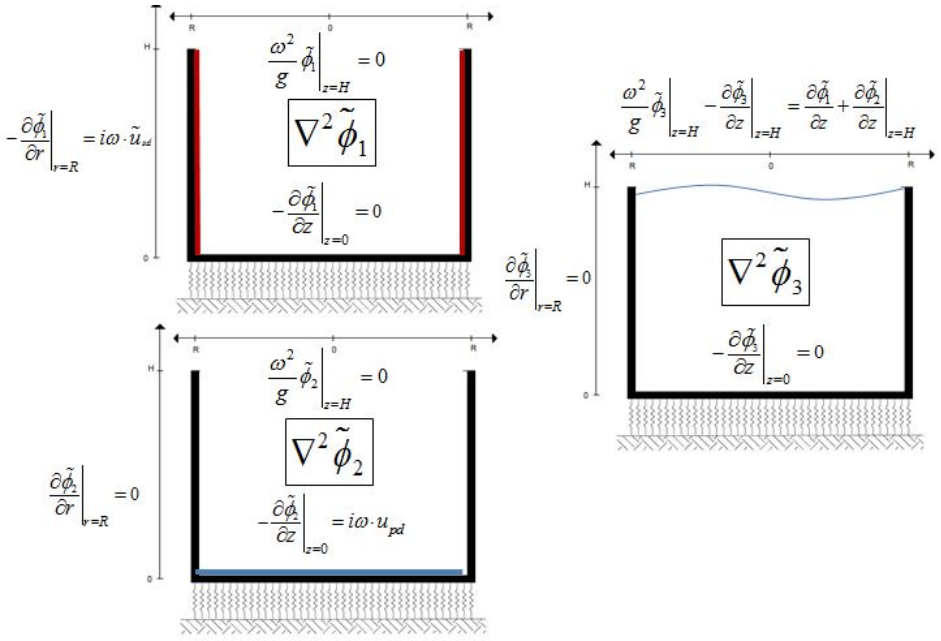

Figure 3.10: Alternative superposition of the fluid potentials

From the above figure, the potential flow can be written as:

$$\tilde{\phi}_{(x,z,\omega)} = \tilde{\phi}_{1(x,z,\omega)} + \tilde{\phi}_{2(x,z,\omega)} + \tilde{\phi}_{3(x,z,\omega)} \tag{3.43}$$

The references such as [5] and [18] separate the sloshing mode completely from the structure boundary conditions. Therefore, using this three superposition method is much easier when comparing the different components with the other journals. For the two superposition method the plate potential is coupled to the sloshing mode. However, for this method the sloshing mode is totally decoupled with the other potentials (compare Figure 3.10 and Figure 3.9).

3.6. MATCHING MODES MODAL ANALYSIS

From the equations of motion and structure-liquid kinematic boundary condition, one could understand that the structure mode and the liquid equations of motion are completely coupled. The method of matching modes is used to solve the coupled equations. The matching modes is used also by *Bauer and Siekmann* in their journals [4],[14]. This method is an analytical method since it utilizes the orthogonality principle in dynamics.

Nonetheless, this principle has its disadvantage. It can be considered as a weak form since it uses integration form. Therefore the convergence check (see Figure 3.36) is needed to satisfy the boundary condition in every exact point. For the first trial, the modes that will be analyzed are the first **six modes**. The convergence determines, whether using the six modes is enough to fulfill the exact boundary condition in every point.

From the Flowchart in Figure 3.2, one can learn that before matching the modes-shapes, liquid and structure shape functions have to be calculated first. The liquid shape functions are obtained from equations 3.42. Meanwhile, the structure shape function is obtained from *structure eigenvalue analysis*. The general solution of the liquid and structure equation can be written as the following:

$$\begin{aligned} \tilde{\phi}_{(x,z,\omega)} &= \sum_{n=1}^{\infty} \tilde{\phi}_{n(x,z,\omega)} \\ \tilde{u}_{(x,z,\omega)} &= \sum_{k=1}^{\infty} \tilde{u}_{k(x,z,\omega)} \end{aligned} \tag{3.44}$$

The solution of the structure can be written in the expanded form:

$$\tilde{u}_{(\bar{x},\omega)} = \sum_{k=1}^{\infty} U_k \times X_{k(\bar{x})} \tag{3.45}$$

The newly redefined $\bar{x}$ here is the argument of the mode shape $X_{k(\bar{x})}$, a generalized coordinate which along the length of the beam. Where the U_k is the amplitude and X_k is the mode shapes are used as the shape function. The modes consist of both axis-symmetric modes and asymmetric modes.

The calculation of the structure shape function is based on *structural homogeneous equations*. This means that the earthquake loading is not yet included to the equations. Based on the reference [21], the earthquake loading can be coupled to the rigid body translation. The inertial term is related to the total displacement (see equation 2.17). Meanwhile the stiffness term is related to the relative displacement. Therefore the total displacement of the structure can be written as the following list.

THE FIRST WALL

$$\underbrace{\tilde{u}_{1(z,\omega)\text{total}}}_{\text{Total Displacement}} = \underbrace{\sum_{k=1}^{\infty} U_k \times X_{1k(z)}}_{\text{Relative Displacement}} + u_{earthquake} \tag{3.46}$$

THE SECOND WALL

$$\underbrace{\tilde{u}_{2(z,\omega)\text{total}}}_{\text{Total Displacement}} = \underbrace{\sum_{k=1}^{\infty} U_k \times X_{2k(z)}}_{\text{Relative Displacement}} + u_{earthquake} \tag{3.47}$$

THE PLATE

$$\underbrace{\tilde{u}_{3(z,\omega)\text{total}}}_{\text{Total Displacement}} = \underbrace{\sum_{k=1}^{\infty} U_k \times X_{3k(z)}}_{\text{Relative Displacement}} + w_{earthquake} \tag{3.48}$$

As the whole structure is considered as a single system, the number of unknowns from the equation is only one, which is the value of the amplitude. A point to remember that the orthogonality is only when the full path is integrated as described in the following:

$$\int_0^H X^1_{k(z)} \times X^1_{j(z)}\, dz + \int_0^L X^3_{k(x)} \times X^3_{j(x)}\, dx + \int_0^H X^2_{k(z)} \times X^2_{j(z)}\, dz = \Gamma \times \delta_{kj} \tag{3.49}$$

The symbol δ_{kj} is the Kronecker delta. After obtaining the shape function, these solutions (equation 3.46 to 3.48) are substituted into the equation where the structure and the liquid are coupled. These equations are the kinematic boundary conditions between liquid and the structure and also the equation of motions.

As the internal structural boundary conditions are already fulfilled via the mode shape, there is no need to substitute the shape function to the inner structure boundary condition. Solving the orthogonality will be continued in the Appendix D at the section D.3. From the equations that are described there, a matrix operation can be derived. The matrix is composed with the equations.

$$\underline{\underline{\mathbf{A}}} \times \begin{bmatrix} C_{1\mathrm{n}} \\ D_{1\mathrm{n}} \\ A_{2\mathrm{n}} \\ B_{2\mathrm{n}} \\ U_k \end{bmatrix} = \underline{\mathbf{B}} \tag{3.50}$$

The matrix $\underline{\underline{\mathbf{A}}}$ is a population of both orthogonal part and non-orthogonal part. The matrix size will be $[4 \cdot n + 1 \cdot k] \times [4 \cdot n + 1 \cdot k]$. The system of equations can be solved by using linear algebra.

3.7. RESULTS

In order to achieve the results, the basic properties are set as the following values in the table below. The tank are modeled as a concrete tank with the length of 20 m and the height of 15 m.

Table 3.1: Model Properties

Properties	Value	Unit
Length (L)	20	m
Height (H)	15	m
Wall Thickness (h_w)	0.5	m
Plate Thickness (h_p)	0.5	m
Wall Young's Modulus (E_w)	30000	MPa
Plate Young's Modulus (E_p)	30000	MPa
Soil Stiffness (k)	50000	kN/m2
Structural Density (ρ_s)	2.5	ton/m3
Liquid Density (ρ_w)	1.0	ton/m3
Earthquake Acceleration (a_e)	1.0	m/s2
Frequency Independent Damping (c)	0.001	

From the Section 2.1.3, one already knows that most of the time the earthquakes are recorded in terms of acceleration. Therefore with Fourier transform, the acceleration can be expressed in the following form:

$$\begin{aligned} \tilde{a}_e &= (i \cdot \omega)^2 \cdot u_e \\ u_e &= -\frac{1}{\omega^2} \end{aligned} \tag{3.51}$$

In the calculation, prestressing and the static loads are not included in the dynamic calculation since it has been separated before in the previous Section 3.3. The prestress calculation could eliminate the static pressure. From the definition, it can be concluded that there is no initial stress in the dynamic calculation.

3.7.1. FREQUENCY RANGE

The natural frequency is divided into 3 ranges which are:

1. **The Low Frequency Range** 0.09-1.0 Hz
2. **The Medium Frequency Range** 1.0-5.0 Hz
3. **The High Frequency Range** 5.0-24 Hz

In reality, the earthquake hardly ever exceed frequencies of 3 to 4 Hz [17]. Meanwhile the number of 0.09 Hz, comes from the lowest frequency that can be ever record in the practice. Lower than 0.09 Hz, the record still has a significant amount of disturbances from white noise such as wind and other vibrations [17]. The high frequency value is taken, due to the need to include the sixth excitation as it has been discussed earlier that the number of modes that will be used is six.

3.7.2. EMPTY TANK

From the calculation of empty tank mode-shapes, the system has both asymmetric modes and axis-symmetric modes. These mode shapes are shown in the following figure:

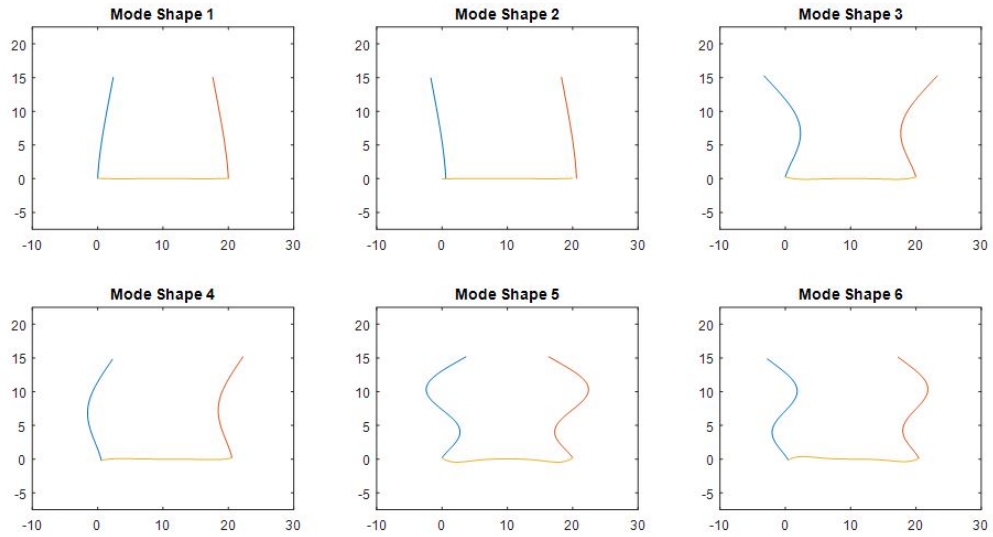

Figure 3.11: The mode shape of the empty tank]

These mode shapes are excited in the following frequencies :

f_1 (Hz)	f_2 (Hz)	f_3 (Hz)	f_4 (Hz)	f_5 (Hz)	f_6 (Hz)
0.981	1.265	6.336	6.880	19.995	20.753

Depends on the direction of the force, different type of modes are excited. For instance, axis-symmetric force dominantly resonates the axis-symmetric frequency. Meanwhile, for asymmetric loading, it dominantly resonates asymmetric modes. However, the frequency of the system stays the same regardless what direction of the external load that acts in the tank. The reference point for empty tank displacement response is located at $x = 0$ and $z = H$. This coordinate is picked due to the maximum values are occurred in this particular location. The following figure depicts the location of the referred point (*the red point*):

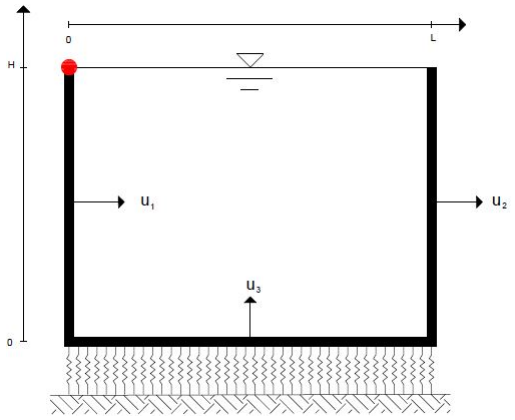

Figure 3.12: Location of the referred point

The excitation of the empty tank response in both x and z seismic direction is shown in the subsequently plotted graph.

HORIZONTAL SEISMIC LOADING

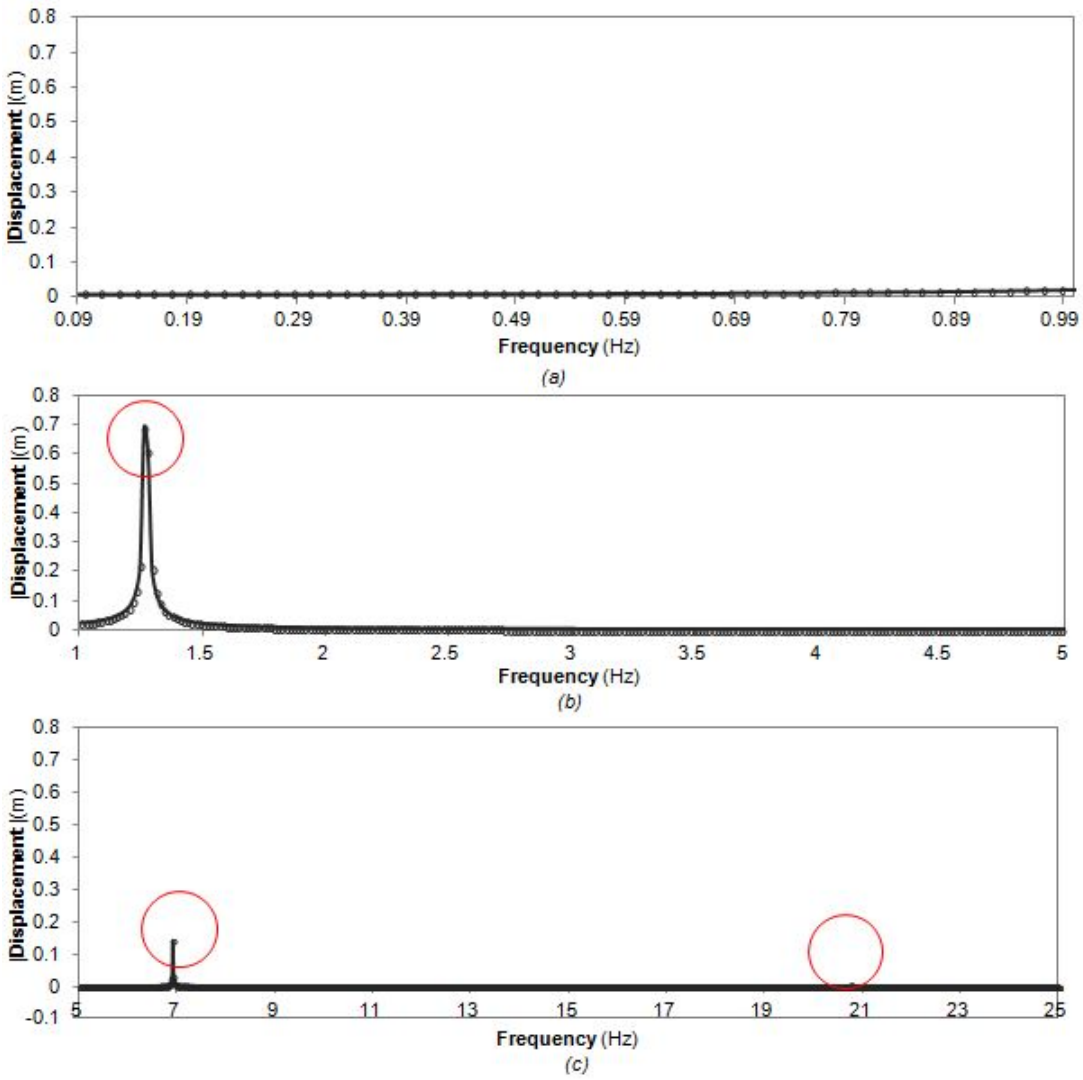

Figure 3.13: Frequency response in term of deformation for empty tank under seismic loading in horizontal direction: (a) low frequency range;(b) medium frequency range ;(c) high frequency range

VERTICAL SEISMIC LOADING

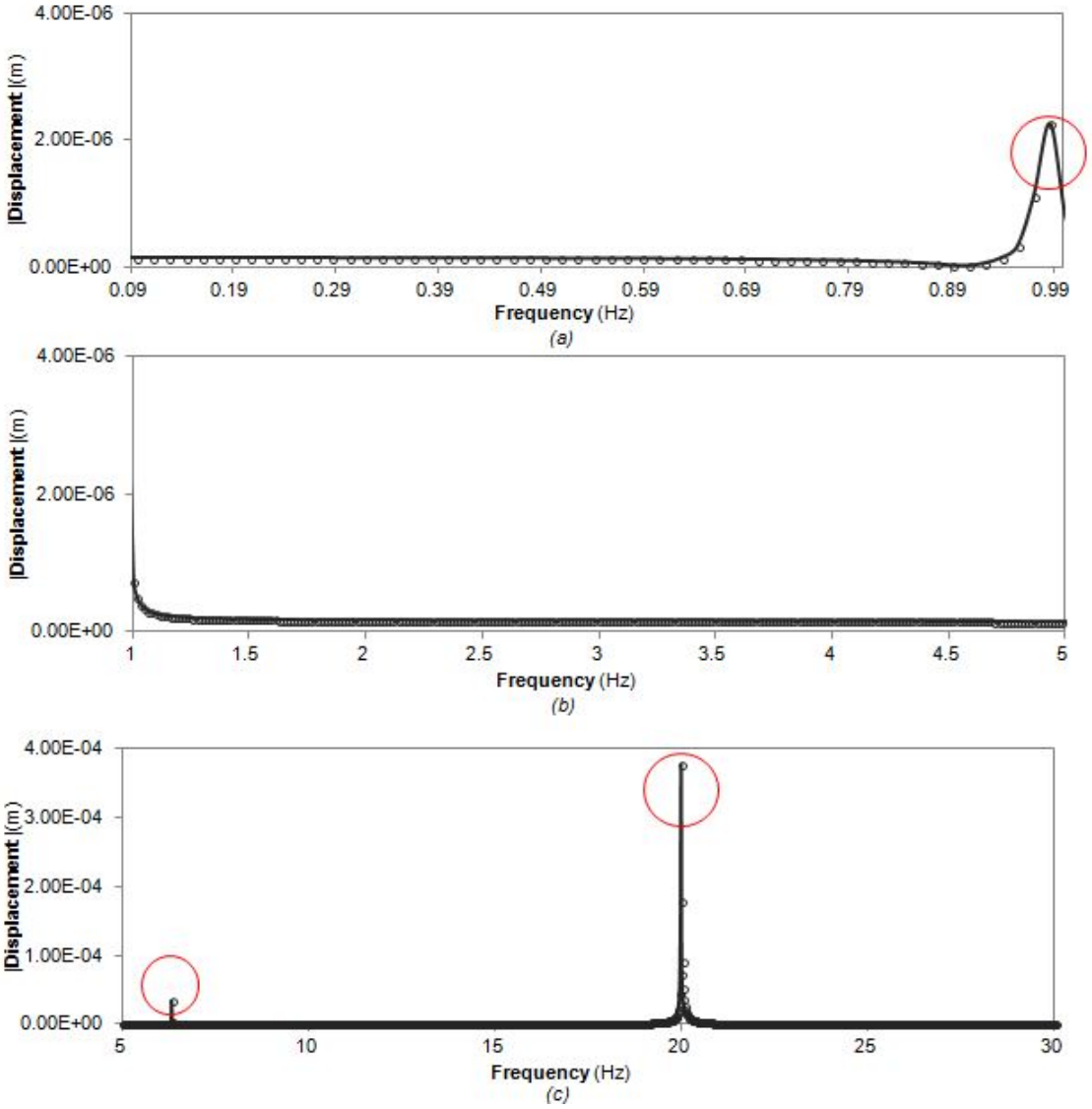

Figure 3.14: Frequency response in term of deformation for empty tank under seismic loading in vertical direction: (a) low frequency range;(b) medium frequency range ;(c) high frequency range

In the subsequent table, it is shown the dominant excitation of empty tank's natural frequency depends on different direction of earthquake loading:

Table 3.2: Empty tank seismic loading in horizontal and vertical directions, natural frequency excitation

Frequency	Seismic loading in X	Seismic loading in Z
f_1 (Hz)	1.257	0.981
f_2 (Hz)	6.876	6.88
f_3 (Hz)	20.74	19.99

CONCLUSION

From the figures above, one can see that the seismic in horizontal direction excites dominantly asymmetric modes. Seismic in vertical direction excites the axisymmetric modes. However, the empty tank has the same natural frequencies which are the 6 frequencies regardless the direction of the loading. This result is due to external load does not have any influence on satisfying the determinant of the matrix equals to zero.

3.7.3. STATIC PRESSURE

From the previous Section 3.2.2, the pressure in a static fluid is derived from the weight of the fluid. The expression is written in the following:

$$P = \rho_{liq} \times g \times (z - H) \tag{3.52}$$

In this expression, we can see that the pressure varies with height. In the static load case, the free surface elevation is equals to zero. This condition results in zero pressure on the surface level ($z = H$). The static pressure is depicted in the following graph:

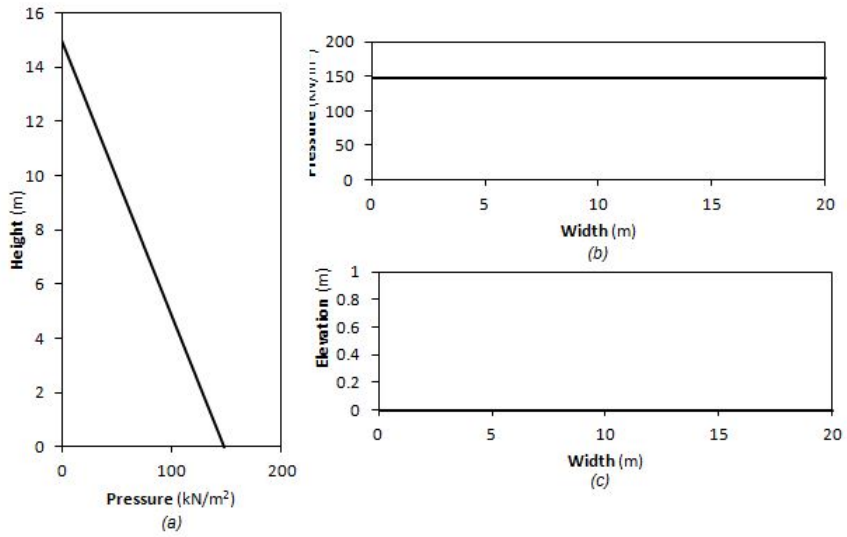

Figure 3.15: Static pressure: (a) wall static pressure; (b) static pressure at z=0; (c) free surface elevation at z=H

3.7.4. HYDRODYNAMIC PRESSURE RESPONSE

The point of reference to plot the pressure response is located at $z = 0$. This location is chosen due to most of the maximum values are located in the that point. The location will be shown in the following figure:

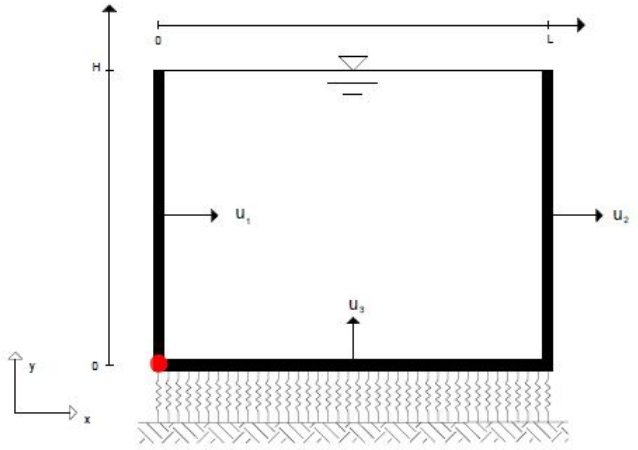

Figure 3.16: Location of the referred point for response pressure plotting

In the following table and graphics, the resonance peak frequencies can be identified:

Table 3.3: Resonance peak frequencies under loading in vertical and horizontal directions

Model	$f_s(Hz)$	$f_1(Hz)$	$f_2(Hz)$	$f_3(Hz)$
Seismic Loading X	0.19	0.87	3.504	13.98
Seismic Loading Z	-	0.492	3.21	12.78

HORIZONTAL SEISMIC LOADING

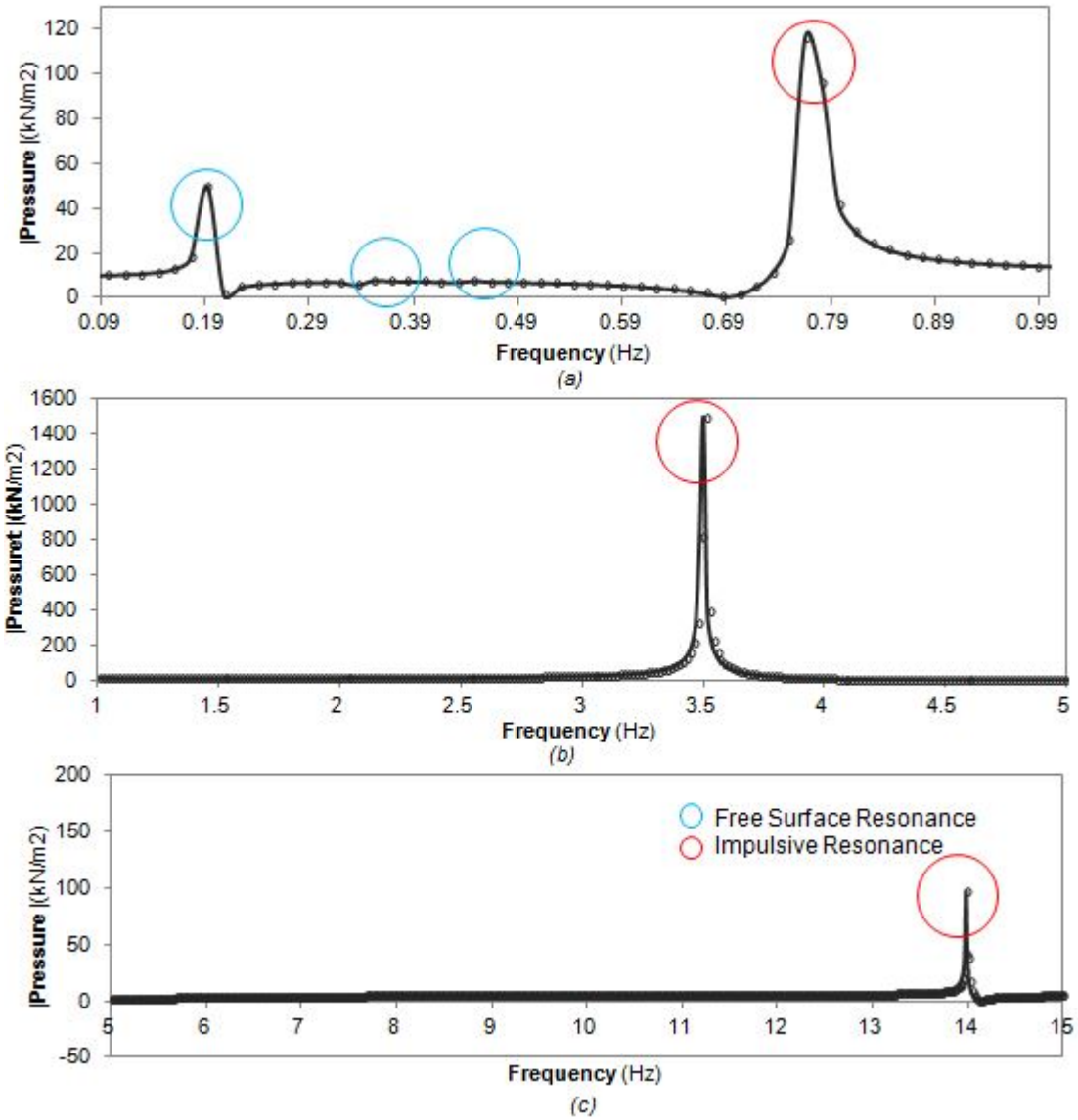

Figure 3.17: Frequency response in term of pressure under seismic loading in horizontal direction: (a) low frequency range;(b) medium frequency range ;(c) high frequency range

VERTICAL SEISMIC LOADING

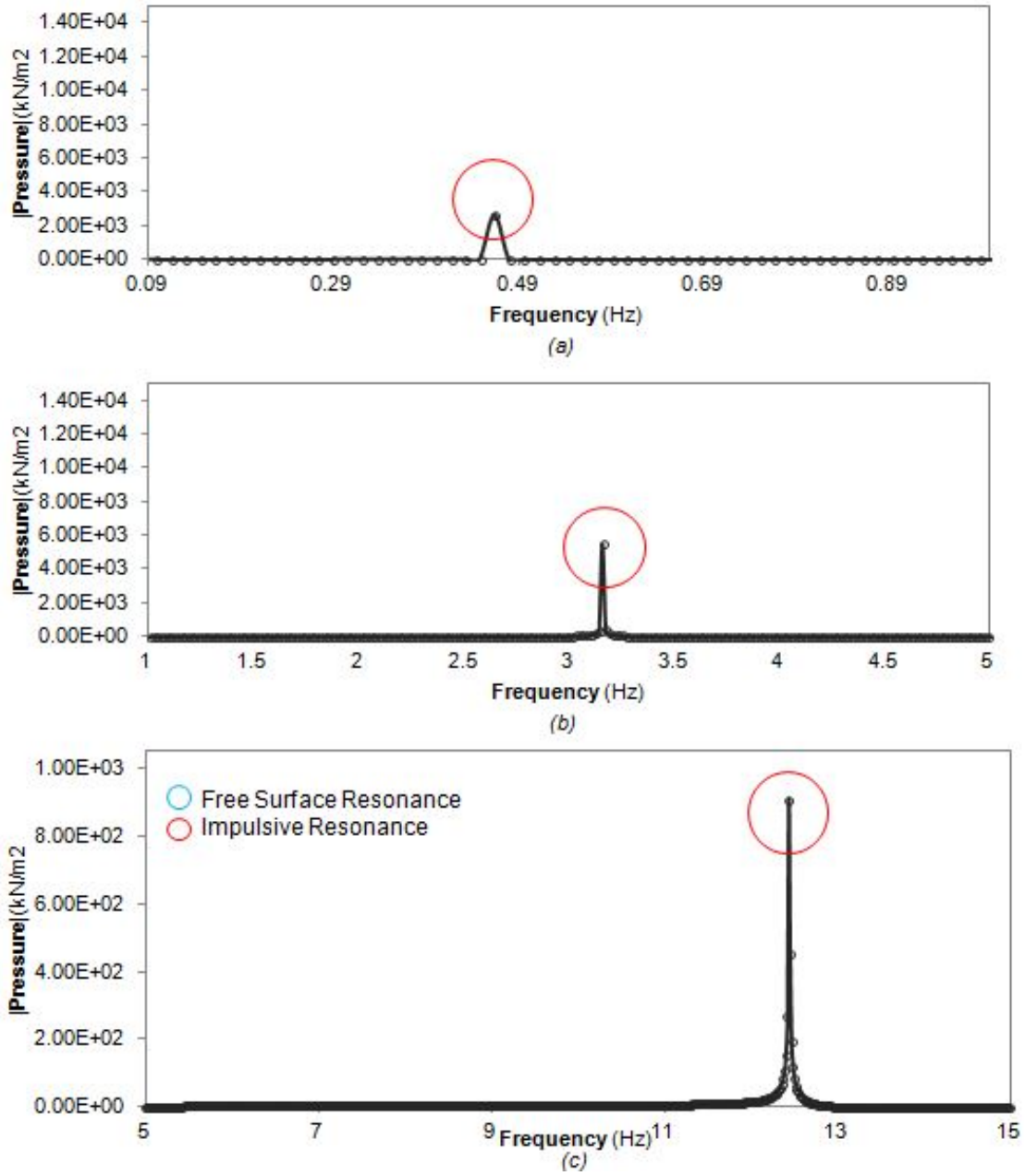

Figure 3.18: Frequency response in term of pressure under seismic loading in vertical direction:
(a) low frequency range;(b) medium frequency range ;(c) high frequency range

CONCLUSION

From the plotted graph, one can see that the natural frequencies of the filled tank are 60% *lower on average* than the empty tank. The declining natural frequency is due to added mass which is derived from the pressure. The added mass concept is later explained in the Section 3.10. Based on the simple discrete model which Housner has derived, it is known that the bigger the mass the lower the natural frequency it becomes since from the simple frequency derivation:

$$\omega = \sqrt{K/m} \tag{3.53}$$

For the structure and liquid interaction, the structure stiffness does not change. The dynamic mass changes, as the liquid and the structure are coupled entirely. From the plotted graphs above, there are other additional

peaks due to the free surface wave frequencies.

For the vertical seismic loading, we can see that there are no peak resonance for the sloshing frequency. Why there is no sloshing frequency in the vertical loading is can be seen in the mathematical derivation. It is more straightforward for this concept, if we consider the derivation in the alternative three superpositions for rigid case. Since we know that the axisymmetric and asymmetric mode shapes is orthogonal the calculation can be totaly seperated. The liquid axisymmetric shape function is under the index of 0. The axisymmetric potential is written in the following:

$$\begin{aligned} \tilde{\phi}_{10} &= C_{l0}(z-H) && \textit{The plate coupled potential} \\ \tilde{\phi}_{20} &= 0 && \textit{The wall coupled potential} \\ \tilde{\phi}_{30} &= B_{l0} && \textit{The sloshing potential} \end{aligned} \tag{3.54}$$

If we analyze the sloshing potential separately from the other two potentials, likewise in journals [18], [8], therefore the sloshing boundary condition can be written as follows:

$$\begin{aligned} \frac{\omega^2}{g}\tilde{\phi_{30}}\Big|_{z=H} &= \frac{\partial\tilde{\phi}_{30}}{\partial z}\Big|_{z=H} \\ \frac{\omega^2}{g}B_{l0} &= 0 \\ \omega &= 0 \end{aligned} \tag{3.55}$$

To solve the trivial solution for the equation above the ω should be zero. If the frequency range shifted and started from zero, we would find the resonance peak of the sloshing frequency.

3.7.5. HYDRODYNAMIC PRESSURE

In journals [18],[7] and Eurocode [5], the impulsive and convective pressure is always assigned with the worst case combination. This combination is the convective pressure has the same direction as the impulsive pressure which results to a higher pressure. This way of calculating pressure will result in a more conservative design. Meanwhile physically this combination will not always be accurate since in some frequencies both pressures might have different signs. This difference in sign can be seen in the following Figure 3.20. The different sign in convective pressure will result in a negative pressure in $z = H$, creating a smaller pressure throughout the height compared to the conservative pressure.This explanation is depicted in the following figure:

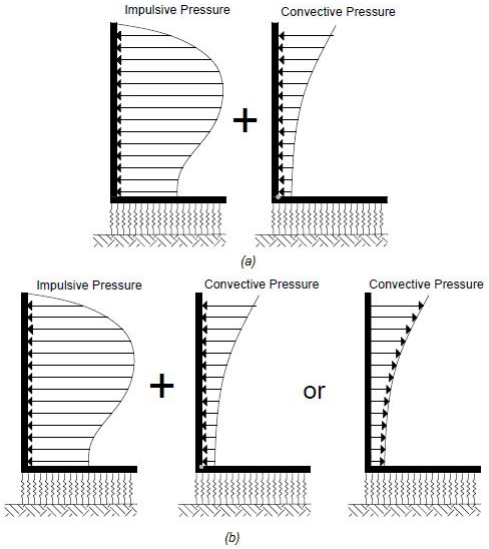

Figure 3.19: Conservative vs actual hydrodynamic pressure: (a) conservative total pressure; (b) actual total pressure

The actual pressure can also be written as follows:

$$P_{\text{conservative total pressure}} = \sqrt{p_i^2 + p_c^2} \tag{3.56}$$

HORIZONTAL SEISMIC DIRECTION

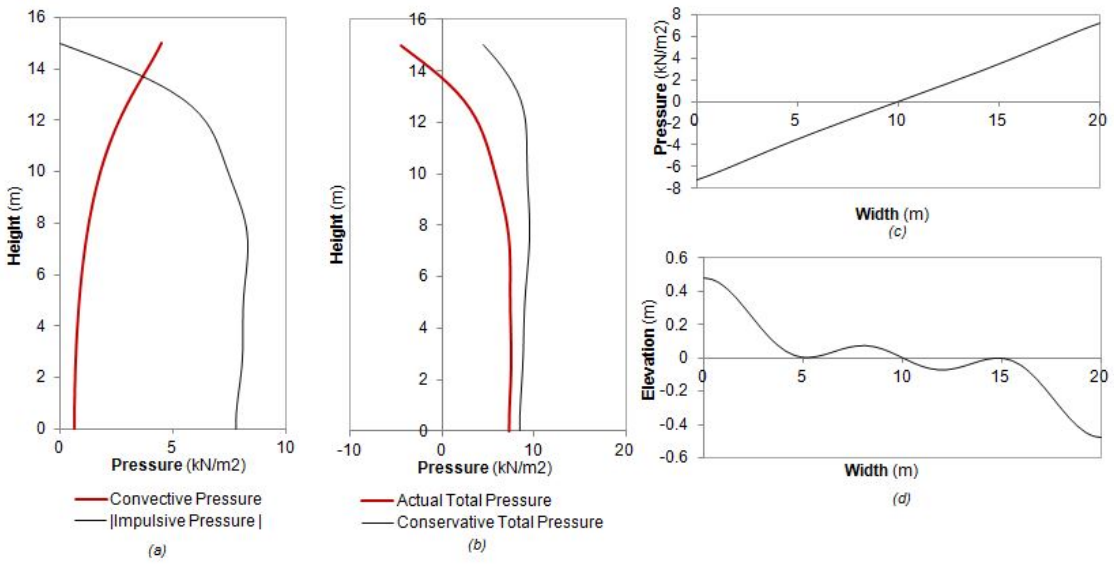

Figure 3.20: Pressure and free surface elevation seismic loading in x direction at 0.318 Hz:
(a) convective and impulsive pressure; (b) conservative and actual pressure;
(c) plate pressure; (d) free surface elevation

From the above figures, one can learn that the conservative pressure is always bigger than the actual pressure. However since one already understand the difference between the two pressures now, the next plotted graphs are the actual pressure instead of the conservative one.

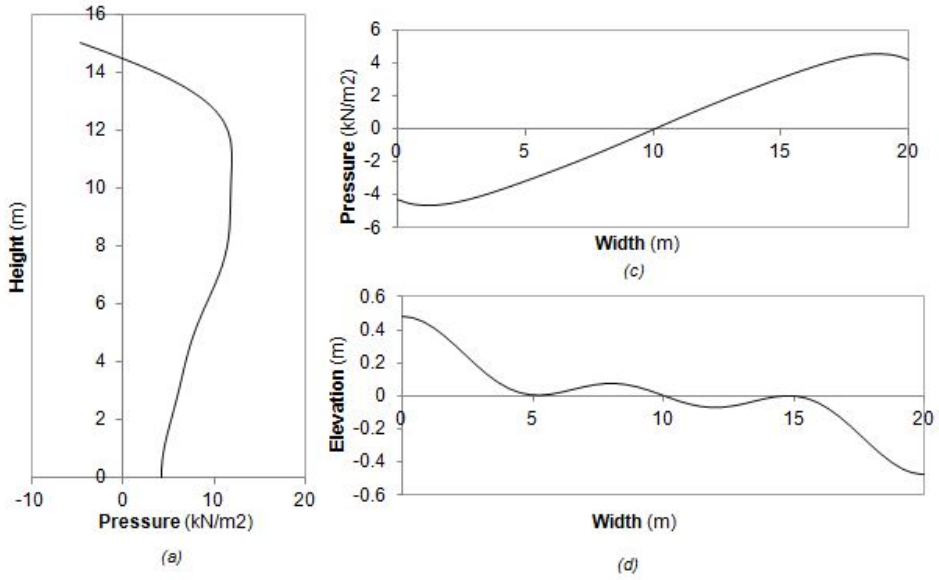

Figure 3.21: Pressure and free surface elevation seismic loading in x direction at 0.955Hz:
(a) wall pressure; (b) plate pressure; (c) free surface elevation

VERTICAL SEISMIC DIRECTION

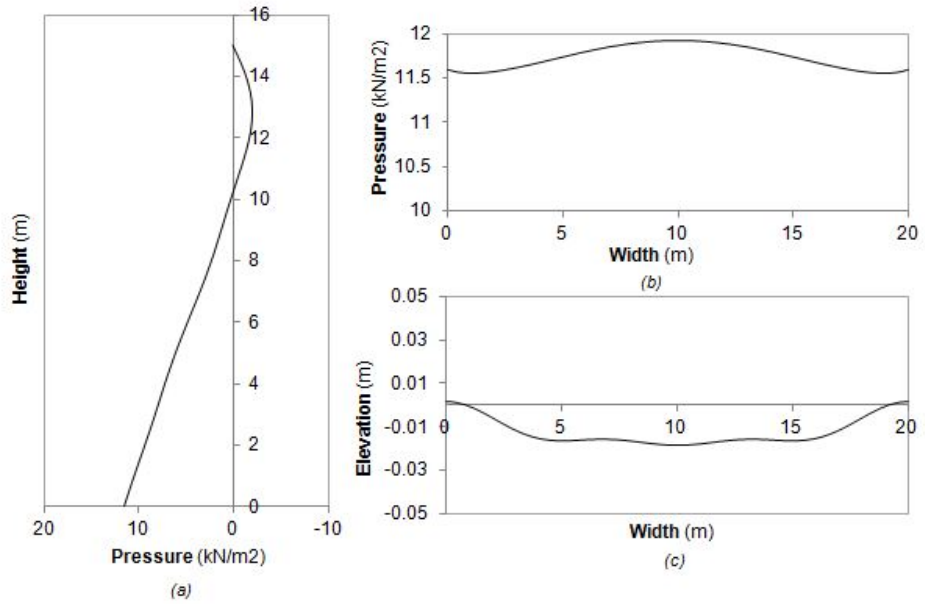

Figure 3.22: Pressure and free surface Elevation seismic loading in z direction at 1.431 Hz:
(a) wall pressure; (b) plate pressure; (c) free surface elevation

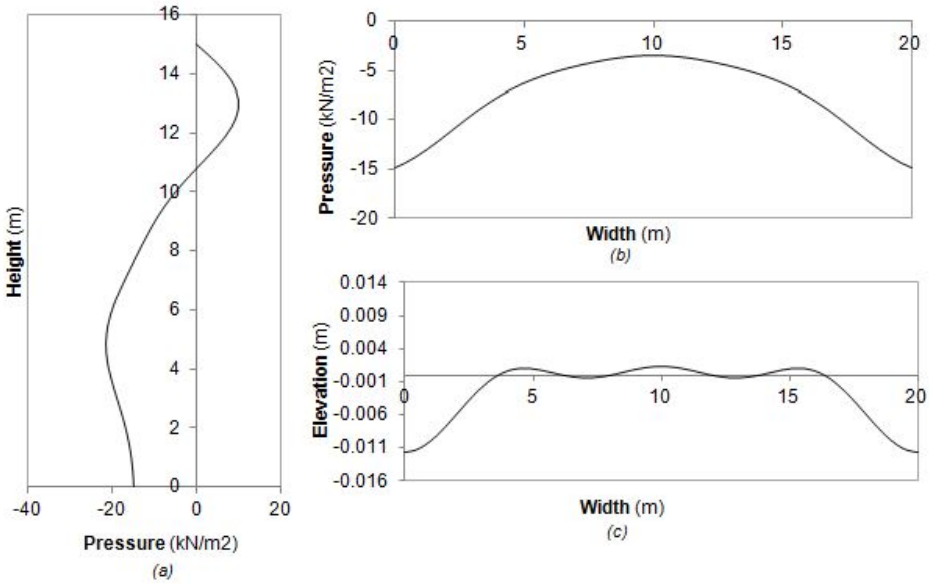

Figure 3.23: Pressure and free surface elevation seismic loading in z direction at 3.425 Hz:
(a) wall pressure; (b) plate pressure; (c) free surface elevation

CONCLUSION

For the seismic loading in the x-direction, the pressure in the first wall is the opposite sign to the other wall. This opposite sign is due to in the beginning in this thesis it is first defined that the pressure is in the normal direction of the structure surface (see Figure 3.5). Horizontal earthquakes loading in the positive x-axis resulting the first wall has a suction pressure which is the negative sign of pressure. Meanwhile, the other wall has a positive sign due to compression. For the vertical seismic loading, the pressure signs are different from the horizontal seismic loading. Since the load is axis-symmetric, the response would also be axis-symmetric. Both the walls have the same sign, either compression or suction pressure in the walls. However, this is not the case if the phase difference is included. If the phase difference is included, the load would not be axis-symmetric any longer.

From the above figures, one can see that the pressure of the vertical loading might be higher than the horizontal loading. However, in most cases, the horizontal loading have a higher effect on the structure due to the overturning moment that it caused. For the vertical loading, the moment due to the hydrodynamic pressure in the first wall is eliminated by the second wall. Nonetheless, the overturning moment for the horizontal load is the summation of both walls due to the same signs. The explanation of the overturning moment can be clearly seen in the following figure:

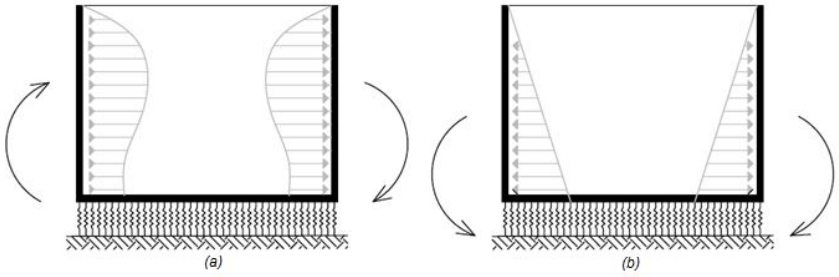

Figure 3.24: Overturning Pressure (a) Horizontal Loading (b) Vertical Loading

From the figures, one can see that the lower the frequency, the higher the significance of the free surface pressure to the total pressure. This due to the sloshing frequency is located in the low-frequency range. The other reason of this phenomenon in this calculation only six modes that is included for the sloshing. Therefore the higher frequency of the sloshing motion is also neglected. Since the total pressure consists of the summation between the impulsive and the convective pressure, hence the free surface pressure will be more significant in the pressure in low-frequency excitation.

According to the journal [8], the convective pressure is small and sometimes neglected for vertical seismic loading. From this statement, we can relate with what we have for the pressure seismic loading vertical direction. The wall pressure at $z = H$ is nearly zero due to small convective pressure.

3.8. PARAMETER STUDY

In this subsection, a parameter study is performed. However since the two-dimensional model is not the main model of this thesis, the purpose of the parameter study in this model is to grasp the understanding of the liquid and the structure interaction. This parameter study will only include a smaller scope and more through parameter study is performed in the three-dimensional model. This sensitivity study consist of changing the following parameters:

- Liquid Precentage
- Flexibility of the structure

3.8.1. LIQUID PERCENTAGE

Through service life, the liquid volume always changes. It can be either empty or half filled or even a completely filled tank. The effect of the liquid volume percentage can be seen in the natural frequency, response plotted graph and also the liquid pressure. This sensitivity study purpose is knowing how the volume of the liquid take influence with a constant geometry and stiffness of the structure to the whole system. In the next figure will be depicted the result for the parameter study in the liquid percentage. The point of reference for plotting the frequency response function in term of pressure is located in Figure 3.16. In the following figures, the frequency response function in term of pressure are plotted:

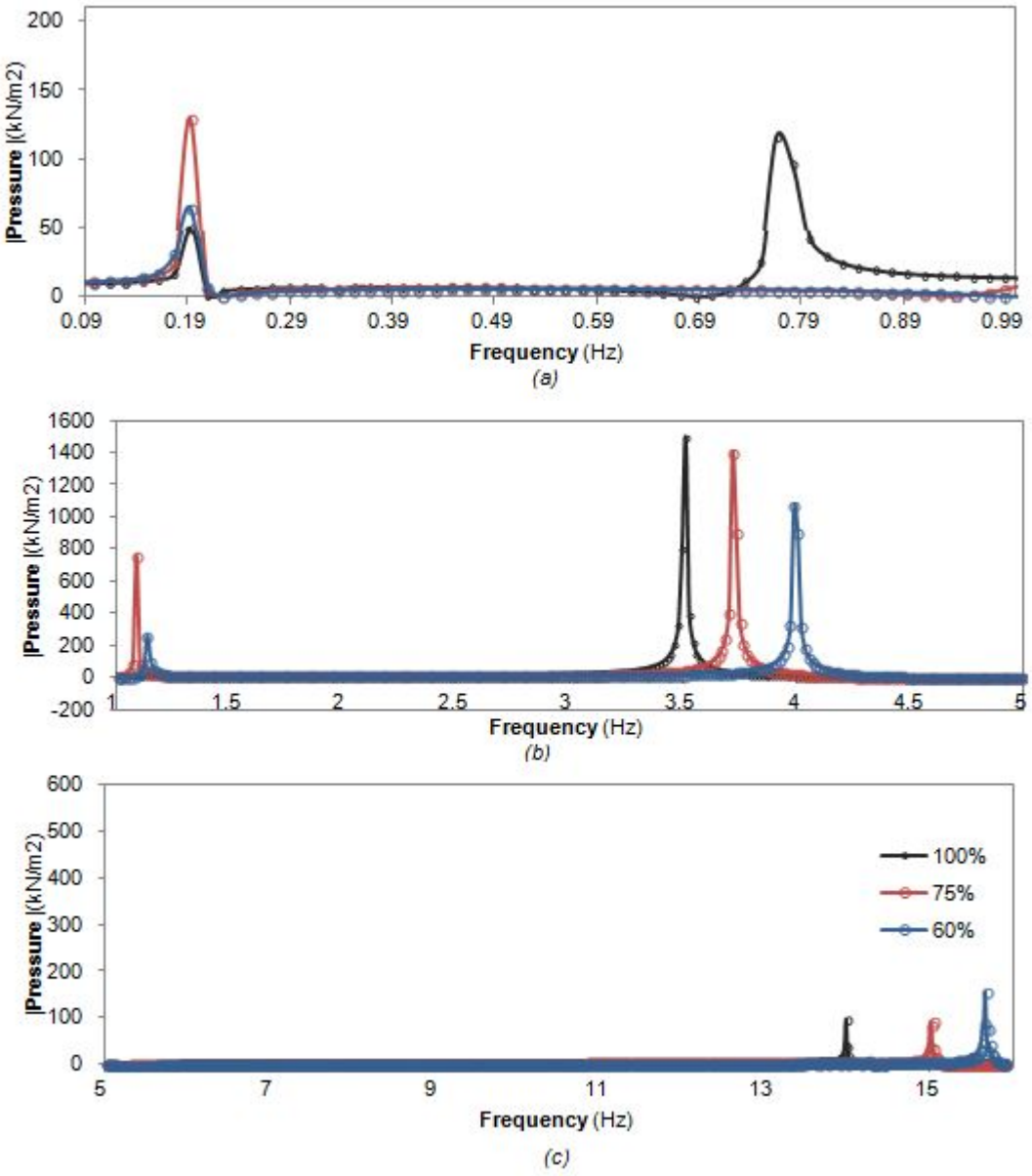

Figure 3.25: Frequency response in term of pressure for different liquid volume under seismic loading in horizontal direction: (a) low frequency range;(b) medium frequency range ;(c) high frequency range

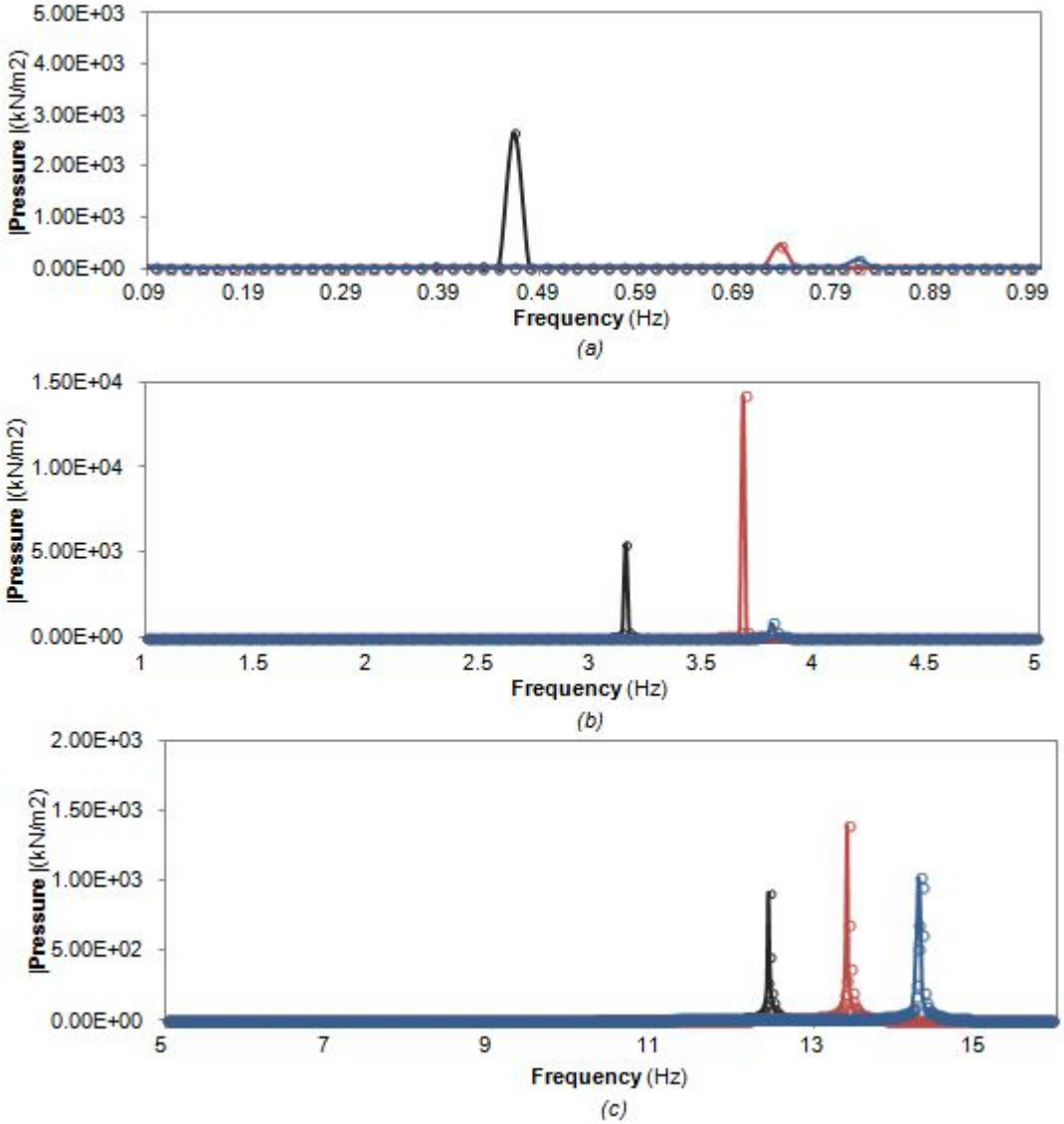

Figure 3.26: Frequency response in term of pressure for different liquid volume under seismic loading in vertical direction: (a) low frequency range;(b) medium frequency range ;(c) high frequency range

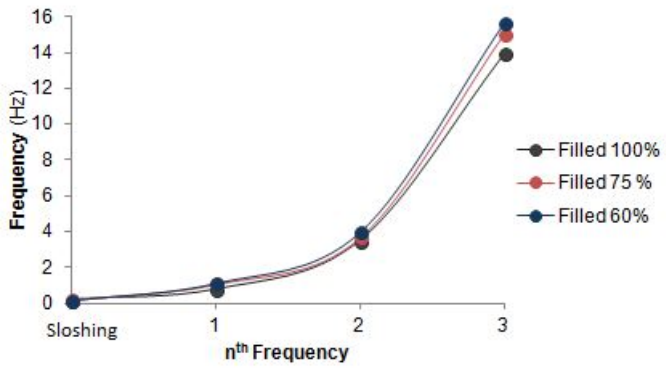

Figure 3.27: Change of frequencies in the different liquid volume for Seismic loading in X direction

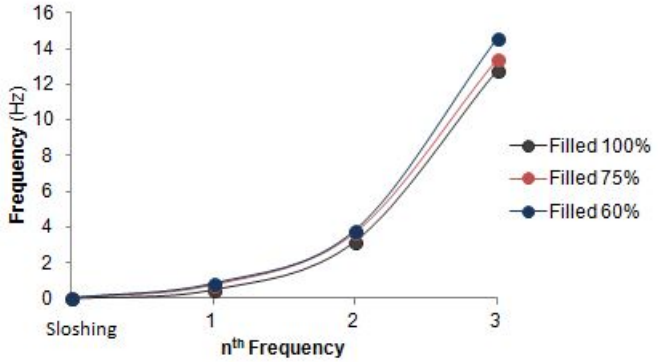

Figure 3.28: Change of frequencies in the different liquid volume for Seismic loading in Z direction

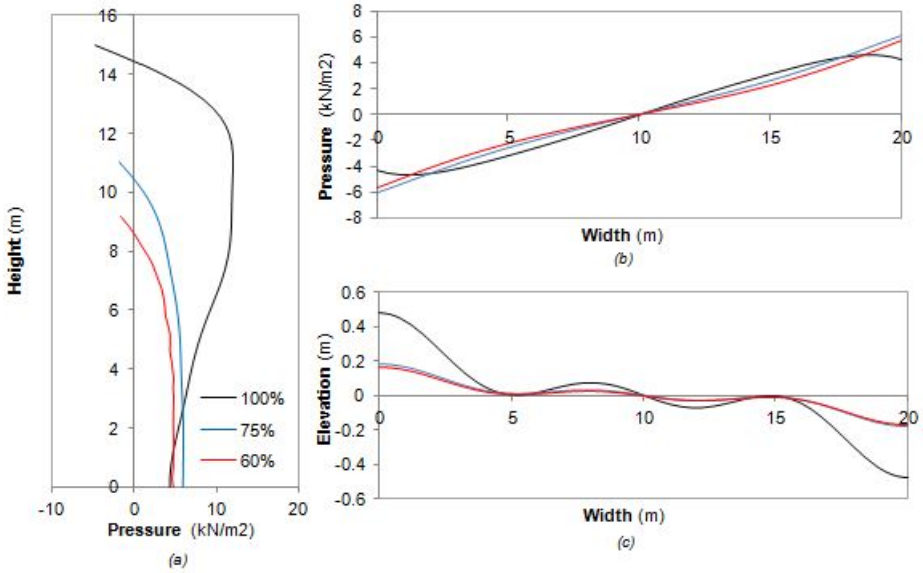

Figure 3.29: Wall Pressure for Liquid Volume Percentage Seismic Loading in x Direction at frequency 0.59 Hz:
(a) Wall Pressure (b) Plate Pressure (c) Free Surface Elevation

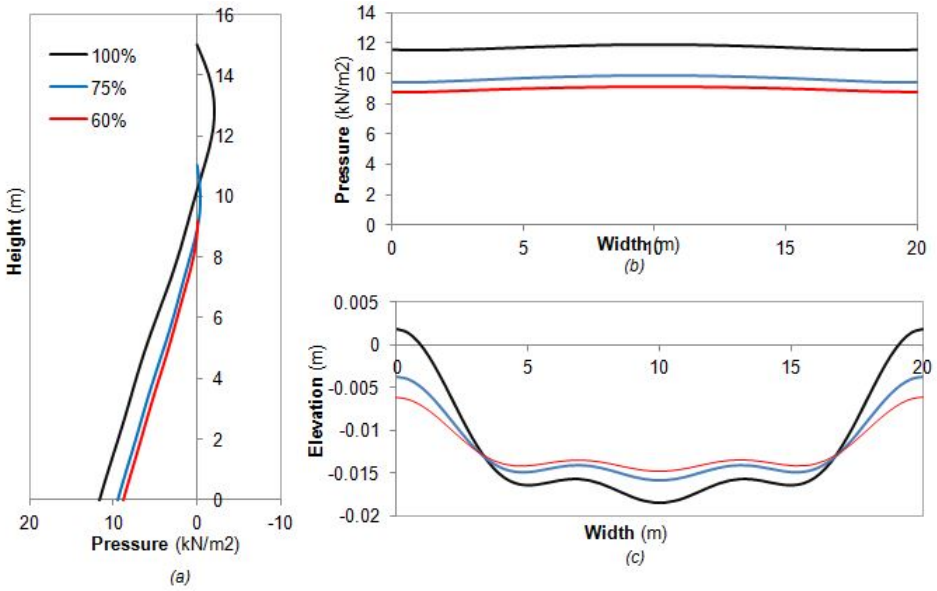

Figure 3.30: Wall Pressure for Liquid Volume Percentage Seismic Loading in z Direction at frequency 1.43 Hz: (a) Wall Pressure (b) Plate Pressure (c) Free Surface Elevation

Table 3.4: Resonance Peak Seismic excitation in X and Z direction

Model	$f_s(Hz)$	$f_1(Hz)$	$f_2(Hz)$	$f_3(Hz)$
Seismic Loading X				
100%	0.195	0.765	3.50	13.98
75%	0.180	1.07	3.63	15.00
60%	0.177	1.1320	3.982	15.669
Seismic Loading Z				
100%	-	0.492	3.21	12.78
75%	-	0.73	3.68	13.41
60%	-	0.81	3.81	14.58

CONCLUSION

We can see that the frequencies are gradually increasing as the liquid percentage in the tank is decreasing. The more significant the liquid volume in the total system, the higher reduction in the natural frequencies. The reason behind this phenomenon is the more filled the tank, the higher pressure it has. This higher pressure induces greater additional mass in the system. This relation is also explained in the next subsection's equation 3.59. Therefore, it would result to lower natural frequencies.

There is also a change in the sloshing frequencies for horizontal direction. The sloshing frequencies are decreasing as the liquid height is reduced. In a rigid tank frequency that is derived by Housner in the equation of 2.52. The frequency is in the term of tanh. This hyperbolic function characteristic is shown in the behavior of the decreasing sloshing natural frequencies for both rigid and flexible structure.

The third conclusion that we can derive from the result is the change in the pressure. In general, the pressure in the wall is decreasing along the reduction of the liquid volume. For both directions of the seismic loading, the pressure in the wall behaves more rigid when the liquid volume is smaller. This is a logical pattern since the mass of the liquid is decreasing. Therefore the peak resonance of the structure is shifted to the right-hand side. This shifting frequency cause that in the frequency, the fundamental mode have not excited yet for 75% and 60% liquid filled tank.

Regardless the direction of the seismic loading, the free surface elevation is decreasing as the liquid percentage decrease.

3.8.2. STRUCTURE FLEXIBILITY

In this subsection is discussed the effect of specific element's flexibility. Most of the simplified calculations for liquid filled tank disregard the plate stiffness or even the wall stiffness (Reference: [7], [18]). Therefore in this section is discussed whether each element's stiffness plays a significant role in the whole system. In order to obtain infinite rigidity, in the program the stiffness are multiplied by 1000. By multiplying with such high value, we can numerically approach the infinite rigidity. The following response of different structure flexibility can be seen in the following:

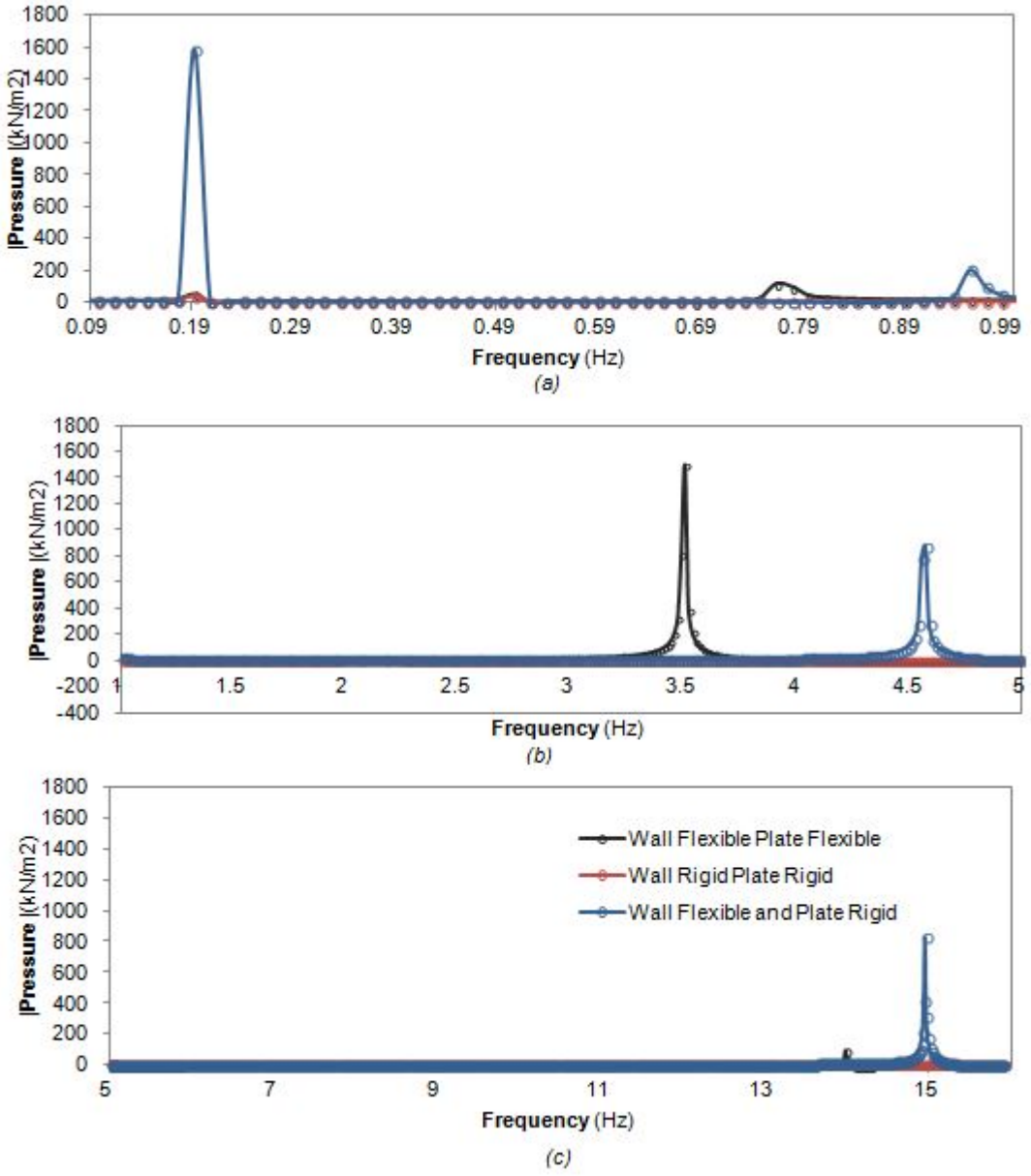

Figure 3.31: Frequency response in term of pressure for different flexibility under seismic loading in horizontal direction: (a) low frequency range;(b) medium frequency range ;(c) high frequency range

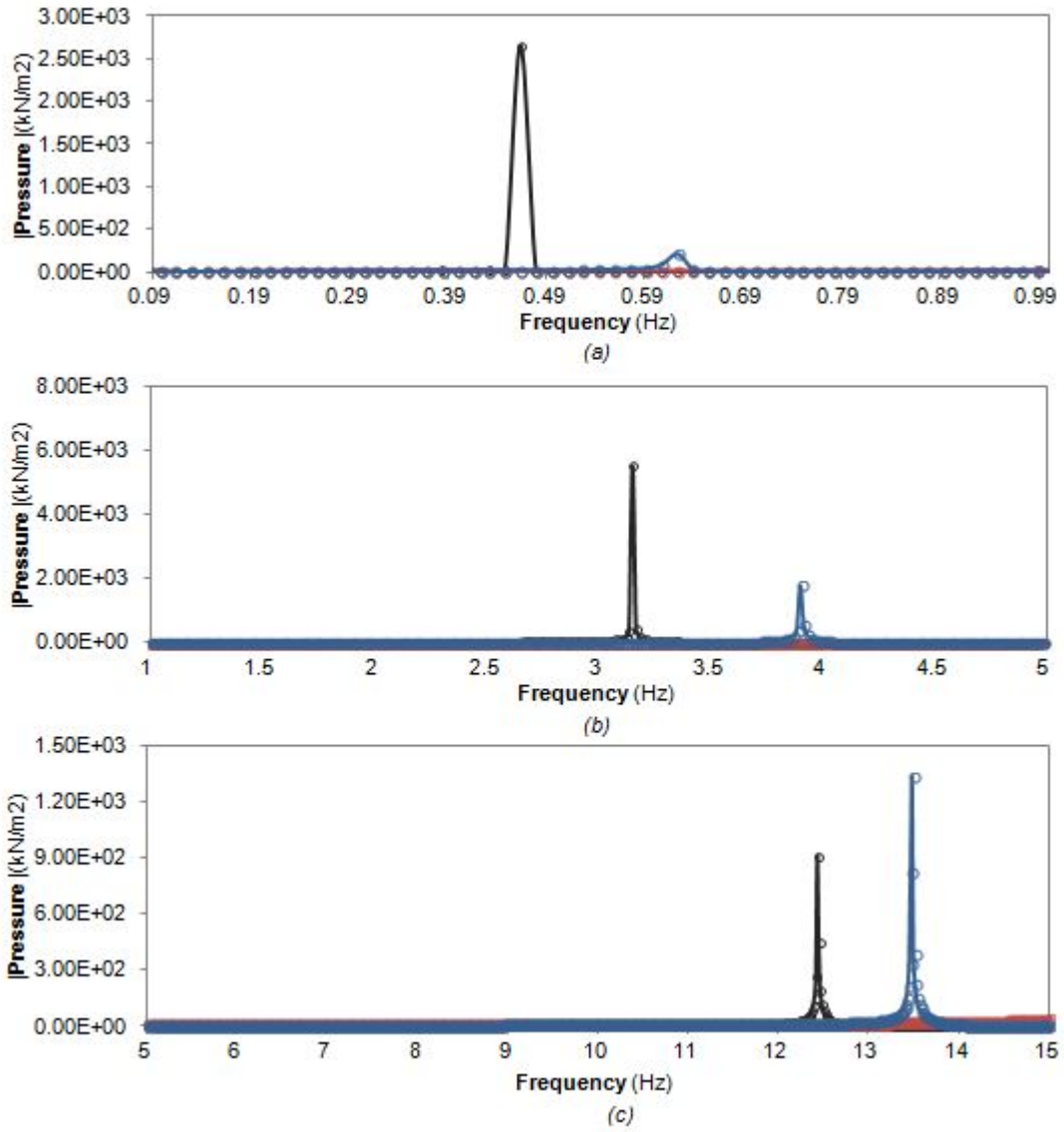

Figure 3.32: Frequency response in term of pressure for different liquid volume under seismic loading in vertical direction: (a) low frequency range;(b) medium frequency range ;(c) high frequency range

Table 3.5: Resonance peak under seismic excitation in horizontal and vertical direction with different types flexibility

Model	$f_s(Hz)$	$f_1(Hz)$	$f_2(Hz)$	$f_3(Hz)$
Seismic Loading X				
Flexible Wall- Flexible Plate	0.272	0.463	3.154	12.437
Rigid Wall- Rigid Plate	0.272	-	-	-
Flexible Wall- Rigid Plate	0.272	0.622	3.918	13.488
Seismic Loading Z				
Flexible Wall- Flexible Plate	-	0.4632	3.1543	12.437
Rigid Wall- Rigid Plate	-	-	-	-
Flexible Wall- Rigid Plate	-	0.622	3.92	13.489

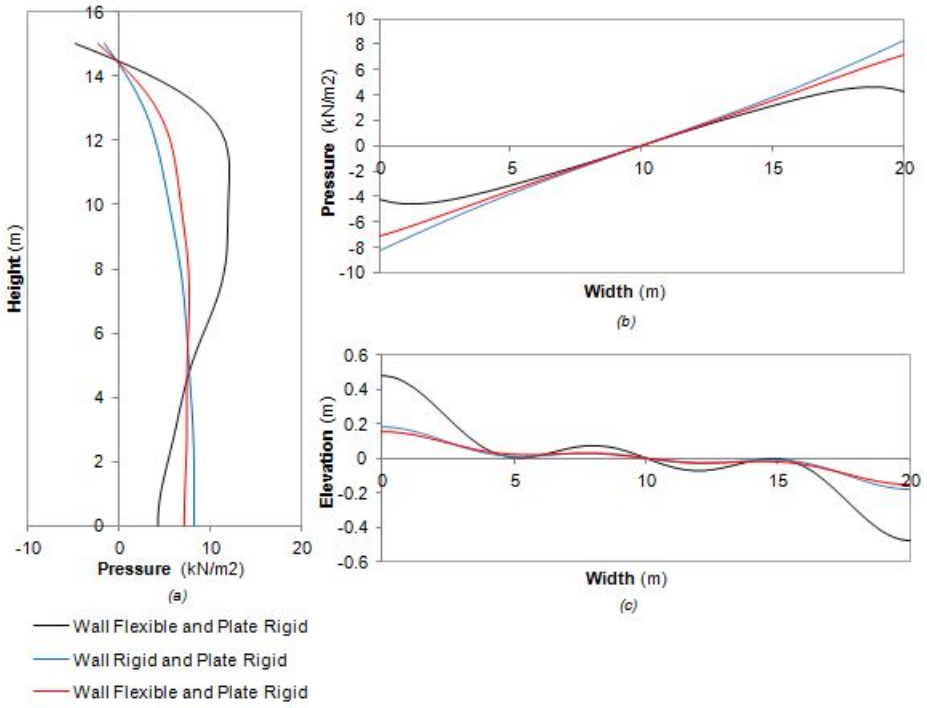

Figure 3.33: Pressure and free surface elevation for different Flexibility Seismic Loading in x Direction at frequency 0.3847 Hz: (a) wall pressure; (b) plate pressure; (d) free surface elevation

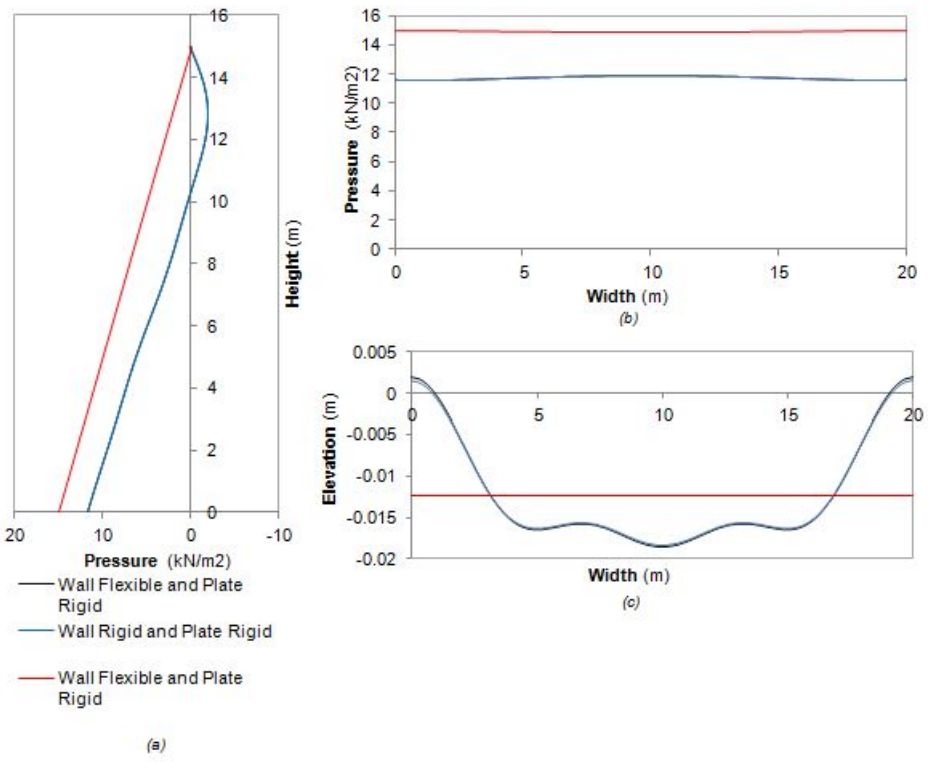

Figure 3.34: Pressure and free surface elevation for different Flexibility Seismic Loading in z Direction at frequency 1.43 Hz: (a) wall pressure; (b) plate pressure; (d) free surface elevation

CONCLUSION

In general, the natural frequency of both vertical and horizontal loading increases as the flexibility increases. This result is expected from the general equation to obtain frequency, equation 2.12. From the plotted response, one can see that the rigid structure results to a constant pressure and independent from the frequency. There is also no change or only small change for the sloshing natural frequency. This because of the sloshing is mainly depended on the geometry, not with the flexibility. This small dependency of the sloshing natural frequency with the flexibility is the main reason why most of the journal simplified by neglecting flexibility effect in the sloshing frequency.

Flexibility of the plate and the wall influence the free surface elevation and the pressure. It is essential to understand that using the assumption of the rigid wall and rigid plate might underestimate or even overestimate the pressure of the liquid and free surface elevation. Since the flexibility also plays an important role in amplifying the structure velocity, therefore the pressure that exerted in the might be higher compared to the rigid structures.

3.9. MODEL VALIDATION

Model verification is essential to assure whether the model is correct. In the two-dimensional model case, the model verification is performed in three main subjects which are the empty tank frequency, the pressure calculation, and the sloshing frequency.

3.9.1. EMPTY TANK FREQUENCY

The verification for the empty tank frequency is comparing the result of an empty tank frequency using the SAP 2000 software.

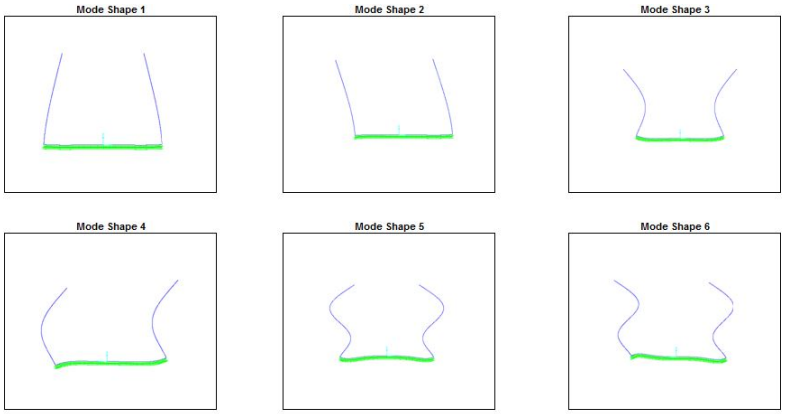

Figure 3.35: Mode Shape From SAP 2000

with the following frequencies and error gap:

Table 3.6: Matlab and SAP 2000 comparison for empty tank natural frequencies

Frequency	SAP 2000	Matlab	Error
ω_1	0.979 Hz	0.981 Hz	0.17%
ω_2	1.263 Hz	1.265 Hz	0.19%
ω_3	6.301 Hz	6.334 Hz	0.51%
ω_4	6.851 Hz	6.875 Hz	0.35%
ω_5	19.66 Hz	20.00 Hz	1.68%
ω_6	20.50 Hz	20.75 Hz	1.17%

From the table, it can be seen that the present's natural frequencies and SAP 2000 have small gap difference. The error percentage is 0.7% on the average. In this thesis such error gap is acceptable. Therefore, the eigenvalue analysis of the empty tank is verified.

3.9.2. CONVERGENCE

During the derivation in the Section 3.6, integration is used to solve the orthogonality for structure and liquid system. However, using such method has its disadvantage. If integration is used then the kinematic boundary condition and the equation of motion itself is a weak form. It is concluded as a weak form due to the integral over the length is different with each point. In actual, the equation should be satisfied in every each point of the liquid and tank condition.

The convergence check is to determine whether the mode that is used in the modal analysis already enough to satisfy all the equation. The concept of the convergence can be seen in the following figure:

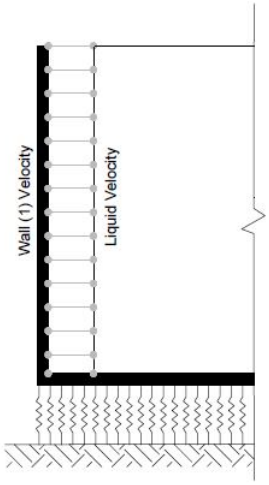

Figure 3.36: Convergence Concept between Wall and liquid velocity

After understanding the convergence concept, the comparison between the liquid and the wall velocity can be seen in the following figures:

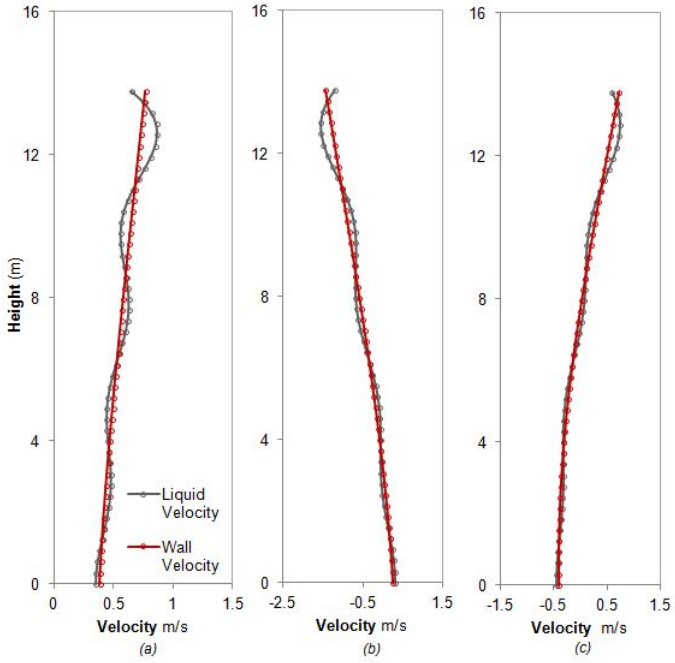

Figure 3.37: Convergence between Wall and liquid velocity for (a) frequency 0.32 Hz ; (b) frequency 0.64 Hz; (c) frequency 1.28 Hz

The difference between the two velocities per each point is less than 10% for only using 6 number of modes.In this thesis this number is acceptable for the convergence check. However, the more modes that is used in the process the more accurate the result : *the velocity of the liquid equals to the wall velocity*. Please note that the number of required modes might be different fo different properties. This statement underlines the important of checking the convergence.

3.9.3. THE FUNDAMENTAL SLOSHING FREQUENCY

For the sloshing frequency, it can be compared with other literature study and standard. For rectangular tank George Housner [7], derived the calculation for the sloshing frequency in the following expression for the rigid tank:

$$\omega^2 = \sqrt{\frac{5}{2}\frac{g}{L}}\tanh\sqrt{\frac{5H}{2L}} \tag{3.57}$$

According to the Eurocode 8 [5] exclusively for the rectangular section, the sloshing frequency is:

$$T = 2\pi\left(\frac{L/g}{\frac{\pi}{2}\tanh\left(\frac{\pi H}{2L}\right)}\right)^{0.5} \tag{3.58}$$

For both the Eurocode and Housner determined that L is the half width of the total length of the structure. Therefore the result can be compared into the following table.

Table 3.7: Matlab, Eurocode 8 [5], and Housner [7] comparison for sloshing frequencies

Matlab	**Eurocode 8**	**Housner**
0.196 Hz	0.196 Hz	0.196 Hz

From the result between these three frequencies it can be seen that the values are almost the same with difference under 0.1%. For this thesis, the error gap is accepted. Therefore the fundamental natural frequency of the sloshing is validated.

3.9.4. LIQUID PRESSURE

For the verification of the pressure, there are some journals that is going to be compared. These journals are Housner [7], Versluis[19],and Jae Kwan Kim [10]. Validation for the rigid tank case is performed by comparing the result with Housner, Versluis and Kim. In this program the structure stiffnesses are multiplied by the factor of 1000 to numerically approach the rigid stiffness. The comparison between the present model with Housner and Versluis is depicted in the figure below:

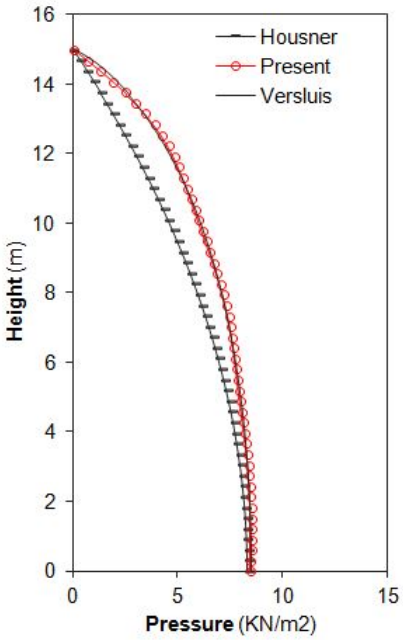

Figure 3.38: Comparison of rigid wall pressure with Housner and Versluis

From the following figure, it can be seen that the comparison between the analytical result with the journal at the frequency before the first excitation is almost the same especially the rigid structure. For rigid structure with only using the **first 6 modes**, result an error of 2.34% and 8.21% for Housner. For the flexible wall, the Journal from Jae Kwan Kim, Hyun Moo Koh, and Im Jong Kwahk [10] is compared. The parameters that is determined by Jae Kwan et. al is written in the following table:

Table 3.8: The properties of the tank that is defined by Jae Kwan Kim et.al [10]

Properties	Value	Unit
Length (L)	9.8	m
Container Height (H)	12.3	m
Liquid Height (H_l)	11.8	m
Wall Thickness (h_w)	0.5	m
Wall Young's Modulus (E_w)	30000	MPa
Soil Stiffness (k)	50000	kN/m2
Structural Density (ρ_s)	2.3	ton/m3
Liquid Density (ρ_w)	1.0	ton/m3

The comparison between the present analysis with the Jae Kim is visualized in the following figure:

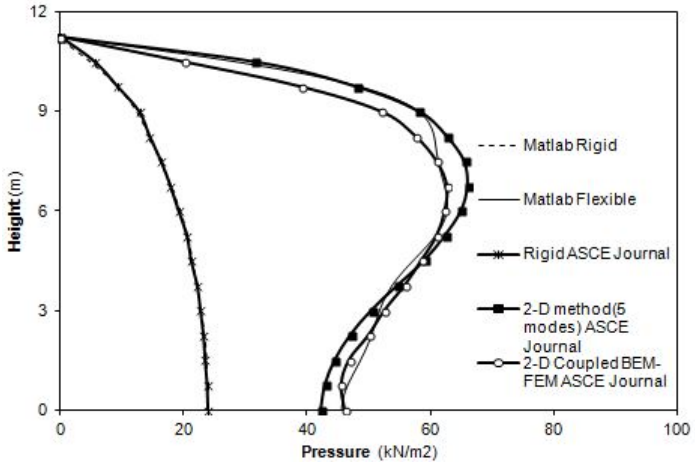

Figure 3.39: Pressure Comparison with other journals (a) Seismic Pressure at 0.3184 Hz, and (b) 0.614 Hz

For the calculation, it can be seen that using this thesis method and the referred journal, the difference for rigid pressure is 1.86% and for flexible, the difference is 5%. The gap can be considered acceptable in this thesis. From the comaparisson, we can also see that the pressure plotted are not a defined smooth curve as the reference. In order to obtain a better curve, use more number of modes.

3.10. THE PHYSICS EXPLANATION

In the literature such as Eurocode 8 [5], Velestos [18],PIANC [8] and Housner [7] the fluid motion is usually separated into two liquid modes: the impulsive mode, and the convective mode. Housner and other simplified methods mostly use a discrete calculation with a representation of impulsive mass and convective mass. In the following will also be explained how to achieve the added mass and it influences the natural frequency.

Since most of the calculation for rectangular tank is done for the rigid case, therefore the comparison will be done in the rigid with infinite thickness for wall and plate. However as the infinite cannot be numerically achieve, therefore the stiffness of the plate and the wall will be times 1000 to reach the numerically closer to a rigid structure. The calculation is included for only 6 first modes. Since the Housner and tha PIANC sets for the acceleration will be set for 1 unit m/s^2. Therefore for the analytical calculation we will set the the displacement in term of 1 unit acceleration.

Eurocode only mentioned more detailed information about the cylindrical tank cases, and less specified explanation for the rectangular tank. Therefore, the formulation in PIANC is more accurate for the rectangular tank. PIANC is the standard for Design of lock Gates under seismic actions.

3.10.1. IMPULSIVE MODES

This modes describe the motion of the liquid together with the walls and the base slab while the free surface boundary condition is not satisfied, i.e., a pressure release boundary is assumed instead at $z = -H$ in our case, a potential of this type is $\tilde{\phi}_2(x,z,\omega)$ which moves in phase with the walls of the tank while the free surface waves are not generated. In the Eurocode 8 for cylindrical tank, the calculation is expressed with the ratio for between added impulsive mass and the total mass. In the analytical calculation the added impulsive can be obtained from the integration of the pressure divided by the acceleration (Newton Second law)

$$\begin{aligned} F_{liq} &= \int_0^H P_{liq}(z)dz \\ m_{liq} &= \frac{F_{liq}}{a_e} \end{aligned} \tag{3.59}$$

the equation above can be expanded in the following form:

$$m_{liq} = \frac{\int_0^H P_{liq}(z)dz}{a_e} \tag{3.60}$$

P_{liq} = liquid pressure;
F_{liq} = liquid force;
m_{liq} = liquid added mass from the dynamic loading;

The conversion from liquid pressure to liquid force can be seen in the following figure:

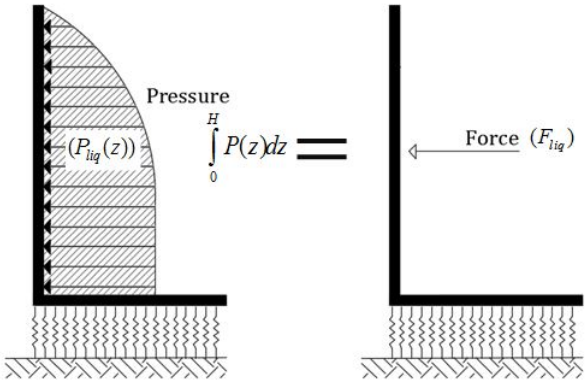

Figure 3.40: Conversion from liquid pressure to force

3.10.2. CONVECTIVE MODES:

The convective modes solely consider the free surface waves while all other boundary condition are assumed homogeneous i.e. $\frac{\partial\phi}{n} = 0$ (see Figure 4.11). The convective modes and its natural periods depend solely on tank dimensions, i.e. H/L ratios. In our case, potential $\tilde{\phi}_1(x,z,\omega)$ is in a way similar to the conditions described above in the limit case of $E_p I_p \to \infty$, Then $\frac{\partial\phi}{\partial z} = 0\Big|_{z=0}$ and the modes calculated are independent of plate and wall flexibility i.e. convective modes.

3.10.3. ADDED MASS IN OTHER JOURNALS

In this subsection, is written the added mass calculation in different journals for rectangular tank.

HOUSNER METHOD

The PIANC code reffered to journal from Housner. However, the calculation for PIANC is more detailed compare to Housner which is more numerical then PIANC. Housner himself formulates a simplified discrete model. The impulsive pressure and mass that is derived from Housner is written in equation 2.49. For the convective pressure and mass, they are expressed in equation 2.50. According to Housner, the overall effect of the fluid pressure in the wall for added mass is multiplied by two if the load is symmetry. However, if the load is not symmetry, then the total pressure for the added mass is the summation of the first wall and the second wall pressure. The pressure is integrated concerning the height likewise equation 3.59 to obtain the total pressure of each wall the pressure that varies over the height. The summation between the convective and the impulsive has to be around equals to the total mass ($m_{tot} = m_i + \sum m_c$).

PIANC CALCULATION [8]

In the PIANC journal there is no specification of added mass likewise in Housner or in the Eurocode 8. However the pressure expression is provided instead. In this code, the pressure is also divided into two term which are the convective and the impulsive with the same explanation as the previous. Both pressure is expressed into the following expressions:

$$p_i = \Big(\sum_{n=1}^{+\infty} \frac{4\rho_{liq} L'}{(2n-1)^2 \pi^2} \frac{\cosh(2n-1) * \pi z/L}{\cosh(2n-1) * \pi H_l/L} - \frac{\rho liq L'}{2} \Big) \ddot{X} t \tag{3.61}$$

and

$$p_c = \Big(\sum_{n=1}^{+\infty} \frac{4\rho_{liq} L'}{(2n-1)^2 \pi^2} \frac{\cosh(2n-1) * \pi z/L'}{\cosh(2n-1) * \pi H_l/L'} \Big) r_n(t) \tag{3.62}$$

Where for the r_n is the response acceleration of a single degree of freedom oscilator

$$\frac{\partial^2 r_n}{\partial t^2} + \omega_n^2 r_n(t) = \ddot{x}_t \tag{3.63}$$

with the following natural frequency of the sloshing as in the following:

$$\omega_n = \frac{(2n-1)\pi g}{L} \tanh\Big(\frac{(2n-1)\pi H_l}{L} \Big) \tag{3.64}$$

The symbol definitions for PIANC formulation are:

ρ_{liq}	= liquid density;
g	= gravitational acceleration;
L	= lock chamber length (for liquid tank cases: the tank width);
H_l	= liquid Height;
ω_n	= sloshing circular n^{th} frequency;
$\ddot{X}(t)$	= ground acceleration due to earthquake ;

EUROCODE 8

The Eurocode 8 provide two ways to calculate the impulsive and convective mode for rigid tank. The impulsive mass according to analytical Eurocode equation is

$$m_i = m \times 2\gamma \sum_{n=0}^{\infty} \frac{I_1(\upsilon_n/\gamma)}{\upsilon_n^3 \times I_1'(\upsilon_n/\gamma)} \tag{3.65}$$

and for the convective mass is expressed in the following equation

$$m_c = m \frac{2\tanh \lambda_n \gamma}{\gamma \lambda_n (\lambda_n^2 - 1)} \tag{3.66}$$

where
m = the total mass;
I_1 = the first kind of modified Bessel function;
γ = H/R;
$\upsilon_n = (2n+1)\pi/2$;
λ_n = 1.841, 5.331, 8.5336,...
For practical calculation Eurocode 8 provide table that include both mass ratio of a convective and impulsive mode as explained in the previous Chapter 2.

ANALYTICAL METHOD

For the calculation of the Analytical method, the impulsive and the convective part it is once again referred to equation 3.59. However, as the calculation consists of 2 potentials, where the free surface potentials are coupled with the plate potentials, there will be an additional calculation for computing the convective mass. The convective part and impulsive part can be done in 2 ways which are:

- By setting the potential superposition into three instead of two. This calculation is explained in the previous section of "Alternative Solution for Liquid Superposition." By using this combination instead of the previous one, the convective pressure can be directly achieved from the $\tilde{\phi}_3$.
- By seperating the total pressure into two different pressures. The first pressure is the pressure from neglecting the free surface condition(P_1). The second pressure is by taking into accont the free surface condition (P_2). For the P_1, the free surface boundary condition in the second potentials is set to be 0. The first pressure results to the impulsive pressure (P_1). The total pressure is obtained from the second pressure (P_2). The total pressure can be defined as the summation of convective pressure and impulsive pressure. From the definition of the total pressure, the convective pressure can be obtained.

Since the potentials are separated into two potentials for this thesis, the method that is applied to obtain the added mass is the later method. From the pressure, one can obtained the impulsive and convective mass by applying the formulation in equation 3.59. The total pressure can be defined as two times pressure for the total added mass, due to there is no phase difference in the loading.

The following figure is the comparison result from the added mass between the available journals and this thesis:

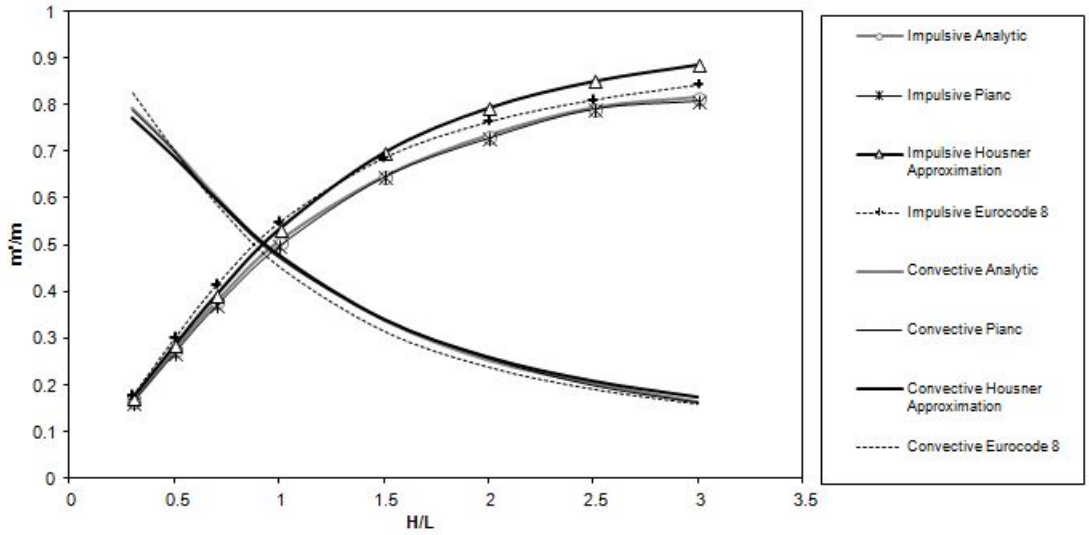

Figure 3.41: Impulsive and Convective Mass ratio for Rigid Tank

From the above figure, it can be seen that the impulsive and the convective mass is changed as the height and length ratio is altered.

By adding the two-components together (*the impulsive mass and the convective mass*), the total mass is less than 1, approximately 0.97. If the calculation is accurate, which is using all the modes, this summation is closer to 1. The ratio 1 is describing the total mass of the whole structure. Due to in the analytic calculation, only six modes are regarded, this ration is always less than 1. From this result, one could understand that by using only 6 modes the calculation almost satisfies the required condition within only under 3% of error.

3.11. REVIEW FOR CHAPTER 3

From the analytical derivation, there are essential decisions to be made along the process:

- **Fourier Transform**
  Since the Fourier transform used in this thesis, the transient phase is neglected during the process. Which means the calculation that is performed concerns about the steady state of the structure solely.
- **Seismic loading superposition**
  The earthquake loading in the structure is considered with no dependency between the two directions. Therefore the calculation between the two can be separated and then the total response is the summation of the two.
- **Liquid Properties**
  The liquid is considered *inviscous, incompressible and linear*. This linear assumption is the underlined reason why the superposition can be used to solve the calculation. Due to the mathematic principle the superposition can only be done if the structure is linear.
- **Structure Properties**
  The structure properties is considered as the linear material, rigid shear stiffness, negligible inertia rotation, and inextensible. By applying these structural properties, *the classic Euler Bernoulli beam theory* is used. In the two dimensional model, the inextensibility of the beams lead to no axial stresses and no soil springs in the transverse direction.

Seeing the result from the case study and the parameter study, one can derive some behavior from the liquid structural interaction in a rectangular container. In a nutshell, the conclusions are written in the following points:

- **Added Mass is derived from the liquid interaction to the structure.** The liquid and the structure interaction under dynamic loading exerted the hydrodynamic pressure. Since the integration of pressure per acceleration (equation 3.59) results in the mass, this added mass **lowers the natural frequencies** of the entire structure. The frequencies of the filled tank are lower compared to the empty container.
- **Sloshing Frequencies are dominantly located in the low frequency**. The sloshing frequencies are dominantly located in the low-frequency range, or one can also define that the sloshing has a longer period than the impulsive pressure. Therefore the free surface water pressure mostly takes effect in the total pressure for the low-frequency domain. The higher the frequency, the less impact from the sloshing to the total pressure.
- **Flexibility of the structure has a significant effect for the entire structure**. The flexibility influence both frequency and the pressure exerted in both wall and plate. The more flexible the structure, the lower the frequency. Moreover, at the certain frequencies, there are some points that the pressure from the flexible structure higher than the rigid structure.

4

THREE DIMENSIONAL ANALYTICAL DERIVATION

This fourth chapter will cover the analytical derivation of the three-dimensional model. From the two dimensional model in Chapter 3, we can obtain the basic knowledge on how the liquid-structure interaction works in the two dimensional model. The governing equations of motion for the three-dimensional are derived in Subsection 2.3.4 for shell vibrations and in Subsection 2.4 for the liquid potential flow. Since the three-dimensional model is more complex than the two-dimensional model, the derivation and the result is separated in the Chapter 5, unlike the two-dimensional model. The purpose of this separation is to have better explanation for both result and derivation in three-dimensional model.

4.1. GENERAL PROCEDURE

The plate and the wall are described as *shell structures* in cylindrical coordinates (r, θ and z). The plate is defined as the circular plate, the circular shell with zero curvature. The wall is modeled as a cylindrical shell. Since the liquid is in the cylindrical tank medium, the potential flow of the liquid is also defined in the cylindrical coordinates. The following figure depicts the three-dimensional model:

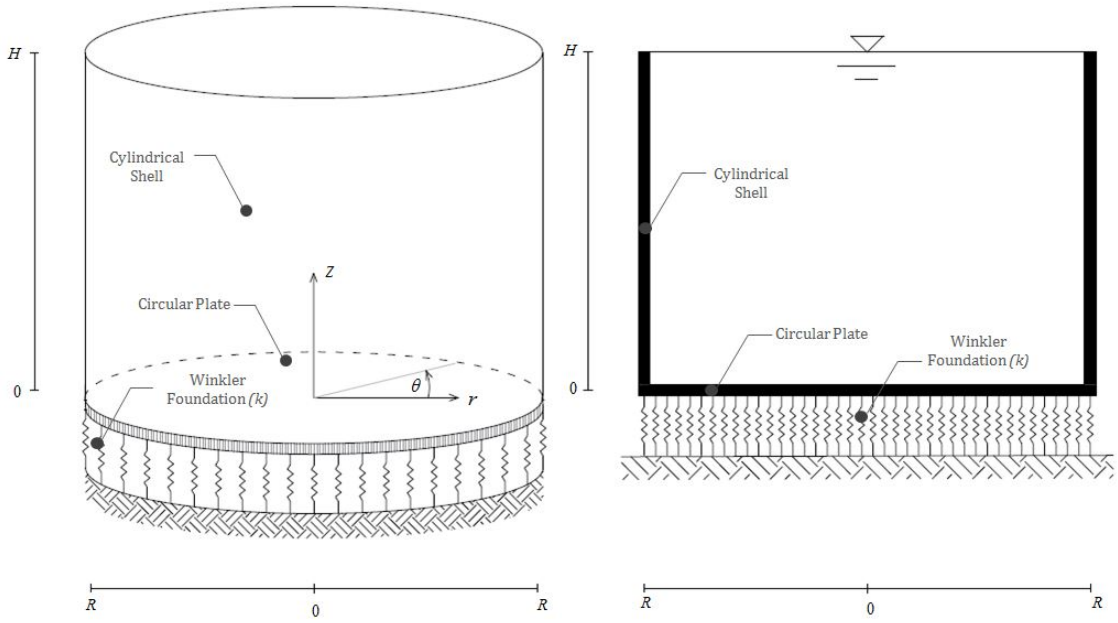

Figure 4.1: The three-dimensional Model, The three dimensional preview *(left)* and cross sectional preview *(right)*

4.1.1. THE PROCESS FLOWCHART

Before we consider the derivations and the calculation, let us firstly consider the overall procedure of the process. This flowchart provides an overview on how the liquid structure works using the modal analysis. The process flowchart is similar to the previous two-dimensional flowchart in Figure 3.2. However, due to the higher level complexity, the three-dimensional flowchart model can be expanded in the following:

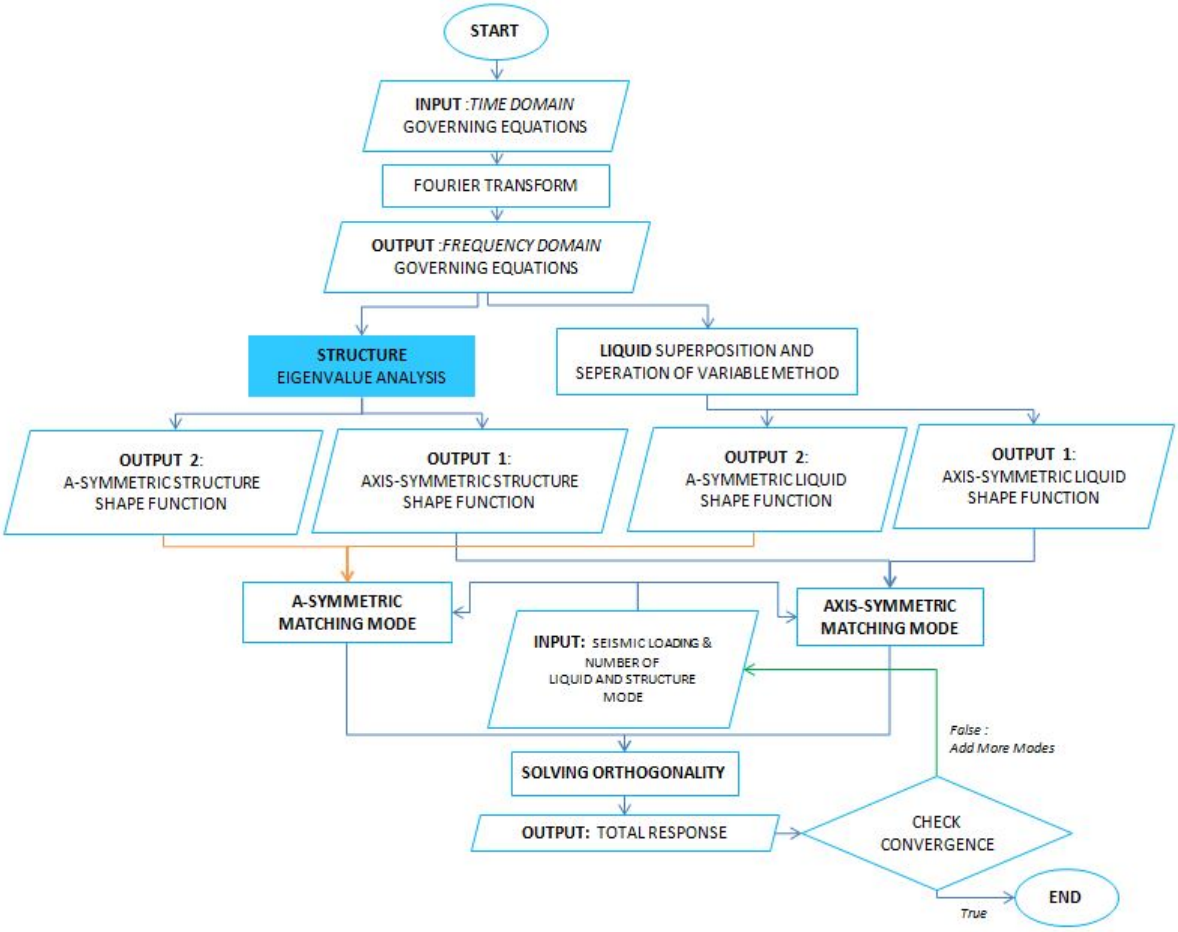

Figure 4.2: The three-dimensional process flowchart

Similarly as the two-dimensional model, most of the processes in this model are analytically performed. The only process that is numerically performed is again the eigenvalue analysis. From the flowchart in Figure 4.2, it is also clear that the process of the three-dimensional model is more complex than the two-dimensional model.

4.1.2. THE ASSUMPTIONS

Once again, the assumptions are re-written in the general description of the model. These assumptions are crucial to derive and solve the three-dimensional model. The liquid assumptions are the same as the two-dimensional model and written in Section 3.1.2. The only thing that differs is: the liquid flow motion is also described in **the three-dimensional plane** and **cylindrical coordinates**. The structural materials are considered *linear*, as with the two-dimensional model.

STRUCTURE ASSUMPTIONS

For modeling the structure, the following assumptions are used in this three-dimensional model:

- **Thin Shell/Plate theory**.
  Thin shell/ plate theory is used to model the plate and the walls. Specifically *Kirchoff-Love theory* is used for the shell modeling - an expansion derivation from *Euler Bernoulli classical beam theory*. In his argument, *Augustus E. H. Love* derives the shell expression based on the assumption from *Gustav Kirchhoff* which are: the rigid shear stiffness and negligible effect of inertial rotation. This theory can be justified since most of the tanks are made of thin elements.
- **Infinite stiffness in in-plane direction for the circular plate**
  This assumption is based on the inertia in the in-plane direction is way higher than the out-plane directions. Since the in-plane stiffness is relative high, the plate is assumed as an inextensible element in the in-plane direction.
- **Neglected roof in the structure.**
  In this thesis, the roof is neglected. This decision is due to the roof structure does not play a part in the liquid-structure interaction.

4.2. GOVERNING EQUATIONS OF MOTION

From section 4.1, the process starts with composing the governing equations of motion in the time domain. Unlike the two-dimensional model, all the governing equations of motion are derived in the cylindrical coordinates. The governing equations of motion in time domain consist of the seismic ground excitation, cylindrical shell, and circular plate equations.

4.2.1. SEISMIC GROUND EXCITATION

As done in the two dimensional model, the seismic ground excitation can be defined as a displacement propagating along the free surface of the soil. Due to the linearity of the model, the seismic loading can be treated separately for the vertical and the horizontal direction. The horizontal loading is projected from the Cartesian to the cylindrical coordinate into two components which are θ and r. Once again, the phase shift in the three dimensional model is disregard. The earthquakes loading in cylindrical tank shown in the following figure:

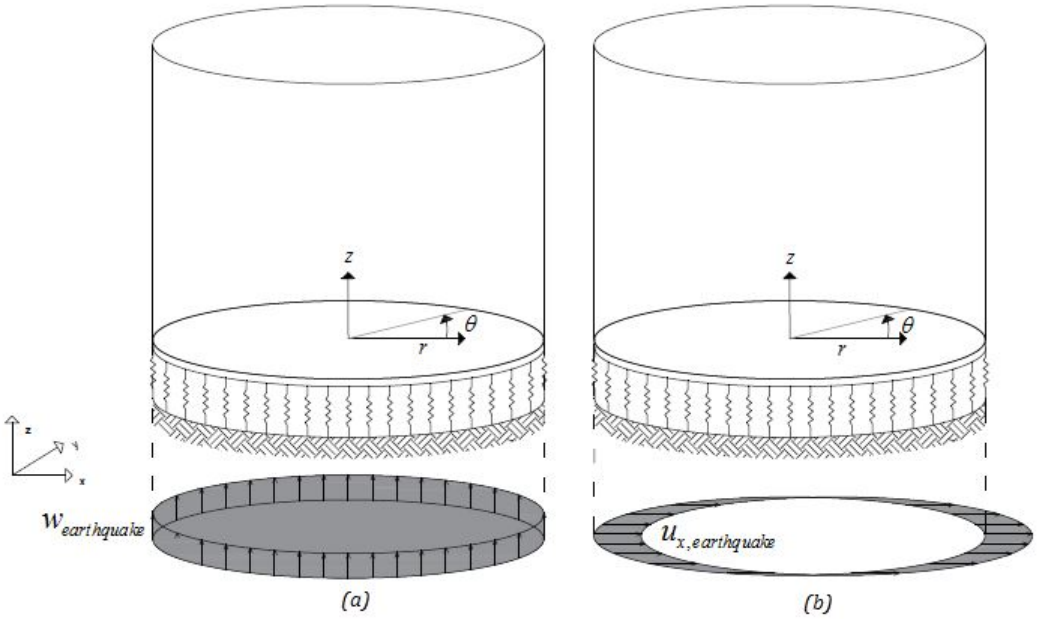

Figure 4.3: The earthquake loading in cylindrical tank. (a) Vertical seismic loading; (b) Horizontal Seismic loading

VERTICAL SEISMIC EXCITATION

The cylindrical coordinates are at r, θ, and z axes. Since the vertical seismic loading is in the z-direction, no projection is performed. Therefore the earthquake loading yields to:

$$w_{earthquakes}(t) = w_{earthquake} \exp(i\omega t) \tag{4.1}$$

HORIZONTAL SEISMIC EXCITATION

The horizontal seismic is in the x direction of the Cartesian coordinates. Therefore, projection is required for the horizontal loading. The projection of the earthquakes is shown in the following figure:

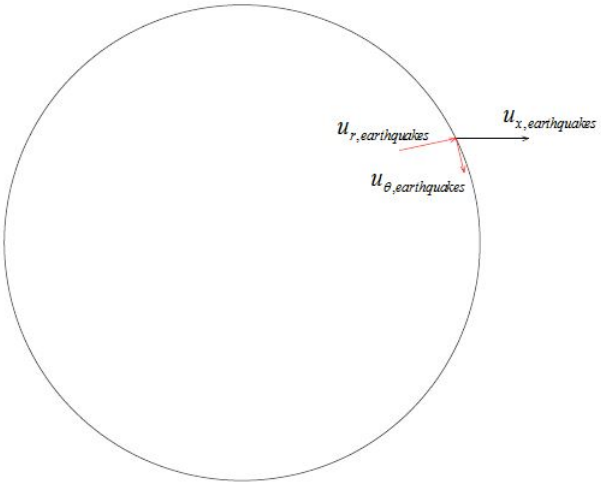

Figure 4.4: The projection of horizontal seismic loading

The initial earthquake loading in Cartesian coordinates is written as:

$$u_{x:earthquakes} = u_e \exp(i\omega) \tag{4.2}$$

From the equation 4.2, the horizontal earthquakes loading is projected in polar coordinates which are (see figure 4.4):

$$\begin{aligned} u_{r:earthquakes} &= u_e \exp(i\omega t)\cos\theta \\ u_{\theta:earthquakes} &= u_e \exp(i\omega t)\sin\theta \end{aligned} \tag{4.3}$$

The application of the seismic loading in the system is depicted in the following figure:

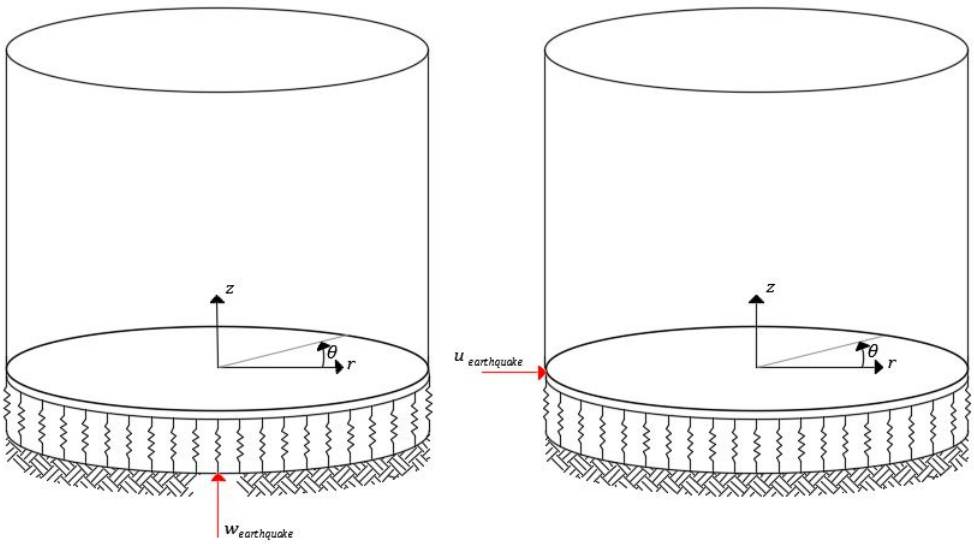

Figure 4.5: The application of seismic loading : vertical seismic loading *(left)* and horizontal seismic loading *(right)*

From the Figure 4.5,the horizontal loading and vertical loading are applied in the different level similar to the two-dimensional model in Figure 3.4. This placement is due the assumption of no soil stiffness on transverse direction. By stating this assumption, we neglect the soil-structure interaction in transverse direction. Therefore, the horizontal loading can be directly applied on the bottom of cylindrical shell as in Figure 4.5.

4.2.2. PLATE EQUATION OF MOTION

The plate vibration derivation is already discussed in the previous Section 2.3.4. From the Section 4.1.2, the assumptions are explained. One of the assumptions is the rigid in-plane mode of the circular plate. This assumption is justified in this thesis, due to the relatively high stiffness compare to the out-plane motion. From this statement, one can conclude that *out-plane motion is highly governing* in the overall circular plate motions.

From the two-dimensional model, one can learn that the liquid pressure direction is normal to the structure surface (see figure 3.5). In the Section 2.3.4, it can be seen that the cylindrical shell in Figure 2.18 and the circular plate in Figure 2.17 have a different positive direction of θ. To avoid mistake, the axes of the plate are converted to match the cylindrical shell axis. These converted axes are shown in the figure below:

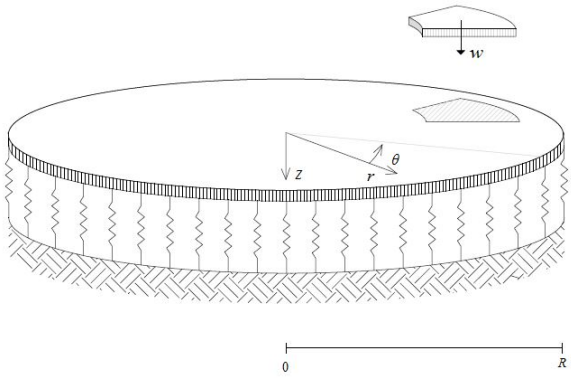

Figure 4.6: Circular plate axis and degree of freedom

From Figure 4.6 and Figure 3.5, one can derive the plate equation of motion subjected to **Seismic loading in horizontal Direction** in the following expression:

$$D\nabla^4 \cdot w(r,\theta,t) + \rho_p h_p \ddot{w}(r,\theta,t) + k_p \cdot w(r,\theta,t) = P_{liq}(r,z=0,\theta,t) \tag{4.4}$$

Where it can be extended into the following form:

$$D\nabla^4 \cdot w(r,\theta,t) + \rho_p h_p \ddot{w}(r,\theta,t) + k_p \cdot w(r,\theta,t) = \rho_{liq}\Big(\frac{\partial\phi(r,z,\theta,t)}{\partial t}\Big|_{z=0} + g \cdot H\Big) \tag{4.5}$$

For **Seismic loading in vertical direction**, in the equation of motion, the loading is introduced on the bottom tip of the spring as in Figure 4.5. Therefore, the equation of motion for the vertical loading is:

$$\begin{aligned} D\nabla^4 \cdot w(r,\theta,t) + \rho_p h_p \ddot{w}(r,\theta,t) + (k_p \cdot w(r,\theta,t) - w_{r:earthquake}(r,\theta,t) \\ = \rho_{liq}\Big(\frac{\partial\phi(r,z,\theta,t)}{\partial t}\Big|_{z=0} + g \cdot H\Big) \end{aligned} \tag{4.6}$$

The Laplace form for the circular plate is:

$$\nabla^2(\cdot) = \frac{\partial^2(\cdot)}{\partial r^2} + \frac{1}{r}\frac{\partial(\cdot)}{\partial r} + \frac{1}{r^2}\frac{\partial^2(\cdot)}{\partial\theta^2} \tag{4.7}$$

4.2.3. CYLINDRICAL SHELL (WALL)

In the Section 2.3.4, the derivation of the cylindrical shell has been discussed. The cylindrical shell has three degrees of freedom in which the three of them are coupled in the three of the equations of motion. The motions of the cylindrical shell are tangential displacement (u_θ), radial displacement (u_r), and z displacement u_z. In the following figure, the structure and axis of the cylindrical shell are depicted:

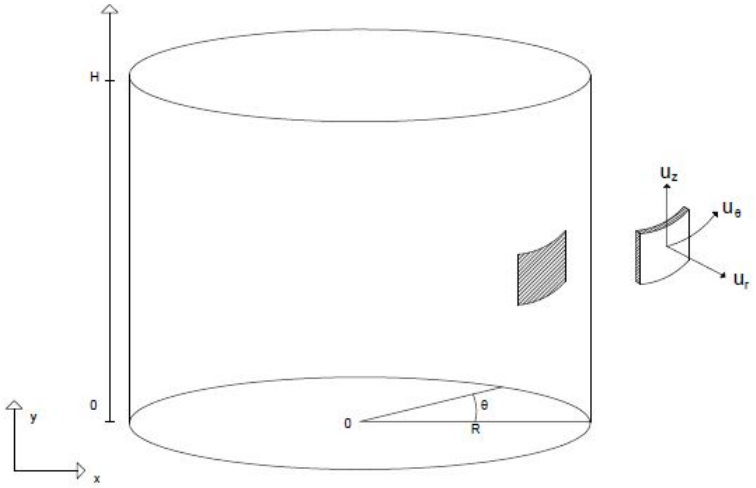

Figure 4.7: Cylindrical Shell axis and degree of freedom

Before writing the equations of motion, in the following figure can be seen the pressure direction in a cylindrical shell:

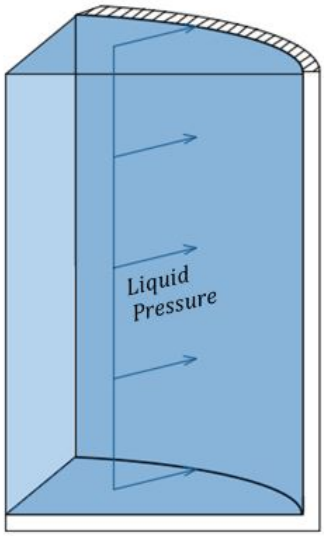

Figure 4.8: Liquid Presure in the cylindrical container

From the Figure 4.8, it can be seen that the liquid pressure acts only in normal to the surface axis. Therefore one can simply write the equations of motion as equation 4.8 to 4.11.

LONGITUDINAL VIBRATION ALONG THE AXIS OF REVOLUTION

$$\frac{\partial(N_{zz})}{\partial z}+\frac{1}{R}\frac{\partial(N_{\theta z})}{\partial \theta}-\rho_w h\ddot{u}_z=0 \tag{4.8}$$

LONGITUDINAL VIBRATION ALONG THE CIRCUMFERENTIAL DIRECTION

$$\frac{\partial(N_{z\theta})}{\partial z}+\frac{1}{R}\frac{\partial(N_{\theta\theta})}{\partial \theta}-\frac{1}{R}Q_{\theta r}-\rho_w h_w\ddot{u}_\theta=0 \tag{4.9}$$

TRANSVERSAL VIBRATION ALONG THE NORMAL TO THE SURFACE AXIS

$$\frac{\partial(Q_{zr})}{\partial z}+\frac{1}{R}\frac{\partial(Q_{\theta r})}{\partial \theta}-\rho_w h_w\ddot{u}_r=P_{liq}(r=R,z,\theta,t) \tag{4.10}$$

or also can be written in the following formulation

$$\frac{\partial(Q_{zr})}{\partial z}+\frac{1}{R}\frac{\partial(Q_{\theta r})}{\partial \theta}-\rho_w h_w\ddot{u}_r=\rho_{liq}\Big(\frac{\partial\phi(r,z,\theta,t)}{\partial t}\Big|_{r=R}+g(z-H)\Big) \tag{4.11}$$

The coupled equations of motion can be written in matrix form. The matrix consists of mass matrix and stiffness matrix as in the following equation:

$$\underbrace{\underline{\underline{[\mathbf{M}]}}}_{\text{Mass Matrix}}\times\underline{u}+\underbrace{\underline{\underline{[\mathbf{K}]}}}_{\text{Stiffness Matrix}}\times\underline{u}=\underline{F} \tag{4.12}$$

From the derivation in the Appendix E, the mass matrix **M**, can be written as the following

$$\underline{\underline{[\mathbf{M}]}}=\begin{bmatrix}m_{11}&0&0\\0&m_{22}&0\\0&0&m_{33}\end{bmatrix} \tag{4.13}$$

Where each of the following component are:

$$\begin{aligned}m_{11}&=-2\rho_w h_w\frac{\partial(\cdot)}{\partial t}\\m_{22}&=-2\rho_w h_w\frac{\partial(\cdot)}{\partial t}\\m_{33}&=2\rho_w h_w\frac{\partial(\cdot)}{\partial t}\end{aligned} \tag{4.14}$$

For the vector u is written in the following:

$$\underline{u}=\begin{Bmatrix}u_z(z,\theta,t)\\u_\theta(z,\theta,t)\\u_r(z,\theta,t)\end{Bmatrix} \tag{4.15}$$

Last but not least, the stiffness matrix is **K**:

$$\underline{\underline{[\mathbf{K}]}}=\begin{bmatrix}L_{11}&L_{12}&L_{13}\\L_{21}&L_{22}&L_{23}\\L_{31}&L_{32}&L_{33}\end{bmatrix} \tag{4.16}$$

For shell equation of motion, the significant characteristic is the symmetric matrix. Where from the above matrix, one can simply write that $L_{12}=L_{21}$, and $L_{13}=L_{31}$, as well as $L_{23}=L_{32}$. Each of the matrix components

is written as:

$$
\begin{aligned}
L_{11} &= \frac{-h_w E_w}{(\mu^2-1)R^2}\left(2R^2\frac{\partial^2(\cdot)}{\partial z^2} - \frac{\partial^2(\cdot)}{\partial\theta^2}\mu + \frac{\partial^2(\cdot)}{\partial\theta^2}\right)\\
L_{22} &= \frac{12E_w h_w}{(12\mu^2-12)R^4}\left(R^2(-1+\mu)\frac{\partial^2(\cdot)}{\partial z^2} - 2\frac{\partial^2(\cdot)}{\partial\theta^2}\right)\left(R^2+\frac{1}{12}h^2\right)\\
L_{33} &= \frac{E_w h_w}{(6\mu^2-6)R^4}\left(R^4\frac{\partial^4(\cdot)}{\partial z^4}h^2 + \left(\frac{\partial}{\partial^4(\cdot)z^2\partial\theta^2}+12\right)R^2 + \frac{\partial^4}{\partial\theta^4}h^2\right)\\
L_{12} &= L_{21} = -\frac{E_w h_w}{R(-1+\mu)}\frac{\partial^2(\cdot)}{\partial z\partial\theta}\\
L_{13} &= L_{31} = -2\frac{E_w h_w \mu}{R(\mu^2-1)}\frac{\partial(\cdot)}{\partial z}\\
L_{23} &= L_{32} = \frac{E_w h_w^3}{R^2(6\mu^2-6)R^4}\frac{\partial^3(\cdot)}{\partial z^2\partial\theta^2} + \frac{E_w h_w}{(6\mu^2-6)R^4}\left(h_w\frac{\partial^3(\cdot)}{\partial\theta^3} - 12R^2\frac{\partial(\cdot)}{\partial\theta}\right)
\end{aligned}
\tag{4.17}
$$

4.2.4. STRUCTURAL BOUNDARY CONDITION AND INTERFACE CONDITION

In this subsection, the internal structural boundary and interface condition are discussed. Since the cylindrical shell is constant edge or in other words fixed circle along the height (z) the boundary conditions are:

$$
\begin{aligned}
N_{zz} = N_{zz}* \quad &\text{or} \quad u_z = u_z*\\
M_{zz} = M_{zz}* \quad &\text{or} \quad \varphi_z = \varphi_z*\\
V_{zr} = V_{zr}* \quad &\text{or} \quad u_r = u_r*\\
T_{z\theta} = T_{z\theta}* \quad &\text{or} \quad u_\theta = u_\theta*
\end{aligned}
\tag{4.18}
$$

In the following figure is shown the number of boundary and interface conditions and their locations:

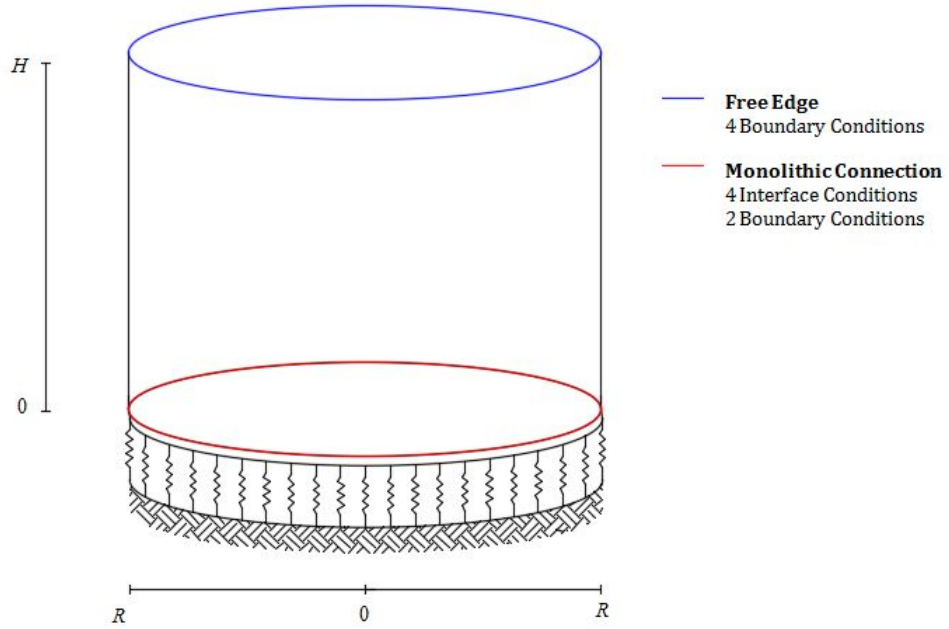

Figure 4.9: Boundary and interface conditions of the cylindrical tank

FREE EDGE AT $z = H$

Since at the $z = H$ is a *free edge* (see Figure 4.9), the boundary condition is either *Dirichlet* or *Newman*. However, in this case, all the boundary conditions are Neumann (Dynamic boundary condition). The moment,shear, and normal forces at $z = H$ have to be equal to zero as there is no constraint or external load in that certain location. This condition leads to no stresses in the free edge.

1. **Normal Force = 0, at** $z = H$:
$$N_{zz}(z,\theta,t)\Big|_{z=H} = 0 \tag{4.19}$$
2. **Moment Force = 0, at** $z = H$:
$$M_{zz}(z,\theta,t)\Big|_{z=H} = 0: \tag{4.20}$$
3. **Shear Force Effective First Kind = 0, at** $z = H$
$$V_{zr}(z,\theta,t)\Big|_{z=H} = 0 \tag{4.21}$$
4. **Shear Force Effective First Kind = 0, at** $z = H$
$$V_{zr}(z,\theta,t)\Big|_{z=H} = 0 \tag{4.22}$$

CONNECTION PLATE AND SHELL AT $z = 0$

As shown in Figure 4.9, the location at $z = 0$ is the monolithic connection between the plate and the wall. In this location, there are boundary conditions and interface conditions. The boundary conditions exist since the in-plane stiffness is considered rigid which leads to constrained in displacement "r" and "θ". However, if the cylindrical shell is excited in the bottom by the earthquake, in this case, the horizontal earthquake (see Figure 4.5), then these boundary conditions alters. In Figure 4.10, the displacement and the forces in the connection are shown. The moment and the forces follow the sign of figure B.6.

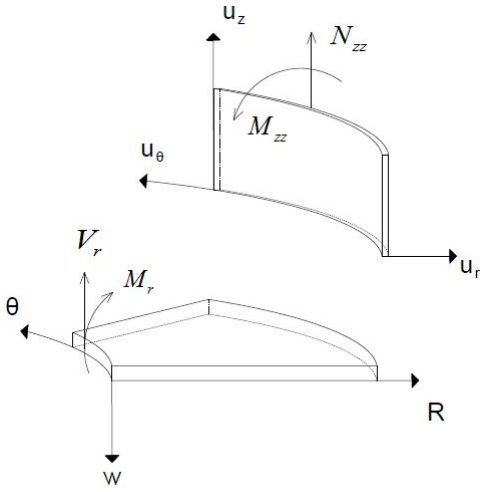

Figure 4.10: Infinitesimal connection between plate and shell with respect to normal/shear force and bending moment

1. **Radial Displacement, at** $z = 0$:

   (a) Earthquake in Vertical loading:

$$u_r(z = 0, \theta, t) = 0 \tag{4.23}$$

   (b) Earthquake in Horizontal loading:

$$u_r(z = 0, \theta, t) = u_{r:earthquake}(r = R, z, \theta, t) \tag{4.24}$$

2. **Tangential Displacement, at** $z = 0$:

   (a) Earthquake in Vertical loading:

$$u_\theta(z = 0, \theta, t) = 0 \tag{4.25}$$

   (b) Earthquake in Horizontal loading:

$$u_\theta(z = 0, \theta, t) = u_{r:earthquake}(r = R, z, \theta, t) \tag{4.26}$$

The connection between the cylindrical shell and the circular plate is described using the following interface conditions which consist of both kinematic and dynamic conditions.

1. **Moment Force, at** $z = 0$:

$$M_{zz}(z, \theta, t)\Big|_{z=0} = M_{plate}(r, \theta, t)|_{r=R} \tag{4.27}$$

2. **Shear Force wall with the Normal Force, at** $z = 0$:

$$N_{zz}(z, \theta, t)\Big|_{z=0} = -V_{plate}(r, \theta, t)|_{r=R} \tag{4.28}$$

3. **Displacement in vertical direction, at** $z = 0$:

$$u_z(z = 0, \theta, t) = -w_{plate}(r = R, \theta, t) \tag{4.29}$$

4. **Rotation in vertical direction, at** $z = 0$:

$$\varphi_z(z, \theta, t)\Big|_{z=0} = \varphi_z(r, \theta, t)\Big|_{r=R} \tag{4.30}$$

The total number of boundary and the interface conditions equal to **ten conditions**.

4.2.5. LIQUID KINEMATIC BOUNDARY CONDITION

In this subsection, the kinematic boundary conditions between liquid and the structure are discussed. The relation between the two is similar to the two-dimensional model which is the velocity of the liquid and the structure. In the following figure are shown the liquid kinematic boundary conditions:

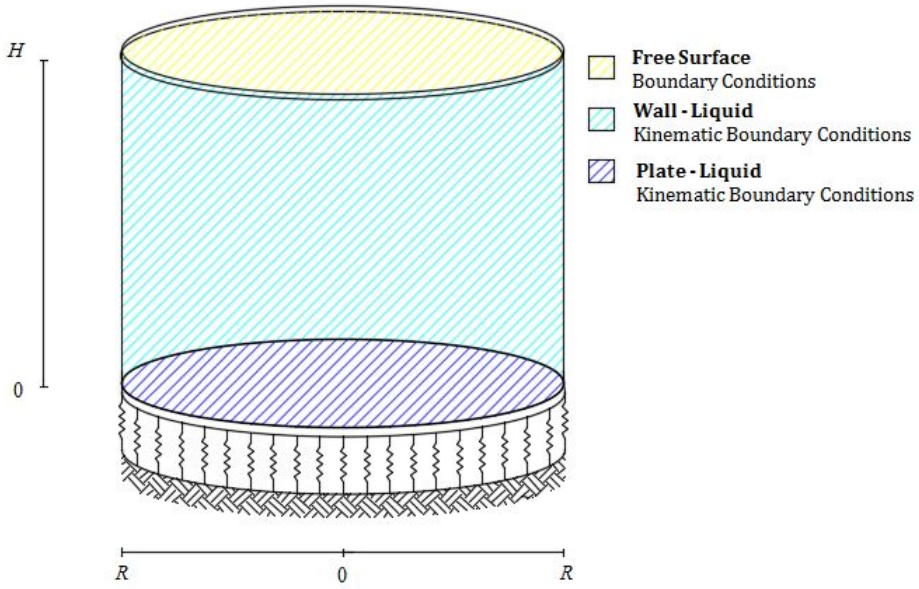

Figure 4.11: Structure and Liquid boundary conditions

From the Figure 4.11, the boundary conditions are expressed in the following form:

1. **Liquid Potential Velocity in r direction at $r = R$:**

$$\frac{\partial \phi(r,z,\theta,t)}{\partial r}\Big|_{r=R} = -\dot{u}_r(z,\theta,t) \tag{4.31}$$

2. **Liquid Potential Velocity in z direction at $z = 0$:**

$$\frac{\partial \phi(r,z,\theta,t)}{\partial z}\Big|_{z=0} = \dot{W}(r,\theta,t)\Big|_{r=R} \tag{4.32}$$

3. **Free Surface at $z = H$:**

$$\frac{1}{g}\frac{\partial \phi(r,z,\theta)}{\partial t}\Big|_{z=H} = \frac{\partial \phi_{(r,z,\theta)}}{\partial z}\Big|_{z=H} \tag{4.33}$$

4.3. SOLUTION IN FREQUENCY DOMAIN

In general, entering the frequency domain for the three-dimensional model has the same steps the previous two-dimensional model as mentioned in Section 3.3. Since in the equations of motion consist of static and dynamic load, the separation between the dynamic response and static response are carried out in this subsection. The method to convert the equation of motion from the time domain to the frequency domain is once again using the Fourier transform with the following equation:

SOLUTION FOR PLATE EQUATION OF MOTION

$$w_{(r,\theta,t)} = w_{s(r,\theta)} + \frac{1}{2\pi}\int_{-\infty}^{\infty} \tilde{W}_{(r,\theta,t)} \exp(i\omega t) d\omega \tag{4.34}$$

SOLUTION FOR CYLINDRICAL SHELL EQUATION OF MOTION

$$\begin{aligned} u_{r(\theta,z,t)} &= u_{rs(\theta,z)} + \frac{1}{2\pi}\int_{-\infty}^{\infty} \tilde{U}_{r(\theta,z)} \exp(i\omega t) d\omega \\ u_{\theta(\theta,z,t)} &= u_{\theta s(\theta,z)} + \frac{1}{2\pi}\int_{-\infty}^{\infty} \tilde{U}_{\theta(\theta,z)} \exp(i\omega t) d\omega \\ u_{z(\theta,z,t)} &= u_{zs(\theta,z)} + \frac{1}{2\pi}\int_{-\infty}^{\infty} \tilde{U}_{zd(\theta,z)} \exp(i\omega t) d\omega \end{aligned} \tag{4.35}$$

SOLUTION FOR LIQUID EQUATION OF MOTION

$$\phi_{(r,z,\theta,t)} = \int_{-\infty}^{\infty} \frac{1}{2\pi} \tilde{\phi}_{((r,z,\theta,\omega)} \cdot \exp(i\omega t) d\omega \tag{4.36}$$

The solutions are substituted to the above equations of motions, equation 4.5, 4.6, 4.8, 4.9, and 4.11. In the following subsections, the derivation for each individual structure element in the frequency domain are performed.

4.4. PLATE DERIVATION IN FREQUENCY DOMAIN

Since the solutions from the Fourier transform are obtained, the plate equation of motion can be converted into the frequency domain. By substituting equation 4.34 into equation 4.4, the governing equation of motion is altered to the frequency domain, and static motion can be separated from the equations. This procedure is carried out in the same manner as the two-dimensional model in Section 3.3.

From the two-dimensional model, one can learn how to obtain the shape functions of the structure. The calculation is performed by considering the governing equations as *homogeneous equations*. These homogeneous equations disregard liquid or external load in the equations. Afterwards, using the matching modal analysis, the coupling of the liquid and the structure are solved with orthogonality principle. By using the solution in the frequency domain, the plate equation of motion can be derived as follows:

$$D_p \nabla^4 \cdot \tilde{W}(r,\theta) - \rho_p h_p \omega^2 \tilde{W}(r,\theta) + k \cdot \tilde{W}(r,\theta) = 0 \tag{4.37}$$

By introducing β_p, the equation can be simplified into the following form:

$$\begin{aligned} \nabla^4 \cdot \tilde{W}(r,\theta) - \beta_p^4 \tilde{W}(r,\theta) &= 0 \\ \beta_p &= \left(\frac{\rho_p \cdot h_p \omega^2 - k}{D_p}\right)^{\frac{1}{4}} \end{aligned} \tag{4.38}$$

The equation above can also be mathematically simplified as in the following equation:

$$\begin{aligned} (\nabla^2 + \beta_p^2)(\nabla^2 - \beta_p^2)\tilde{W}(r,\theta) &= 0 \\ (\nabla^2 \pm \beta_p^2)\tilde{W}(r,\theta) &= 0 \end{aligned} \tag{4.39}$$

From the equation above, it can be seen that $\tilde{W}$ is depended on both variables r and θ. Therefore the **separation method of variables** is introduced. The thorough details of the derivation continues in the Appendix

E in subsection E.2.1. From this section the circular plate solution is defined as follows

$$\tilde{W}_r(s) = \sum_{p=0}^{\infty} (L_p \cdot J_p(\beta_p r) + M_p \cdot I_p(\beta_p r)) \cos(p\theta) \tag{4.40}$$

The constants L_p and M_p are the unknown parameters that are solved later in the *eigenvalue analysis*. The variables J_p and I_p are the first kind and the second kind of Bessel function respectively [1]. The constant p is an integer and starts from 0. The derivation that results in the constant p into integer values is shown in equation E.23. The index zero on p means the **axisymmetric modes**. Meanwhile the other value of p such as $1,2,3,..$ is defined as the **asymmetric modes**. The p is called as the *Diametral mode number*. The more detailed depiction of the diametral mode number of the plate is shown in figures 4.12 and 4.13.

4.5. CYLINDRICAL SHELL IN FREQUENCY DOMAIN

Since the Fourier transform is performed to obtain the solution, the cylindrical shell equations of motion can be calculated in the frequency domain. Similarly with the plate derivation, the cylindrical shell equations of motion are separated into dynamic part and static part. Afterwards, both result can be superimposed to find the total response. This separation only can be performed if it is assumed that the initial stress due to static load is small and the structure is a self-balanced structure toward the static load. From the two-dimensional model, one understands that to obtain the shape function the equation is evaluated as a homogeneous equation, first. Then the interaction between liquid and the structure is solved using orthogonality.

One can assume that the load and the structure have the same form, in which the structure solutions are written in the following expressions:

$$\begin{aligned} \tilde{u}_z &= \sum_{j=0}^{\infty} \tilde{U}_z(z) \cos(j\theta) \\ \tilde{u}_\theta &= \sum_{j=0}^{\infty} \tilde{U}_\theta(z) \sin(j\theta) \\ \tilde{u}_r &= \sum_{j=0}^{\infty} \tilde{U}_r(z) \cos(j\theta) \end{aligned} \tag{4.41}$$

Once again the value of j is an integer to satisfy the additional boundary condition that:

$$\cos(j \cdot 0) = \cos(j \cdot 2\pi) \tag{4.42}$$

The constant j can also be defined as the *circumferential modes number*. The cylindrical shell modes are also divided into two types of modes which are the axisymmetric and the asymmetric modes. In Figure 4.12 and 4.13, the different between the two are represented.

4.5.1. ASYMMETRIC MODES

For the asymmetric modes, the integer j is a non zero value. This non zero value produced the asymmetric vibration (see Figure 4.13).

From the previous section, it is already discussed that the equation of motion is entirely coupled in three axes. Therefore decoupling needed to be performed. The detailed derivation of the decoupling for the cylindrical shell is defined in the E in the section E.2.2. Decoupling the equation will result in the 8th order of differential equations. The result of the decoupled expression is rewritten in here :

$$F_8\lambda^8 + F_6\lambda^6 + F_4\lambda^4 + F_2\lambda^2 + F_0 = 0 \tag{4.43}$$

Since the equation is expressed in the eight order differential equation, the quantity of the unknown constant have the same amount as the order which is **eight constants**. The solution that resulted from decoupling is

defined in the following terms:

$$\begin{aligned}\tilde{U_{rj}}(z) &= \sum_{b=1}^{8} A_{jb} \exp(\lambda_{jb} \cdot z) \\ \tilde{U}_{\theta j}(z) &= \sum_{b=1}^{8} \delta_{jb} \cdot A_{jb} \exp(\lambda_{jb} \cdot z) \cdot \tilde{U}_{rj}(z) \\ \tilde{U}_{zj}(z) &= \sum_{b=1}^{8} \gamma_{jb} \cdot A_{jb} \exp(\lambda_{jb} \cdot z) \cdot \tilde{U}_{rj}(z)\end{aligned} \tag{4.44}$$

The variables A_{jb} are the unknown asymmetric constants. These constants are solved in the eigenvalue analysis process. The parameter δ_{jb} and γ_{jb}, are obtained from the equation E.44.

4.5.2. AXISYMMETRIC MODES

Meanwhile, for the axisymmetric modes, the integer j is always zero. Substituting the $j = 0$ to equation 4.41 results in the following:

$$\begin{aligned}\tilde{u}_{z0} &= \tilde{U}_{z0}(z) \\ \tilde{u}_{\theta 0} &= 0 \\ \tilde{u}_{r0} &= \tilde{U}_{r0}(r)\end{aligned} \tag{4.45}$$

The step for decoupling the axisymmetric modes has the same procedure as the decoupling of asymmetric modes in the E. Since no motion that depends on θ, the final equation of motion is not in the eighth order differential equation. The equation results in **sixth order differential equation** under the following expression:

$$H_6\lambda^6 + H_4\lambda^4 + H_2\lambda^2 + H_0 = 0 \tag{4.46}$$

As the order of the differential equation above is six, the number of unknown constants are the same as the order.

$$\begin{aligned}\tilde{U_{r0}}(z) &= \sum_{b=1}^{6} A_{0b} \exp(\lambda_{0b} \cdot z) \\ \tilde{U}_{\theta 0}(z) &= 0 \\ \tilde{U}_{z0}(z) &= \sum_{b=1}^{6} \gamma_{0b} \cdot A_{0b} \exp(\lambda_{0b} \cdot z) \cdot \tilde{U}_{r0}(z)\end{aligned} \tag{4.47}$$

The parameter A_{0b} are the unknown constants for the axisymmetric modes. The variable γ_{0b} defines the relation between $\tilde{U}_{r0}$ and $\tilde{U}_{z0}$.

The following figures depict the general modes shape for both the circular plate and the cylindrical shell:

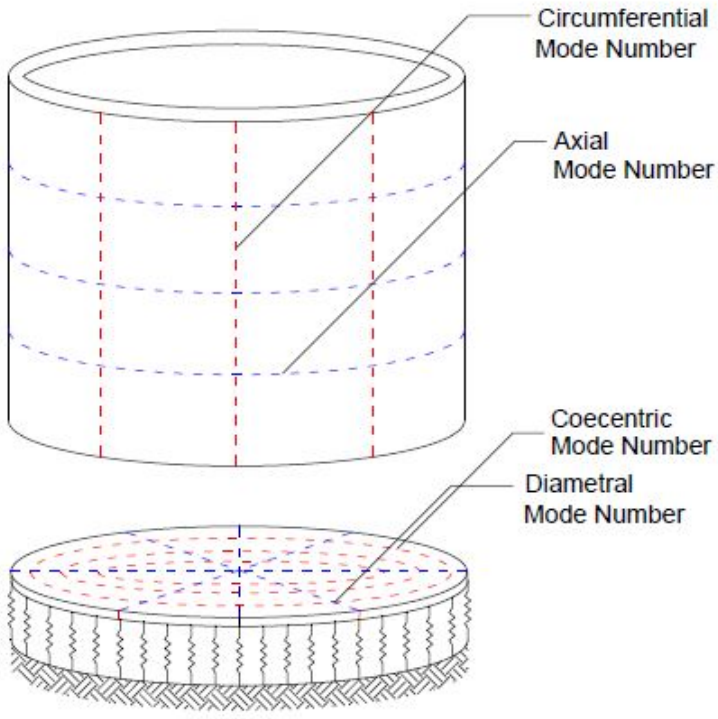

Figure 4.12: Cylindrical Shell and Circular Plate mode number

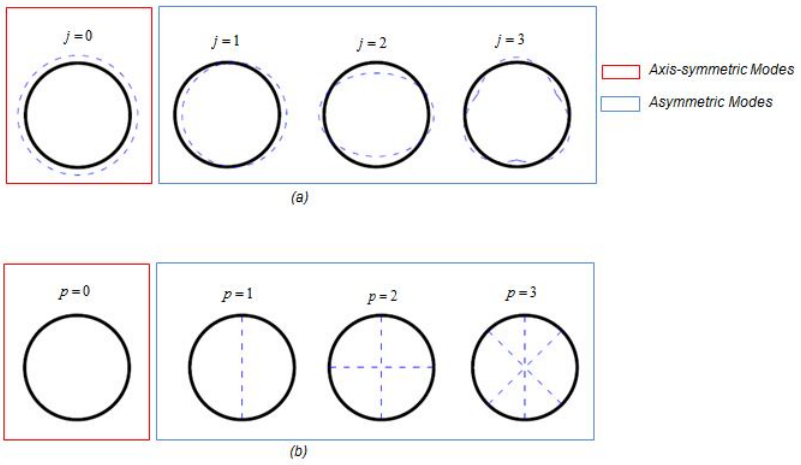

Figure 4.13: Axisymmetric and Asymmetric in both structural systems : (a) Cylindrical Shell (b) Circular Plate

To obtain the concentric mode number for the circular plate and the axial mode number for the cylindrical shell, the boundary conditions and the interface conditions of the internal structure are needed to be solved in the eigenvalue analysis. For the shell in every circumferential mode number, there is a set of infinity amount of axial mode numbers. For the plate, in every diametral mode number, it will have an infinite amount of concentric mode numbers.

The final solution of the cylindrical shell is written in the following:

$$\begin{aligned}\tilde{u}_z &= \sum_{j=0}^{\infty}\sum_{a=0}^{\infty}\tilde{U}_z[j,a](z)\cos(j\theta)\\ \tilde{u}_\theta &= \sum_{j=0}^{\infty}\sum_{a=0}^{\infty}\tilde{U}_\theta[j,a](\theta)\sin(j\theta)\\ \tilde{u}_r &= \sum_{j=0}^{\infty}\sum_{a=0}^{\infty}\tilde{U}_r(r)[j,a]\cos(j\theta)\end{aligned} \tag{4.48}$$

And the final solution of the circular plate is written as follows:

$$\tilde{W}_r(s) = \sum_{p=0}^{\infty}\sum_{a=0}^{\infty}(L[p,a]\cdot J_p(\beta[p,a]r) + M_[p,a]\cdot I_p(\beta[p,a]r))\cos(p\theta) \tag{4.49}$$

Since the plate and the wall are solved together, therefore one can simply say that $j = p$.

4.6. LIQUID DERIVATION IN FREQUENCY DOMAIN

As explained in Appendix C, the potential flow of the liquid consists of a Laplace derivation and potential velocity. The liquid flow motion is described in the equation C.20. However, for the three-dimensional model, the Laplace derivation is no longer in Cartesian coordinates but in the cylindrical coordinates. In general, the potential flow by using the curvilinear coordinates can be written as follows:

$$\nabla^2\tilde{\phi} = 0\nabla^2(\cdot) = \frac{1}{A_1A_2A_3}\left[\frac{\partial(\cdot)}{\partial\alpha_1}\left(\frac{A_2A_3}{A_1}\frac{\partial(\cdot)}{\partial\alpha_1}\right) + \frac{\partial(\cdot)}{\partial\alpha_2}\left(\frac{A_3A_1}{A_2}\frac{\partial(\cdot)}{\partial\alpha_2}\right) + \frac{\partial(\cdot)}{\partial\alpha_3}\left(\frac{A_1A_2}{A_3}\frac{\partial(\cdot)}{\partial\alpha_3}\right)\right] \tag{4.50}$$

For a cylindrical coordinate, it is known that:

$$\begin{aligned} \alpha_1 = r \quad \alpha_2 \quad &= \theta \\ \alpha_3 = x \quad A_1 \quad &= 1 \\ A_2 = r \quad A_3 \quad &= 1 \end{aligned} \tag{4.51}$$

Where the Laplace equation for Cylindrical coordinates are in the following expression:

$$\nabla^2 = \frac{\partial^2(\cdot)}{\partial r^2} + \frac{1}{r}\frac{\partial(\cdot)}{\partial r} + \frac{1}{r}\frac{\partial^2(\cdot)}{\partial\theta^2} + \frac{\partial^2(\cdot)}{\partial z^2} \tag{4.52}$$

For the further calculation, the coordinate system is expressed in a different formulation to solve the differential equation *(Bessel Function)* easier. The conversion of coordinate system is depicted in the figure below:

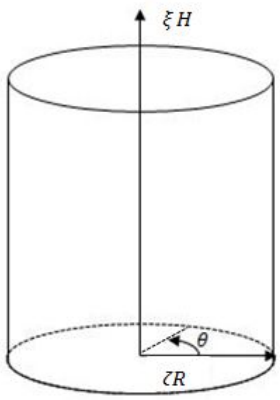

Figure 4.14: Converted Cylindrical coordinate

The coordinates are expressed under ratios:

$$\begin{aligned} \zeta &= r/R \\ \xi &= z/H \\ \alpha &= H/R \end{aligned} \tag{4.53}$$

By substituting the ratios to the Laplace equation in the cylindrical coordinates, the expression results as follows :

$$\nabla^2 = \frac{\partial^2(\cdot)}{\partial\zeta^2} + \frac{1}{\zeta}\frac{\partial(\cdot)}{\partial\zeta} + \frac{1}{\zeta^2}\frac{\partial^2(\cdot)}{\partial\theta^2} + \frac{1}{\alpha^2}\frac{\partial(\cdot)}{\partial\xi^2} \tag{4.54}$$

Similar to the procedure with the two-dimensional liquid derivation, the number of boundary conditions and the number constants are unbalance. Therefore, the liquid superposition is used to solve the imbalance issues. For the three dimensional model, instead of making two superpositions, the three superpositions are used due to several reasons. Firstly, because it is clearer and more simpler to derive the liquid equations. Moreover, it is less complicated to analyze the sloshing mode since it is already separated in the beginning. The liquid superpositions are described in the following figure:

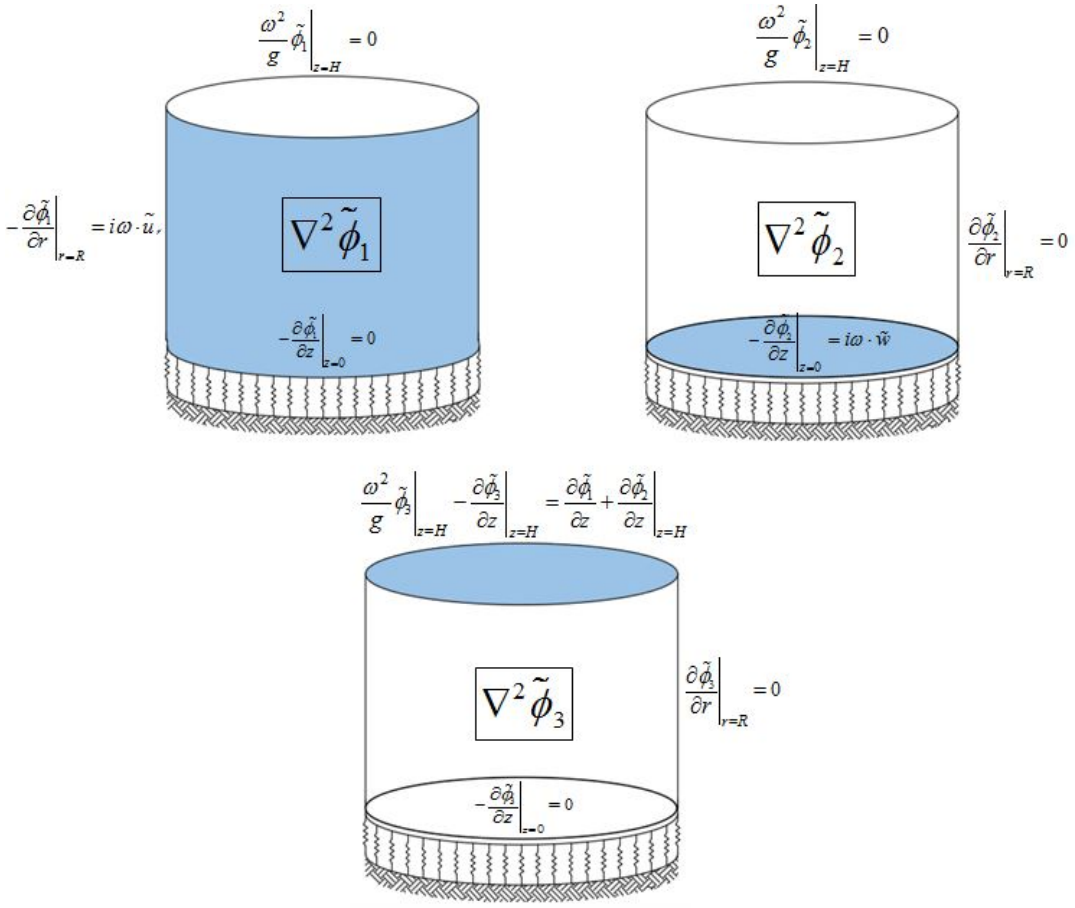

Figure 4.15: Superposition of Liquid in 3D model

The detail of the derivation is expressed in Appendix E in section E.3. To be short, the final equations that are achieved in the appendix are written as the following:

$$\begin{aligned}
&\tilde{\phi}(r,z,\theta) = \tilde{\phi}_1(r,z,\theta) + \tilde{\phi}_2(r,z,\theta) + \tilde{\phi}_3(r,z,\theta)\\
&\tilde{\phi}(r,z,\theta) = \sum_{n=1}^{\infty}\tilde{\phi}_{10n} + \sum_{n=1}^{\infty}\sum_{m=1}^{\infty}\tilde{\phi}_{1mn} + \tilde{\phi}_{200} + \sum_{n=1}^{\infty}\tilde{\phi}_{20n} + \sum_{n=1}^{\infty}\sum_{m=1}^{\infty}\tilde{\phi}_{2mn}\\
&\qquad + \tilde{\phi}_{300} + \sum_{n=1}^{\infty}\tilde{\phi}_{30n} + \sum_{n=1}^{\infty}\sum_{m=1}^{\infty}\tilde{\phi}_{3mn}
\end{aligned} \tag{4.55}$$

$$\begin{aligned}
&\tilde{\phi}_{10n}(r,z,\theta) = C_{l0n}\cdot I_0\Big(\frac{\pi(2n-1)r}{2H}\Big)\cos\Big(\frac{\pi(2n-1)z}{2H}\Big)\\
&\tilde{\phi}_{1mn}(r,z,\theta) = C_{lmn}\cdot I_m\Big(\frac{\pi(2n-1)r}{2H}\Big)\cos\Big(\frac{\pi(2n-1)z}{2H}\Big)\cos(m\theta)\\
&\tilde{\phi}_{200}(r,z,\theta) = A_{l00}(z-H)\\
&\tilde{\phi}_{20n}(r,z,\theta) = A_{l0n}\cdot\Big(\cosh(\varepsilon_{0n}z/R) + \frac{\sinh(\varepsilon_{0n}z/R)}{\tanh(\varepsilon_{0n}H/R)}\Big)J_0(\varepsilon_{0n}r/R)\\
&\tilde{\phi}_{2mn}(\zeta,\xi,\theta) = A_{lmn}\cdot\Big(\cosh(\varepsilon_{mn}z/R + \frac{\sinh(\varepsilon_{mn}z/R)}{\tanh(\varepsilon_{mn}H/R)}\Big)\cos(m\cdot\theta)J_m(\varepsilon_{mn}r/R)\\
&\tilde{\phi}_{300}(r,z,\theta) = B_{l00}\\
&\tilde{\phi}_{30n}(r,z,\theta) = B_{l0n}\cdot\big(\cosh(\varepsilon_{0n}z/R)\big)J_0(\varepsilon_{0n}r/R)\\
&\tilde{\phi}_{3mn}(r,z,\theta) = B_{lmn}\cdot\big(\cosh(\varepsilon_{mn}z/R)\big)\cos(m\cdot\theta)J_m(\varepsilon_{mn}r/R)
\end{aligned} \tag{4.56}$$

The symbol A_l, B_l, and C_l are the unknown liquid constants. These constants are solved through the liquid-structure matching modal analysis.

From the solution, it can be seen that the final equations have a similiar form as what *M. Amabili* writes in his journal [2].

4.7. MATCHING MODAL ANALYSIS

Again, the same procedure which is the matching modal analysis is repeated in three-dimensional model (see flowchart in Figure 4.2). However, there are still the distinguished components in the three-dimensional model due to its complexity. The mode shapes consist of asymmetric mode and axisymmetric modes. These two modes are orthogonal to each other. Therefore, these modes can be solved separately, since they can be fully decoupled through orthogonality. *Bauer and Siekmann*[4] use this approach. In most of the cases, the asymmetric mode shape is governing compare to the axisymmetric modes since axisymmetric modes do not create overturning moment (see Figure 3.24).

From the two-dimensional model and also from the flowchart in Figure 4.2, one can understand that in matching modal analysis there are two input components. These two inputs are the structural shape and the liquid shape function. The liquid shape function is obtained from the equation 4.56. The structure shape function is obtained from the *eigenvalue analysis*.

Since the shape function are obtained from the homogeneous equation, the earthquake loadings are not yet be taken into consideration. With the same manner as the two-dimensional model, the earthquakes loadings are included in the shape function as rigid body translations.

THE CYLINDRICAL SHELL

$$\begin{aligned}
\underbrace{\tilde{u}_z(z,\theta,\omega)}_{\text{Total Displacement}} &= \underbrace{\sum_{j=0}^{\infty}\sum_{a=1}^{\infty}\tilde{U}c_{[j,a]}\times X_z[j,a](z)\times\cos(j\theta)}_{\text{Relative Displacement}} \\
\underbrace{\tilde{u}_\theta(z,\theta,\omega)}_{\text{Total Displacement}} &= \underbrace{\sum_{j=0}^{\infty}\sum_{a=1}^{\infty}\tilde{U}c_{[j,a]}\times X_\theta[j,a](z)\times\sin(j\theta)+\tilde{u}_e\cos(\theta)}_{\text{Relative Displacement}} \\
\underbrace{\tilde{u}_r(z,\theta,\omega)}_{\text{Total Displacement}} &= \underbrace{\sum_{j=0}^{\infty}\sum_{a=1}^{\infty}\tilde{U}c_{[j,a]}\times X_r[j,a](z)\times\cos(j\theta)+\tilde{u}_e\sin(\theta)}_{\text{Relative Displacement}}
\end{aligned} \tag{4.57}$$

THE CIRCULAR PLATE

$$\underbrace{\tilde{w}(r,\theta,\omega)}_{\text{Total Displacement}} = \underbrace{\sum_{j=0}^{\infty}\sum_{a=1}^{\infty}\tilde{U}c_{[j,a]}\times X_w[j,a](r)\times\cos(j\theta)+\tilde{w}_e}_{\text{Relative Displacement}} \tag{4.58}$$

The constants Uc are the unknown amplitudes. These unknown amplitudes are later obtained from solving the matching modal analysis. The symbols X_z, X_θ, X_r, and X_w are the shape functions that are obtained from the eigenvalue analysis.

Before going deeper to the matching modes, the orthogonality of an the structure can be defined as the following expression which is:

$$\begin{aligned}
&\int_0^H\int_0^{2\pi}\tilde{u}_{\theta_{ja}}(z,\theta)\cdot\tilde{u}_{\theta_{ow}}(z,\theta)dzd\theta+\int_0^H\int_0^{2\pi}\tilde{u}_{r_{ja}}(z,r)\cdot\tilde{u}_{r_{ow}}(z,\theta)dzd\theta+ \\
&\int_0^H\int_0^{2\pi}\tilde{u}_{z_{ja}}(z,r)\cdot\tilde{u}_{z_{ow}}(z,\theta)dzd\theta+\int_0^H\int_0^{2\pi}\tilde{w}_{ja}(z,r)\cdot\tilde{w}_{ow}(z,\theta)dzd\theta=\Gamma\delta_{po}\delta_{vw}
\end{aligned} \tag{4.59}$$

Where form the orthogonality principle is if $j\neq o$ and $a\neq w$ the result equals to 0. This statement is written in the above equations as *Kronecker delta* δ_{po} and δ_{vw}. Likewise in the previous the two-dimensional model,

the orthogonality is defined in the full path. From this equation, one can draw a conclusion that axisymmetric and asymmetric modes can be fully separated into the different set of equations. Moreover, each asymmetric mode can also be separated for each j. This is due to these constant are integers and orthogonal for every different j.

The matching modes of axisymmetric and asymmetric modes in the governing equations are discussed in subsection **??**. In this thesis the only first three circumferential mode number are taken into account. The reason behind this decision is based that on only the fundamental circumferential mode number gives a significant contribution. The contribution can be seen mathematically in the orthogonality principle (see section E.4.2).

In short, the kinematic boundary conditions of the liquid structure interaction and the equations of motion can be defined in the following matrix:

$$\underline{\underline{\mathbf{L}}} \times \begin{bmatrix} C_{l0(n+1)} \\ C_{l1(n+1)} \\ C_{l2(n+1)} \\ C_{l3(n+1)} \\ \\ A_{l0n} \\ A_{l1n} \\ A_{l2n} \\ A_{l3n} \\ \\ B_{l0n} \\ B_{l1n} \\ B_{l2n} \\ B_{l3n} \\ \\ U_{c0n} \\ U_{c1a} \\ U_{c2a} \\ U_{c3a} \end{bmatrix} = \underline{\mathbf{B}} \tag{4.60}$$

This matrix will be populated with both orthogonal and non-orthogonal values.The value of n starts from 0. The value of a starts from 1.

4.8. REVIEW FOR CHAPTER 4

From the analytical derivation there are some points that can be learned for the cylindrical shell, circular plate, and liquid components

- **Plate Concentric and Diameter mode number**
  Plate mode number consist of two types which are the concentric and diametric mode numbers. The plate concentric mode numbers are varies along the θ axis. In every concentric mode number, there is a set of an infinite diametric mode numbers.

- **Shell Circumferential and Axis mode number**
  Similarly with the plate, since the shell also three dimensional therefore it also consists of two different mode numbers. The circumferential mode numbers coresponds to the θ direction. Meanwhile, the axial mode number is along the z-axis. In every circumferential mode, there is a set of infinite axis mode number.

- **Structure and Liquid Axisymmetric and Asymmetric mode**
  In the whole structure, there is an axisymmetric mode, where the index of circumferential and concentric mode number equals to 0 regardless what the axis and diametric mode number. If the two circumferential and concentric mode number does not equal to 0, the mode will be an asymmetric mode.

In the previous section is already discussed the definition of both axisymmetric mode and asymmetric mode, one can realize that the two modes are completely orthogonal to each other. Therefore the calculation between the two can be completely decoupled.

5

THREE DIMENSIONAL MODEL AND DISCUSSION

This chapter covers the three-dimensional modeling and sensitivity study of the system. The outline of this chapter is described in the following list:

- ***The tank Properties***
  In this section the tank geometry and structure element properties are written down and illustrated.
- ***Introduction of Shell Vibration***
  This section will discuss the introduction of shell vibration modeling. The purpose of this introduction is to have a better comprehension and to validate each structural element. This section is the application of the equations that we derive in Section 4.
- ***Modeling and Results***
  This third section will cover both the modeling and results. How the liquid and structure interaction works given the assigned properties is also discussed in this chapter.
- ***Parameter Studies***
  The parameter studies are devoted to analyze the sensitivity of the liquid-structure interaction on these following parameters:
  - *Tank Geometry*
  - *Structural Flexibility*
  - *Liquid Volume*

5.1. PROPERTIES DEFINITION

Most of the liquid tanks are built with tapered thickness for the wall and the plate (Source: www.tankconnection.com). By considering the structure element with variable thickness, we can obtain benefits in term of structure and economic perspective. The static pressure of any material is zero at the top and higher on the bottom. Therefore, it would be more convenient to have the wall is thicker at the bottom and thinner at the top. In the subsequent pictures, the example of a steel liquid storage tank are presented:

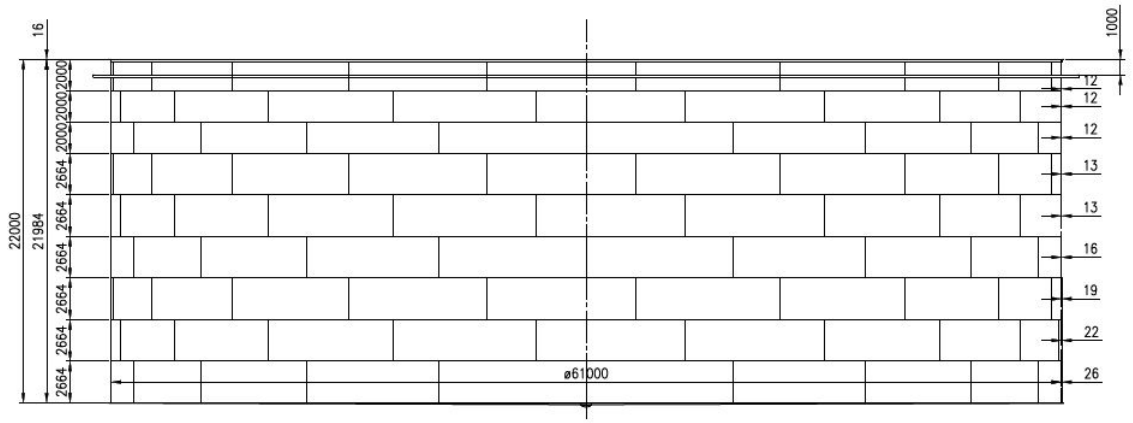

Figure 5.1: Cylindrical shell cross section
Source : Witteveen+Bos

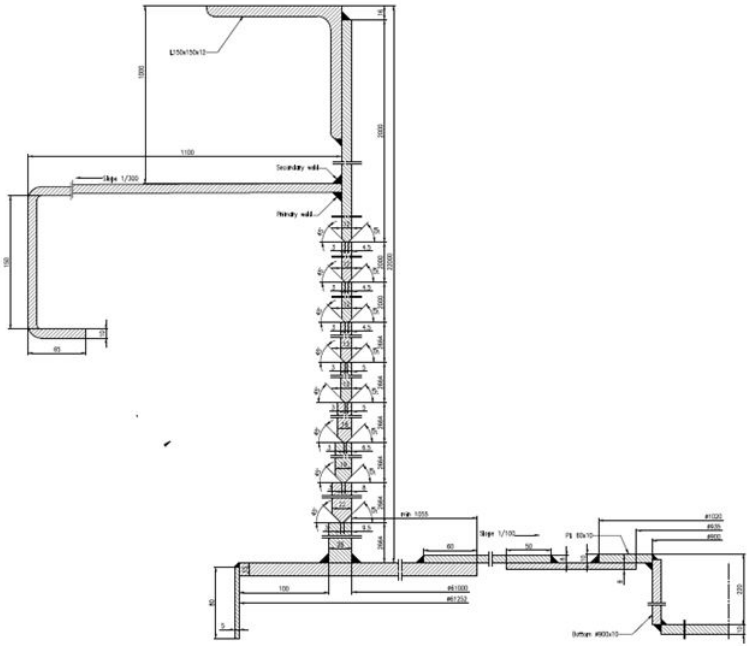

Figure 5.2: Dimension of the wall and bottom plate
Source: Witteveen+Bos

However, this model only uses a uniform thickness for simplification. This decision is justified as according to Eurocode [5], the tapered thickness can be simplified, by representing it with an approximation of equivalent value. This equivalent thickness is the thickness of the wall on one third from the bottom.

The tank data obtained from *Witteveen+Bos* are summarized in the following table:

Table 5.1: Case Study Properties

Properties	Value	Unit
A. General Properties		
Height (H)	22	m
Radius (R)	31	m
Gravitational acceleration (g)	9.81	m/s^2
B. Liquid Properties		
Water Density (ρ_l)	1.00	ton/m^3
C. Wall Properties(Steel)		
Uniform Wall Thickness (h_w)	19	mm
Young's Modulus (E_w)	200,000,000	kN/m^2
Mass Density (ρ_w)	7.85	ton/m^3
Poisson Ratio (μ)	0.27	ton/m^3
D. Plate Properties(Steel)		
Uniform Plate Thickness (h_p)	15	mm
Young's Modulus (E_p)	200,000,000	kN/m^2
Mass Density (ρ_p)	7.85	ton/m^3
Poisson Ratio (μ_p)	0.27	–
Average soil stiffness (k_p)	40,000	kN/m^2

5.2. INTRODUCTION OF SHELL VIBRATION

Before modeling the whole structure, let us validate the individual structural element. This decision is made for the purpose to avoid any mistakes in the entire structure and to give a better comprehension on how the structural element will vibrate.

5.2.1. PLATE

Since the model is not derived entirely with an analytical method, the plate modeling is validated using a reference from literature written by Soedel [16] as an analytical reference. The natural frequency that Soedel derived is the clamped in the edges of the circular plate. The plate is modeled as the clamped edges in this subsection only in order to have an equal comparison to the reference. The boundary conditions are neither rotation nor displacement at $r = R$. The clamped condition is depicted in the following figure:

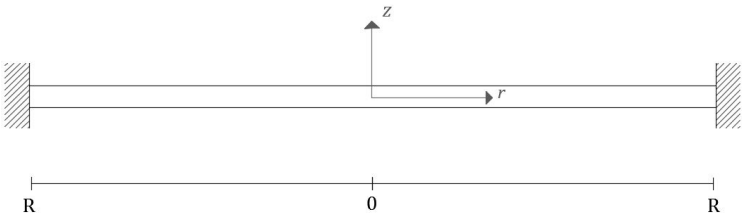

Figure 5.3: Circular plate clamped in the edges

The comparison model between the reference and present work is summarized in the following table:

Table 5.2: Comparison plate vibration frequency

Soedel	**p=0**	**p=1**
n=1 (rad/s^2)	0.241	0.50
n=2 (rad/s^2)	0.939	1.43
n=3 (rad/s^2)	2.105	2.836
Present Study	**p=0**	**p=1**
n=1 (rad/s^2)	0.241	0.50
n=2 (rad/s^2)	0.939	1.43
n=3 (rad/s^2)	2.105	2.836

From Table 5.2, we can see that the difference between the present calculation and what Soedel has calculated is 0.1%. This error gap is from the numerical error and considered acceptable in this thesis. Therefore, the equations and derivations that we have derived for the circular plate in Chapter 4 are verified.

This section also provides the modes shape vibration for both axisymmetric and asymmetric modes to give an idea on the plate vibration. The numerical computation and programming is programmed in *Matlab* software. Here are the following result for the **axisymmetric mode** shape which is obtained from the index $p = 0$:

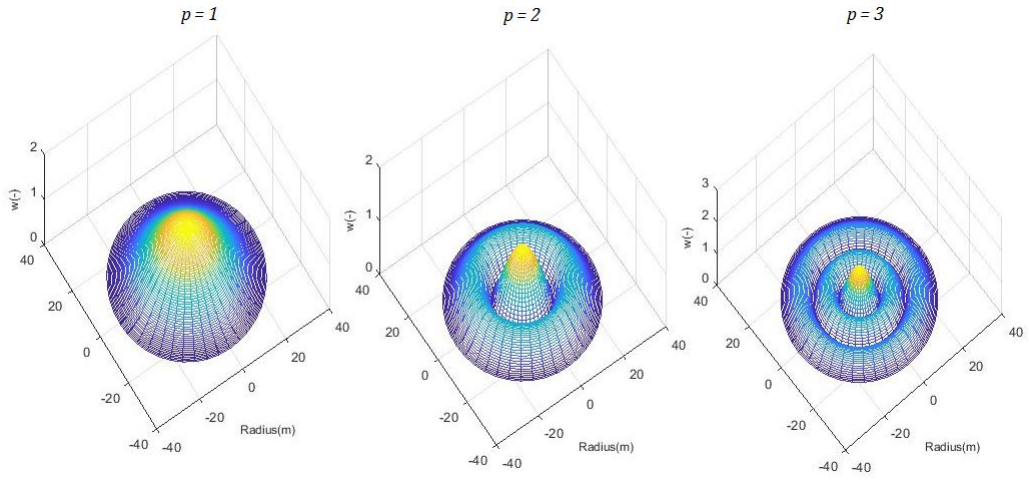

Figure 5.4: Axisymmetric mode shape from Matlab with diametrical mode number(p) = 0

Next, the result of the asymmetric mode is plotted in the following graphs:

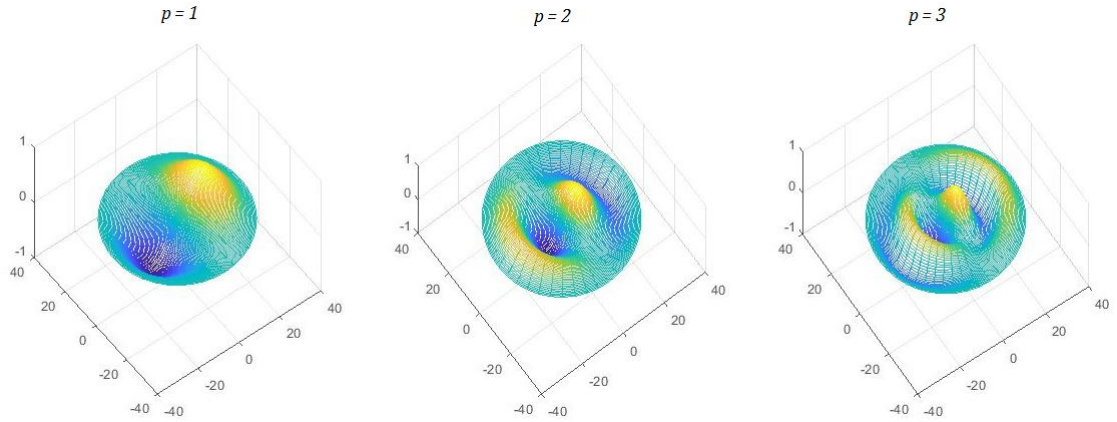

Figure 5.5: Asymetric mode shape with diametrical mode number (p) = 1

From Figure 5.4 and Figure 5.5, we can now differentiate between the concentric and diametrical mode number which previously shown in Figure 4.13. These figures also give us an idea how do the axisymmetric and asymmetric modes behave. Therefore one can relate these figure with the predefined term for the *concentric* and *diametrical mode number* in Figure 4.13.

5.2.2. CYLINDRICAL SHELL (WALL)

The entire model is solved using the semi-analytical method. This term is used due to it is hardly possible to solve the shell with a pure analytical method due to the complexity of the equations. To perform the eigen-analysis, numerical approach is introduced for an efficient and faster performance.

The structure is validated using help from structural program SAP 2000. The model that is used is a **clamped-free cylindrical shell.**. The system is depicted in the following figure:

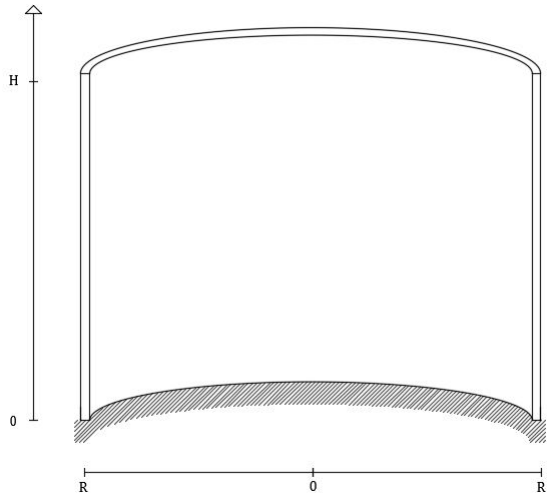

Figure 5.6: The clamped-free cylindrical shell

The boundary conditions of the system in Figure 5.6 are composed in the following lists:

1. **Tangential displacement = 0, at** $z = 0$

$$u_z(z,\theta,t)\Big|_{z=0} = 0 \tag{5.1}$$

2. **Radial displacement = 0, at** $z = 0$

$$u_r(z,\theta,t)\Big|_{z=0} = 0 \tag{5.2}$$

3. **Axial displacement= 0, at** $z = 0$

$$u_z(z,\theta,t)\Big|_{z=0} = 0 \tag{5.3}$$

4. **Rotation = 0, at** $z = 0$

$$\beta_z(z,\theta,t)\Big|_{z=0} = 0 \tag{5.4}$$

5. **Normal Force = 0, at** $z = H$

$$N_{zz}(z,\theta,t)\Big|_{z=H} = 0 \tag{5.5}$$

6. **Moment Force = 0, at** $z = H$

$$M_{zz}(z,\theta,t)\Big|_{z=H} = 0 \tag{5.6}$$

7. **Shear Force Effective First Kind = 0, at** $z = H$

$$V_{zr}(z,\theta,t)\Big|_{z=H} = 0 \tag{5.7}$$

8. **Shear Force Effective First Kind = 0, at** $z = H$

$$V_{zr}(z,\theta,t)\Big|_{z=H} = 0 \tag{5.8}$$

Since the calculation for the clamped system is more straightforward than with the inclusion of the plate, the algorithm to perform eigenvalue analysis is explained for the clamped system. Firstly substitute the solution in the equation 4.44 into the boundary condition. The equation 4.44 consists of eight constants for asymmetric modes. From the boundary condition, a matrix with $8x8$ in size can be derived for each circumferential mode:

$$\underbrace{\underline{\underline{\mathbf{BC}}}}_{\text{Boundary Condition Matrix}} \times \underbrace{\underline{A}}_{\text{Constants Vector}} = 0 \tag{5.9}$$

$$\begin{bmatrix} BC_1(\omega) \\ BC_2(\omega) \\ BC_3(\omega) \\ BC_4(\omega) \\ BC_5(\omega) \\ BC_6(\omega) \\ BC_7(\omega) \\ BC_8(\omega) \end{bmatrix} \times \begin{bmatrix} A_1 \\ A_2 \\ A_3 \\ A_4 \\ A_5 \\ A_6 \\ A_7 \\ A_8 \end{bmatrix} = \mathbf{0} \tag{5.10}$$

To perform the eigenvalues analysis, we have to obtain which ω that results to $det(\underline{\underline{\mathbf{BC}}}) = 0$. However, within such complex equation with eight constants, it is hardly possible to achieve ω analytically. Therefore, the numerical process is introduced: the value ω is numerical and real variable from zero to a certain value.

In the following table will be discussed the comparison between the present study and the SAP 2000.

Table 5.3: Cylindrical Shell Natural Frequency Comparison with SAP 2000

Present	**m=0**	**m=1**	**m=2**	**m=3**
n=1 (Hz)	25.81	19.26	13.06	9.12
n=2 (Hz)	25.99	25.39	23.70	20.96
n=3 (Hz)	26.02	25.77	25.13	24.11
SAP 2000	**m=0**	**m=1**	**m=2**	**m=3**
n=1 (Hz)	25.65	19.07	12.92	9.06
n=2 (Hz)	25.73	25.38	23.72	21.07
n=3 (Hz)	25.80	25.65	25.02	24.21

The circumferential mode is represented as the value of m. Meanwhile, in this table, the axial mode number is symbolized as n. The average error between the two comparisons is 0.54% in a gap. For this thesis, the value of the error between the two is considered well-fitted. The numerical error of 0.54% results from the different step that is used and also the meshing for the software program. To achieve better result smaller step and smaller meshing can result in a convergence between the two. The mode shapes of a clamped system are shown in the following figures:

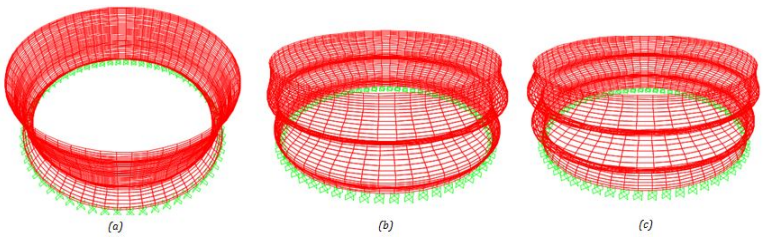

Figure 5.7: Mode shape with *circumferential* mode number(m) = 0 from SAP 2000, (a) axis mode number 1 ;(b) axis mode number 2 ;(c) axis mode number 3

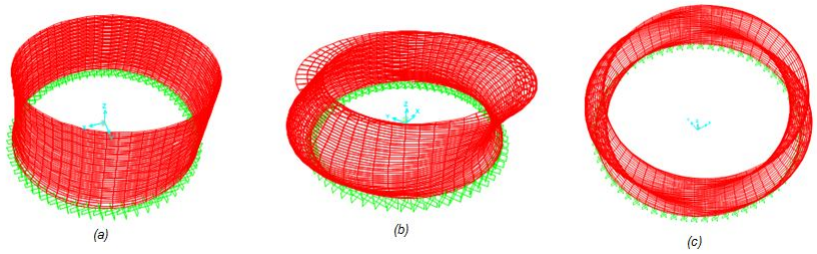

Figure 5.8: Mode shape with *circumferential* mode number(m) = 1 from SAP 2000, (a) axis mode number 1 ;(b) axis mode number 2 ;(c) axis mode number 3

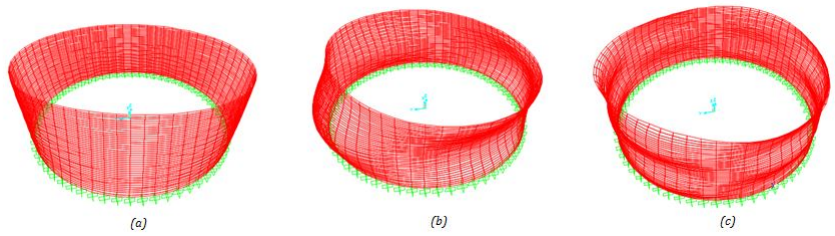

Figure 5.9: Mode shape with *circumferential* mode number(m) = 2 from SAP 2000, (a) axis mode number 1 ;(b) axis mode number 2 ;(c) axis mode number 3

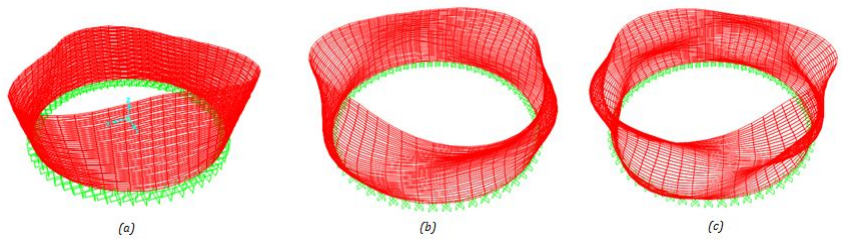

Figure 5.10: Mode shape with *circumferential* mode number(m) = 3 from SAP 2000, (a) axis mode number 1 ;(b) axis mode number 2 ;(c) axis mode number 3

The mode shapes that are derived in this thesis are plotted in the following:

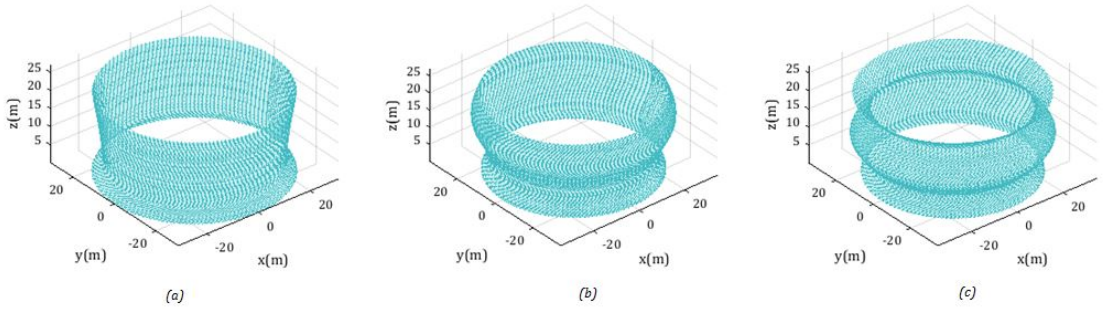

Figure 5.11: Mode shape with *circumferential* mode number(m) = 0 from Matlab, (a) axis mode number 1 ;(b) axis mode number 2 ;(c) axis mode number 3

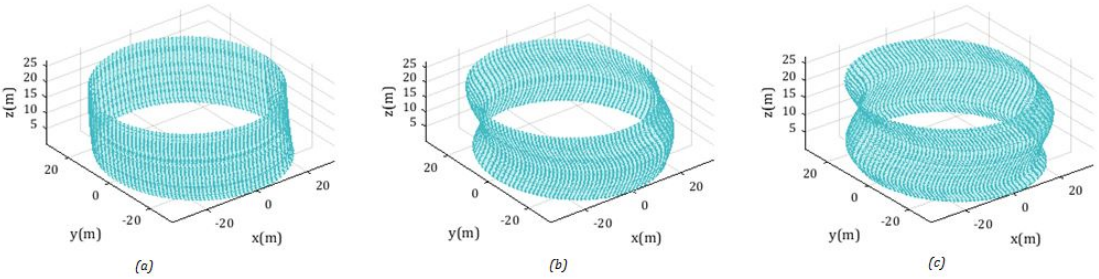

Figure 5.12: Mode shape with *circumferential* mode number(m) = 1 from Matlab, (a) axis mode number 1 ;(b) axis mode number 2 ;(c) axis mode number 3

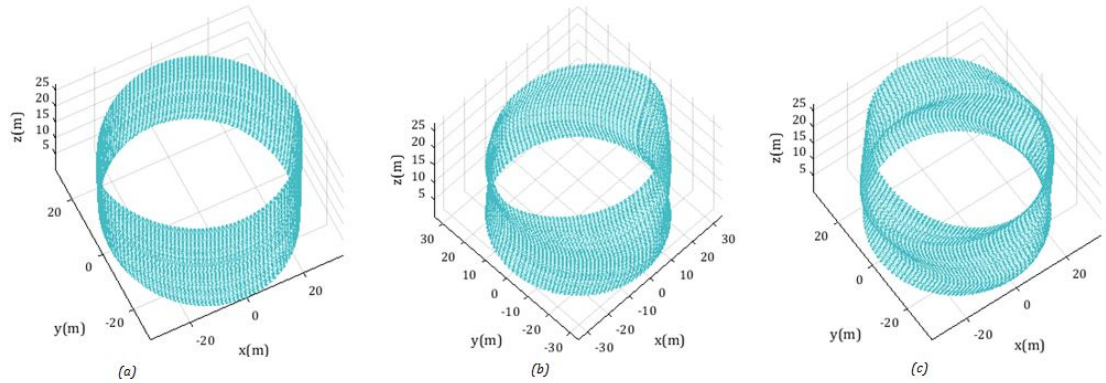

Figure 5.13: Mode shape with *circumferential* mode number(m) = 2 from Matlab, (a) axis mode number 1 ;(b) axis mode number 2 ;(c) axis mode number 3

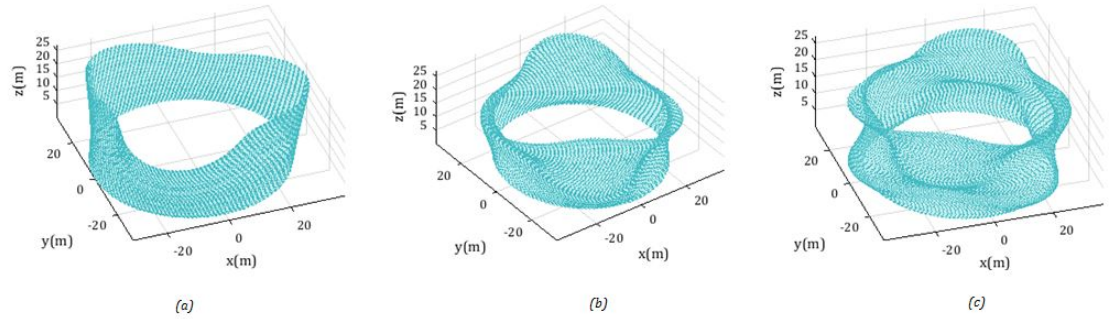

Figure 5.14: Mode shape with *circumferential* mode number(m) = 3 from Matlab, (a) axis mode number 1 ;(b) axis mode number 2 ;(c) axis mode number 3

From these figures, we can see the resemblance between the mode shapes that are obtained from the SAP 2000 and from the model in this thesis (Matlab). We can understand also the difference between the circumferential-mode and the axial mode number just as the Figure 4.13 depicted.

5.3. MODELING AND RESULT

This section consists of the result and discussion of the three-dimensional model. The first results that are presented here are the empty tank. After the discussion of the empty tank, the results of the filled tank are discussed next. Even though the plate thickness is $15mm$, the plate is concreted and the soil stiffness also play roles in the system. Based on the previous statement, one can roughly simplified the model as clamped-free cylindrical shell. However, a conservative approach that can be done is cooperating the slab and the soil structure interaction. The value of soil stiffness $40000kN/m^2$ is already included the concrete slab in the bottom of the tank. The slab incorporation are also more versatile for different tank geometry. This versatility is due to for larger tanks the plate is only resting in compacted soil and without concrete. Due to this explanation, the model that will be performed are these two models, which are the clamped shell and the plate incorporation.

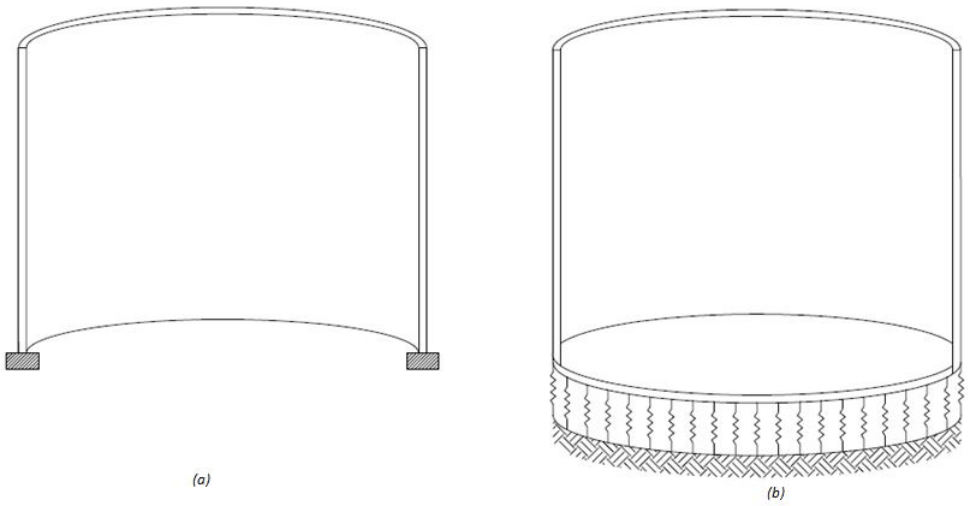

Figure 5.15: The two model that will be used (a) Model A: Clamped Cylindrical Shell; (b) Model B: Cylindrical Shell with Plate

In the process flowchart (see Figure 4.2), it can be seen that the mode numbers are inputted until the kinematic boundary conditions achieve convergence. Therefore before entering the result, let us decide the number of modes for both liquid and structure. This thesis uses ten mode numbers for structural axial mode numbers and three mode numbers for structural circumferential mode numbers. The circumferential mode number is based on the mathematical reason from the statement in Section E.4.2 which is: *only the fundamental circumferential mode number gives the significant contribution to the seismic loading.* Therefore, the circumferential-mode number is limited to three mode numbers with the purpose of still taking into account the effect of higher circumferential mode number while saving computing time. For the structural axial mode numbers, they are obtained from the rule of thumb: for modal analysis, the number of modes is at least **two times the load's frequency range**.

However, there is no restriction on the liquid mode numbers. Therefore for this thesis, the liquid mode numbers are defined in the following list:

ϕ_1 *(the wall-liquid coupled potential)*	= 100 mode numbers;
ϕ_2 *(the plate-liquid coupled potential)*	= 100 mode numbers;
ϕ_3 *(the sloshing potential)*	= 3 mode numbers;

To have an accurate result with an efficient program, the structure-liquid mode (ϕ_1 and ϕ_2) uses 50 mode number meanwhile the sloshing mode uses only three mode number. This difference in number for sloshing mode number is due to the sloshing on earthquake loading has small effect as it located in the long period. Therefore, the sloshing potential is limited to three mode numbers to have less expensive computing time.

Please note that this number is not a definitive number and can change for other different cases. Therefore convergence check is needed to be performed at the end (see process flowchart in Figure 4.2).

5.3.1. EIGENVALUE ANALAYSIS FOR EMPTY TANK

Since the plate in the Model A is considered rigid in the three directions, which are θ, radial, and axial axis the frequency that will be expected is higher compare to the Model B. For the model B the plate is modeled lies in a Winkler foundation that incoorperate the concreting and the soils stiffness. The Model B will be less stiff compared to Model A. Here are the following natural frequency for each model

Table 5.4: Model A and Model B eigenvalue analysis

Model A	**m=0**	**m=1**
n=1 (Hz)	25.81	19.266
n=2 (Hz)	25.99	25.407
n=3 (Hz)	26.01	25.780
n=4 (Hz)	26.03	25.926
n=5 (Hz)	26.07	26.008
Model B	**m=0**	**m=1**
n=1 (Hz)	7.90	6.721
n=2 (Hz)	25.97	22.655
n=3 (Hz)	26.00	25.407
n=4 (Hz)	26.01	25.806
n=5 (Hz)	26.03	25.926

From these natural frequencies, we can see that the Model B is more flexible than the Model A. Since the natural frequency is almost 3 times smaller, therefore using Model A which is a simplification from Model B is overestimating the stiffness of the Winkler foundation. Therefore Model B would be a better representation compare to the Model A. In the following figures are shown the Model B mode shapes both axisymmetric and asymmetric modes:

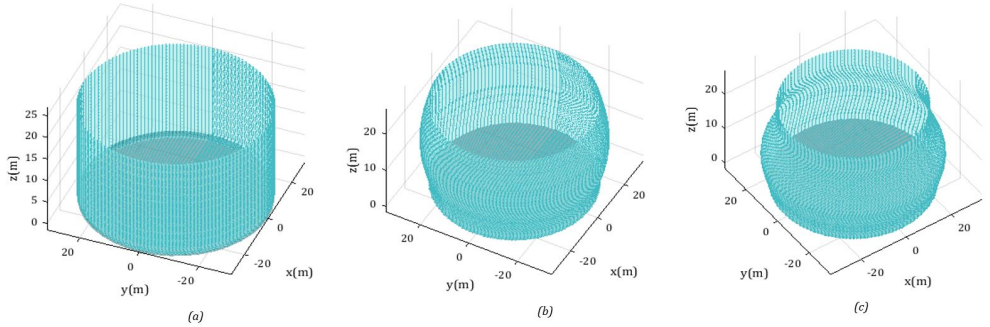

Figure 5.16: Model B mode shape with *circumferential* mode number(m) = 0 from Matlab, (a) axis mode number 1 ;(b) axis mode number 2 ;(c) axis mode number 3

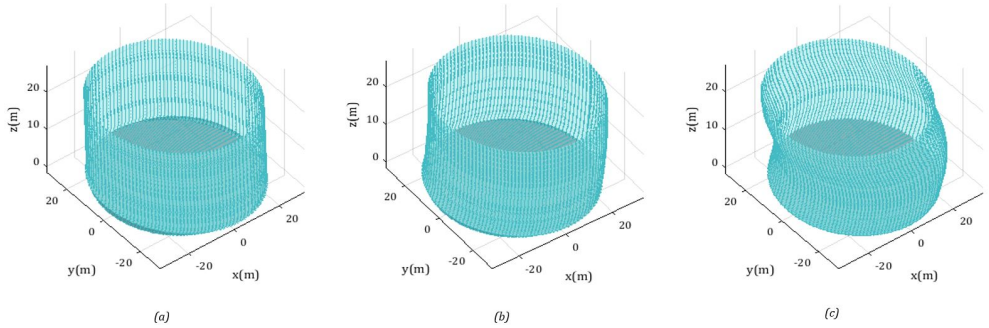

Figure 5.17: Model B mode shape with *circumferential* mode number(m) = 1 from Matlab, (a) axis mode number 1 ;(b) axis mode number 2 ;(c) axis mode number 3

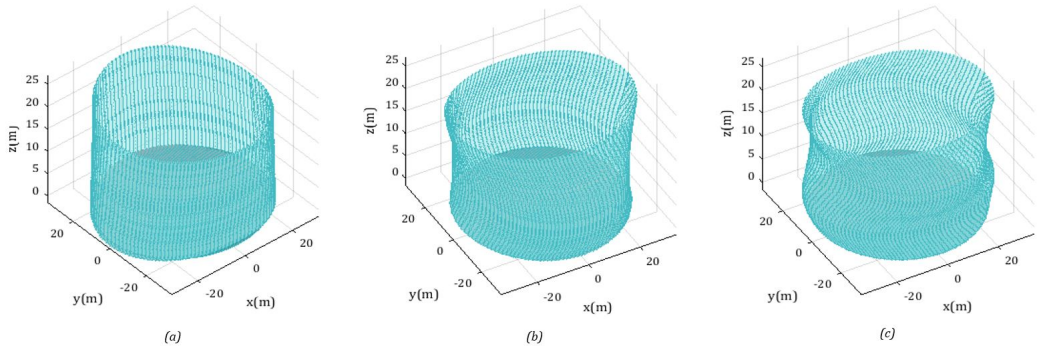

Figure 5.18: Model B mode shape with *circumferential* mode number(m) = 2 from Matlab, (a) axis mode number 1 ;(b) axis mode number 2 ;(c) axis mode number 3

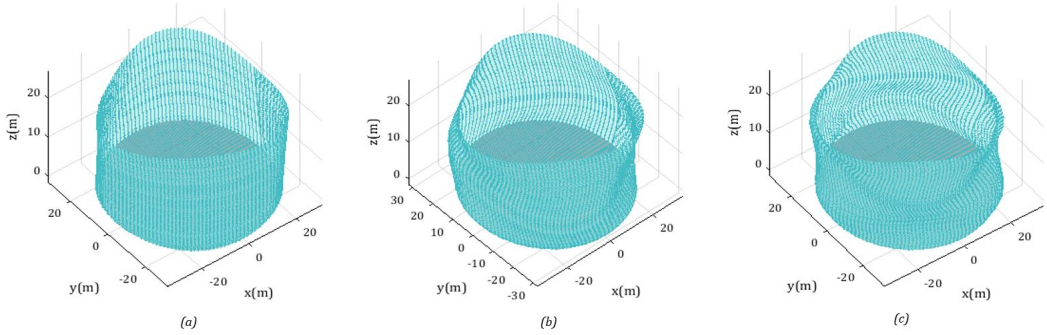

Figure 5.19: Model B mode shape with *circumferential* mode number(m) = 3 from Matlab, (a) axis mode number 1 ;(b) axis mode number 2 ;(c) axis mode number 3

5.3.2. HYDRODYNAMIC PRESSURE FREQUENCY RESPONSE AND HYDRODYNAMIC PRESSURE UNDER HORIZONTAL SEISMIC LOADING

Since the earthquake loading has two axes of propagation as explained in the two-dimensional case, therefore the calculation is divided into two which is horizontal and vertical loading. In this section, the primary focus is the horizontal seismic loading. The pressure response is plotted based on a point that is located at the $z = 0$, $r = R$, and $\theta = 0$ coordinate. This location is chosen due to most of the maximum values are found at this point. The location of the reference point is shown in the following figure:

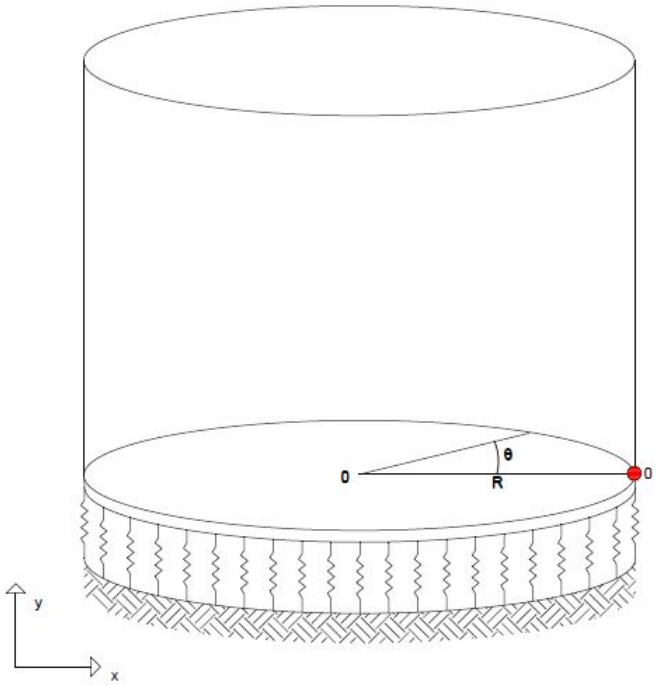

Figure 5.20: Location of the referred point for pressure response

From the picked location the frequency response of the pressure is plotted and depicted as the following figure:

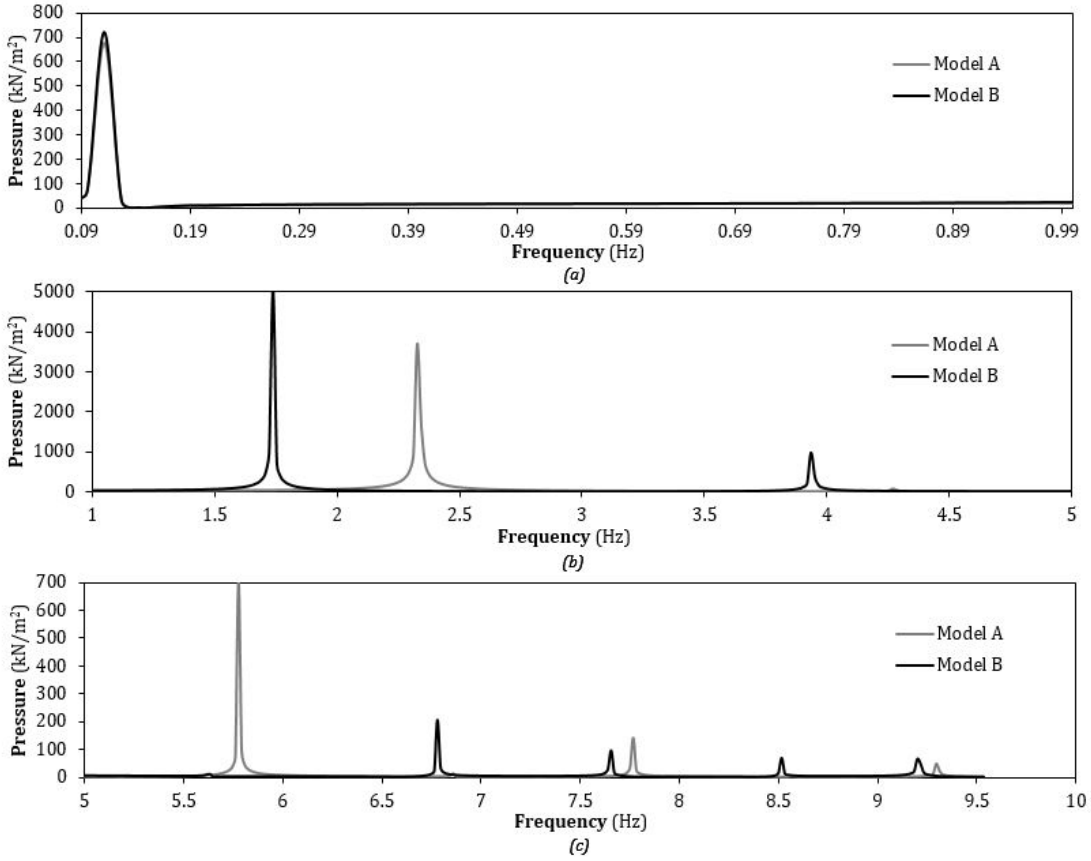

Figure 5.21: Frequency response of Model A and Model B wall pressure in term of pressure under horizontal loading: (a) low frequency range; (b) medium frequency range; (c) high frequency range

The frequency difference between the two models is summarized in the following table:

Table 5.5: The resonance peak for seismic in horizontal direction

Model	$f_s(Hz)$	$f_1(Hz)$	$f_2(Hz)$	$f_3(Hz)$	$f_4(Hz)$	$f_5(Hz)$	$f_6(Hz)$
Model A	0.111	2.357	4.379	6.210	7.484	8.678	9.713
Model B	0.111	1.720	3.997	5.669	6.863	7.643	8.408

In the next subsection, the pressure exerted on the wall and plate as well as the sloshing elevation are plotted. The pressures and sloshing elevation are plotted based on the following cross section *(red line)*:

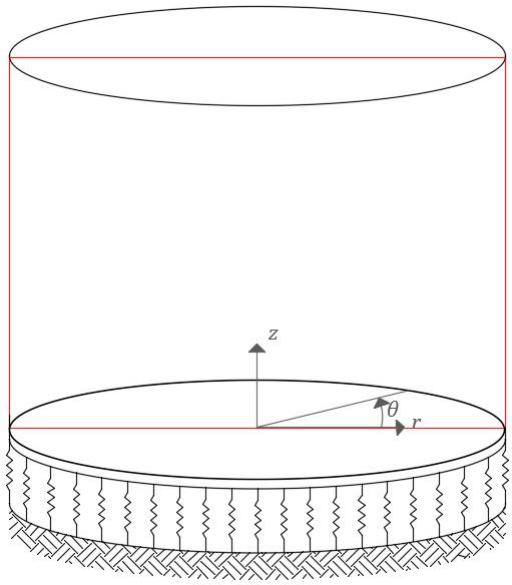

Figure 5.22: The cross section that the pressure is plotted

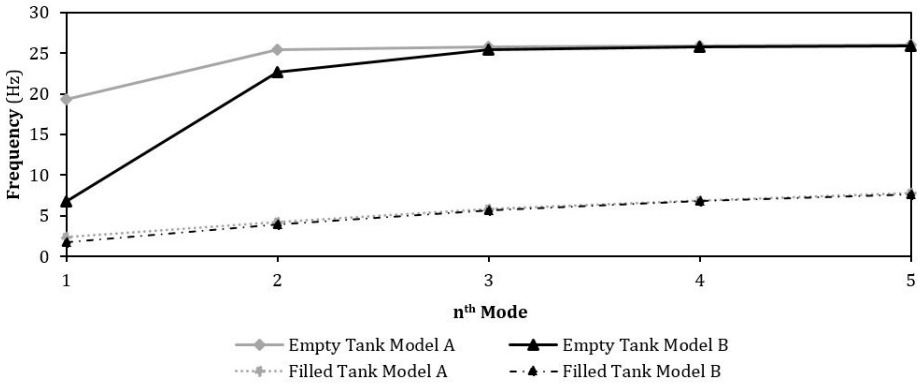

Figure 5.23: gatau

MODEL A

The pressure and sloshing elevation is plotted in the frequency 0.700 Hz and 1.97 Hz. These frequencies are chosen due to in 0.7 Hz to see the pressure before the excitation of the impulsive component. Meanwhile for 1.97 Hz is used to see the pressure after the first resonance peak for the Model B. The pressure and sloshing elevation for the first model (clamped shell) is shown in the following figures:

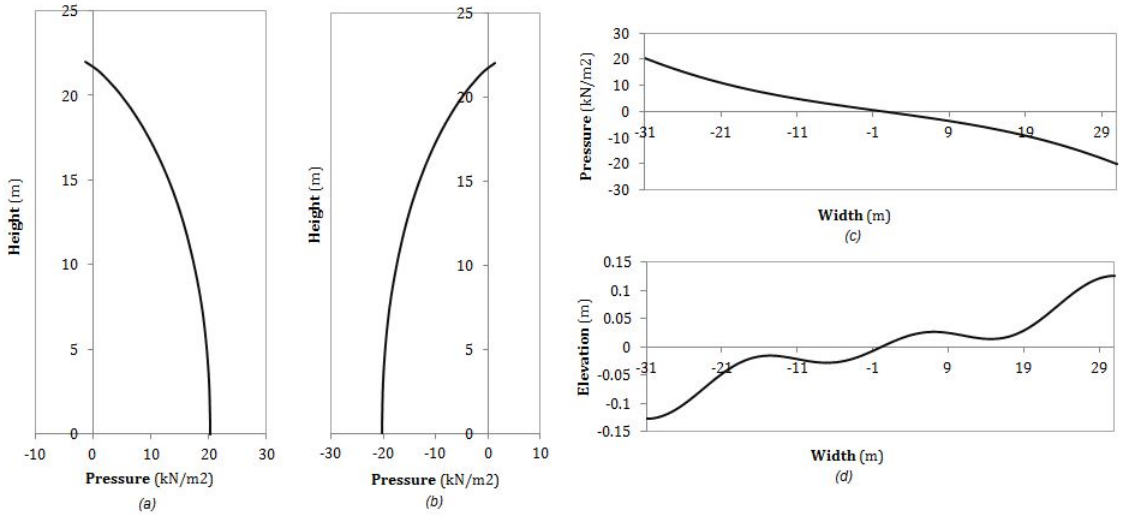

Figure 5.24: Pressure and free surface elevation seismic loading in horizontal direction at **0.700 Hz** for Model A: (a) wall Pressure at $\theta = 0$ (b) wall Pressure at $\theta = \pi$ (c) plate pressure (d) free surface elevationn

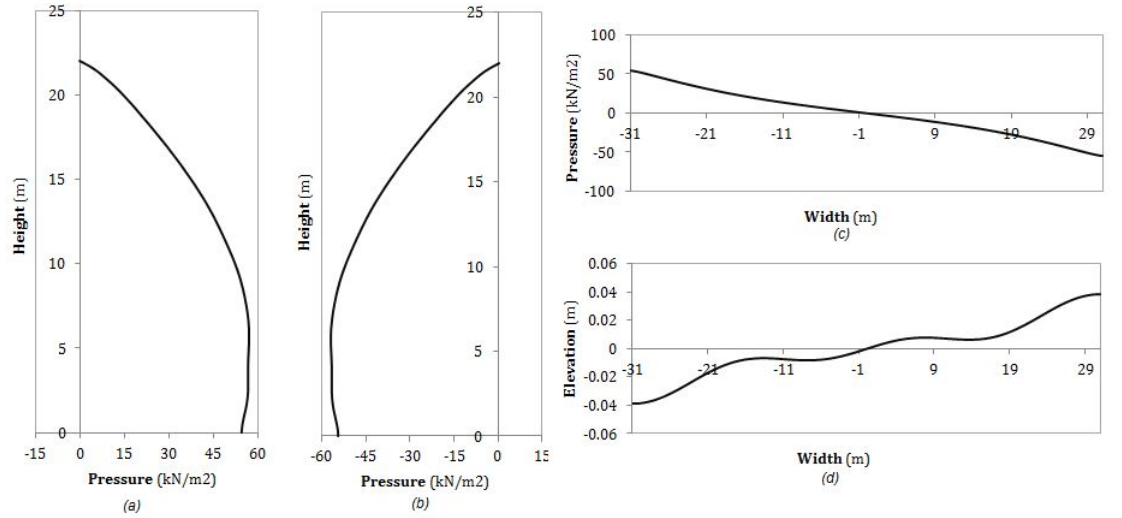

Figure 5.25: Pressure and free surface elevation seismic loading in horizontal direction at **1.97 Hz** for Model A: (a) wall Pressure at $\theta = 0$;(b) wall pressure at $\theta = \pi$; (c) plate pressure; (d) free surface elevation

MODEL B

The figures below depicted the pressure and the free surface elevation for the second model (plate inclusion) at the frequency 0.7 and 1.97 Hz:

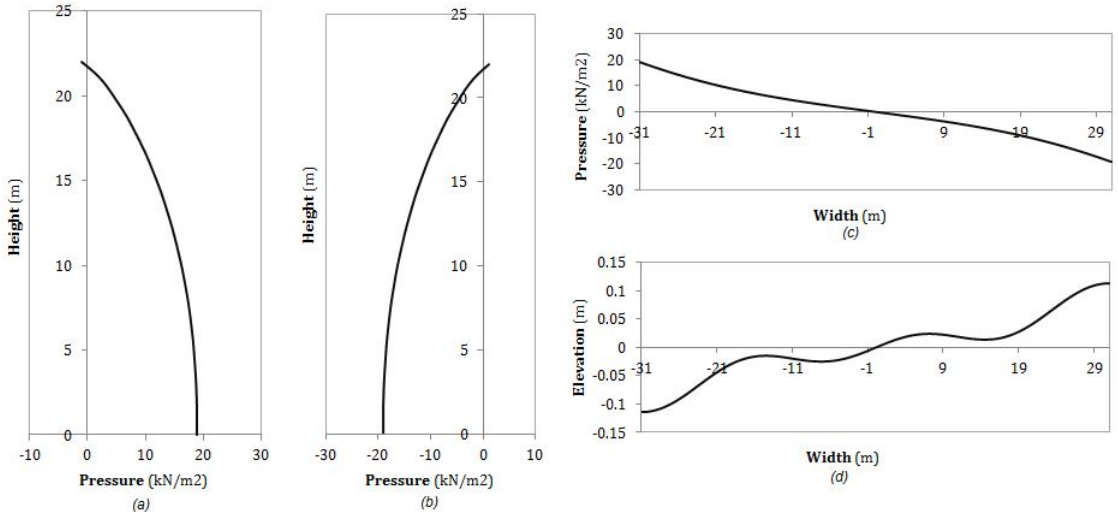

Figure 5.26: Pressure and free surface elevation seismic loading in horizontal direction at **0.700 Hz** for Model B: (a) wall pressure at $\theta = 0$; (b) wall pressure at $\theta = \pi$; (c) plate pressure; (d) free surface elevation

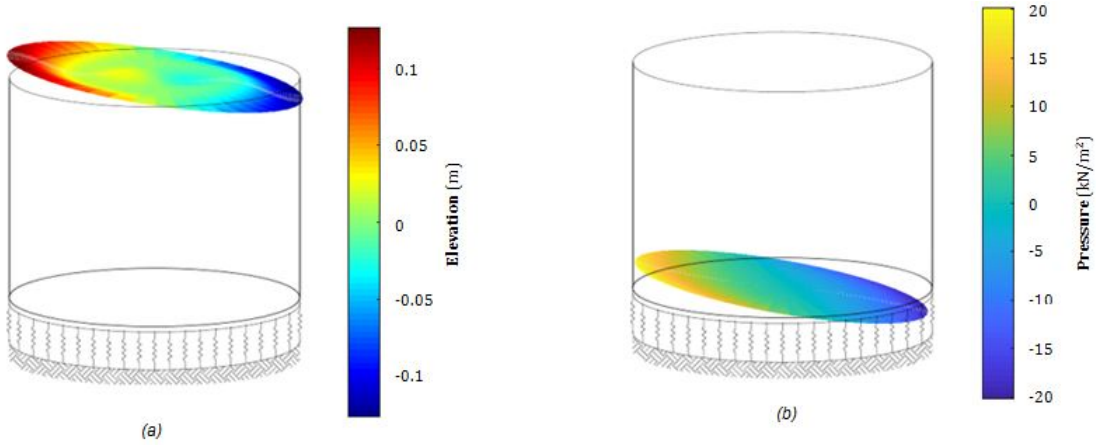

Figure 5.27: Plate pressure and free surface Elevation Seismic loading in horizontal direction at **0.700 Hz** in 3D cross section for Model B: (a) free surface elevation; (b) plate pressure

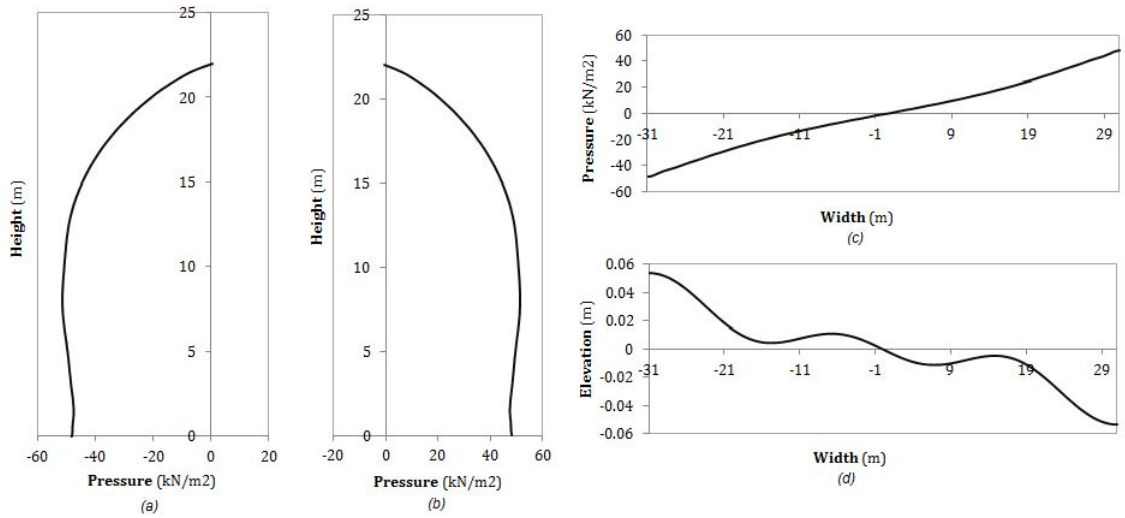

Figure 5.28: Pressure and free surface elevation seismic loading in horizontal direction at **1.97 Hz** for Model B: (a) wall Pressure at $\theta = 0$; (b) wall pressure at $\theta = \pi$; (c) plate pressure; (d) free surface elevation

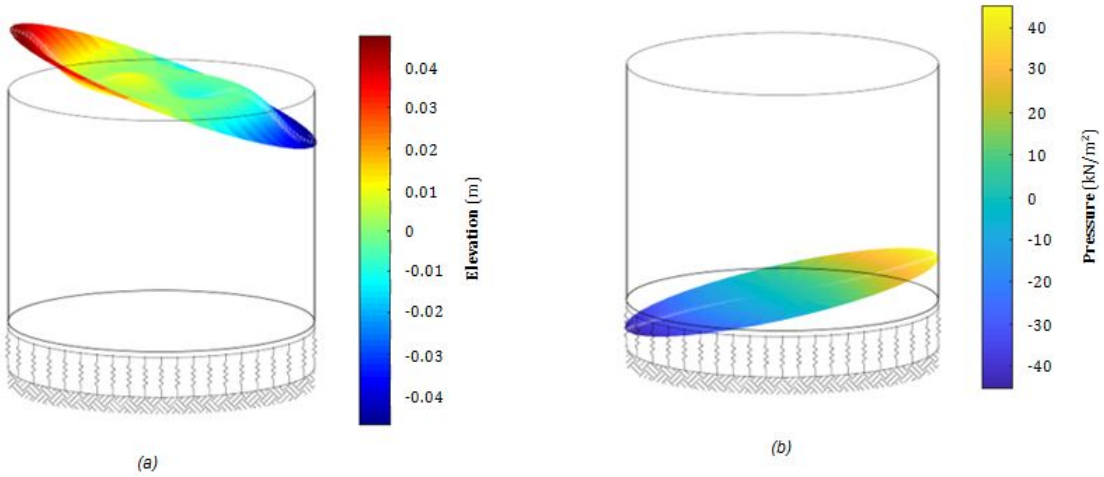

Figure 5.29: Plate pressure and free surface elevation seismic loading in horizontal direction at **1.97 Hz** in 3D cross section for Model B: (a) free surface elevation; (b) plate pressure

Let us also discuss the modes contribution under the horizontal loading. The modes contribution is plotted before the first excitation and at the first excitation. The modes contributions that are analyzed are the structure modes contribution and the liquid modes contribution. Since the liquid pressure for asymmetric loading is dominantly comes from the first potential, therefore the liquid mode contribution that is plotted is the first liquid potential. In the following charts, the mode contributions are depicted:

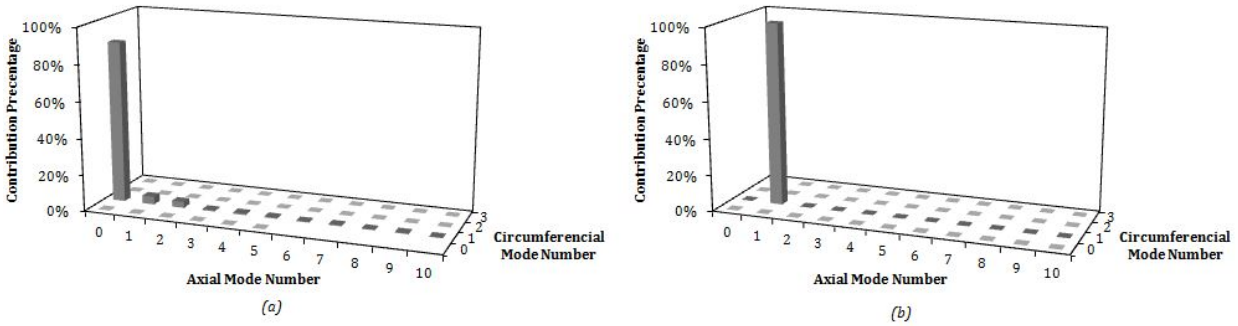

Figure 5.30: Mode contribution under horizontal loading before the first resonance peak at (0.7 Hz):
(a) structure contribution ; (b) liquid mode (ϕ_1) contribution

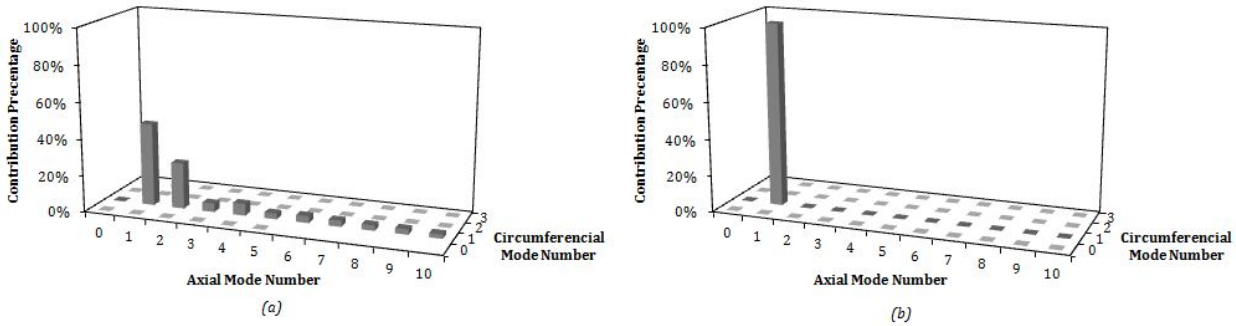

Figure 5.31: Mode contribution under horizontal loading at the first resonance peak at (1.72 Hz):
(a) structure mode contribution ; (b) liquid mode (ϕ_1) contribution

5.3.3. HYDRODYNAMIC PRESSURE FREQUENCY RESPONSE AND HYDRODYNAMIC PRESSURE UNDER VERTICAL SEISMIC LOADING

This subsection is written for the earthquake loading in the vertical direction. The pressure response is plotted in the point reference that is located at $z = 0$, $r = R$, and $\theta = 0$ (see Figure 5.20). From the point of reference the pressure response are plotted in the following graph:

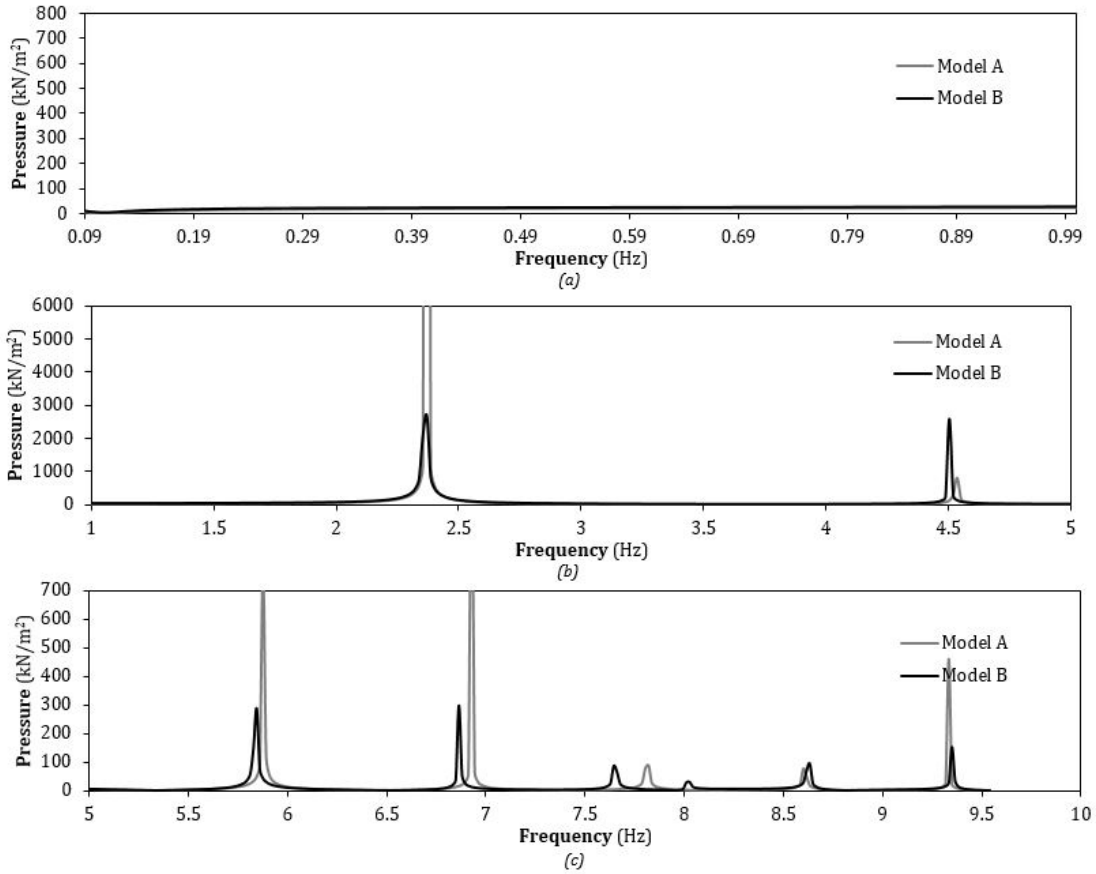

Figure 5.32: Frequency response of Model A and Model B wall pressure in term of pressure under vertical loading: (a) low frequency range; (b) medium frequency range; (c) high frequency range

The natural frequencies between the two models are summarized in the following table:

Table 5.6: The resonance peak for seismic in vertical direction

Model	$f_1(Hz)$	$f_2(Hz)$
Model A	2.388	4.618
Model B	2.372	4.51

From the explanation of two-dimensional model (See Figure 3.24), we understand that there is no overturning moment in the vertical loading due to symmetrical loading. Therefore, the vertical loading is discussed less detail than the horizontal seismic loading. Since from the horizontal loading we can see that the Model B is more critical than Model A. Therefore the pressure that is discussed here is the Model B. In the following figures are shown the pressure and free surface elevation of Model B based on the cross section Figure 5.22:

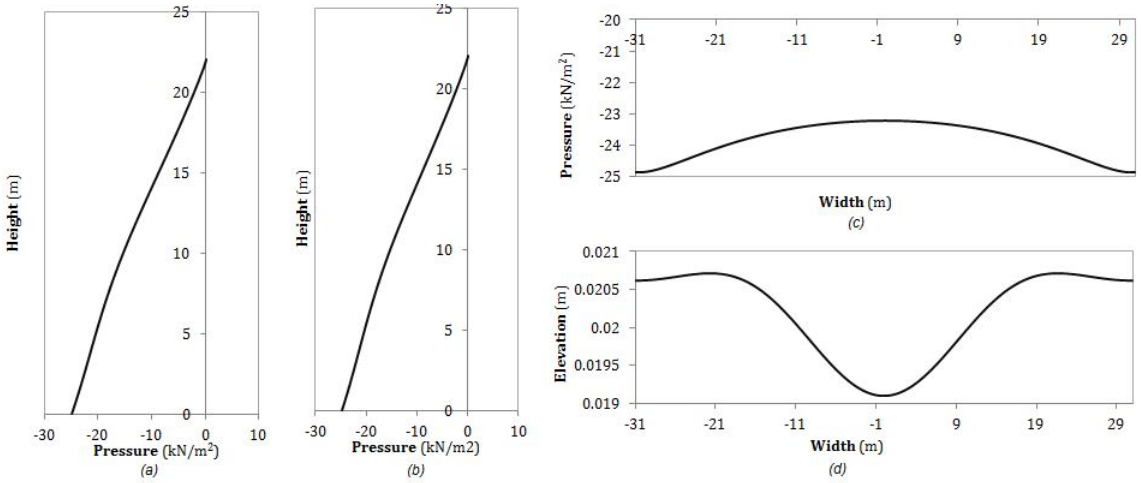

Figure 5.33: Pressure and free surface elevation seismic loading in vertical direction at **1.20 Hz** for Model B: (a) wall Pressure at $\theta = 0$; (b) wall pressure at $\theta = 2\pi$; (c) plate pressure; (d) free surface elevation

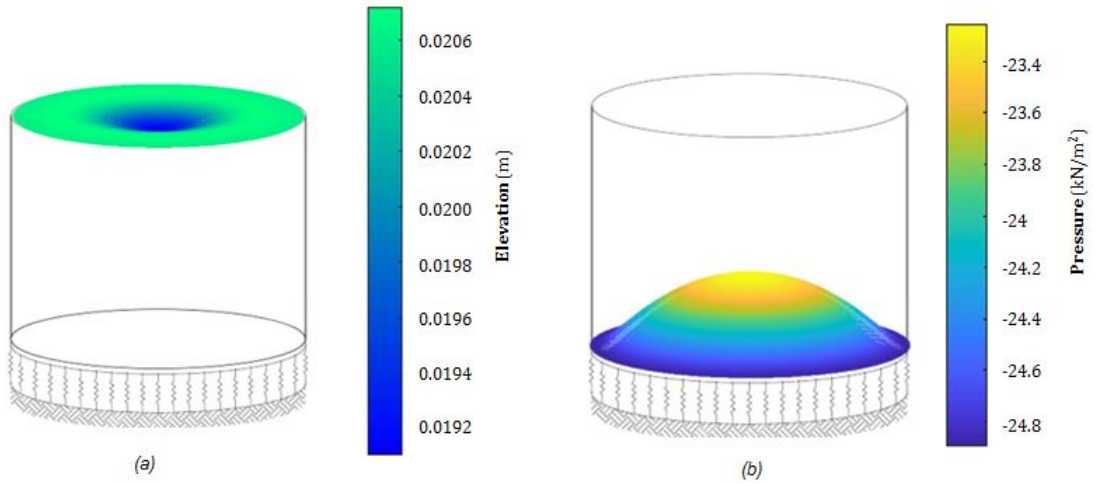

Figure 5.34: Plate pressure and free surface Elevation Seismic loading in vertical direction at **0.700 Hz** in 3D cross section for Model B: (a) free surface elevation; (b) plate pressure

The pressure and free surface elevation below is plotted as negative values due to the earthquake loading is in the positive z direction. However, please note that the earthquake motion in reality goes ups and downs. Which means that **the governing pressure will be the absolute value** of the pressure and free surface elevation plotted in Figure 5.33.

From Figure 5.32, we could see that there is a dip in 0.1 Hz. This dip is due to the compulsive component and the impulsive component in the total pressure response. From the equation 3.55. We can understand that the sloshing frequency under vertical loading is at 0 Hz. However the higher the frequency, the less contribution it has. From the figure 5.35 we can see that the impulsive and compulsive component have different sign. The total pressure at the reference point for frequency response plotting is almost zero in Figure 5.35.

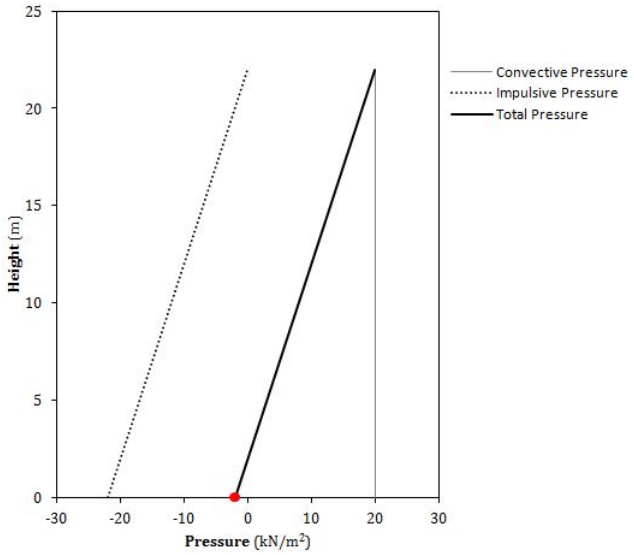

Figure 5.35: Impulsive, convective and total pressure under vertical loading at 1 Hz

The mode contributions for the axisymmetric vertical loading are also divided into two which are structure and liquid mode contributions. For the axisymmetric loading, instead of the first liquid potential, the biggest liquid mode contribution comes from the second liquid potential. In the following figures, the mode contribution for the vertical loading is depicted:

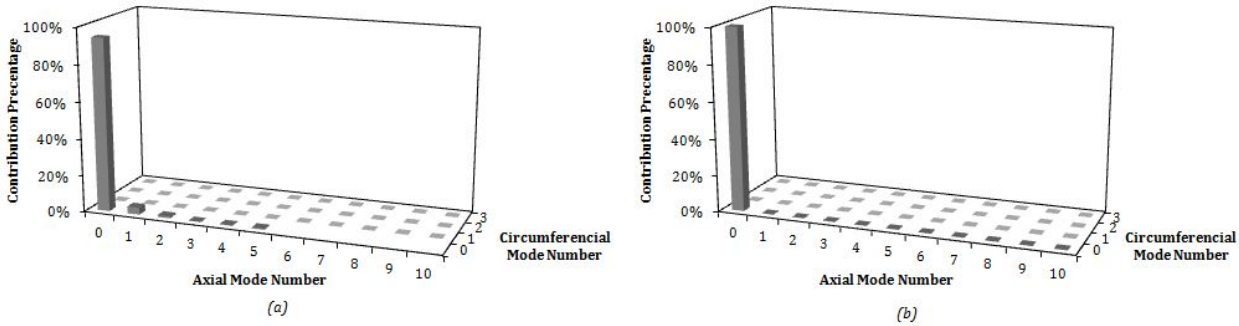

Figure 5.36: Mode contribution under vertical loading before the first resonance peak at (0.4 Hz):
(a) structure contribution ; (b) liquid mode (ϕ_2) contribution

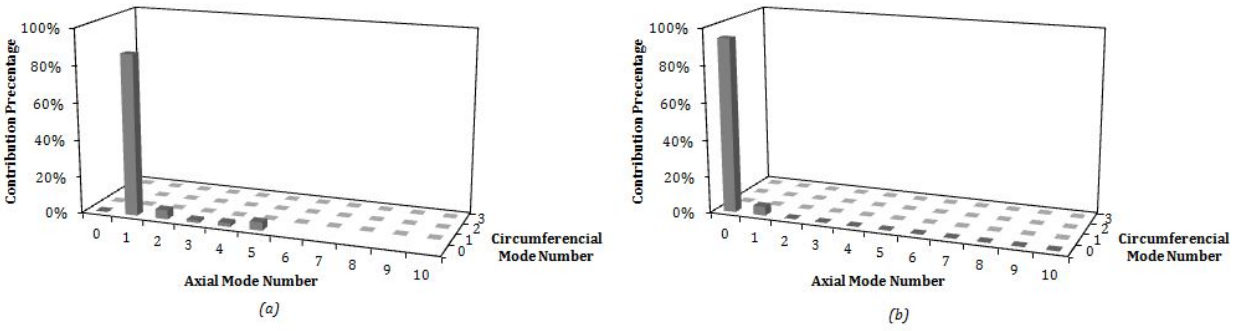

Figure 5.37: Mode contribution under vertical loading at the first resonance peak at (2.55 Hz):
(a) structure mode contribution ; (b) liquid mode (ϕ_2) contribution

5.3.4. CONCLUSION

From the frequency response for the pressure (see Figure 5.21 and 5.32), we can see that the flexibility of the plate in Model B influences the entire system dynamic behavior. Since the structure is more flexible than Model A, it is expected that the resonance peak Model B is lower than Model A. The Model A fundamental natural frequency is higher than the Model B with the following percentages: 33.3% under the horizontal loading and 98% under the vertical loading. Therefore we could conclude that neglecting the soil structure interaction in this case study leads to an overestimation of the impulsive natural frequencies. This period elongation is due to the soil-structure interaction.

Based on the plotted frequency response, we also can see that the fundamental sloshing frequency is almost the same for the Model A and Model B with the difference of 0.012%. The same behavior is also found in the two dimensional model. In a nutshell, we can conclude that the soil-structure interaction and plate flexibility for this case study has a considered small effect on the sloshing frequencies. This relation is also the reason why these journals ([5], [18],[7]) do not include the soil-structure interaction and the plate flexibility in the fundamental sloshing frequency (for an example see equation 2.45). In the next section the flexibility parameters study are discussed in more detail.

From the result for vertical and horizontal loading, we can understand that the pressure and free surface shapes accordance to the shape of the loading. Since the vertical loading in Figure 4.3 are axisymmetric, we can also see that the pressure are also axisymmetric. For the horizontal loading which the load is asymmetric, the pressure on the wall and the plate are also asymmetric. Please also note that for the vertical loading the absolute values for pressure and free surface elevation are the governing combination for the total response.

How the pressure shapes function follows the type of loading can also be seen from the modes contribution (see Figure 5.30, 5.31, 5.36, and 5.37). For the axisymmetric loading, only the axisymmetric modes (circumferential mode number 0), that contributes in the total response. The total pressure under vertical loading is dominantly contributed by the rigid body component of the liquid potential (ϕ_{200}) both before and at the first resonance peak. Due to the ϕ_{200} is dominant with the contribution percentage of 94.8%, in Figure 5.34 we can see that the plate pressure along the radius produce almost a constant value with an average of $23.851 kN/m^2$ and standard deviation of $0.54 kN/m^2$ at the first resonance peak. For the asymmetric loading in Figure 5.30 and 5.31, we can also see that only the first circumferential mode number that gives contribution to the total response. This result is expected since we can clearly seen how the orthogonality works on equation E.119. From Figure 5.31, we can notice that the higher axial mode numbers do give contributions to the total response : the second and the third axial mode number contributions are 25.4% and 4.65% respectively. Therefore, neglecting higher mode numbers might be less representative in this case to describe the dynamic behavior of the liquid-structure interaction.

From the pressure figures (see Figure 5.24, 5.25, 5.26, and 5.28), it can be seen that the free surface wave elevation is higher on the lower frequency. The higher the frequencies range, the lower the free surface elevation. This means that the free surface water pressure decreases as the frequency increase. This because seeing the pressure response the peak resonance that the sloshing frequency located in the lower range. The other

reason is the in the number of modes selection the sloshing frequencies that are used is only three which will not cover the rest sloshing in the higher frequency. This phenomenon can also be explained the figure below:

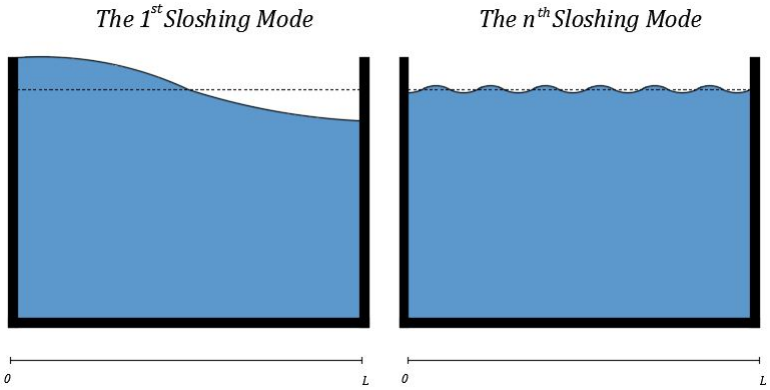

Figure 5.38: The asymmetric sloshing modes : the first sloshing mode (left) and the n sloshing mode (right)

From the figure above we can see that the first sloshing mode number has the highest effect. Based on the equation 5.11, we also understand that it located is in the longest period among other mode numbers. Therefore, from this wave geometry properties we can correlate to the statement above: *the lower the frequency the higher the sloshing effect.*

$$\lambda = \frac{L \times n}{2}$$
$$T = \frac{\lambda}{v} \tag{5.11}$$

where:

L	= the length of the tank;
n	= the mode order;
λ	= the wave length;
v	=the wave velocity;

As the Model B is more flexible than the Model A, therefore the pressure that is obtained from this model has a higher mode function compare to the Model A pressure. This flexibility result in the pressure and sloshing elevation are higher in some frequecies.

In the result we also see the same behavior in the frequency response in vertical loading as the two dimensional model where there is no sloshing frequencies. The result can be explained mathematically in equation 3.19.

5.4. PARAMETER STUDY

As explained in the opening of this chapter, the parameter study is to analyze several variables effect in the system. These parameters are the liquid volume, tank geometry, and tank flexibility. Seeing from the response that the hydrodynamic pressure most of the time higher in model B. Therefore the default model that is used throughout the parameter study is model B. The parameter study is focused on horizontal seismic loading only since the horizontal loading is more critical due to the overturning moment. However, please do note that the effect of the parameters can still be seen in the vertical loading.

5.4.1. LIQUID VOLUME PRECENTAGE

During the service life, liquid tank will have a different volume over time. It can be fully filled, half filled or empty. In the following will be plotted the response of the pressure with the same location as shown in Figure 5.20. In the following figures are plotted the response for different liquid volumes:

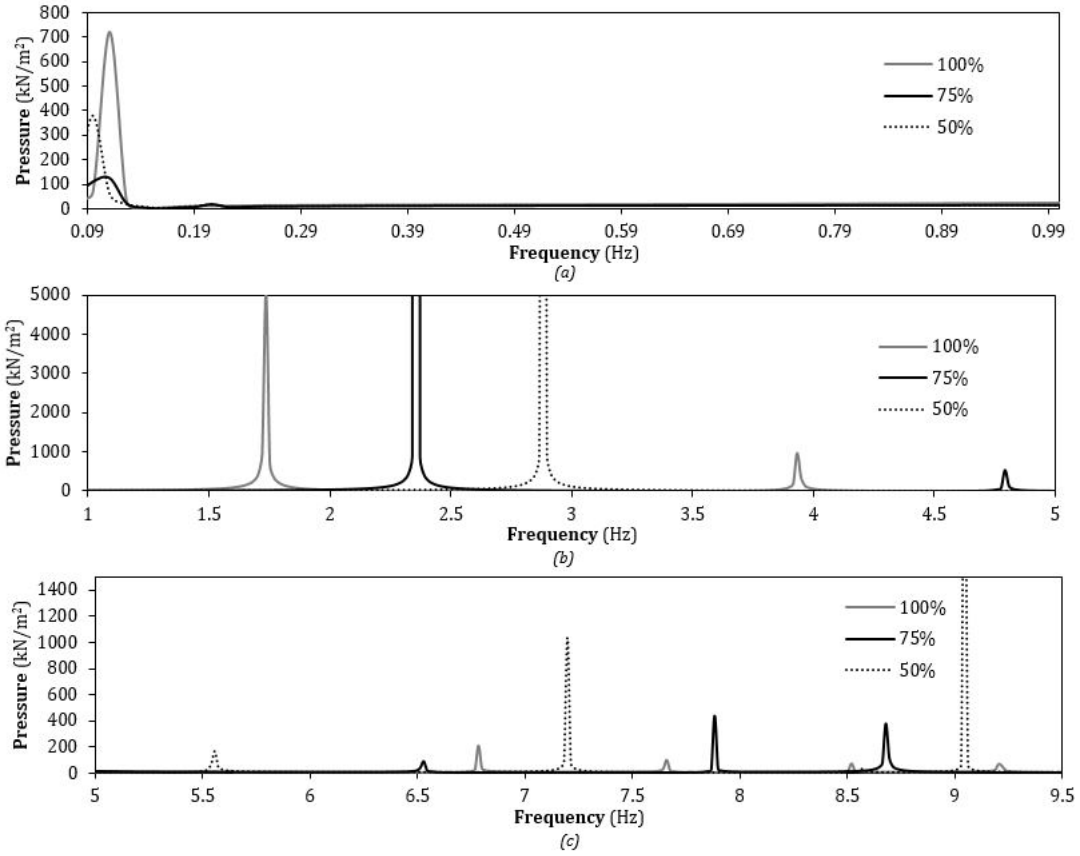

Figure 5.39: Frequency response of the wall pressure for different liquid volume under horizontal loading: (a) low frequency range; (b) medium frequency range; (c) high frequency range

The different between the natural frequency of the three different volume condition can be seen in the plotted graph:

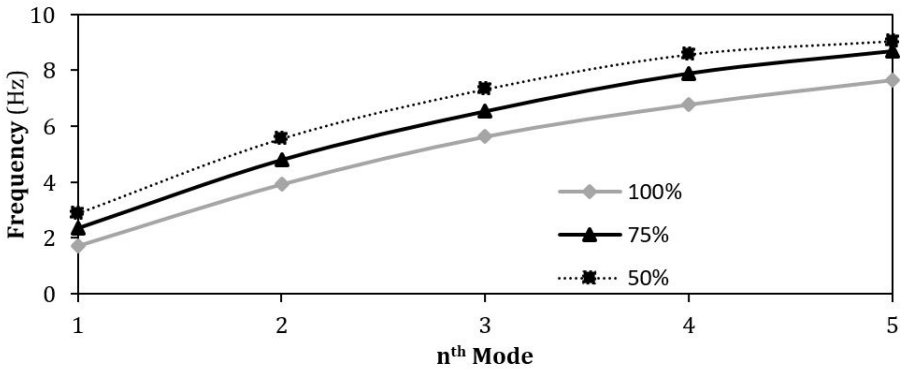

Figure 5.40: Frequency difference for different liquid volume frequency under horizontal loading

The pressures for different liquid volumes are also plotted in these following figure:

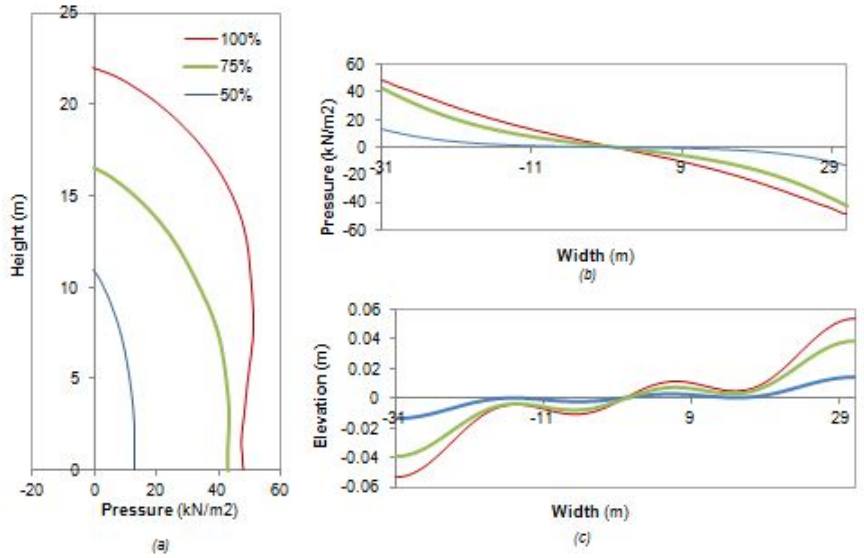

Figure 5.41: Pressure and free surface elevation at 1.97 Hz under horizontal loading: (a) wall pressure at $\theta = 0$; (b) plate pressure; (c) free surface elevation

CONCLUSION

Once again, the three-dimensional model shows the same behavior as the two-dimensional model. Firstly one can clearly see that there is a change in a frequency. The more liquid inside of the tank the higher the pressure, while in the other hand the lower the frequency. By decreasing the volume to 75% and 50% the fundamental natural frequency is increasing 1.37 and 1.95 times respectively. The lower frequency is due to the pressure that is coupled to the structure will result in a mass. Therefore bigger volume result to bigger mass. From the fundamental equation to obtain the natural frequency in equation 2.12, we can expect that the bigger mass leads to lower frequency. This physics explanation is written in Section 3.10.

The sloshing frequencies however change: the bigger the volume, the lower the natural frequencies. This phenomenon can be explained mathematically based on the Housner equation the higher the ratio between H/R which is a wider tank the longer the period it travels and in contrary with a narrow tank.

From Figure 5.41, we can say that mostly the pressure in this case is more critical as the liquid volume increases. One can conclude that the pressure in higher liquid volume has a higher mode. This is due to the location of the frequency. Since the frequencies decrease for higher liquid volume, the tank with more volume is already excited first compare to the other tank with less liquid volume.

5.4.2. WALL AND BOTTOM PLATE THICKNESS

In this subsection, the highlighted point is the wall and the plate thickness. This thickness is highly corelated to the flexibility of the tank structure. The thinner the structural thickness, the higher also the moment of inertia.

WALL THICKNESS

The parameter study for the wall thickness is executed by changing the default wall thickness. The first model's wall thickness is half the size of the default wall thickness. The second model's wall thickness is twice the size of the default wall thickness. These two models will be increasing or decreasing the moment inertia with the factor of $2^3 = 8$ times. Then they are compared to the pressure from the default wall thickness model. The pressure responses are taken from the same location on Figure 5.20 and depicted in the following figure:

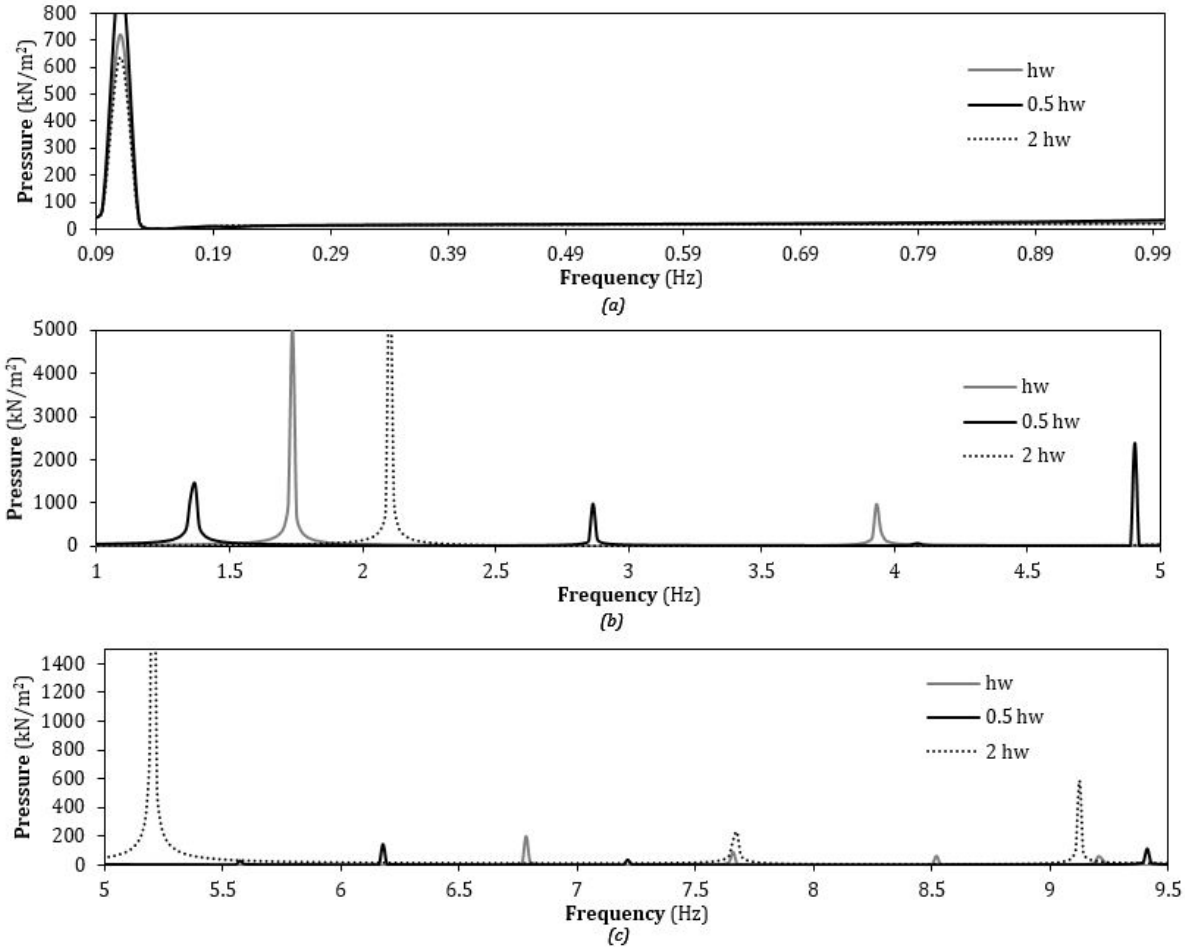

Figure 5.42: Frequency response of pressure for different wall thickness under horizontal loading: (a) low frequency range; (b) medium frequency range; (c) high frequency range

The difference between the natural frequency of these three wall thickness are depicted in the following graph: Let us also compare to the Eurocode in the equation 2.45 for the impulsive frequency. The Eurocode

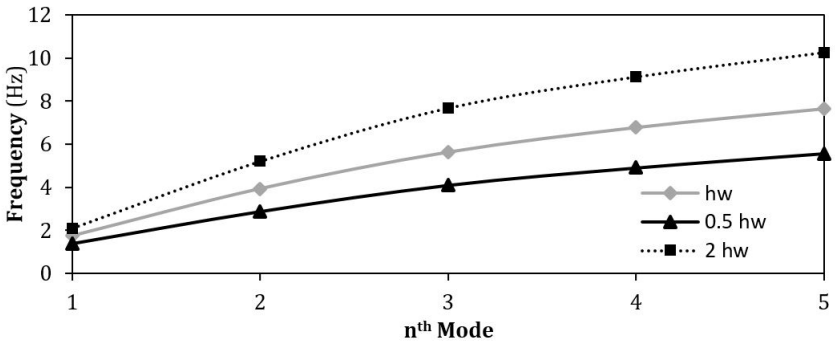

Figure 5.43: Difference natural frequency in for different wall thickness under horizontal loading

in equation 2.45 considers the plate as rigid and we know that:

$$T_{imp} = C_i \frac{1}{\sqrt{h_w/R}} \tag{5.12}$$

Since the only variable that change in the equation is the wall thickness we can define the equation above as the following:

$$\begin{aligned} f_1(n \times h_w) &= \sqrt{n \times h_w} f_1(h_w) \\ f_1(2 \times h_w) &= \sqrt{2 \times h_w} f_1(h_w) \\ &= 1.41 f_(h_w) \\ f_(0.5 \times h_w) &= \sqrt{0.5 \times h_w} f_1(h_w) \\ &= 0.71 f_(h_w) \end{aligned} \tag{5.13}$$

Let us also compared to the Model A to the Eurocode for fair comparison. The fundamental impulsive frequency for different wall thickness in Model A is depicted as follows:

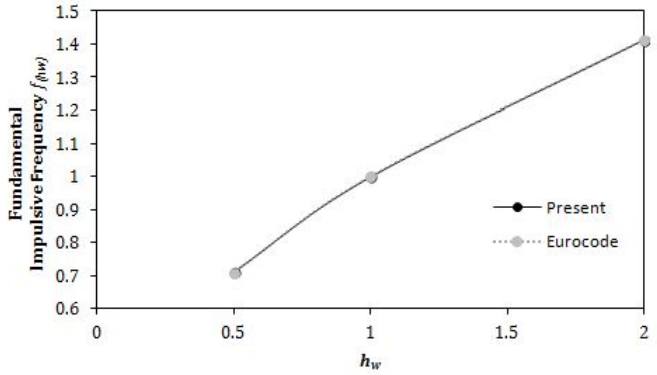

Figure 5.44: Fundamental frequency difference for different wall thickness

Let us also analyzed the Model A, if the wall structure is extremely flexible. Flexible structures sometimes yields in the closely located impulsive and sloshing frequencies. Where these two components may interdependent to each other. In the following figure are shown in the case that the structure's flexibility influence the sloshing frequency:

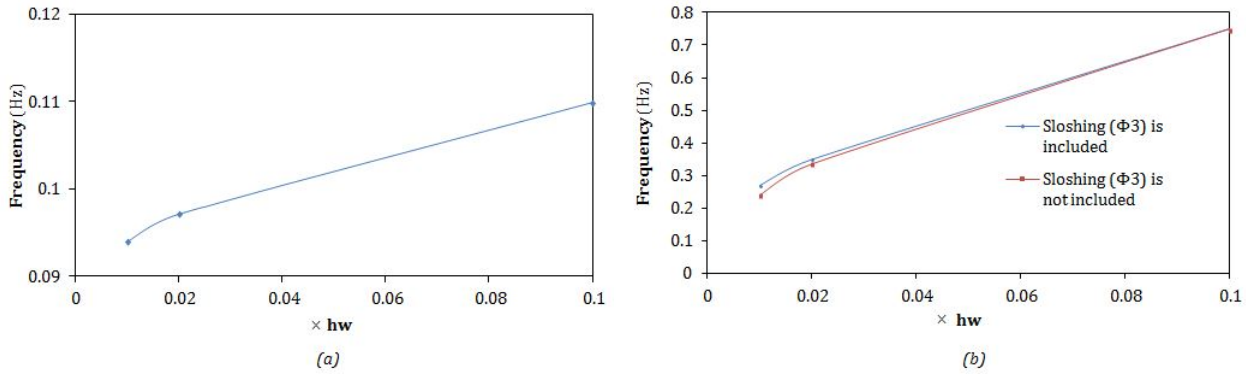

Figure 5.45: Interdependent sloshing and impulsive frequency in a very flexible structure :
(a) sloshing frequencies, (b) impulsive frequencies (with and without the sloshing component)

PLATE THICKNESS

The same manner from the parameter study of the wall thickness also applies for the parameter study of the plate thicknes. The impact of the difference plate thickness are shown in the following figure:

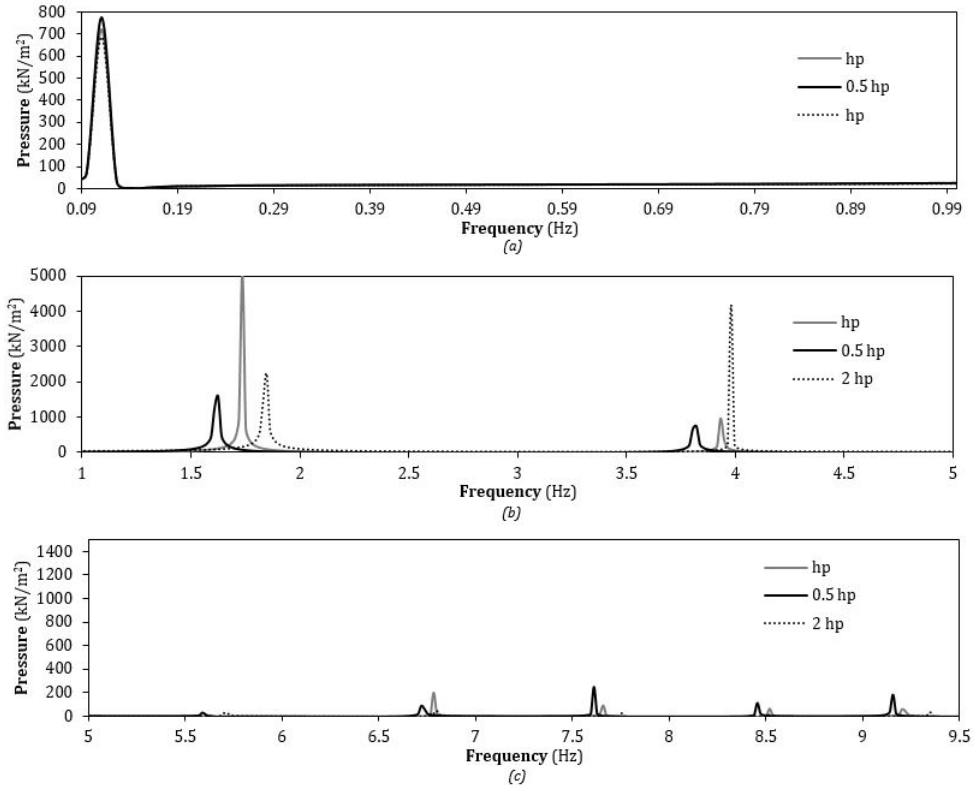

Figure 5.46: Frequency response of pressure for different plate thickness under horizontal loading: (a) low frequency range; (b) medium frequency range; (c) high frequency range

Where the difference in each excitation is plotted in the following graph

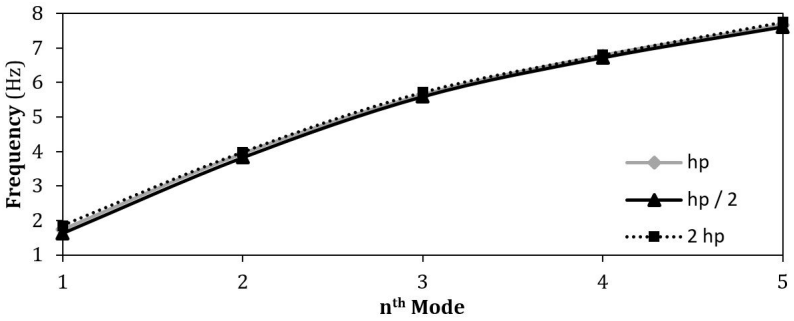

Figure 5.47: Difference natural frequency for different plate thickness under horizontal loading

CONCLUSION

As expected, the frequencies are increasing as the structural elements get thicker and in contrary for thinner structural elements. The plate and wall thickness is one of the critical aspects that defined the structural stiffness. Therefore, we can relate the correlation between the structural stiffness and the natural frequency in the equation 2.12.

From the parameter study for the wall thickness, the fundamental impulsive frequency is decreasing 0.78 times when the thickness is only half of the default thickness. While, for the two times thicker wall the frequency is increasing 1.21 times. The Model A is compared to the Eurocode and have the ratio of 0.71 and 1.41 times for $0.5h_w$ and $2h_w$ respectively. When these numbers are compared to the Eurocode in the equation 5.13, they have the difference of 0.32 % on the average. This difference is considered acceptable in this thesis. The correlation between the cylindrical shell width for Model A is a quadratic relation. However there are some difference between the Model A and Model B, regarding the ratio for different wall thickness. This difference is due to the Model B take into account the soil-structure interaction.

From Figure 5.42 and Figure 5.46, we can see that the sloshing frequencies are hardly changing. The reason behind this unchanged sloshing frequencies is the distance between the convective and impulsive frequencies are relatively *distant with almost the power one or two.* Due to such distance, we can almost conclude that the flexibility hardly gives effect to the sloshing frequency. This is why most of the journal separate these two-components for the sake of simplification. This separation means that the sloshing frequencies is assumed independent to the flexibility of the structure. This assumption is only valid if the sloshing frequencies and impulsive frequencies are far apart. Therefore in most of the journals [18], [5] and [4], the sloshing can be decoupled into separate component that yields into the following equations:

$$\frac{\omega^2}{g}\tilde{\Phi}_3(r,\theta,z=H) = \frac{\partial\tilde{\Phi}_3(r,\theta,z=H)}{\partial z} \tag{5.14}$$

From this equation, we can assume that the sloshing is independent of other potentials (Φ_1 or Φ_2). Where we can directly obtained the sloshing frequency as follows:

$$\omega = \sqrt{g \times \varepsilon[m,n] \times \tanh\left(\varepsilon[m,n]H/R\right)/R} \tag{5.15}$$

However in the case that the two components are closely related, the sloshing frequencies depend on the impulsive frequencies and also the other way around (see Figure 5.45).Therefore equation 5.15 is no longer valid. From Figure 5.45, we can also learn that flexible structures also tend to decrease the sloshing frequencies.

The effect of the wall stiffness in dynamic loading is more dominant than the plate stiffness. The change fundamental natural frequency are smaller compare to the parameter study on the wall thickness. We can regard the plate is more stiff when it compared to the wall, as the plate is resting in elastic bedding. This elastic bedding gives contribution to the plate stiffness.

5.4.3. TANK GEOMETRY

In this parameter study, we will investigate on how the tank geometry (H/R) influence the dynamic behavior. Three models are studied for the geometry sensibility, which are tank geometry of $H/R = 0.35$, 1.4, and 0.7. The comparison between the three geometries is depicted in the following figure:

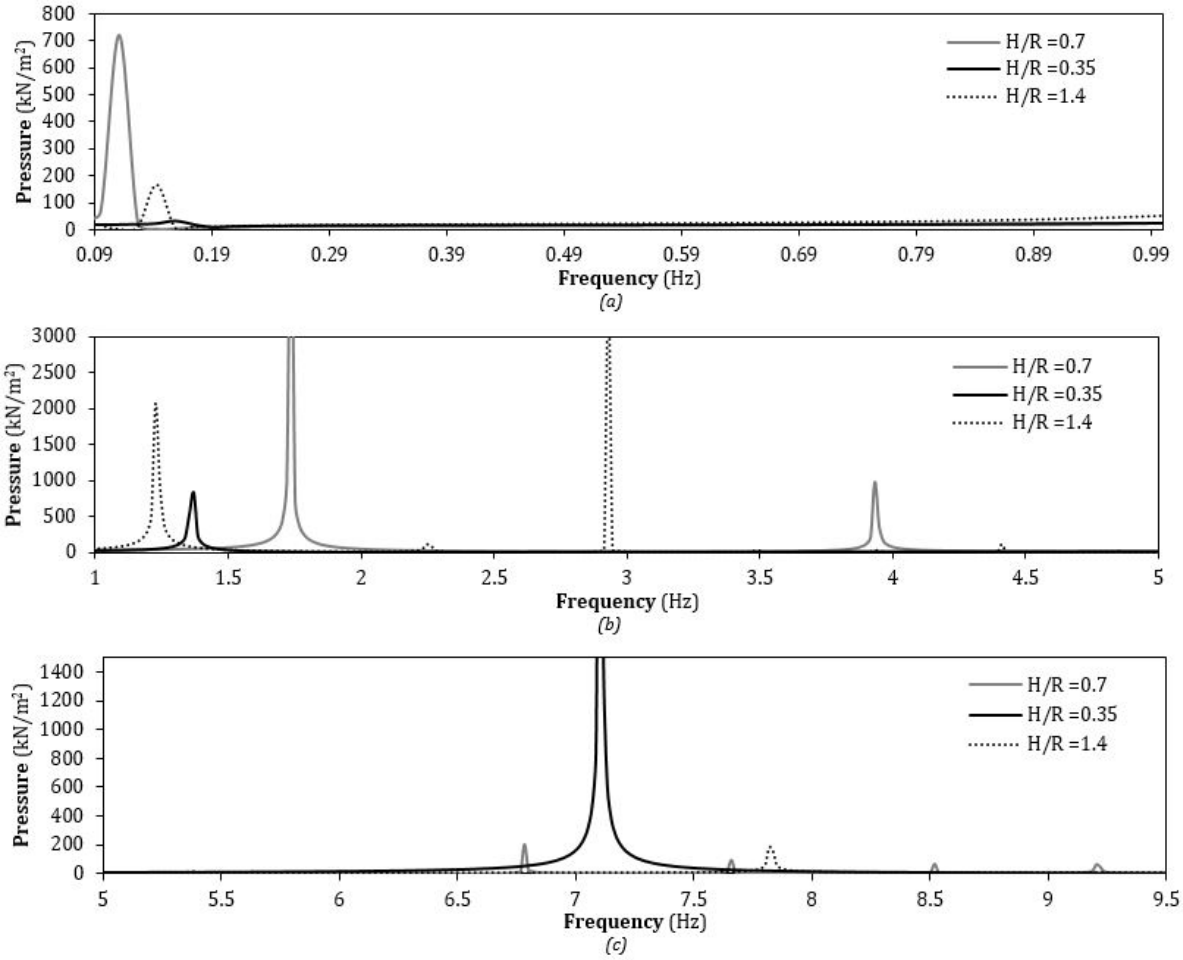

Figure 5.48: Frequency response of pressure for different From Geometry under horizontal loading:(a) low frequency range; (b) medium frequency range; (c) high frequency range

CONCLUSION

From equation 5.15, we can see clearly that the only determining factor on frequency is the geometry. Let us also compare the natural frequency of the sloshing from separated form in equation 5.15 and from Figure 5.48:

Table 5.7: The sloshing frequency for different geometry

Model	$f(H/R = 0.35)$	$f(H/R = 0.7)$	$f(H/R = 1.4)$
Simplification (equation 5.15)	0.06 Hz	0.11 Hz	0.17 Hz
Actual	0.06 Hz	0.11 Hz	0.17 Hz

The difference between the two methods is 0.58% in this case. Therefore, from this sample of case study, we can understand why in some journals ([5],[18]) the sloshing component can be totaly seperated from the strucutre flexibility components (ϕ_1 and ϕ_3).

Since the parameter R is the variant, therefore the wider the tank, the more flexible it is. It can be seen in how the frequency shifted to the left hand side. It will be a different result if the parameter H is the variant.

5.5. TIME DOMAIN ANALYSIS

By using the Fourier Transform in equation 2.70, all the result in the previous section is in the frequency domain. However most of the time, the earthquake acceleration are recorded in the time domain. Therefore in this section, we will address the example of a time domain analysis. The following figure are shown the seismic time history in the two directions (horizontal and vertical):

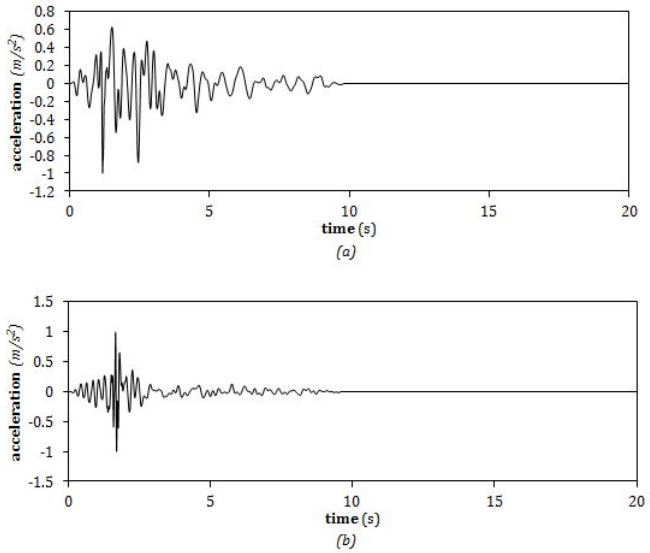

Figure 5.49: Sample of Groningen earthquake acceleration:(a) earthquake acceleration in the horizontal direction (b) earthquake acceleration in the vertical direction
Source: Witteveen+Bos

Using the Fourier transform (see equation 2.70), the earthquake acceleration spectrum is converted into the frequency domain. However, changing the acceleration spectrum in the frequency domain will result in complex functions which are composed of both real and imaginary function. In the following figure is the frequency domain earthquake acceleration:

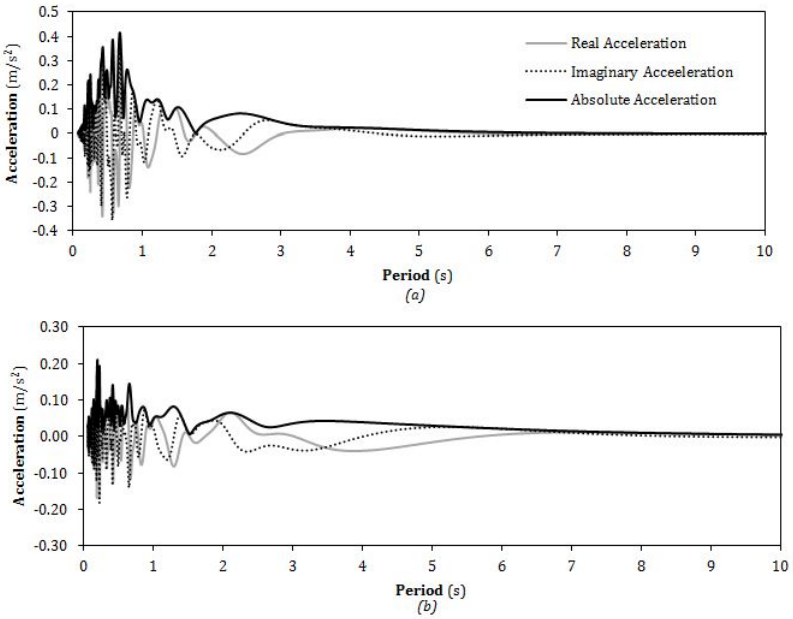

Figure 5.50: Groningen earthquake acceleration in frequency domain
: (a) earthquake acceleration in the horizontal direction (b) earthquake acceleration in the vertical direction

From the Inverse Fourier Transform, we can obtain the response of the structure in the real time domain which is yielded from following equation:

$$\begin{aligned} FR_{horizontal}(t) &= \frac{1}{\pi}\int_0^{2\pi} \tilde{ae}_{horizontal}(\omega) \times F\tilde{R}F_{horizontal}(\omega) \exp i\omega t d\omega \\ FR_{vertical}(t) &= \frac{1}{\pi}\int_0^{2\pi} \tilde{ae}_{vertical}(\omega) \times F\tilde{R}F_{vertical}(\omega) \exp i\omega t d\omega \\ FR_{total}(t) &= FR_{horizontal}(t) + FR_{vertical}(t) \end{aligned} \tag{5.16}$$

From the equation above, the pressure response in the time domain under the specific loading can be plotted as the figure bellow

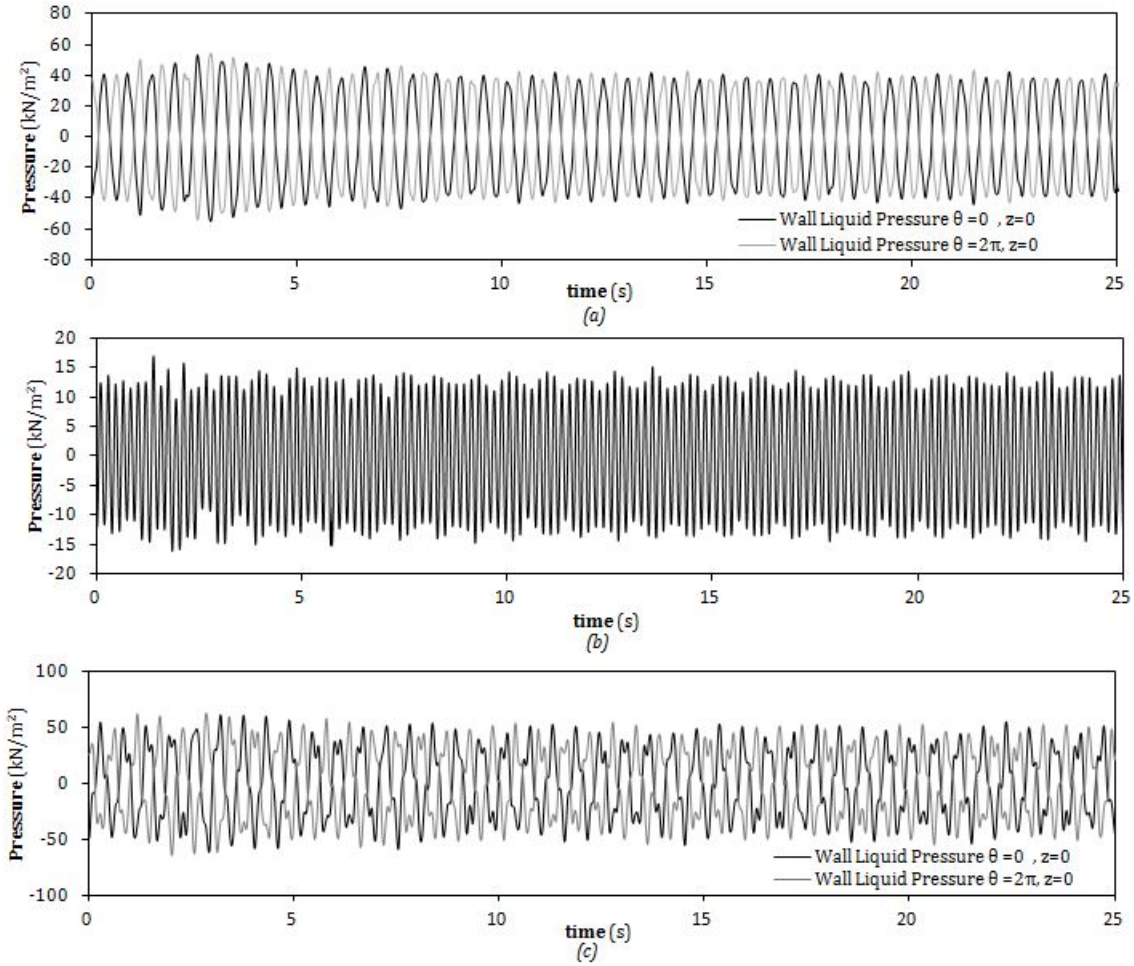

Figure 5.51: Pressure Response in the time domain
: (a) Wall pressure response under earthquake loading on the horizontal direction
(b) Wall pressure response under earthquake loading on the horizontal direction
(c) Total pressure response

CONCLUSION

From figure 5.51, we can analyze the example of time history analysis in the time domain. At the beginning of the parameter determination, the structural damping coefficient is already inputted. However, the system time response is not damped out. This situation means that the structural damping is too small to damp the whole mass of the system. In case of the empty tank, the seismic response damps out, and it is shown in the following figure:

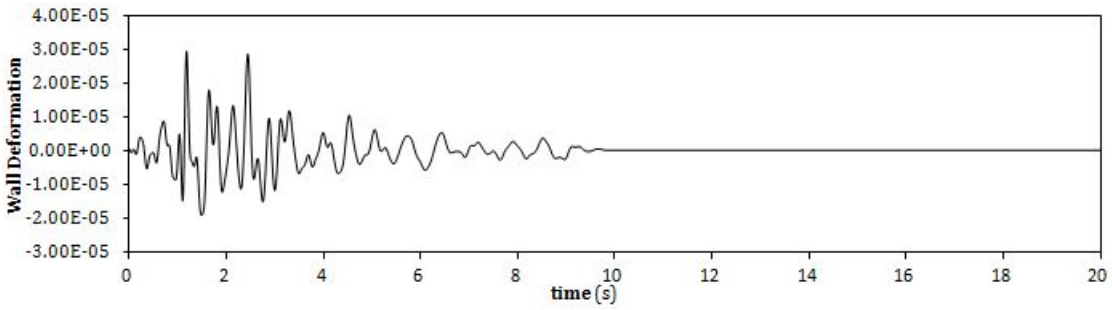

Figure 5.52: Empty tank pressure response in time domain under horizontal loading

From the result and the parameter studies, we understand that the liquid contributes as added masses in this system. This statement means that the total mass now is not only composed by the structure but also from the liquid. This undamped situation might be unrealistic since, at the certain point when the earthquake acceleration stops, the system should damp out due to the material damping. The crucial missing point in the system is the **liquid damping**. Liquid has its own material damping likewise any other structural materials.

5.6. VALIDATION AND VERIFICATION

The validation is an essential step that needs to be performed. From the validation, we can be sure that both the derivation and the implementation of the model are correct. The model is verified in two aspects which are:

1. **Convergence**
   From the two-dimensional model, we already discussed that the modal analysis uses a weak form to satisfy the boundary condition. Instead of satisfying the kinematic boundary condition in every location, the modal analysis uses the integral form. The main issue for the three-dimensional model is: *the boundary conditions are no longer edges but surfaces*, therefore double integration is used to solve the conditions. This double integration leads to a weaker formulation and requirement for more amount of modes to satisfy the convergence.

2. **Journal Comparison**
   The other type of validation is the comparison with the available journals and standards. The parameters that are compared to the journal are the hydrodynamic pressure and the combined system (structure and fluid) eigenvalues.

5.6.1. CONVERGENCE

In this subsection, the convergence of the structure and liquid velocities are checked. The basic principle of checking the convergence is the same as the two-dimensional model (see Figure 3.36). For the sake of legibility, the number of modes shapes are rewritten in the following:

n_p *(the asymmetric mode number)*	= 10 mode numbers;
n_0 *(the axisymmetric mode number)*	= 5 mode numbers;
ϕ_1 *(the wall-liquid coupled potential)*	= 100 mode numbers;
ϕ_2 *(the plate-liquid coupled potential)*	= 100 mode numbers;
ϕ_3 *(the sloshing potential)*	= 3 mode numbers;

In the following figures are shown how converged the both velocities (*wall velocity-liquid velocity* and *plate velocity-liquid velocity*) are:

From the convergence check in Figure 5.53, most of the points difference is under 10%. However, there are some errors in $z = H$ where the difference is higher than 10%. This error is due to the lack of structural mode numbers. However, in this thesis, the convergence check is considered acceptable, as the average error is less than 10% and adding more modes is slowing the computational time. In the following table and plotted graph is discusses how choosing mode numbers take effect on the convergence.

From the table-figure 5.55 and 5.54, we can see that the number of liquid modes plays a dominant role to obtain the convergence. The amount of the structure mode numbers that are used are not giving that impact to the total convergence as the liquid mode numbers. However, using higher quantities of structural mode numbers helps to achieve minor error in the higher frequencies.

5.6.2. REFERENCE COMPARISON

This model is compared with the two references. The first reference is by Velestos and Yang [18]. Their pressure derivation is discussed in the Chapter 2. This journal is being published since the late 70's and become the foundation of the liquid tank under seismic calculation in some standards, including Eurocode [5]. The other journal that is compared to the model is Habenberger in his dissertation [6]. The method from the Habenberger is more accurate than Velestos and Yang. This accuracy is achieved since Habenberger considers the structural modes.

VELESTOS AND TANG [18]

The disadvantage of using the formulation from Velestos and Yang is the missing of higher order modes. They solely consider the fundamental axial mode and circumferential mode for the structural mode number and represent it as an infinite amount of modes. For the sake of legibility, the mode numbers are written as follows:

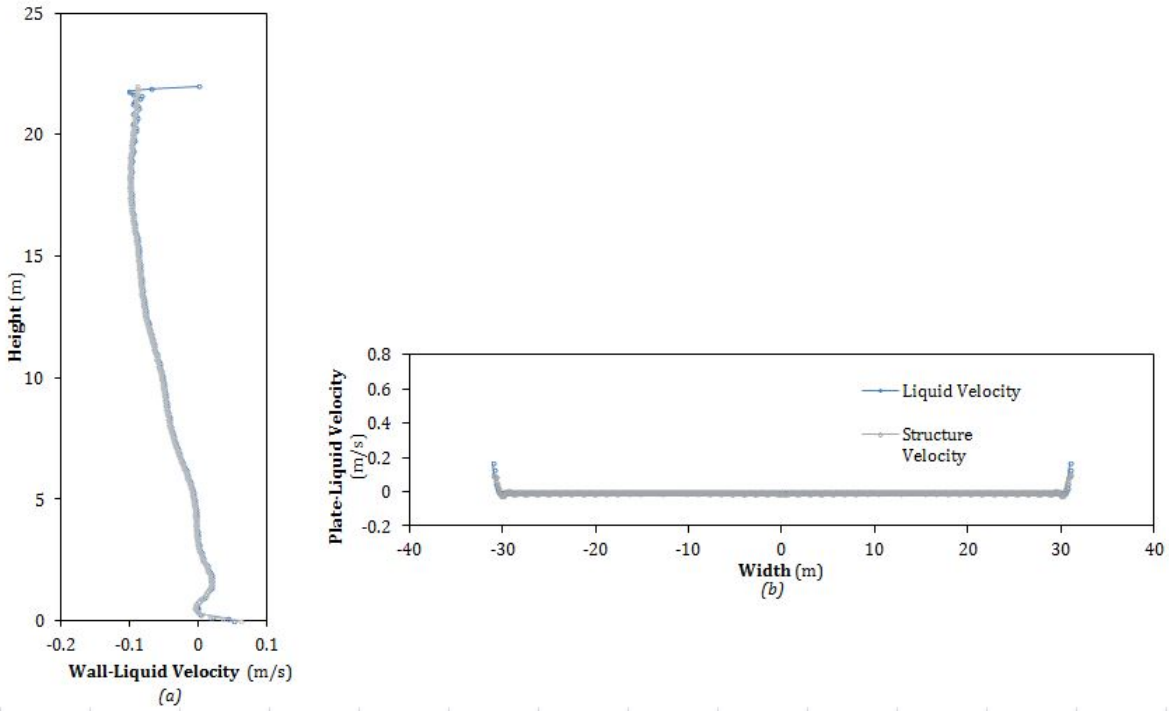

Figure 5.53: Convergence check under horizontal loading at 2.55 Hz : (a) wall convergence at $\theta = 0$; (b) bottom plate convergence

	Structural Mode Number : 10 Liquid Mode Number : 10		Structural Mode Number : 10 Liquid Mode Number : 20		Structural Mode Number : 10 Liquid Mode Number : 50		Structural Mode Number : 10 Liquid Mode Number : 100	
	Frequency (Hz)		Frequency (Hz)		Frequency (Hz)		Frequency (Hz)	
	2.55	8.76	2.55	8.76	2.55	8.76	2.55	8.76
Unconverged Points	31.22%	81.90%	11.76%	82.81%	6.79%	48.87%	4.98%	6.33%
Average Error	17.40%	121.40%	9.88%	71.46%	4.87%	22.79%	4.08%	4.18%
Convergence Figure Axis x : Velocity (m/sec) Axis y : Height (m)	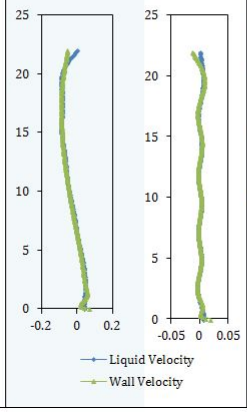		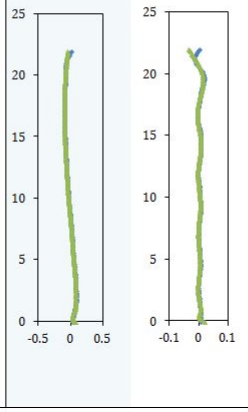		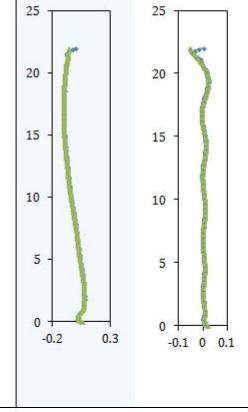		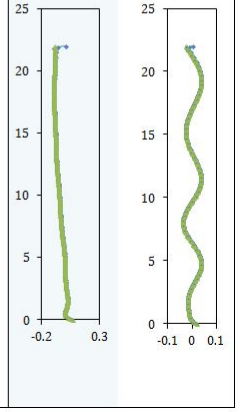	

Figure 5.54: The effect of different liquid mode number to the convergence

n_p *(the asymmetric mode number)*	= 1 mode numbers;
n_0 *(the axisymmetric mode number)*	= 1 mode numbers;
ϕ_1 *(the wall-liquid coupled potential)*	= 100 mode numbers;
ϕ_2 *(the plate-liquid coupled potential)*	= 100 mode numbers;
ϕ_3 *(the sloshing potential)*	= 3 mode numbers;

This assumption might be justified in some cases since from the previous eigenvalue analysis for this case's cylindrical shell empty tank had a relatively high frequency and located in the outside range of the seismic response frequency. However, from the Figure 5.31, we can clearly see that for this case, there are contribution from the higher axial mode numbers: the second and the third axial mode number contributions are 25.4%

	Structural Mode Number : 1 Liquid Mode Number : 100		Structural Mode Number : 5 Liquid Mode Number : 100		Structural Mode Number : 10 Liquid Mode Number : 100		Structural Mode Number : 15 Liquid Mode Number : 100	
	Frequency (Hz)		Frequency (Hz)		Frequency (Hz)		Frequency (Hz)	
	2.55	8.76	2.55	8.76	2.55	8.76	2.55	8.76
Unconverged Points	7.69%	8.60%	6.79%	8.60%	4.98%	6.33%	4.52%	4.98%
Average Error	4.81%	3.29%	5.61%	4.42%	4.08%	4.18%	2.67%	2.75%
Convergence Figure Axis x : Velocity (m/sec) Axis y : Height (m)	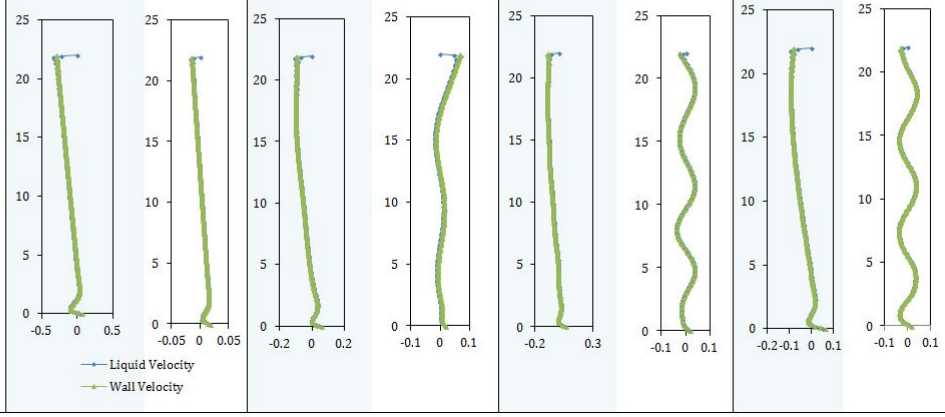							

Figure 5.55: The effect of different vacuo-shell mode number to the convergence

and 4.65% respectively.

To obtain the rigid pressure, the structural elements stiffness are set by multiplying with 10000. This multiplication is a numerical approach to achieve infinite stiffness. In the following figures are shown the comparison between Velestos and Yang with the present result for both flexible and rigid pressure:

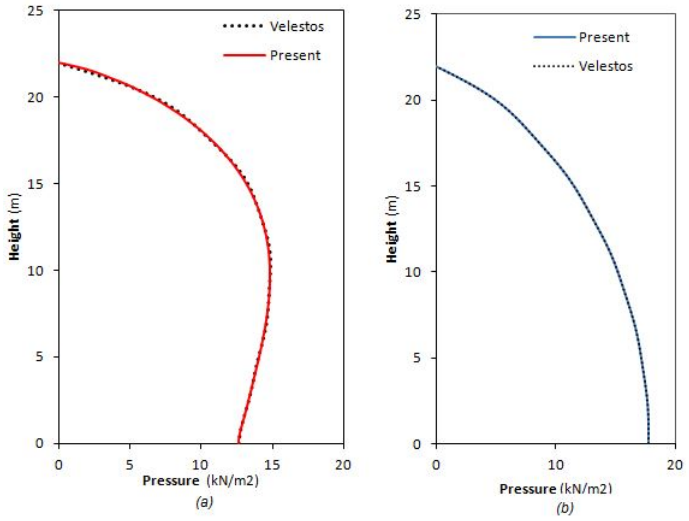

Figure 5.56: Hydrodynamic wall pressure ($\theta = 0$) comparison with Velestos [18] under horizontal loading at the first resonance peak: (a) flexible pressure; (b) rigid pressure

The error between the two hydrodynamic pressure is 0.3%. The difference between the two can be considered as insignificant. This error might derived from numerical in the process such as the usage of numerical integration instead of analytical integration. When we also compared to the two dimenisonal model.

HABENBERGER [6]

In his journal, Habenberger uses the first four axial mode numbers for each circumferential mode. In the following list, let us define the number of modes:

n_p *(the asymmetric mode number)* = 4 mode numbers;
n_0 *(the axisymmetric mode number)* = 4 mode numbers;
ϕ_1 *(the wall-liquid coupled potential)* = 100 mode numbers;
ϕ_2 *(the plate-liquid coupled potential)* = 100 mode numbers;
ϕ_3 *(the sloshing potential)* = 3 mode numbers;

This consideration makes the calculation more accurate compared to the derivation by Velestos and Yang formulation. The tank properties that is set by Habenberger are the following:

Table 5.8: The properties as used by Habenberger [6]

Properties	Value	Unit
A. General Properties		
Height (H)	18.28	m
Diameter ($2R$)	18.28	m
Gravitational acceleration (g)	9.81	m/s^2
B. Liquid Properties		
Water Density (ρ_l)	1.00	ton/m^3
C. Wall Properties(Steel)		
Wall Thickness (h_w)	18.28	mm
Young's Modulus (E_w)	210,000,000	kN/m^2
Mass Density (ρ_w)	7.85	ton/m^3
Poisson Ratio (μ)	0.3	ton/m^3

In the following graph are depicted the hydrodynamic pressure and the natural frequency of the system accordance with Habenberger's properties:

Table 5.9: Liquid Tank Natural Frequency Comparison with Habenberger

Habenberger (rad sec)	**Present** (rad sec)
24.757	25.1
46.969	47.7
65.869	66.0
81.601	79.9

In addition to the natural frequency, the hydrodynamic pressure is compared in the following figure:

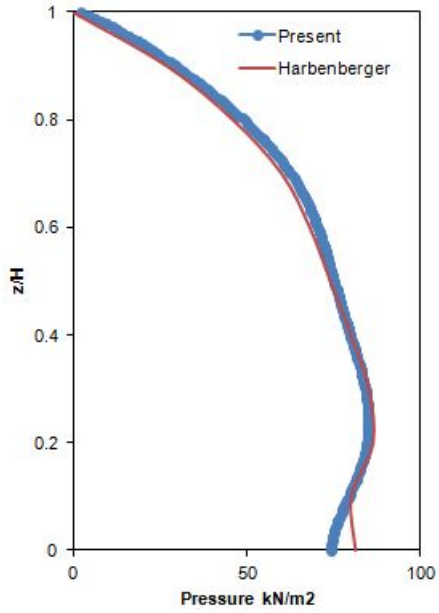

Figure 5.57: Hydrodynamic wall pressure ($\theta = 0$) compare to Habenberger under horizontal loading

From the above figure and table, the difference between present work and Habenberger [6] is relatively small. The natural frequency error is 1.31%, and the hydrodynamic pressure average error is 3.84%. Some errors are expected since some aspects are different from this journal. One of them is the different derivation for the shell structure equations. Last but not least is due to the numerical error and the usage of a different number of liquid modes. In the next section, the comparison between other method is addressed.

5.7. REVIEW FOR CHAPTER 5

From the result, parameter study, and validation, there are some points that one can underline to see the behavior of liquid and structure interaction which are:

- **Foundation and plate stiffness**.
  In this thesis, there are two models. The first model is the clamped free system (Model A), wherein this case the soil-structure interaction is disregarded. The second model is the Model B where the plate flexibility and soil-structure interaction is represented as a Winkler foundation. In both conditions which are filled and empty tank, the Model B always have lower frequencies. For the empty and filled tank, the fundamental asymmetric natural frequency of Model B decreases about 0.32 and 0.71 times from Model A for this case. These lower frequencies are expected due to the later model is more flexible than the first model. In this thesis, these numbers are considered high. Therefore, the soil-structure interaction is regarded a critical parameter to design the liquid storage tank. However, the sloshing frequencies are almost not changing even though the soil-structure interaction is included.

- **Added Mass derived from the liquid interaction to the structure.**
  The three-dimensional model also shown the same behavior as the second-dimensional model which is the liquid pressure decreases the frequency of the system. This frequency decrement is due to the liquid pressure resulting in an added mass in the system. The mass addition to the mass yields to lower frequency based on what we have learned from equation 2.12.

- **Sloshing frequency are located in low frequency range**.
  The sloshing frequencies are located in the low-frequency range for the considered geometry. This statement leads to the free surface water elevation are higher in the low-frequency range. The free surface water elevation has the direct correlation with the free surface water pressure. Therefore, we can also conclude that the free surface water pressure mostly takes effect in the total pressure on the low-frequency domain. The higher the frequency, the less impact that is given from the free surface waves to the total pressure.

- **Axisymmetric and asymmetric seismic loading.**
  The vertical loading is an axisymmetric loading. From the results, we can see that the vertical loading cause axisymmetric liquid pressure. The horizontal loading is an asymmetric loading which results in the asymmetric liquid pressure. Therefore we can conclude that the response whether it is asymmetric or axisymmetric is accordance with the type of the loading. This pattern is shown in both the two-dimensional and three-dimensional model.

- **Modes Contribution**
  How the response follows the load can also be seen from the modes contribution. For axisymmetric loading, only axisymetric modes that contribute in the system. This also applies contrary to the asymmetric loading. We can also understand that only the fundamental circumferential mode number that contributes in the dynamic behavior under horizontal loading. We also learn that choosing the mode number needs a careful consideration. For this case, the second and the third axial mode number have considered significant contribution which are 25.4% and 4.65% respectively. Therefore by only using the axial fundamental mode might be less representative in this case. For the vertical loading, the dominant contribution comes from the rigid body component with 94.8%. Therefore from Figure 5.30, 5.31, 5.36, and 5.37, we can see that these chosen structural mode number has achieved more than 90 % for the total contribution. Which we can also come to a conclusion that for this case the number of structural modes is acceptable.

- **Liquid Volume**.
  From the previous point, we can understand that the liquid contributes mass to the whole system. Since mass and volume is closely related, it is expected that the change in liquid volume influences the impulsive frequencies. The higher the volume, the lower the impulsive frequencies. The decreasing frequencies are due to higher volume leads to higher mass and smaller frequency from equation 2.12. By decreasing the volume to 75% and 50%, the fundamental natural frequency is increasing 1.37 and 1.95 times respectively.

- **Flexibility of the structure gives significant effect for the entire structure**.
  The flexibility influence both the natural frequencies and the pressure exerted on both wall and plate. The flexibility also influences the impulsive frequency. However, this might not be the case for the sloshing frequency. For this specific case study, the difference between the sloshing and the impulsive frequency is the ten to the power of two. We can say both frequencies are almost independent. The flexibility hardly influences the sloshing frequencies, unless the frequencies are closely excited. The relation between the fundamental impulsive frequency and the wall thickness is quadratic. The flexibility of the wall have more significant impact compare to the flexibility of the plate.

- **Tank dimension (H/R) of the Structure strongly influence the sloshing frequency**.
  Since from the previous point we can learn that the flexibility wall and flexibility of the plate can be seperated from the sloshing. Therefore the frequency can be roughly calculated in the equation 5.15. Where we can see that there is no dependency on the flexibility of the structure and the components that composed the sloshing frequency equation are only g (gravity acceleration) and tank H/R ratio. The comparison between the seperated analysis of sloshing potential and this present study (see Table 5.7) for this case has a considerable small error which is 0.54 %.

- **Comparison with the other journal**.
  From the journal that is written by Velestos and Yang [18], there is a fundamental assumption which is: they only consider that the structural fundamental frequency and disregard higher order modes. However, the journal that is written by Habenberger [6] considers only the first four modes. Therefore in order to have a fair comparison between the two models, the number of structural modes are adjust

to the two references. Only by adjusting the mode number, we can see that the pressure from this thesis has acceptable difference with other journals.

- **Higher number of modes to reach convergence in the three dimensional model**.
  From the convergence check, the error for this thesis is acceptable. The number of modes that is use by default for this case are in the following list:

  n_p *(the asymmetric mode number)* = 5 mode numbers;
  n_0 *(the axisymmetric mode number)* = 10 mode numbers;
  ϕ_1 *(the wall-liquid coupled potential)* = 100 mode numbers;
  ϕ_2 *(the plate-liquid coupled potential)* = 100 mode numbers;
  ϕ_3 *(the sloshing potential)* = 3 mode numbers;

  In the convergence check we can learn that for a three-dimensional model more modes are needed to achieve convergence with a small difference as the two-dimensional model has. Such phenomenon is well predicted since the from the equation 4.59 exist double integration. This double integration makes the equation form weaker.

6

CONCLUSIONS AND RECOMMENDATIONS

The last chapter covers the complete conclusion for both two-dimensional and three-dimensional model. In addition to the conclusions, we also discuss some limitations and suggestions for the current model. Within numerous assumptions, the model will need some development to achieve an actual representation and versatility for other actual cases. Therefore some of this suggestions, hopefully, will help to complete this model for future development.

6.1. CONCLUSIONS

From both the two-dimensional and three-dimensional model, we can conclude some points on how the model and the dynamic behavior of the liquid tank .

- This thesis presents a novel method to solve for the dynamics of a tank-liquid system subjected to seismic excitation. In the adopted solution approach, the total system is divided into two subsystems, i.e. the tank structure and the contained liquid. The response of the structure is expressed in terms of the in-vacuo shell modes which can be obtained by formulating a standard eigenvalue problem for the shell consisting of the plate and the wall of the tank. The fluid motion is separated into a number of linear potentials. The satisfaction of the kinematic continuity at the shell-liquid interfaces allows one to correlate the modal coefficients of the shell structure to those of the fluid potentials. The forced response can subsequently be found by solving the forced equations of motion of the tank including the seismic excitation and the exerted pressure of the stored liquid at the inner side of the shell.

- The semi-analytical method of solution is computationally inexpensive and accurate. Moreover, the inexpensiveness is also due to the fact that the tank structure is represented by the in-vacuo shell modes, the latter do not change with varying liquid height. Thus, one needs to solve the eigenvalue problem of the shell structure only once for a given tank geometry and subsequently use this modal set for any filling height of the liquid. The accuracy of the method is demonstrated via comparison with other documented results in the literature [18] and [6].

- A parametric study is contacted which has shown that in the case of tanks made of steel, the flexibility of the tank needs to be considered. The dynamic behaviour of the liquid-structure interaction in the storage tank is dependent to the tank geometry and liquid volume as well. Additionally, the number of fluid modes to accurately capture the pressure at the inner side of the wall of the tank needs careful consideration. In this study we have shown that to achieve satisfactory convergence in terms of the displacement continuity at the fluid-tank interfaces higher order modes need to be accounted for in the modal summation. This is something that is often overlooked in the literature.

- On deriving the liquid shape function, the superposition of three potentials is more convenient to analyze the convective and the impulsive component separately than using the two potentials. Moreover, the rigid body motions of liquid shape function for z-direction dependent potentials are more straightforward to obtain using the three superposition. The only disadvantage of using the three superposition derivation is relatively lengthier than using the two superposition Regardless, these two ways of liquid superposition will yield the same result at the end.

- The introduction of liquid damping is essential to describe the system more accurately. We can conclude that even though the structural damping is regarded, the time history response does not damp out even after the earthquake loading stop. The total mass of the system in the filled tank is heavier than the empty tank due to the additional contribution of the liquid hydrodynamic pressure. Therefore liquid damping should be included since the structural damping is insufficient to damps out all the system mass.

6.2. RECOMMENDATIONS

In this subsection will be discuss the thing that can be improved in this thesis which are the uncomplete structure element, soil structure interaction, liquid assumption and the material.

- The results are highly sensitive to the choice of the spring constants to represent the effect of soil-structure interaction. Since an accurate determination of the spring constants is very difficult, a more detailed description of the soil is needed. This can be achieved without much computational effort in the adopted modelling approach since the addition of the soil will add one extra substructure in the total system. The dynamic stiffness of the soil-foundation substructure can be obtained independently and then coupled to the already obtained tank-liquid system presented in this thesis. A layered soil stratum can also be included with no additional computational costs. Better modelling of the soil structure interaction can also capture the seismic travelling waves along the ground surface(i.e. Rayleigh wave) in a more refine manner .This point is missing in the present model since the soil springs are modelled only in one direction. Meanwhile, the travelling waves can propagate in two directions. This component is essential for tanks of large diameter in which the motion of the base is non-synchronous

- In this thesis only the wall and the plate of the tank are modelled. An extension of the model to include the dome of the tank is needed in some case but this is quite straightforward (and thus not of added scientific value in this thesis). The only extra step that needs to be considered to include the dome of the tank is to modify slightly the eigenproblem that one needs to solve to obtain the eigenvalues and eigenshapes of the tank structure (in vacuo modes).

- Since geometrical non-linearity is disregarded, any buckling failure modes cannot be analyzed in this thesis. There are two buckling failure modes under dynamic loading, which are the elephant foot buckling and the diamond shape buckling. Elephant foot buckling is the result from combined action of vertical compressive stresses and hoop tension close to the critical stress. The other type of buckling which is diamond shaped buckling is elastic buckling in shell. The main cause is due to the high axial compressive stresses. This axial stress can be caused from the rocking motion that occurs at the base of unanchored tanks.

BIBLIOGRAPHY

[1] ABRAMOWITZ, M., STEGUN, I. A., AND MILLER, D. Handbook of Mathematical Functions With Formulas, Graphs and Mathematical Tables (National Bureau of Standards Applied Mathematics Series No. 55), 1965.

[2] AMABILI, M., PAÏDOUSSIS, M., AND LAKIS, A. Vibrations of Partially Filled Cylindrical Tanks With Ring-Stiffeners and Flexible Bottom. *Journal of Sound and Vibration 213*, 2 (1998), 259–299.

[3] ARON, C., AND JONAS, E. Structural Element Approaches for Soil-Structure Interaction, 2012.

[4] BAUER, H. F., AND SIEKMANN, J. Dynamic interaction of a liquid with the elastic structure of a circular cylindrical container. *Ingenieur-Archiv 40*, 4 (1971), 266–280.

[5] EUROPEAN COMMITEE FOR STANDARDIZATION. EN 1998-4:2006 - Eurocode 8: Design of structures for earthquake resistance - Part 4: Silos, tanks and pipelines. *Eurocode 8: Design of structures for earthquake resistance 4*, 2006 (2006), 84.

[6] HABENBERGER, J. Beitrag zur Berechnung von nachgiebig gelagerten Behältertragwerken unter seismischen Einwirkungen. *Deposit.Ddb.De* (2001), 185.

[7] HOUSNER, G. W. Earthquakes Pressures on Fluid Containers. Tech. rep., Office Naval Research, Pasadena, California, 1954.

[8] INLAND NAVIGATION COMMISSION. Tech. rep.

[9] J.M.J., S., A.W.C.M., V., AND E.C., K. *Structural Dynamics CT 4140*. 2005.

[10] KIM, J. K., KOH, H. M., KWAHK, I. J., AND METHODS, A. Dynamic Response of Rectangular Flexible Fluid Containers. *Engineering 122*, 9 (1996), 807–817.

[11] KRAMER, S. L. *Geotechnical Earthquake Engineering*. Prentice Hall, New Jersey, 1996.

[12] METRIKINE, A. *Dynamics, Slender Structures and an Introduction to Continuum Mechanics CT 4145*. Delft.

[13] ORLIC, B. Geomechanical effects of CO2 storage in depleted gas reservoirs in the Netherlands: Inferences from feasibility studies and comparison with aquifer storage. *Journal of Rock Mechanics and Geotechnical Engineering 8*, 6 (2016), 846–859.

[14] RAOUF A. IBRAHIM. *Liquid Sloshind Dynamics: Theory and Applications*, first edit ed. Cambridge University Press, Cambridge, 2005.

[15] SEZEN, H., LIVAOGLU, R., AND DOGANGUN, A. Dynamic analysis and seismic performance evaluation of above-ground liquid-containing tanks. *Engineering Structures 30*, 3 (2008), 794–803.

[16] SOEDEL, W., AND QATU, M. S. *Vibrations of Shells and Plates, Third Edition*, third edit ed., vol. 117. Marcel Dekker,Inc., New York, 2005.

[17] TSOUVALAS, A. Semi-analytical modeling of the earthquake response of an LNG tank using the dynamic sub-structuring technique, 2012.

[18] VELETSOS, A. S., AND YANG, J. Y. Dynamics of fixed-base liquid storage tanks. In *U.s. Japan Seminar on Earthquake Engineering Research with Emphasis on Lifeline Systems* (Tokyo, 1976), The Kajima Foundation.

[19] VERSLUIS, M. Hydrodynamic pressures on large lock structures, 2010.

[20] VROUWENVELDER, A. *Random Vibration CIE 5145*. Delft, 1995.

[21] W. WEAVER, J., TIMOSHENKO, S. P., AND YOUNG, D. H. *Vibration Problems in Engineering*, fifth edit ed. John Wiley & Sons, New York, 1990.

A

VIBRATION OF CONTINUOUS SYSTEM

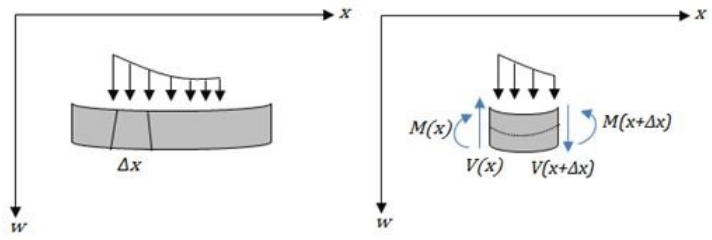

Figure A.1: Beam undergoing transverse motion *(left)* differential element of the beam subject to the shear force bending moment and external load *(right)*

Using kinematic relations that is depicted in the figure A.1, the derivation begins with *kinematic relation.* For Euler Bernoulli beam, the kinematic components are:

$$\begin{aligned} \varphi &= -\frac{dw}{dx} \\ \kappa &= \frac{d\varphi}{dx} \\ \varepsilon &= z\kappa \end{aligned} \tag{A.1}$$

The first equation is a result from an assumption that implies there is *no shear deformation* occurs, or the *cross section is considered remaining perpendicular to the neutral line.* As for the third relationship is a result of the assumption that plane cross-section is remaining in plain or *t*hestrain is linear over the height of the beam.

After definition of the kinematic relation is obtained, the constitutive relation can be determined. The basic principle of this relation is *the Hooke's law.* The derivations are defined as follows:

$$\sigma = \epsilon(z)E \tag{A.2}$$

By substituting the equation A.1 to the equation A and integrating the result, the bending moment can be achieved as the equation below:

$$\sigma = z\kappa \cdot E \tag{A.3}$$

$$M(x) = \int (z\sigma(z))dA \tag{A.4}$$

$$M = EI\kappa \tag{A.5}$$

By using the second law of Newton, the vibration in x direction will result as follows:

$$\sum F_x = Ma_x \tag{A.6}$$

$$\begin{aligned} dV + q\,dx &= \rho A\,dx \frac{\partial^2 w}{\partial t^2} \\ \frac{d^2 M}{dx^2} + q &= \rho A \frac{\partial^2 w}{\partial t^2} \end{aligned} \tag{A.7}$$

Substituting this equation above to the equation A.5 results to the *Euler-Bernoulli beam theory's governing equation of motion*:

$$EI\frac{d^4 w}{dx^4} + \rho A \frac{\partial^2 w}{\partial t^2} = q \tag{A.8}$$

B

VIBRATION PLATE AND SHELL DERIVATION

The derivations of vibration plate and shell in this Appendix are referred to Soedel derivation [16]. The derivations consist of three main sections which are:

1. Curvilinear coordinates definition
2. Strain - Displacement Relationship *(kinematic relation)*
3. Love simplification for thin shell
4. Membrane Forces and Bending Moment *(constitutive relation)*
5. Hamilton Principle *(derivation for equations of motion)*

B.1. SHELL COORDINATES AND INFINITESIMAL DISTANCES IN SHELL LAYER

Before going through depth in the derivation, let us firstly define the shell as *thin*, *isotrpohic*, and *homogeneous shell* element for easier derivation. The next step before deriving the shell motion is to define the curvilinear coordinates of the shell. In the following figure the infinitesimal element and the reference surface is defined :

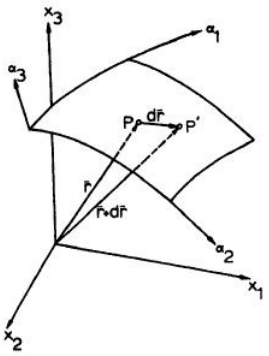

Figure B.1: Reference Surface
Source : Vibration of Shell and Plates, Soedel [16]

For the cartesian coordinates, we can define the location of the point in Figure B.1 as follows:

$$x_1 = f_1(\alpha_1, \alpha_2, \alpha_3), \quad x_2 = f_2(\alpha_1, \alpha_2, \alpha_3), \quad x_3 = f_3(\alpha_1, \alpha_2, \alpha_3) \tag{B.1}$$

The location of point P in Figure B.1 on the neutral surface can also be written in vector form, which is:

$$\overline{r} = f_1(\alpha_1, \alpha_2)\overline{e}_1 + f_2(\alpha_1, \alpha_2)\overline{e}_2 + f_3(\alpha_1, \alpha_2)\overline{e}_3 \tag{B.2}$$

As the coordinate can be explained in the equations B.1 and B.2, The infinitesimal distance between the two points which are point P and point P' on the neutral surface $(d\overline{r})$is:

$$d\overline{r} = \frac{\partial \overline{r}}{\partial \alpha_1} d\alpha_1 + \frac{\partial \overline{r}}{\partial \alpha_2} d\alpha_2 \tag{B.3}$$

The magnitude of the distance of $d\overline{r}$ can be achieved as follows:

$$(ds)^2 = d\overline{r} \cdot d\overline{r} \tag{B.4}$$

$$\begin{aligned} (ds)^2 &= \frac{\partial \overline{r}}{\partial \alpha_1} d\alpha_1 + \frac{\partial \overline{r}}{\partial \alpha_2} d\alpha_2 \cdot \frac{\partial \overline{r}}{\partial \alpha_1} d\alpha_1 + \frac{\partial \overline{r}}{\partial \alpha_2} d\alpha_2 \\ (ds)^2 &= \frac{\partial \overline{r}}{\partial \alpha_1} \frac{\partial \overline{r}}{\partial \alpha_1} (d\alpha_1)^2 + \frac{\partial \overline{r}}{\partial \alpha_2} \frac{\partial \overline{r}}{\partial \alpha_2} (d\alpha_2)^2 + 2 \frac{\partial \overline{r}}{\partial \alpha_1} \frac{\partial \overline{r}}{\partial \alpha_2} d\alpha_1 \cdot d\alpha_2 \end{aligned} \tag{B.5}$$

The *third term is zero*, because of only curvilinear coordinates that coincide with the *curvature of the neutral surface*. Therefore the first and the two terms can be defined as follows:

$$\begin{aligned} \frac{\partial \overline{r}}{\partial \alpha_1} \frac{\partial \overline{r}}{\partial \alpha_1} &= A_1^2 \\ \frac{\partial \overline{r}}{\partial \alpha_2} \frac{\partial \overline{r}}{\partial \alpha_2} &= A_2^2 \end{aligned} \tag{B.6}$$

Where it can be simplified as the equation bellow:

$$(ds)^2 = A_1^2 (d\alpha_1)^2 + A_2^2 (d\alpha_2)^2 \tag{B.7}$$

The equation B.7 is defined as *the fundamental form* and the A_1 and A_2 are called the *fundamental form parameters* or *Lamé parameters*. These Lamé parameters is very convenient for deriving the equation of motion in any shape. This convenience is because of the Lameé parameter can be defined uniquely for every type of shapes of shells.

The fundamental form can be intrepeted as defining the hypotenuse ds of the right triangle as depicted in Figure B.2. This hypotenuse are infinitesimal distance along the surface coordinates of the shell.

$$(ds)^2 = (dx)^2 + \alpha^2 (d\theta)^2 \tag{B.8}$$

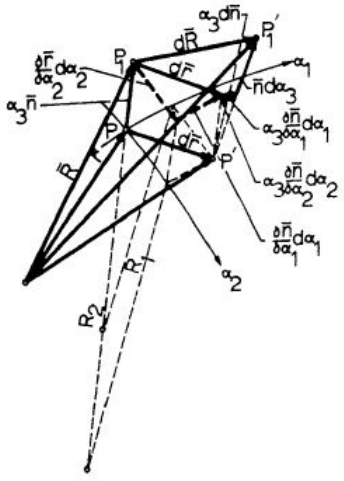

Figure B.2: Distance between two points removed from the reference surface
Source : Vibration of Shell and Plates, Soedel [16]

For general case, the simplification can be done in the shell derivation. The simplification is by defining the

infinitesimal distance between a point P_1 normal to P and a point of P_1' wnormal to P and a point P_1' normal to P' . The point P_1 is located at a distance α_3 *from the neutral surface.*The figure B.2describe the geometry of these points The P_1' is located in $(\alpha_3 + d\alpha_3)$ from the neutral surface. Therefore the location of the P_1 as:

$$\overline{R}(\alpha_1, \alpha_2, \alpha_3) = \overline{r}(\alpha_1, \alpha_2) + \alpha_3 \overline{n}(\alpha_1, \alpha_2) \tag{B.9}$$

Referred to Soedel the equation can be simplified as follows:

$$(ds)^2 = A_1^2\Big(1 + \frac{\alpha_3}{R_1}\Big)^2 (d\alpha_1)^2 + A_2^2\Big(1 + \frac{\alpha_3}{r_2}\Big)^2 (d\alpha_2)^2 + (d\alpha_3)^2 \tag{B.10}$$

B.2. STRESS-STRAIN RELATIONSHIP

Similar as the continous beam, one can relate the strain with the stress relationship by using the *constitutive relation.* Therefore the equation for the stress-strain relationship according the Hooke's Law are:

$$\begin{aligned}
\varepsilon_{11} &= \frac{1}{E}[\sigma_{11} - \mu(\sigma_{22} + \sigma_{33})] \\
\varepsilon_{22} &= \frac{1}{E}[\sigma_{22} - \mu(\sigma_{11} + \sigma_{33})] \\
\varepsilon_{33} &= \frac{1}{E}[\sigma_{33} - \mu(\sigma_{11} + \sigma_{22})] \\
\varepsilon_{12} &= \frac{\sigma_{12}}{G} \\
\varepsilon_{13} &= \frac{\sigma_{13}}{G} \\
\varepsilon_{23} &= \frac{\sigma_{23}}{G}
\end{aligned} \tag{B.11}$$

Where ε is strain of the element in different direction. From the strain, the stresses in the element can be depicted in the following figure:

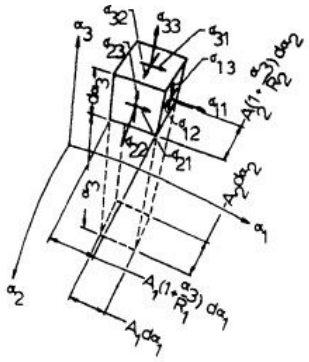

Figure B.3: Stress Acting in the Element
Source : Vibration of Shell and Plates, Soedel [16]

The shear stresses can be derived as follows:

$$\begin{aligned}
\sigma_{12} &= \sigma_{21} \\
\sigma_{13} &= \sigma_{31} \\
\sigma_{23} &= \sigma_{32}
\end{aligned} \tag{B.12}$$

For a simplification, the normal stresses σ_{33} thhat acts in the normal direction to the neutral surface is neglected.

$$\sigma_{33} = 0 \tag{B.13}$$

From this assumptions and stresses, one can define the strain in term of stress, as the following definitions :

$$\begin{aligned}\varepsilon_{11} &= \frac{1}{E}(\sigma_{11} - \mu\sigma_{22}) \\ \varepsilon_{22} &= \frac{1}{E}(\sigma_{22} - \mu\sigma_{11}) \\ \varepsilon_{12} &= \frac{\sigma_{12}}{G} \\ \varepsilon_{33} &= -\frac{\mu}{E}(\sigma_{11} + \sigma_{22})\end{aligned} \tag{B.14}$$

B.3. STRAIN-DISPLACEMENT RELATIONSHIP

From Section B.2, one can see that the infinitesimal distance between the two points of P_1 and P_1'. In this chapter the equation can be also defined into the following equations:

$$\begin{aligned}A_1^2\left(1+\frac{\alpha_3}{R_1}\right)^2 &= g_{11}(\alpha_1,\alpha_2,\alpha_3) \\ A_2^2\left(1+\frac{\alpha_3}{R_2}\right)^2 &= g_{22}(\alpha_1,\alpha_2,\alpha_3) \\ 1 &= g_{33}(\alpha_1,\alpha_2,\alpha_3)\end{aligned} \tag{B.15}$$

Or one can write in term of distance, that is obtained by summing all the equations in equation B.15

$$(ds)^2 = \sum_{i=1}^{3} g_{ii}(\alpha_1,\alpha_2,\alpha_3)(d\alpha_i)^2 \tag{B.16}$$

As the previous equation is in the *underformed state*, as the shell is deformed the point of P_1 which originally located in $(\alpha_1,\alpha_2,\alpha_3)$ is deflected in the α_1 direction by U_1 and it will be the same for the other index. Therefore the deflection U_i and coordinate change ξ_i

$$U_i = \sqrt{g_{ii}(\alpha_1,\alpha_2,\alpha_3)}x_i \tag{B.17}$$

For the point P_1' which originally at $(\alpha_1+d\alpha_1,\alpha_2+d\alpha_2,\alpha_3+d\alpha_3)$ when it deflected it will located in $(\alpha_1+d\alpha_1+\xi_1,\alpha_2+d\alpha_2+\xi_2,\alpha_3+d\alpha_3+\xi_3)$/ therefore the distance of two points P_1 and P_1' in the deflected state will be

$$(ds)^2 = \sum_{i=1}^{3} g_{ii}(\alpha_1+\xi_1,\alpha_2+\xi_2,\alpha_3+\xi_3)(d\alpha_i+d\xi_i)^2 \tag{B.18}$$

By using the taylor series since the the $g_{ii}(\alpha_1+\alpha_2+\alpha_3)$ is a continuous system, one can re-written the above equation into:

$$g_{ii}(\alpha_1+\xi_1,\alpha_2+\xi_2,\alpha_3+\xi_3) = g_{ii}(\alpha_1,\alpha_2,\alpha_3) + \sum_{j=1}^{3}\frac{\partial_i i(\alpha_1,\alpha_2,\alpha_3)}{\partial\alpha_j}\xi_j \tag{B.19}$$

It can also be written from The equation [B.19] that:

$$(d\alpha_i + dxi_i) = (d\alpha_i)^2 + 2d\alpha_i d\xi_i + (d\alpha_i)^2 \tag{B.20}$$

In order to have a consistent approximation to the **linear theory** the third term is disregard from the equation. Therefore, differential $d\xi_i$ is written as follows:

$$d\xi_i = \sum_{j=1}^{3}\frac{\partial\xi_i}{\partial\alpha_j}d\alpha_j \tag{B.21}$$

Substituting the equation B.21 to the equation B.20 the equation can be written as the following:

$$(d\alpha_i+\xi_i) = (d\alpha_i)^2 + 2d\alpha_i d\sum_{j=1}^{3}\frac{\partial\xi_i}{\partial\alpha_j}(d\alpha_j) \tag{B.22}$$

Afterwards, the equation B.22 is substituted to the deflected state main equation B.18,

$$(ds)^2 = \sum_{i=1}^{3}\left[g_{ii}(\alpha_1,\alpha_2,\alpha_3) + \sum_{j=1}^{3}\frac{\partial g_{ii}(\alpha_1,\alpha_2,\alpha_3)}{\partial \alpha_j}\xi_j\right] \times\left[(d\alpha_i)^2 + 2d\alpha_i d\sum_{j=1}^{3}\frac{\partial \xi_i}{\partial \alpha_j}(d\alpha_j)\right] \tag{B.23}$$

The equation above can be expanded into the following:

$$g_{ii}(\alpha_1,\alpha_2,\alpha_3) = g_{ii} \tag{B.24}$$

Therefore the equation (B.23) will result in the following

$$(ds')^2 = \sum_{i=1}^{3}\left[\left(g_{ii} + \sum_{j=1}^{3}\frac{\partial g_{ii}}{\partial \alpha_j}(d\alpha_j)^2\right) + g_{ii}\sum_{j=1}^{3}\frac{\partial \xi) j}{\partial \alpha_j}d\alpha_j + 2d\alpha_i\sum_{j=1}^{3}\frac{\partial g_{ii}}{\partial \alpha_j}\xi_j\sum_{j=1}^{3}\frac{\partial \xi_j}{\partial \alpha_j}\alpha_j\right] \tag{B.25}$$

An assumption are made for the shell derivation which is the *initial stresses does not influence the vibration* or one can say that the system is *linear* such as no buckling. From this assumption the third term can be disregard from the equation. Therefore by replacing the j into k, the equation results as follows:

$$(ds')^2 = \sum_{i=1}^{3}\left(g_{ii} + \sum_{k=1}^{3}\frac{\partial g_{ii}}{\partial \alpha_k}(d\alpha_i)^2\xi_k\right) + \sum_{i=1}^{3}\sum_{j=1}^{3} g_{ii}\frac{\partial \xi_j}{\partial \alpha_j}d\alpha_j d\alpha_i + \sum_{i=1}^{3}\sum_{j=1}^{3} g_{ii}\frac{\partial \xi_j}{\partial \alpha_j}d\alpha_j d\alpha_i \tag{B.26}$$

By utilizing *kronecker delta*, one can simplifies the first term into the following equation:

$$\sum_{i=1}^{3}\sum_{j=1}^{3}\left(g_{ii} + \sum_{k=1}^{3}\frac{\partial g_{ii}}{\partial \alpha_k}(d\alpha_k)^2\xi_k\right)\delta_{ij}d\alpha_i d\alpha_j \tag{B.27}$$

While the last two term can be written in symmetric form by noticing that:

$$\sum_{i=1}^{3}\sum_{j=1}^{3} g_{ii}\frac{\partial \xi_i}{\partial \alpha_j}d\alpha_j d\alpha_i = \sum_{i=1}^{3}\sum_{j=1}^{3} g_{jj}\frac{\partial \xi_j}{\partial \alpha_i}d\alpha_i d\alpha_j \tag{B.28}$$

Therefore by substituting back to the main equation, the distance formulation can be written in the following:

$$(ds')^2 = \sum_{i=1}^{3}\sum_{j=1}^{3}\left[\left(g_{ii} + \sum_{k=1}^{3}\frac{\partial g_{ii}}{\partial \alpha_k}(d\alpha_k)^2\xi_k\right)\delta_{ij} + g_{ii}\frac{\partial \xi_i}{\partial \alpha_j} + g_{jj}\frac{\partial \xi_j}{\partial \alpha_i}\right]d\alpha_i d\alpha_j \tag{B.29}$$

Let us introduce the variable G_{ij} to compact the equation above:

$$G_{ij} = \left(g_{ii} + \sum_{k=1}^{3}\frac{\partial g_{ii}}{\partial \alpha_k}(d\alpha_k)^2\xi_k\right)\delta_{ij} + g_{ii}\frac{\partial \xi_i}{\partial \alpha_j} + g_{jj}\frac{\partial \xi_j}{\partial \alpha_i} \tag{B.30}$$

This equation results as:

$$(ds')^2 = \sum_{i=1}^{3}\sum_{j=1}^{3} G_{ij}d\alpha_i d\alpha_j \tag{B.31}$$

Note that $G_{ij} = G_{ji}$. In general the displacement can be written as follows:

$$\begin{aligned}(ds)^2_{ii} &= g_{ii}(d\alpha_i)^2\\ (ds')^2_{ii} &= G_{ii}(d\alpha_i)^2\\ (ds)^2_{ij} &= g_{ii}(d\alpha_i)^2 + g_{jj}(d\alpha_j)^2\\ (ds')^2_{ii} &= G_{ii}(d\alpha_i)^2 + G_{jj}(d\alpha_j)^2 - 2G_{ij}d\alpha_i d\alpha_j\end{aligned} \tag{B.32}$$

From these equations B.32, the strain can be formulated into the following equation:

$$\varepsilon_{ii} = \frac{du}{dx} = \frac{(ds')_{ii} - (ds)_{ii}}{(ds)_{ii}} = \sqrt{\frac{G_{ii}}{g_{ii}}} - 1 \tag{B.33}$$

Once again, the *taylor series expansion* is used, where the equation will result in the following:

$$\varepsilon_{ii} = \frac{G_{ii} - g_{ii}}{2 \times g_{ii}} \tag{B.34}$$

As for the shear strain, the strain is defined as the *angular change of an infinitesimal element* and illustrated in the following equation:

$$\varepsilon_{ij} = \frac{\pi}{2} - \theta_{ij} \tag{B.35}$$

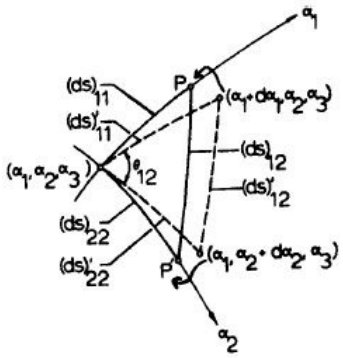

Figure B.4: Shear deformation in plane of the reference surface
Source : Vibration of Shell and Plate, Soedel [16]

Based on the figure B.4 and equation (B.32) by utilizing the cosine law, one can compute the angle into the following:

$$\begin{aligned} (ds')^2_{ii} &= (d'_{ii})^2 + (d'_{jj})^2 - 2(d'_{ii})(d'_{jj})\cos\theta_{ij} \\ \cos\theta_{ij} &= \frac{G_{ij}}{\sqrt{G_{ii}G_{jj}}} \end{aligned} \tag{B.36}$$

The above equation is substituted back to the equation B.3. Which then result in:

$$\cos\left(\frac{\pi}{2} - \varepsilon_{ij}\right) = \sin\varepsilon_{ij} = \frac{G_{ij}}{\sqrt{G_{ii}G_{jj}}} \tag{B.37}$$

Since for reasonable shear strain magnitudes are considerable small therefore it can be simplified that:

$$\sin\varepsilon_{ij} = \varepsilon_{ij}\frac{G_{ij}}{\sqrt{G_{ii}G_{jj}}} = \frac{G_{ij}}{\sqrt{g_{ii}G_{jj}}} \tag{B.38}$$

Substitution into the general equation B.15 it will result the strain with index 1,2,3:

$$\begin{aligned} \varepsilon_{11} &= \frac{1}{A_1(1+\alpha_3/R_1)}\left(\frac{\partial U_1}{\partial\alpha_1} + \frac{U_2}{A_2}\frac{\partial A_1}{\partial\alpha_2} + u_3\frac{A_1}{R_1}\right) \\ \varepsilon_{22} &= \frac{1}{A_1(1+\alpha_3/R_2)}\left(\frac{\partial U_2}{\partial\alpha_2} + \frac{U_1}{A_1}\frac{\partial A_2}{\partial\alpha_1} + U_3\frac{A_2}{R_2}\right) \\ \varepsilon_{33} &= \frac{\partial U_3}{\partial\alpha_3} \end{aligned} \tag{B.39}$$

And the shear strain is expanded as follows:

$$\begin{aligned}
\varepsilon_{12} &= \frac{A1(1+\alpha_3/R_1)}{A_2(1+\alpha_3/R_2)}\frac{\partial}{\partial\alpha_2}\left(\frac{U_1}{A_1(1+\alpha_3/R_1)}\right) \\
&+ \frac{A2(1+\alpha_3/R_2)}{A_2(1+\alpha_3/R_1)}\frac{\partial}{\partial\alpha_1}\left(\frac{U_2}{A_2(1+\alpha_3/R_2)}\right) \\
\varepsilon_{13} &= A_1\left(1+\frac{\alpha_3}{R_1}\right)\frac{\partial}{\partial\alpha_3}\left(\frac{U_1}{A_1(1+\alpha_3/R_1}\right)+\frac{1}{A_1(1+\alpha_3/R_1)}\frac{\partial U_3}{\partial\alpha_1} \\
\varepsilon_{23} &= A_2\left(1+\frac{\alpha_3}{R_2}\right)\frac{\partial}{\partial\alpha_3}\left(\frac{U_2}{A_2(1+\alpha_3/R_2}\right)+\frac{1}{A_2(1+\alpha_3/R_1)}\frac{\partial U_3}{\partial\alpha_2}
\end{aligned} \tag{B.40}$$

B.4. LOVE SIMPLIFICATION

In this case love simplification can be used. In his argument, Love simplified the derivation based on the assumption of thin shell. Thin structure means that the displacement in the α_1 and α_2 directions vary linearly through the shell thickness, whereas displacements in the α_3 direction are independent or constant of α_3. The equation can be written from these consideration into the following:

$$\begin{aligned}
U_1(\alpha_1,\alpha_2,\alpha_3) &= u_1(\alpha_1,\alpha_2)+\alpha_3\cdot\beta_1(\alpha_1,\alpha_2) \\
U_2(\alpha_1,\alpha_2,\alpha_3) &= u_2(\alpha_1,\alpha_2)+\alpha_3\cdot\beta_2(\alpha_1,\alpha_2) \\
U_3(\alpha_1,\alpha_2,\alpha_3) &= u_3(\alpha_1,\alpha_2)
\end{aligned} \tag{B.41}$$

Where in this case $beta_1$ and $beta_2$ are angles. If the shear deflection is neglected based on *Love simplification*. Therefore $\varepsilon_{13}=\varepsilon_{23}=0$

Substitution this condition and equation B.41 into the equation B.40 to achieve the value of β_1 and β_2:

$$\begin{aligned}
\beta_1 &= \frac{u_1}{R_1}-\frac{1}{A_1}\frac{\partial u_3}{\partial\alpha_1} \\
\beta_2 &= \frac{u_2}{R_2}-\frac{1}{A_2}\frac{\partial u_3}{\partial\alpha_2}
\end{aligned} \tag{B.42}$$

As the value of β_1 and β_2 is obtained, substitute to the equation B.41 to equation B.39 while recognizing that:

$$\frac{\alpha_3}{R_1}\ll 1, \quad \frac{\alpha_3}{R2}\ll 1 \tag{B.43}$$

Therefore the total equation for the strain is:

$$\begin{aligned}
\varepsilon_{11} &= \varepsilon_{11}^o+\alpha_3 k_{11} \\
\varepsilon_{22} &= \varepsilon_{22}^o+\alpha_3 k_{22} \\
\varepsilon_{33} &= 0 \\
\varepsilon_{13} &= 0 \\
\varepsilon_{23} &= 0 \\
\varepsilon_{12} &= \varepsilon_{12}^o+\alpha_3 k_{12}
\end{aligned} \tag{B.44}$$

where with the ε^o are the membrane strains in the element which is defined as follows:

$$\begin{aligned}
\varepsilon_{11}^o &= \frac{1}{A_1}\frac{\partial u_1}{\partial\alpha_1}+\frac{u_2}{A_1A_2}\frac{\partial A_1}{\partial\alpha_2}+\frac{u_3}{R_1} \\
\varepsilon_{22}^o &= \frac{1}{A_2}\frac{\partial u_2}{\partial\alpha_2}+\frac{u_1}{A_1A_2}\frac{\partial A_2}{\partial\alpha_1}+\frac{u_3}{R_2} \\
\varepsilon_{12}^o &= \frac{A_2}{A_1}\frac{\partial}{\partial\alpha_1}\left(\frac{u_2}{A_2}\right)+\frac{A_1}{A_2}\frac{\partial}{\partial\alpha_2}\left(\frac{u_1}{A_1}\right)
\end{aligned} \tag{B.45}$$

The change in curvature k or bending strains are written as follows:

$$\begin{aligned} k_{11} &= \frac{1}{A_1}\frac{\partial \beta_1}{\partial \alpha_1} + \frac{\beta_2}{A_1 A_2}\frac{\partial A_1}{\partial \alpha_2} \\ k_{22} &= \frac{1}{A_2}\frac{\partial \beta_2}{\partial \alpha_2} + \frac{\beta_1}{A_1 A_2}\frac{\partial A_2}{\partial \alpha_1} \\ k_{12} &= \frac{A_2}{A_1}\frac{\partial}{\partial \alpha_1}\frac{\beta_2}{A_2} + \frac{A_1}{A_2}\frac{\partial}{\partial \alpha_2}\frac{\beta_1}{A_1} \end{aligned} \tag{B.46}$$

B.5. MEMBRANE FORCES AND BENDING MOMENTS

By combining the three previous sections : section B.2, section B.3, and section B.4, the complete solution of the stresses in the structure element can be expanded as:

$$\begin{aligned} \sigma_{11} &= \frac{E}{1-\mu^2}[\varepsilon^o_{11} + \mu\varepsilon^o_{22} + \alpha_3(k_{11} + \mu k_{22})] \\ \sigma_{22} &= \frac{E}{1-\mu^2}[\varepsilon^o_{22} + \mu\varepsilon^o_{11} + \alpha_3(k_{22} + \mu k_{11})] \\ \sigma_{12} &= G(\varepsilon^o_{12} + \alpha_3 k_{12}) \end{aligned} \tag{B.47}$$

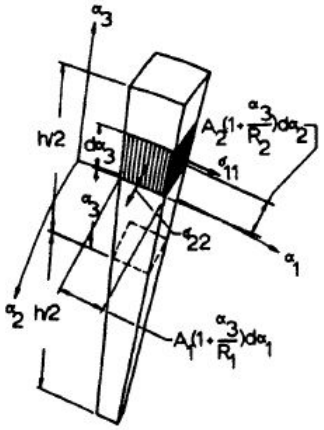

Figure B.5: Cut infinitesimal cross-sectional dimensions

B.5.1. MEMBRANE FORCES

From Figure B.5, the force in the α_1 direction acting on a strip of the element face of **height**: $d\alpha_3$ and with **width**: $A_2(1+\alpha_3/R_2)d\alpha_2$ is:

$$\int_{\alpha_3=-h/2}^{\alpha_3=h/2} \sigma_{11} A_2 \left(1+\frac{\alpha_3}{R_2}\right) d\alpha_2 d\alpha_3 \tag{B.48}$$

Therefore the force per unit length in the neutral surface as in Figure B.5 $A_2 d\alpha_2$ is:

$$N_{11} = \int_{-h/2}^{h/2} \sigma_{11}\left(1+\frac{\alpha_3}{R_2}\right) d\alpha_3 \tag{B.49}$$

By neglecting the second term since from the Love simplification the value of α_3/R_2 is very small and substitution to the equation B.47 the normal force is written as follows:

$$\begin{aligned} N_{11} &= \int_{-h/2}^{h/2} \sigma_{11} d\alpha_3 \\ N_{11} &= K(\varepsilon^o_{11} + \mu\varepsilon^o_{22}) \\ K &= \frac{Eh}{1-\mu^2} \end{aligned} \tag{B.50}$$

Where K is defined as the membrane stiffness. The procedure above also applied to obtain forces in other indexes. The rest of forces are:

$$\begin{aligned} N_{22} &= K(\varepsilon^o_{22} + \mu\varepsilon^o_{11}) \\ N_{21} = N_{12} &= \frac{K(1-\mu}{2}(\varepsilon^o_{22}) \end{aligned} \tag{B.51}$$

In order to obtain bending moment, the basic principle is to multiply the membrane forces with the level arm therefore an additional term in the previous equation is a multiplication of α_3:

$$\begin{aligned} M_{11} &= \int_{-h/2}^{h/2} \sigma_{11}\alpha_3 d\alpha_3 \\ M_{11} &= D(k_{11} + \mu k_{22}) \\ D &= \frac{Eh^3}{12(1-\mu^2)} \end{aligned} \tag{B.52}$$

While D is mostly called as the bending stiffness. Similarly with the other indexes. The rest bending moments are:

$$\begin{aligned} M_{11} &= D(k_{22} + \mu k_{11}) \\ M_{12} = M_{21} &= \frac{D(1-\mu)}{2} k_{12} \end{aligned} \tag{B.53}$$

B.5.2. TRANSVERSE SHEAR FORCE

In the previous section, it is described according to *Love Simplification* the strains ε_{13} and ε_{23} are negligible. But please note that **this assumption does not means that the stress integration is neglected**. Therefore the transverse shear are written as follows:

$$\begin{aligned} Q_{13} &= \int_{-h/2}^{h/2} \sigma_{13} d\alpha_3 \\ Q_{23} &= \int_{-h/2}^{h/2} \sigma_{23} d\alpha_3 \end{aligned} \tag{B.54}$$

B.5.3. STRESS EXPRESSION

Therefore the force can be reversed back in term of the stresses, it may result into the following:

$$\begin{aligned} \sigma_{11} &= \frac{N_{11}}{h} + \frac{12M_{11}}{h^3}\alpha_3 \\ \sigma_{22} &= \frac{N_{22}}{h} + \frac{12M_{22}}{h^3}\alpha_3 \\ \sigma_{12} &= \frac{N_{12}}{h} + \frac{12M_{12}}{h^3}\alpha_3 \end{aligned} \tag{B.55}$$

B.6. HAMILTON PRINCIPLE

After the kinematic and the consecutive relation have been derived, to derive the governing equation of motion, Hamilton's principle is used. Hamilton's principle is defined by the principle of stationary action. According to *William Rowan Hamilton* the **integral of difference energies equals to stationary which is 0.** Therefore one can simply write the energy expression under the Hamilton's principle as follwos:

$$\begin{aligned} \delta\int_{t_o}^{t_1} (U - K - W_{ln})dt = 0 \\ \int_{t_o}^{t_1} \delta U dt - \int_{t_o}^{t_1} \delta K - \int_{t_o}^{t_1} \delta W_{ln} = 0 \end{aligned} \tag{B.56}$$

Where U, K, and W_{ln} is the stain, kinetic,and total input energy respectively. The total input energy consists of these two components which are the boundary force and moment E_B and distributed external loading E_L.

$$W_{ln} = E_B + E_L \tag{B.57}$$

Each of these energy that composed the Hamilton's principle are discussed in the next subsection.

B.6.1. STRAIN ENERGY EXPRESSION

The strain energy U is stored in one infinitesimal element that is acted on by stresses σ_{ij}. Which can be written as follows:

$$\begin{aligned} dU &= \frac{1}{2}\sigma\varepsilon dV \\ dU &= \frac{1}{2}(\sigma_{11}\varepsilon_{11}+\sigma_{22}\varepsilon_{22}+\sigma_{12}\varepsilon_{12}+\sigma_{13}\varepsilon_{13}+\sigma_{23}\varepsilon_{23}+\sigma_{33}+\varepsilon_{33})dV \end{aligned} \tag{B.58}$$

However the transverse shear term has to be considered. The infinitesimal volume is given by from the figure B.5 is written as follows:

$$dV = A_1A_2\Big(1+\frac{\alpha_3}{R_1}\Big)\Big(1+\frac{\alpha_3}{R_2}\Big)d\alpha_1 d\alpha_2 d\alpha_3 \tag{B.59}$$

Therefore integrating the equation would result

$$\begin{aligned} U &= \int_{\alpha_1}\int_{\alpha_2}\int_{\alpha_3} F dV dt \\ F &= \frac{1}{2}(\sigma_{11}\varepsilon_{11}+\sigma_{22}\varepsilon_{22}+\sigma_{12}\varepsilon_{12}+\sigma_{13}\varepsilon_{13}+\sigma_{23}\varepsilon_{23}+\sigma_{33}+\varepsilon_{33}) \end{aligned} \tag{B.60}$$

Substitution to the **Hamilton's Expression**, the integration part by part for the strain energy can be write in the following:

$$U = \int_{t_o}^{t_1}\int_{\alpha_1}\int_{\alpha_2}\int_{\alpha_3}\delta F dV dt \tag{B.61}$$

Where:

$$\delta F = \frac{\partial F}{\partial\varepsilon_{11}}\delta\varepsilon_{11}+\frac{\partial F}{\partial\varepsilon_{22}}\delta\varepsilon_{22}+\frac{\partial F}{\partial\varepsilon_{12}}\delta\varepsilon_{12}+\frac{\partial F}{\partial\varepsilon_{13}}\delta\varepsilon_{13}+\frac{\partial F}{\partial\varepsilon_{23}}\delta\varepsilon_{23} \tag{B.62}$$

Examining the first term from this equation by substituting the the equation B.65 to the equation above, it can be found that:

$$\frac{\partial F}{\partial\varepsilon_{11}}\delta\varepsilon_{11} = \frac{1}{2}\Big(\frac{\partial\sigma_{11}}{\partial\varepsilon_{11}}\varepsilon_{11}+\sigma_{11}+\varepsilon_{22}\frac{\partial\sigma_{22}}{\partial\varepsilon_{11}}\Big)\delta\varepsilon_{11} \tag{B.63}$$

Substitution to the stress equation it can be found that:

$$\frac{\partial F}{\partial\varepsilon_{11}}\delta\varepsilon_{11} = \sigma_{11}\delta\varepsilon_{11} \tag{B.64}$$

Therefore likewise for the other term the strain energy can be derived into the following equations and by considering the small value of: α_3/R_1 and α_3/R_2

$$\begin{aligned} \int_{t_o}^{t_1}\delta U = \int_{t_o}^{t_1}\int_{\alpha_1}\int_{\alpha_2}\int_{\alpha_3}(&\sigma_{11}\delta\varepsilon_{11}+\sigma_{22}\delta\varepsilon_{22}+\sigma_{12}\delta\varepsilon_{12}+ \\ &\sigma_{13}\delta\varepsilon_{13}+\sigma_{23}\delta\sigma_{23})A_1A_2 d\alpha_1 d\alpha_2 d\alpha_3 dt \end{aligned} \tag{B.65}$$

Afterwards, the equation above is substituted in the equation B.44 which in the extended form for the strain. Integration with the respect term α_3 will result to force and moment resultant. For the sake of liability of the equation, the first term will be firstly discussed:

$$\begin{aligned} &\int_{t_o}^{t_1}\int_{\alpha_1}\int_{\alpha_2}\int_{\alpha_3}(\sigma_{11}\delta\varepsilon_{11}+A_1A_2 d\alpha_1 d\alpha_2 d\alpha_3 dt \\ =&\int_{t_o}^{t_1}\int_{\alpha_1}\int_{\alpha_2}\int_{\alpha_3}\Big[\sigma_{11}\Big(A_2\frac{\partial(\delta u_1)}{\partial\alpha_1}+\delta u_2\frac{\partial A_1}{\partial\alpha_2}+\frac{A_1A_2}{R_1}\delta u_3\Big) \\ &+\alpha_3\sigma_{11}\Big(A_2\frac{\partial\delta\beta_1}{\partial\alpha_1}+\delta\beta_2\frac{\partial A_1}{\partial\alpha_2}\Big)\Big]d\alpha_1 d\alpha_2 d\alpha_3 dt \end{aligned} \tag{B.66}$$

Substitution to the equation B.50 and B.52, the first term result into the following:

$$\begin{aligned} \int_{t_o}^{t_1}\int_{\alpha_1}\int_{\alpha_2}\Big[&N_{11}\Big(A_2\frac{\partial(\delta u_1)}{\partial\alpha_1}+\delta u_2\frac{\partial A_1}{\partial\alpha_2}+\frac{A_1A_2}{R_1}\delta u_3\Big) \\ &+M_{11}\Big(A_2\frac{\partial\delta\beta_1}{\partial\alpha_1}+\delta\beta_2\frac{\partial A_1}{\partial\alpha_2}\Big)\Big]d\alpha_1 d\alpha_2 dt \end{aligned} \tag{B.67}$$

The integration part by part on the first term may result into the following equation:

$$\begin{aligned}&\int_{t_o}^{t_1}\int_{\alpha_1}\int_{\alpha_2} N_{11}\Big(A_2\frac{\partial(\delta u_1)}{d\alpha_1}\Big)\delta u_1 d\alpha_1 d\alpha_2\\ &=\int_{\alpha_2} N_{11}A_2\delta u_1 d\alpha_2-\int_{\alpha_1}\int_{\alpha_2}\frac{\partial(N_{11}A_2)}{\partial\alpha_1}\delta d\alpha_1 d\alpha_2\end{aligned}\tag{B.68}$$

Continue with the other term, the full equation will result:

$$\begin{aligned}\int_{t_o}^{t_1}\delta U dt=\int_{t_o}^{t_1}\int_{\alpha_1}\int_{\alpha_2}\Big[\Big(&-\frac{\partial(N_{11}A_2)}{\partial\alpha_1}-\frac{\partial(N_{21}A_1)}{\partial\alpha_2}-N_{12}\frac{\partial A_1}{\partial\alpha_2}+\\ &N_{22}\frac{\partial A_2}{\partial\alpha_1}-Q_{13}\frac{A_1A_2}{R_1}\Big)\delta u_1+\\ &\Big(-\frac{\partial(N_{12}A_2)}{\partial\alpha_1}+N_{11}\frac{\partial A_1}{\partial\alpha_2}-N_{21}\frac{\partial A_2}{\partial\alpha_1}-Q_{23}\frac{A_1A_2}{R_2}\Big)\delta u_2+\\ &\Big(N_{11}\frac{A_1A_2}{R_1}+N_{22}-\frac{\partial(Q_{13}A_2)}{\partial\alpha_1}-\frac{\partial(Q_{23}A_1)}{\partial\alpha_2}\Big)\delta u_3+\\ \Big(-\frac{\partial(M_{21}A_1)}{\partial\alpha_2}-M_{12}\frac{\partial A_1}{\partial\alpha_2}+M_{22}\frac{\partial A_1}{\partial\alpha_1}-\frac{\partial(M_{11}A_2)}{\partial\alpha_1}+Q_{13}A_1A_2\Big)&\delta\beta_1+\\ &\Big(-\frac{\partial(M_{12}A_2)}{\partial\alpha_1}-\frac{\partial(M_{22}A_1)}{\partial\alpha_2}-M_{21}\frac{\partial A_2}{\partial\alpha_1}+\\ &M_{11}\frac{\partial A_1}{\partial\alpha_2}+Q_{23}A_1A_2\Big)\delta\beta_2\Big]d\alpha_1 d\alpha_2 dt+\\ \int_{t_o}^{t_1}\int_{\alpha_2}(N_{11}\delta u_1+M_{11}\delta\beta_1+N_{12}\delta u_2+M_{12}\delta\beta_2+Q_{13}\delta u_3)A_2 d\alpha_2 dt+&\\ \int_{t_o}^{t_1}\int_{\alpha_1}(N_{22}\delta u_2+M_{22}\delta\beta_2+N_{21}\delta u_1+M_{21}\delta\beta_1+Q_{23}\delta u_3)A_1 d\alpha_1 dt&\end{aligned}\tag{B.69}$$

B.6.2. KINETIC ENERGY EXPRESSION

The kinetic energy of one infinitesimal element is written as follows:

$$\begin{aligned}dK&=\frac{1}{2}mv^2\\ dK&=\frac{1}{2}\rho(\dot U_1^2+\dot U_2^2+\dot U_3^2)dV\end{aligned}\tag{B.70}$$

Substitution to the equation B.41 and by integration the kinetic energy is:

$$\begin{aligned}dK=\frac{\rho}{2}\int_{\alpha_1}\int_{\alpha_2}\int_{\alpha_3}\Big[&\dot u_1^2+\dot u_2^2+\dot u_3^2+\alpha_3^2(\dot\beta_1^2+\dot\beta_2^2)\\ +2\alpha_3(\dot u_1\dot\beta_1+\dot u_2\dot\beta_2\Big]&A_1A_2\Big(1+\frac{\alpha_3}{R_1}\Big)\Big(1+\frac{\alpha_3}{R_2}\Big)d\alpha_1 d\alpha_2 d\alpha_3\end{aligned}\tag{B.71}$$

As it is already mentioned before that the α_3/R_1 and α_3/R_2 is negligible, and by integrating over the thickness of the shell ($\alpha_3=-h/2$ to $\alpha_3=h/2$):

$$dK=\frac{\rho h}{2}\int_{\alpha_1}\int_{\alpha_2}\Big[\dot u_1^2+\dot u_2^2+\dot u_3^2+\frac{h^2}{12}(\dot\beta_1^2+\dot\beta_2^2)\Big]A_1A_2 d\alpha_1 d\alpha_2\tag{B.72}$$

Substituting to the **Hamilton Equation**, therefore the equation would result into the following:

$$\begin{aligned}\int_{t_o}^{t_1}\delta K dt=\rho h\int_{t_o}^{t_1}\int_{\alpha_1}\int_{\alpha_2}\Big[&\dot u_1\delta\dot u_1+\dot u_2\delta\dot u_2+\dot u_3\delta\dot u_3+\\ &\frac{h^2}{12}(\dot\beta_1\delta\dot\beta_1+\dot\beta_2\delta\dot\beta_2)\Big]A_1A_2 d\alpha_1 d\alpha_2 dt\end{aligned}\tag{B.73}$$

For the sake of convenience each integration is performed part by part. The first terms will result into:

$$\int_{t_o}^{t_1}\dot u_1\delta\dot u_1 dt=[\dot u_1\delta u_1]_{t_o}^{t_1}-\int_{t_o}^{t_1}\ddot u_1\delta u_1 dt\tag{B.74}$$

As the virtual displacement is 0, $t = t_o$ and $t = t_1$ the equation above will result into the following

$$\int_{t_o}^{t_1} \ddot{u}_1 \delta \dot{u}_1 \, dt = -\int_{t_o}^{t_1} \ddot{u}_1 \delta u_1 \, dt \tag{B.75}$$

The same applies to the other terms therefore the equation will result

$$\begin{aligned} \int_{t_o}^{t_1} \delta K \, dt = \rho h \int_{t_o}^{t_1} \int_{\alpha_1} \int_{\alpha_2} \Big[& \ddot{u}_1 \delta u_1 + \ddot{u}_2 \delta u_2 + \ddot{u}_3 \delta u_3 + \\ & \frac{h^2}{12} (\ddot{\beta}_1 \delta \beta_1 + \ddot{\beta}_2 \delta \beta_2) \Big] A_1 A_2 \, d\alpha_1 \, d\alpha_2 \, dt \end{aligned} \tag{B.76}$$

From the **classical Bernoulli-Euler** beam the influence of **rotatory inertia** ($\ddot{\beta}$) **is neglected**. Therefore the complete term for this case is:

$$\int_{t_o}^{t_1} \delta K \, dt = \rho h \int_{t_o}^{t_1} \int_{\alpha_1} \int_{\alpha_2} \Big[\ddot{u}_1 \delta u_1 + \ddot{u}_2 \delta u_2 + \ddot{u}_3 \delta u_3 \Big] A_1 A_2 \, d\alpha_1 \, d\alpha_2 \, dt \tag{B.77}$$

B.6.3. INPUT ENERGY

The input energy W_{Ln} is consisted of the energy from the boundary force and moment resultants and also from the distributed loading on the reference surface. Firstly, it will be discussed the boundary force and the moment resultant in the following figure:

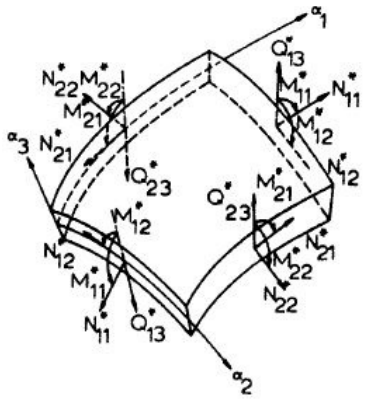

Figure B.6: Boundary force and moment resultant
Source : Vibration of Shell and Plates, Soedel [16]

From Figure B.6, the boundary force and moment resultant along α_2 (constant) and α_1 (constant lines) is:

$$\begin{aligned} \delta E_B = & \int_{\alpha_1} (\delta u_2 N^*_{22} + \delta u_1 N^*_{21} + \delta u_3 Q^*_{23} + \delta \beta_2 M^*_{22} + \delta \beta_1 M^*_{21}) A_1 \, d\alpha_1 \\ & + \int_{\alpha_2} (\delta u_1 N^*_{11} + \delta u_2 N^*_{12} + \delta u_3 Q^*_{13} + \delta \beta_1 M^*_{11} + \delta \beta_2 M^*_{12}) A_2 \, d\alpha_2 \end{aligned} \tag{B.78}$$

Where for the distributed loading on the reference surface is depicted in the following figure:

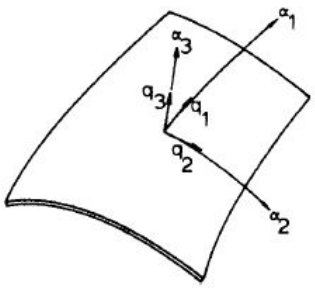

Figure B.7: Distributed loading on the reference surface
Source : Vibration of Shell and Plates, Soedel [16]

Where from the picture above it can be derived that:

$$\delta E_L = \int_{\alpha_1}\int_{\alpha_2} (q_1\delta u_1 + q_2\delta u_2 + q_3\delta u_3) A_1 A_2 d\alpha_1 d\alpha_2 \tag{B.79}$$

Substitution to the **Hamilton Equation**, likewise the other energies above, the equation would result into the following The boundary force and moment resultant:

$$\begin{aligned}\delta E_B = &\int_{t_o}^{t_1}\int_{\alpha_1} (\delta u_2 N_{22}^* + \delta u_1 N_{21}^* + \delta u_3 Q_{23}^* + \delta\beta_2 M_{22}^* + \delta\beta_1 M_{21}^*) A_1 d\alpha_1 \\ &+ \int_{t_o}^{t_1}\int_{\alpha_2} (\delta u_1 N_{11}^* + \delta u_2 N_{12}^* + \delta u_3 Q_{13}^* + \delta\beta_1 M_{11}^* + \delta\beta_2 M_{12}^*) A_2 d\alpha_2\end{aligned} \tag{B.80}$$

Distributed load in reference surface :

$$\delta E_L = \int_{t_o}^{t_1}\int_{\alpha_1}\int_{\alpha_2} (q_1\delta u_1 + q_2\delta u_2 + q_3\delta u_3) A_1 A_2 d\alpha_1 d\alpha_2 \tag{B.81}$$

B.6.4. HAMILTON EXPRESSION AND EQUATION MOTION

Since each energy from the Hamilton's expression in equation B.56, the fully equation of Hamilton can be calculated by inputting equation B.69, equation B.77, equation B.80 and equation B.81 in the following expression:

$$\begin{aligned}\int_{t_o}^{t_1}\delta U dt = \int_{t_o}^{t_1}\int_{\alpha_1}\int_{\alpha_2}\Big[\Big(&\frac{\partial(N_{11}A_2)}{\partial\alpha_1} + \frac{\partial(N_{21}A_1)}{\partial\alpha_2} + N_{12}\frac{\partial A_1}{\partial\alpha_2} - \\ &N_{22}\frac{\partial A_2}{\partial\alpha_1} + Q_{13}\frac{A_1A_2}{R_1} - (q_1 - \rho h\ddot{u}_1)A_1A_2\Big)\delta u_1 + \\ &\Big(\frac{\partial(N_{12}A_2)}{\partial\alpha_1} + \frac{\partial(N_{22}A_1)}{\partial\alpha_2} + N_{21}\frac{\partial A_2}{\partial\alpha_1} - N_{11}\frac{A_1}{\partial\alpha_2} + \\ &Q_{23}\frac{A_1A_2}{R_2} + (q_2 - \rho h\ddot{u}_2)A_1A_2\Big)\delta u_2 + \\ &\Big(\frac{\partial(Q_{13}A_2)}{\partial\alpha_1} + \frac{\partial(Q_{23}A_1)}{\partial\alpha_2} - \Big(\frac{N_{11}}{R_1} + \frac{N_{22}}{R_2}\Big)A_1A_2 + (q_3 - \rho h\ddot{u}_3)A_1A_2\Big)\delta u_3 + \\ &\Big(\frac{\partial(M_{11}A_2)}{\partial\alpha_1} + \frac{\partial(M_{21}A_1)}{\partial\alpha_2} + M_{12}\frac{\partial A_1}{\partial\alpha_1} - M_{22}\frac{\partial A_2}{\partial\alpha_1} - Q_{13}A_1A_2\Big)\delta\beta_1 + \\ &\Big(\frac{\partial(M_{12}A_2)}{\partial\alpha_1} + \frac{\partial(M_{22}A_1)}{\partial\alpha_2} + M_{21}\frac{\partial A_2}{\partial\alpha_1} - M_{11}\frac{\partial A_1}{\partial\alpha_2} - Q_{23}A_1A_2\Big)\delta\beta_2\Big] d\alpha_1 d\alpha_2 dt + \\ &\int_{t_o}^{t_1}\int_{\alpha_2}[(N_{22}^* - N_{22})\delta u_2 + (N_{21}^* - N_{21})\delta u_1 + (Q_{23}^* - Q_{23})\delta u_3 + \\ &(M_{22}^* - M_{22})\delta\beta_2 + (M_{21}^* - M_{21})\delta\beta_1] A_1 d\alpha_1 dt \\ &\int_{t_o}^{t_1}\int_{\alpha_2}[(N_{11}^* - N_{11})\delta u_1 + (N_{12}^* - N_{12})\delta u_2 + (Q_{13}^* - Q_{13})\delta u_3 + \\ &(M_{11}^* - M_{11})\delta\beta_1 + (M_{12}^* - M_{12})\delta\beta_2] A_2 d\alpha_2 dt = 0\end{aligned} \tag{B.82}$$

The equation can be only satisfied only if each of triple and the double integral their self equals to 0. Therefore for the triple integration the equation would be in the following:

$$-\frac{\partial(N_{11}A_2)}{\partial\alpha_1}-\frac{\partial(N_{21}A_1)}{\partial\alpha_2}-N_{12}\frac{\partial A_1}{\partial\alpha_2}+N_{22}\frac{\partial A_2}{\partial\alpha_1}-Q_{13}\frac{A_1A_2}{R_1}+\rho hA_1A_2\ddot{u}_1=A_1A_2q_1 \tag{B.83}$$

$$-\frac{\partial(N_{12}A_2)}{\partial\alpha_1}-\frac{\partial(N_{22}A_1)}{\partial\alpha_2}-N_{21}\frac{\partial A_2}{\partial\alpha_1}+N_{11}\frac{A_1}{\partial\alpha_2}-Q_{23}\frac{A_1A_2}{R_2}+\rho hA_1A_2\ddot{u}_2=A_1A_2q_2 \tag{B.84}$$

$$-\frac{\partial(Q_{13}A_2)}{\partial\alpha_1}-\frac{\partial(Q_{23}A_1)}{\partial\alpha_2}+\left(\frac{N_{11}}{R_1}+\frac{N_{22}}{R_2}\right)A_1A_2+A_1A_2\rho h\ddot{u}_3=A_1A_2q_3 \tag{B.85}$$

The transverse shear can be defined in the following:

$$\frac{\partial(M_{11}A_2)}{\partial\alpha_1}+\frac{\partial(M_{21}A_1)}{\partial\alpha_2}+M_{12}\frac{\partial A_1}{\partial\alpha_1}-M_{22}\frac{\partial A_2}{\partial\alpha_1}-Q_{13}A_1A_2=0 \tag{B.86}$$

$$\frac{\partial(M_{12}A_2)}{\partial\alpha_1}+\frac{\partial(M_{22}A_1)}{\partial\alpha_2}+M_{21}\frac{\partial A_2}{\partial\alpha_1}-M_{11}\frac{\partial A_1}{\partial\alpha_2}-Q_{23}A_1A_2=0 \tag{B.87}$$

These five equations are more commonly known as the **Love's Equations**. In this governing equations of motion, shear deflection and rotatory inertia are neglected.

C

FLUID POTENTIAL FLOW DERIVATION

Deriving the equation motion for the fluid is described in the following steps

C.1. COORDINATE SYSTEM

As for liquid the velocity is in the vector field the description of a flow as function of the space and time coordinate can be defined. Basically there are two method to describe flow : Eulerian and Lagrangian method. Suppose that fluid element is labeled with an unique label of . The position of the liquid is explained in the vector . Therefore the velocity of the fluid element is equal to:

$$\underline{V} = \frac{d\underline{X}(t;a)}{dt} \tag{C.1}$$

In *Lagrangian principle* the description of a and t are independent to the coordinates and trajectory $\underline{X}(t;a)$ is the dependent variable. The capital $\underline{X}$ is to draws distinction between the fluid element and the position vector in a Cartesian coordinate system $x = (x, y, z) = (x_1, x_2, x_3)$.

C.2. MATERIAL DERIVATIVE

Consider a function of $G(x,t)$ as a continuously differentiable function of the coordinates x, t. Defining G as the property of a fluid element where is located in the position of $\underline{X}(t) = \underline{x}$. One can consider the total differential of G as a function of $\underline{x}$ and t.

$$\frac{dG}{dt} = \frac{\partial G}{\partial t} + \frac{dx}{dt}\frac{\partial G}{\partial x} + \frac{dy}{dt}\frac{\partial G}{\partial y} + \frac{dz}{dt}\frac{\partial G}{\partial z} = \frac{dG}{dt} + \frac{dx_i}{dt}\frac{\partial G}{\partial x_i} \tag{C.2}$$

The vector of $(dx/dt, dy/dt, dz/dt)$ describes as an arbitrary path through three-dimensional space as a function time. The first time derivative of the space is equal to the velocity u_i of the fluid element at the position of u_i of the fluid element in the position of x_i. Therefore the equation can be written as:

$$\frac{DG}{Dt} = \frac{\partial G}{\partial t} + (u \cdot \text{grad})G \tag{C.3}$$

$$\frac{DG}{Dt} = \frac{\partial G}{\partial t} + u_i\frac{\partial G}{\partial x_i} \tag{C.4}$$

Above one is expressing the value G of scalar property. However the material derivation can be also developed to a vector property.

C.3. CONSERVATION MASS

Before discussing the conservation of mass principle, one can consider a fixed volume V (where the volume does not move with the flow) with surface boundary of A . In the surface, is defined a pointing normal vector of n.

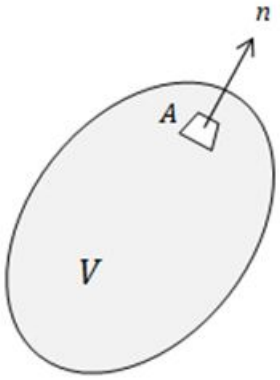

Figure C.1: Illustration of Geometry of the volume V

Conservation is defined as the change mass in V should be equal to the net influx of the surface A. Therefore the equation based on this statement is:

$$\frac{\partial M}{\partial t} \equiv \frac{\partial}{\partial t} \iiint_V \rho dV = \iint_A \rho \cdot \mathbf{u} \cdot \mathbf{n} \cdot dA \tag{C.5}$$

The minus sign is result from the vector is taken positive when it points outward. The first divergence of Gauss theory is defined as this following equation:

$$\iiint_V \text{div}\mathbf{u} \cdot dV = \iint_S \mathbf{u} \cdot \mathbf{n} \cdot dS \tag{C.6}$$

$$\iiint_V \text{div} \cdot \mathbf{u} \cdot dV = \iint_S u_i \cdot n_i \cdot dS \tag{C.7}$$

Therefore with the help from equation (C.6), the equation (C.5) will result in the following definition:

$$\iiint_V \frac{\partial \rho}{\partial t} dV = -\iiint_V \text{div}(\rho \cdot \mathbf{u}) dV \tag{C.8}$$

From this equation this relationship must be valid for an arbitrary volume V, one can continue the equation as:

$$\frac{\partial \rho}{\partial t} + \text{div}(\rho \cdot \mathbf{u}) = 0 \tag{C.9}$$

Using the definition from the previous equation C.4 the equation can also be defined as the following:

$$\frac{D\rho}{Dt} + \rho \cdot \text{div}(\mathbf{u}) = 0 \tag{C.10}$$

Based on these two equations above it can be interpreted the concept of divergence. Regards a fluid element with a volume of δV from the continuum hypothesis that $\rho = \lim_{\delta V \to 0} \delta M / \delta V$ and δM is the mass. The conservation of mass for the fluid element will result:

$$\frac{D\delta M}{Dt} = 0 \tag{C.11}$$

In order to fulfill the theory of conservation mass, one must understand that this fluid element on its path the flow and for that reason the equation above material derivative is used. Substituting the equation (C.11) and (C.10), the equation will be:

$$\text{div} \cdot \mathbf{u} = \frac{1}{\delta V} \frac{D\delta V}{Dt} = \Delta \tag{C.12}$$

From this equation, one can defined that the divergence of the velocity result of the local relative change of volume δ that a fluid element experiences in the flow field. For the sake of simplification, firstly assume that the density of the fluid does not change during the fluid element takes through the flow (incompressible) or simply saying that $D\rho/Dt = 0$ Therefore the equation will result to:

$$\text{div} \cdot \mathbf{u} = 0 \tag{C.13}$$

The fluid that have a velocity fluid satisfying this condition is mostly called *solenoidal*.

C.4. VELOCITY FIELD AND POTENTIAL FLOW

From the equation (C.12) it can be seen that:

$$\text{div} \cdot \mathbf{u} = \Delta \tag{C.14}$$

Assume that the is not an rotational flow, the rotation is not computed in this calculation. The decomposing the equation it would result that Helmholtz decomposition. And the Helmholtz decomposition for a free rotational fluid is :

$$\begin{aligned} \nabla \cdot \mathbf{u} &= \Delta \\ \nabla \cdot \mathbf{u} &= 0 \end{aligned} \tag{C.15}$$

In order to fulfilling the equation it can be defined that :

$$\mathbf{u} = \nabla\phi = \frac{\partial\phi}{dx} i + \frac{\partial\phi}{\partial y} j + \frac{\partial\phi}{\partial z} k \tag{C.16}$$

Where ϕ is called velocity potential for u. As for incompressible as it explained in in the previous conservation mass, the equation (C.13) therefore the equation will result in the following:

$$\begin{aligned} \text{div} \cdot \mathbf{u} &= 0 \\ \Delta \cdot \mathbf{u} &= 0 \\ \nabla \times \nabla\phi &= 0 \\ \nabla^2\phi &= 0 \end{aligned} \tag{C.17}$$

The above equation usually called the Laplace equation. and the general solution of Laplace equation is called a harmonic equation. In some references there are some different reference axis and notation. In order avoid mistakes in the future, let defined in this following terms due to the axis reference:

$$\begin{aligned} v_x &= \frac{\partial\phi}{\partial x} \\ v_y &= \frac{\partial\phi}{\partial y} \\ v_z &= \frac{\partial\phi}{\partial z} \end{aligned} \tag{C.18}$$

The governing equation will be:

$$\frac{\partial^2\phi}{\partial x^2} + \frac{\partial^2\phi}{\partial y^2} + \frac{\partial^2\phi}{\partial z^2} = 0 \tag{C.19}$$

or it can also be described as in the following:

$$\begin{aligned} \nabla^2 \times \phi &= 0 \\ \nabla^2 &= \frac{\partial^2(\cdot)}{\partial x^2} + \frac{\partial^2(\cdot)}{\partial y^2} + \frac{\partial^2(\cdot)}{\partial z^2} \end{aligned} \tag{C.20}$$

This will result a motion equation in term of pressure for incompressible liquid:

$$\frac{\partial^2 p}{\partial x^2} + \frac{\partial^2 p}{\partial y^2} + \frac{\partial^2 p}{\partial z^2} = 0 \tag{C.21}$$

D

Two Dimensional Derivation

D.1. Fourier Transform

The response will be expressed in the frequency domain with one important reason which is the simplicity of the analytical further derivations. To obtain the expression in frequency domain, the method that will be used is Fourier transform. The fourier transform function it self will be consisted of complex-value function of frequency. The solution for the liquid and the beam displacement are:

Solution for Beam Equation of Motion

$$u_{(x \text{ or } z,t)} = u_{s(x \text{ or } z)} + \frac{1}{2\pi}\int_{-\infty}^{\infty} \tilde{u}_{d(x \text{ or } z,t)} \exp(i\omega t) d\omega \tag{D.1}$$

Solution for Liquid Equation of Motion

$$\phi_{(x,z,t)} = \int_{-\infty}^{\infty} \frac{1}{2\pi} \tilde{\phi}_{(x,z,\omega)} \cdot \exp(i\omega t) d\omega \tag{D.2}$$

Afterwards, the fourier transform will be substituted back to the governing equations.

D.1.1. Liquid Equation of Motion

For the liquid equation of motion the Fourier transform may result in the following equation:

$$\begin{aligned} \frac{\partial^2 \phi_{(x,z,t)}}{\partial x^2} + \frac{\partial^2 \phi_{(x,z,t)}}{\partial z^2} &= 0 \\ \frac{\partial^2 \tilde{\phi}_{(x,z,\omega)}}{\partial x^2} + \frac{\partial^2 \tilde{\phi}_{(x,z,\omega)}}{\partial z^2} &= 0 \end{aligned} \tag{D.3}$$

From the equation it can be seen that the result of the equation of motion will be completely coupled in x and z dependent. Therefore to solve he equation the separation method is used to solve the coupled partial differential equation. Therefore the equation would result in the following:

$$\tilde{\phi}_{(x,z,\omega)} = \tilde{\phi}_{x(x,\omega)} \cdot \tilde{\phi}_{z(z,\omega)} \tag{D.4}$$

Through the substitution the liquid equation of motion will result as follows:

$$\tilde{\phi}_{z(z,\omega)} \frac{d^2 \tilde{\phi}_{x(x,\omega)}}{dx^2} + \tilde{\phi}_{x(x,\omega)} \frac{d^2 \tilde{\phi}_{z(z,\omega)}}{dz^2} = 0 \tag{D.5}$$

Dividing this expression bt $\tilde{\phi}_x$ and $\tilde{\phi}_z$ and introducing the separation constant c the expression would result in the following:

$$\frac{1}{\tilde{\phi}_{x(x,\omega)}} \frac{d^2 \tilde{\phi}_{x(x,\omega)}}{dx^2} = -\frac{1}{\tilde{\phi}_{z(z,\omega)}} \frac{d^2 \tilde{\phi}_{z(z,\omega)}}{dz^2} = -c^2 \tag{D.6}$$

However by the existence of the separation constant, the quantity of the kinematic boundary conditions are not enough to satisfy all of the liquid constants. The number of kinematic boundary conditions are four, while on the other hand the number of constants are five: two in x, another two constants in z, and also the separation constants. In the next section the liquid superposition will be explained, in order to solve the problem.

D.1.2. SEISMIC EXCITATION IN VERTICAL DIRECTION

In this subsection onward the dynamic and the static equation will be completely treated separately as explained above

WALL 1 EQUATION OF MOTION

For the dynamic part a transformation in the frequency domain yields:

$$E_w \cdot I_w \cdot \frac{d^4 \tilde{u}_{1d(z,\omega)}}{dz^4} - \omega^2 \rho_s A_w \tilde{u}_{1d(z,\omega)} = -\rho_{liq} i\omega \tilde{\phi}_{(x=0,z,t)} \tag{D.7}$$

For the static part the equation would result in the following, where the time dependent term is totally separated from the equation:

$$E_w \cdot I_w \cdot \frac{d^4 u_{1s(z)}}{dz^4} = -\rho_{liq} g(z-H) \tag{D.8}$$

WALL 2 EQUATION OF MOTION

The same principle also applied for the second wall equation. The dynamic part the wall equation after the Fourier transform results in the following:

$$E_w \cdot I_w \cdot \frac{d^4 \tilde{u}_{2d(z,\omega)}}{dz^4} - \omega^2 \rho_s A_w \tilde{u}_{2d(z,\omega)} = \rho_{liq} i\omega \tilde{\phi}_{(x=0,z,t)} \tag{D.9}$$

For the static part the equation would result as follows:

$$E_w \cdot I_w \cdot \frac{d^4 u_{2s(z)}}{dz^4} = \rho_{liq} g(z-H) \tag{D.10}$$

PLATE EQUATION OF MOTION

Likewise the first and the second wall the equation of plate in the dynamic part is defined as:

$$E_p \cdot I_p \cdot \frac{d^4 \tilde{u}_{3d(x,\omega)}}{dx^4} - (\omega^2 \rho_s A_p - k)\tilde{u}_{3d(x,\omega)} - k \cdot \tilde{We}_{(x,\omega)} = -\rho_{liq} i\omega \tilde{\phi}_{(x,z=0,t)} \tag{D.11}$$

For the static part the equation would result as:

$$E_w \cdot I_w \cdot \frac{d^4 u_{3s(z)}}{dz^4} + k \cdot u_{3s(z)} = -\rho_{liq} g(H) \tag{D.12}$$

BOUNDARY CONDITION AND INTERFACE CONDITION OF STRUCTURES

Through the substitution of the solution the time domain boundary conditions can be converted into the frequency domain boundary conditions:

1. **Moment of the wall 1 at** $z = H$**,** $(x = 0)$

$$\frac{d^2 \tilde{u}_{1d(z,\omega)}}{dz^2}\Big|_{z=H} = 0 \tag{D.13}$$

2. **Moment of the wall 2 at** $z = H$**,** $(x = L)$

$$\frac{d^2 \tilde{u}_{2d(z,\omega)}}{dz^2}\Big|_{z=H} = 0 \tag{D.14}$$

3. **Shear force of the wall 1 at** $z = H$**,** $(x = 0)$

$$\frac{d^3 \tilde{u}_{1d(z,\omega)}}{dz^2}\Big|_{z=H} = 0 \tag{D.15}$$

4. **Shear force of the wall 1 at** $z = H$**,** $(x = L)$

$$\frac{d^3 \tilde{u}_{2d(z,\omega)}}{dz^2}\Big|_{z=H} = 0 \tag{D.16}$$

5. **Wall deformation due to the in-extensibility of plate at** $z = 0$, $(x = 0, L)$

$$\tilde{u}_{1d(z,t)} = \tilde{u}_{2d(z=0,t)} = 0 \tag{D.17}$$

6. **Shear Force due to the in-extensibility of the plate at** $z = 0$, $(x = 0, L)$

$$-\rho AH\omega^2 \tilde{u}_{1(z,\omega)}\Big|_{z=0} = E_w \cdot I_w \cdot \Big(-\frac{d^3\tilde{u}_{1(z,\omega)}}{dz^3} + \frac{d^3\tilde{u}_{2(z,\omega)}}{dz^3}\Big)\Big|_{z=0} \tag{D.18}$$

7. **Rotation of the plate and the wall 1 at** $x = 0$ **and** $z = 0$

$$\frac{d\tilde{u}_{1d(z,\omega)}}{dz}\Big|_{z=0} = -\frac{d\tilde{u}_{3d(x,\omega)}}{dx}\Big|_{x=0} \tag{D.19}$$

8. **Rotation of the plate and the wall 2 at** $x = L$ **and** $z = 0$

$$\frac{d\tilde{u}_{2d(z,\omega)}}{dz}\Big|_{z=0} = -\frac{d\tilde{u}_{3d(z,\omega)}}{dx}\Big|_{x=L} \tag{D.20}$$

9. **Moment of the plate and the wall 1 at** $x = 0$ **and** $z = 0$

$$E_w \cdot I_w \frac{d^2\tilde{u}_{1d(z,t)}}{dz^2}\Big|_{z=0} = E_p \cdot I_p \frac{d^2\tilde{u}_{3d(x,t)}}{dx^2}\Big|_{x=0} \tag{D.21}$$

10. **Moment of the plate and the wall 2 at** $z = 0$, $x = L$

$$E_w \cdot I_w \frac{d^2\tilde{u}_{2d(z,\omega)}}{dz^2}\Big|_{z=0} = -E_p \cdot I_p \frac{d^2\tilde{u}_{3d(x,\omega)}}{dx^2}\Big|_{x=0} \tag{D.22}$$

11. **Shear force of the Plate at** $x = 0$

$$\rho_w \cdot A_w \cdot H \frac{d^2\tilde{u}_{3d(x,\omega)}}{dt^2}\Big|_{x=0} = E_w \cdot I_w \cdot \frac{d^3\tilde{u}_{3d(x,\omega)}}{dx^3}\Big|_{x=0} \tag{D.23}$$

12. **Shear force of the Plate at** $x = L$

$$\rho_w \cdot A_w \cdot H \frac{d^2\tilde{u}_{3d(x,\omega)}}{dt^2}\Big|_{x=L} = -E_w \cdot I_w \cdot \frac{d^3\tilde{u}_{3d(x,\omega)}}{dx^3}\Big|_{x=L} \tag{D.24}$$

KINEMATIC BOUNDARY CONDITIONS FOR LIQUID STRUCTURE INTERACTION

The boundary condition that describes liquid and structure interaction in the frequency domain is:

1. **Wall 1 and liquid velocity** $x = 0$

$$i \cdot \omega \cdot \tilde{u}_{1d(z,\omega)} = -\frac{\partial\tilde{\phi}_{(x,z,\omega)}}{\partial x}\Big|_{x=0} \tag{D.25}$$

2. **Wall 2 and liquid velocity** $x = L$

$$i \cdot \omega \cdot \tilde{u}_{2d(z,\omega)} = -\frac{\partial\tilde{\phi}_{(x,z,\omega)}}{\partial x}\Big|_{x=L} \tag{D.26}$$

3. **Plate and liquid velocity** $z = 0$

$$i \cdot \omega \cdot \tilde{u}_{3d(z,\omega)} = -\frac{\partial\tilde{\phi}_{(x,z,\omega)}}{\partial z}\Big|_{z=0} \tag{D.27}$$

4. **Free Surface** $z = H$

$$\frac{\omega^2}{g}\tilde{\phi}_{(x,z,\omega)}\Big|_{z=H} + \frac{\partial\tilde{\phi}_{(x,z,\omega)}}{\partial z}\Big|_{z=H} = 0 \tag{D.28}$$

The set of the equations complete the statement of the problem in the frequency domain under vertical seismic excitation. The calculations is repeated for the structure under horizontal seismic loading.

D.1.3. SEISMIC ANALYSIS IN HORIZONTAL DIRECTION

As explained in the previous section, the governing equations would have the same form as the seismic analysis in vertical direction and would only differs for plate equation and boundary condition number (5).

PLATE EQUATION OF MOTION

$$E_p \cdot I_p \cdot \frac{\partial^4 u_{3(x,\omega)}}{\partial x^4} + \rho_s A_p \ddot{u}_{3d(x,\omega)} + k(u_{3d(x,\omega)}) = -\rho_{liq}\left(\frac{\partial \phi_{(x,z=0,\omega)}}{\partial \omega}\right) \tag{D.29}$$

The different boundary conditions are (5), (6), (11), and (12) which result in the following terms:

5. **Wall deformation due to the in-extensible plate at** $x = 0, L$ **and** $z = 0$

$$\tilde{u}_{1d(z=0,\omega)} = \tilde{U}_{e(x,\omega)} \tag{D.30}$$

D.2. LIQUID SUPERPOSITION

As explained in the chapter the liquid is consisted of two potentials. The main general equation will be rewritten for the convenience of the reader:

$$\tilde{\phi}_{(x,z,\omega)} = \tilde{\phi}_{1(x,z,\omega)} + \tilde{\phi}_{2(x,z,\omega)} \tag{D.31}$$

The first potential velocity satisfies the z dependent boundary condition, while for the x dependent boundary condition it will result to homogeneous conditions. As for the second potential velocity it satisfies the contrary with the first potential.

KINEMATIC BOUNDARY CONDITION FOR $\tilde{\phi}_1$

In the following will be described the kinematic boundary condition for the first potential velocity. The walls are assumed to be rigid. This implies that the effects of free surface wave is directly influenced by the flexibility of the plate:

1. **Liquid potential velocity in x direction at** $x = 0$

$$\frac{\partial \tilde{\phi}_{1(x,z,\omega)}}{\partial x}\bigg|_{x=0} = 0 \tag{D.32}$$

2. **Liquid potential velocity in x direction at** $x = L$

$$\frac{\partial \tilde{\phi}_{1(x,z,\omega)}}{\partial x}\bigg|_{x=L} = 0 \tag{D.33}$$

3. **Liquid potential velocity in z direction at** $z = 0$

$$\frac{\partial \tilde{\phi}_{1(x,z,\omega)}}{\partial x}\bigg|_{z=0} = i \cdot \omega \cdot \tilde{u}_{3(x,\omega)} \tag{D.34}$$

4. **Free Surface Condition at** $z = H$

$$\begin{aligned} \frac{\omega^2}{g}\tilde{\phi}_{1(x,z,\omega)}\bigg|_{z=H} &= \frac{\partial \tilde{\phi}_{(x,z,\omega)}}{\partial x}\bigg|_{z=H} \\ \frac{\omega^2}{g}\tilde{\phi}_{1(x,z,\omega)}\bigg|_{z=H} &= \frac{\partial (\tilde{\phi}_{1(x,z,\omega)} + \tilde{\phi}_{2(x,z,\omega)})}{\partial x}\bigg|_{z=H} \end{aligned} \tag{D.35}$$

KINEMATIC BOUNDARY CONDITION FOR $\tilde{\phi}_2$

In contrast to the first potential velocity, the second potential velocity boundary condition satisfies the total boundary condition in x direction. In the second potential velocity, the plate is considered rigid and the pressure in the free surface wave level equals to 0. Therefore one can synthesized the kinematic boundary condition of the liquid in the following manner:

1. **Liquid potential velocity in x direction at** $x = 0$

$$\frac{\partial \tilde{\phi}_{2(x,z,\omega)}}{\partial x}\bigg|_{x=0} = i \cdot \omega \tilde{u}_{1(z,\omega)} \tag{D.36}$$

2. **Liquid potential velocity in x direction at** $x = L$

$$\frac{\partial \tilde{\phi}_{2(x,z,\omega)}}{\partial x}\Big|_{x=L} = i \cdot \omega \tilde{u}_{2(z,\omega)} \tag{D.37}$$

3. **Liquid potential velocity in z direction at** $z = 0$

$$\frac{\partial \tilde{\phi}_{2(x,z,\omega)}}{\partial x}\Big|_{z=0} = 0 \tag{D.38}$$

4. **Free surface condition at** $z = H$

$$\frac{\omega^2}{g}\tilde{\phi}_{2(x,z,H,\omega)}\Big|_{z=H} = 0 \tag{D.39}$$

D.2.1. SEPARATION OF VARIABLE METHOD

The separation method already been briefly discussed in the previous section which is the foundation why the superposition is needed. The separation method will be performed in both $\tilde{\phi}_1$ and $\tilde{\phi}_2$. Then by solving homogeneous boundary condition the total solution of the liquid can be obtained.

FLUID POTENTIAL FOR $\tilde{\phi}_1$

Likewise the equation D.4,the first potential velocity is contained both x t and z dependent variable:

$$\tilde{\phi}_{1(x,z,\omega)} = \tilde{\phi}_{1x(x,\omega)} \cdot \tilde{\phi}_{1z(z,\omega)} \tag{D.40}$$

By substituting the main equation of motion the equation would result in the following:

$$\tilde{\phi}_{1z(z,\omega)}\frac{d^2\tilde{\phi}_{1x(x,\omega)}}{dx^2} + \tilde{\phi}_{1x(x,\omega)}\frac{d^2\tilde{\phi}_{1z(z,\omega)}}{dz^2} = 0 \tag{D.41}$$

Introduction of the separation constant the equation will be totally separated between z and x dependent:

$$\frac{1}{\tilde{\phi}_{1x(x,\omega)}}\frac{d^2\tilde{\phi}_{1x(x,\omega)}}{dx^2} = -\frac{1}{\tilde{\phi}_{1z(z,\omega)}}\frac{d^2\tilde{\phi}_{1z(z,\omega)}}{dz^2} = -a^2 \tag{D.42}$$

For the **x dependent** differential equation would result in the following:

$$\begin{aligned} \frac{1}{\tilde{\phi}_{1x(x,\omega)}}\frac{\partial^2\tilde{\phi}_{1x(x,\omega)}}{\partial x^2} &= -a^2 \\ \frac{\partial^2\tilde{\phi}_{1x(x,\omega)}}{\partial x^2} + a^2\tilde{\phi}_{1x(x,\omega)} &= 0 \end{aligned} \tag{D.43}$$

The solution for the differential equation can be described into the following form:

$$\tilde{\phi}_{1x(x,\omega)} = A_1 \cdot \cos(a \cdot x) + B_1 \sin(a \cdot x) \tag{D.44}$$

Meanwhile for the **z dependent** differential equation would result in the following:

$$\begin{aligned} -\frac{1}{\tilde{\phi}_{1z(z,\omega)}}\frac{\partial^2\tilde{\phi}_{1z(z,\omega)}}{\partial z^2} &= -a^2 \\ \frac{\partial^2\tilde{\phi}_{1z(z,\omega)}}{\partial z^2} - a^2\tilde{\phi}_{1z(z,\omega)} &= 0 \\ \tilde{\phi}_{1z(z,\omega)} &= C_1 \cdot \cosh(a \cdot z) + D_1 \sinh(a \cdot z) \end{aligned} \tag{D.45}$$

Solving the differential equation would result in the following:

$$\tilde{\phi}_{1z(z,\omega)} = C_1 \cdot \cosh(a \cdot z) + D_1 \sinh(a \cdot z) \tag{D.46}$$

As the result the total equation would be:

$$\begin{aligned} \tilde{\phi}_{1(x,z,\omega)} &= \tilde{\phi}_{1x(x,\omega)} \cdot \tilde{\phi}_{1z(z,\omega)} \\ \tilde{\phi}_{1(x,z,\omega)} &= \big(A_1 \cdot \cos(a \cdot x) + B_1 \sin(a \cdot x)\big) \cdot \big(C_1 \cdot \cosh(a \cdot z) + D_1 \sinh(a \cdot z)\big) \end{aligned} \tag{D.47}$$

After the general solution for the first potential velocity is obtained, the homogeneous boundary conditions are analyzed in order to solve the unknown constants.

1. **Liquid potential velocity at t** $x = 0$

$$\begin{aligned} \frac{\partial \tilde{\phi}_{1(x,z,\omega)}}{\partial x}\Big|_{x=0} &= 0 \\ A_1 \cdot \sin 0 + B_1 \cdot \cos 0 &= 0 \\ B_1 &= 0 \end{aligned} \tag{D.48}$$

2. **Liquid potential velocity in x direction at** $x = L$

$$\begin{aligned} \frac{\partial \tilde{\phi}_{1(x,z,\omega)}}{\partial x}\Big|_{x=L} &= 0 \\ A_1 \cdot \sin a \cdot L &= 0 \\ sin(a \cdot L) &= 0 \\ a &= \frac{n\pi}{L} \end{aligned} \tag{D.49}$$

Therefore the equation would result in the following

$$\begin{aligned} \tilde{\phi}_{1n(x,z,\omega)} &= \big(A_{1\,n} \cdot \cos(a_n \cdot x)\big) \cdot \big(C_{1\,n} \cdot \cosh(a_n \cdot z) + D_{1\,n} \sinh(a_n \cdot z)\big) \\ a_n &= \frac{n\pi}{L}, \text{ with } n = 1, 2, 3, \ldots \end{aligned} \tag{D.50}$$

It can also be condensed into the following form

$$\tilde{\phi}_{1(x,z,\omega)} = \sum_{n=1}^{\infty} \big(C_{1\,n} \cdot \cosh(a_n \cdot z) + D_{1\,n} \sinh(a_n \cdot z)\big)\big(\cos(a_n \cdot x)\big) \tag{D.51}$$

From the following equation it can be seen that there are 2 unknown constants left, which can be satisfied with the other two non-homogeneous boundary conditions.

SEPARATION METHOD FOR $\tilde{\phi}_2$

With the same step as the first potential velocity, it begins with separating the x and z dependent into

$$\tilde{\phi}_{2(x,z,\omega)} = \tilde{\phi}_{2x(x,\omega)} \cdot \tilde{\phi}_{2z(z,\omega)} \tag{D.52}$$

$$\tilde{\phi}_{2z(z,\omega)} \frac{\partial^2 \tilde{\phi}_{2x(x,\omega)}}{\partial x^2} + \tilde{\phi}_{2x(x,\omega)} \frac{\partial^2 \tilde{\phi}_{2z(z,\omega)}}{\partial z^2} \tag{D.53}$$

By introducing the separation constant the equation will be totally separated between z and x dependent.

$$\frac{1}{\tilde{\phi}_{2x(x,\omega)}} \frac{\partial^2 \tilde{\phi}_{2x(x,\omega)}}{\partial x^2} = -\frac{1}{\tilde{\phi}_{2z(z,\omega)}} \frac{\partial^2 \tilde{\phi}_{2z(z,\omega)}}{\partial z^2} = -b^2 \tag{D.54}$$

Which result the total equation of

$$\tilde{\phi}_{2(x,z,\omega)} = \big(A_{2\,n} \cdot \cos(b \cdot x) + B_{2\,n} \sin(b \cdot x)\big) \cdot \big(C_{2\,n} \cdot \cosh(b \cdot z) + D_{2\,n} \sinh(b \cdot z)\big) \tag{D.55}$$

After the general solution for the first potential velocity is obtained, the homogeneous boundary conditions which are the (3) and (4).

3. **Liquid potential velocity in z direction at** $z = 0$

$$\begin{aligned} \frac{\partial \tilde{\phi}_{2(x,z,\omega)}}{\partial x}\Big|_{z=0} &= 0 \\ C_2 \cdot \sinh(0) + D_2 \cosh(0) &= 0 \\ D_2 &= 0 \end{aligned} \tag{D.56}$$

4. **Free Surface Condition at** $z = H$

$$\begin{aligned} \frac{\omega^2}{g}\tilde{\phi}_{2(x,z,\omega)}\Big|_{z=H} &= 0 \\ C_2 \cdot \cosh(b\cdot(H)) &= 0 \\ \cosh^{-1}(0) &= b\cdot H \\ bn &= i\cdot\left(\frac{\pi\cdot(2n-1)}{2H}\right) \end{aligned} \tag{D.57}$$

It can also be condensed and simplified by using trigonometry principle into the following form

$$\begin{aligned} \tilde{\phi}_{2(x,z,\omega)} &= \sum_{n=1}^{\infty}\left(A_{2n}\cdot\cosh(b_n\cdot x)+B_{2n}\cdot\sinh(b_n\cdot x)\right)\cos(b_n\cdot z) \\ b_n &= \frac{\pi\cdot(2n-1)}{2H}, \text{with } n = 1,2,3,... \end{aligned} \tag{D.58}$$

Similarly with the first potential velocity, the second also has 2 unknown constants left that can be satisfied with the rest two other non-homogeneous conditions. With the superposition method, the number of constants can be fully satisfied with the total boundary conditions. Therefore the total equation can be written as the following

$$\begin{aligned} \tilde{\phi}_{(x,z,\omega)} = \sum_{n=1}^{\infty} &\left(C_{1n}\cdot\cosh(a_n\cdot z)+D_{1n}\sinh(a_n\cdot z)\right)\left(\cos(a_n\cdot x)\right) \\ &+\left(A_{2n}\cdot\cosh(b_n\cdot x)+B_{2n}\cdot\sinh(b_n\cdot x)\right)\left(\cos(b_n\cdot z)\right) \end{aligned} \tag{D.59}$$

with the following solved separation constants

$$\begin{aligned} a_n &= \frac{n\pi}{L} \\ b_n &= \frac{\pi\cdot(2n-1)}{2H} \\ n &= 1,2,3,... \end{aligned} \tag{D.60}$$

D.3. STRUCTURE AND LIQUID INTERACTION

After calculating the mode shape of both the liquid and the structure, the next step is to solve the couple system between the two. The one way to solve the coupled interaction between the liquid and the structure is by using the matching modes. Through orthogonality for both the liquid orthogonality for the kinematic boundary condition for structural and liquid, and also structural orthogonality to solve the governing equation of motions

D.3.1. KINEMATIC BOUNDARY CONDITION

From the previous section the rest non homogeneous boundary condition will be solved with the solved mode shape.

LIQUID AND WALL 1 KINEMATIC BOUNDARY CONDITION

$$\begin{aligned} \frac{\partial\tilde{\phi}_{2(x,z,\omega)}}{\partial x}\Big|_{x=0} &= i\cdot\omega\tilde{u}_{1(z,\omega)} \\ \sum_{n=1}^{\infty}\frac{B_{2(n)}\,\pi\,(2\,n-1)}{2H}\cos\left(\frac{\pi\,(2\,n-1)\,z}{2H}\right) &= \sum_{k=1}^{\infty} i\cdot\omega U_k\times X^1_{k(x)} \end{aligned} \tag{D.61}$$

With the use of orthogonality the equation would result in the following equation by multiplying both side with $\left(\cos\frac{1}{2}\frac{\pi(2m-1)z}{H}\right)$ and integrate along $x = 0$ to $x = L$. Which result into the following equation.

$$\begin{aligned} \int_0^H \sum_{n=1}^{\infty}\frac{B_{2(n)}\pi(2n-1)}{2H}\cos\frac{\pi(2n-1)z}{2H}\cdot\cos\frac{\pi(2m-1)z}{2H}dz \\ = \int_0^H\sum_{k=1}^{\infty} i\cdot\omega U_k\times X^1_{k(z)}\cos\frac{\pi(2m-1)z}{2H}dz \end{aligned} \tag{D.62}$$

According to the orthogonality principle when $n = m$ would result is

$$\int_0^H \sum_{n=1}^{\infty} \cos\frac{\pi(2n-1)z}{2H} \cdot \cos\frac{\pi(2m-1)z}{2H} dz = \delta_{mn}\frac{H}{2} \tag{D.63}$$

However for the right hand side the equation will be presist in summation as the structure motion is not orthogonal with the liquid.

$$\frac{1}{4}B_{2n}\pi(2n-1)\delta_{mn} = \int_0^H \sum_{k=1}^{\infty} i\cdot\omega U_k \times X_{k(z)} \cos\Big(\frac{\pi(2m-1)z}{2H}\Big)dz \tag{D.64}$$

LIQUID AND WALL 2 KINEMATIC BOUNDARY CONDITION

Likewise the previous section the kinematic boundary condition between liquid and the wall 2 reads

$$\begin{aligned} \frac{\partial\tilde{\phi}_{2(x=L,z,\omega)}}{\partial x} &= i\cdot\omega\tilde{u}_{2(z,\omega)} \\ \sum_{n=1}^{\infty}\Big(\frac{1}{2H}A_{2(n)}\pi(2n-1)\cdot\sinh\Big(\frac{\pi(2n-1)L}{H}\Big)+ & \\ \frac{1}{2H}B_{2(n)}\pi(2n-1)\cdot\cosh\Big(\frac{\pi(2n-1)L}{H}\Big)\Big) &= \sum_{k=1}^{\infty} i\cdot\omega U_k \times X^2_{k(z)} \end{aligned} \tag{D.65}$$

Using the same concept of orthogonality the equation would result in t he following

$$\begin{aligned} \frac{1}{4}\Big(A_{2n}\pi(2n-1)\sinh\Big(\frac{\pi(2n-1)L}{H}\Big) + B_{2n}\pi(2n-1)\cosh\Big(\frac{\pi(2n-1)L}{H}\Big)\Big)\delta_{mn} & \\ = \int_{-H}^{0}\sum_{k=1}^{\infty} i\cdot\omega U_k \times X^2_{k(z)}\cos\Big(\frac{\pi(2m-1)z}{H}\Big)dz & \end{aligned} \tag{D.66}$$

LIQUID AND PLATE KINEMATIC BOUNDARY CONDITION

The liquid equation will be in the following

$$\frac{\partial\tilde{\phi}_{1(x,z,\omega)}}{\partial z}\Big|_{z=0} = -i\cdot\omega\tilde{u}^3_n(x,\omega) \tag{D.67}$$

Likewise the previous equation the orthogonality would result in the following equation

$$D_{1(m)} \times n \times \Big(\frac{\pi}{2}\Big)\delta_{mn} = \int_0^L \sum_{k=1}^{\infty} i\cdot\omega Uk\cdot X^3_{k(x)}\cdot\cos\Big(\frac{m\pi x}{L}\Big)dx \tag{D.68}$$

FREE WATER SURFACE CONDITION

$$\begin{aligned} \sum_{n=1}^{\infty}\frac{\omega^2}{g}\Big(C_{1(n)}\cosh\Big(\frac{n\pi H}{L}\Big) + D_{1(n)}\sinh\Big(\frac{n\pi H}{L}\Big)\Big)\cos\Big(\frac{n\pi x}{L}\Big) = & \\ \Big(\frac{C_{1(n)}\,n\pi}{L}\sinh\Big(\frac{n\pi H}{L}\Big) + \frac{D_{1(n)}\,n\pi}{L}\cosh\Big(\frac{n\pi H}{L}\Big)\Big)\cos\Big(\frac{n\pi x}{L}\Big) + & \\ \frac{1}{2H}\Big(A_{2(n)}\cdot\cosh\Big(\frac{\pi(2n-1)x}{H}\Big) + B_{2(n)}\cdot\sinh\Big(\frac{\pi(2n-1)x}{H}\Big)\Big) & \\ \pi(2n-1)\sin\Big(\frac{1}{2}\pi(2n-1)\Big) & \end{aligned} \tag{D.69}$$

Using the orthogonality principle by multiplying to $\cos\left(\frac{m\pi x}{L}\right)$ and integrating it from 0 to L, the equation would result in the following

$$\begin{aligned} \frac{\omega^2}{g}\Big(C_{1(n)}\cosh\Big(\frac{n\pi H}{L}\Big) + D_{1(n)}\sinh\Big(\frac{n\pi H}{L}\Big)\Big)\frac{L}{2}\delta_{mn} = & \\ \Big(\frac{C_{1(n)}\,n\pi}{2}\sinh\Big(\frac{n\pi H}{L}\Big) + \frac{D_{1(n)}\,n\pi}{2}\cosh\Big(\frac{n\pi H}{L}\Big)\Big)\delta_{mn} + & \\ \sum_{n=1}^{\infty}\int_0^L\Big[\frac{-1}{2H}\Big(A_{2(n)}\cdot\cosh\Big(\frac{\pi(2n-1)x}{H}\Big) + B_{2(n)}\cdot\sinh\Big(\frac{\pi(2n-1)x}{H}\Big)\Big) & \\ \pi(2n-1)\sin\Big(-\frac{1}{2}\pi(2n-1)\Big)\Big]\cos\frac{m\pi x}{L} & \end{aligned} \tag{D.70}$$

In total the unknowns $U_n, C_{1(n)}, D_{1(n)}, A_{2(n)}, B_{2(n)}$ where $n = 1,2,3,4,...$ and $k = 1,2,3,4,...$ The number of unknowns are not only satisfied through kinematic boundary conditions but also from the equation of motion in which will be derived in the following equations.

WALL 1 EQUATION OF MOTION

The equation of motion from the First wall is

$$\frac{d^4\tilde{u}^1_{k(z\omega)}}{dz^4} - \beta^4_w u^1_{k(z,\omega)} = \rho_{liq} i\omega\tilde{\phi}_{(x=0,z,t)}$$
$$\beta^4_w = (\omega^2 \rho_s A_w) \tag{D.71}$$

Which can be expand into the following form

$$\sum_{k=1}^{\infty}\left[U_k \frac{d^4 X^1_{k(z)}}{dz^4} - \beta^4_w U_k X^1_{k(z)}\right] = \sum_{n=1}^{\infty}\left[C_{1(n)}\cosh\left(\frac{n\pi z}{L}\right) + D_{1(n)}\sinh\left(\frac{n\pi z}{L}\right) + A_{2(n)} \times \cos\left(\frac{\pi(2n-1)z}{2H}\right)\right] \times \frac{i\cdot\omega\dot{\rho}_{liq}}{E_w I_w} \tag{D.72}$$

and by integrating the equation form H to 0 and multiply by the structural mode shape, the equation in the following will be expanded

$$\int_0^H \sum_{k=1}^{\infty}\left(\frac{U_k}{\beta^4_w}\frac{d^4 X^1_{k(z)}}{dx^4}\right)X^1_{j(z)}dz - \int_0^H \sum_{k=1}^{\infty} U_k X^1_{k(z)}\cdot X^1_{j(z)}dz =$$
$$\int_0^H \sum_{n=1}^{\infty}\left[C_{1(n)}\cosh\left(\frac{n\pi z}{L}\right) + D_{1(n)}\sinh\left(\frac{n\pi z}{L}\right) + A_{2(n)} \times \cos\left(\frac{\pi(2n-1)z}{2H}\right)\right] \times \frac{i\cdot X^1_{j(z)}\cdot\omega\cdot\rho_{liq}}{E_w I_w \beta^4_w}dz \tag{D.73}$$

The summation would not be crossed out by a Kronecker's delta δ_{mn} as the orthogonality can only be achieved by the full path of the length. However as in the previous section the homogeneous calculation has been performed which is in the following expression:

$$\frac{d^4\tilde{u}^1_{k(z\omega)}}{dz^4} - \beta_{w}{}^4_k u^1_{k(z,\omega)} = 0$$
$$\frac{d^4\tilde{u}^1_{k(z\omega)}}{dz^4} = \beta_{w}{}^4_k u^1_{k(z,\omega)} \tag{D.74}$$

Therefore through substitution the equation D.74, the expression would result in the following

$$\int_0^H \sum_{k=1}^{\infty}\left(\left(\frac{\beta_{wk}}{\beta_w}\right)^4 - 1\right)U_k X^1_{k(z)}\cdot X^1_{j(z)}dz =$$
$$\int_0^H \sum_{n=1}^{\infty}\left[C_{1(n)}\cosh\left(\frac{n\pi z}{L}\right) + D_{1(n)}\sinh\left(\frac{n\pi z}{L}\right) + A_{2(n)} \times \cos\left(\frac{\pi(2n-1)z}{2H}\right)\right] \times \frac{i\cdot X^1_{j(z)}\cdot\omega\cdot\rho_{liq}}{E_w I_w \beta^4_w}dz \tag{D.75}$$

WALL 2 EQUATION OF MOTION

For the equation of motion of the Second wall is defined by the following expression:

$$\frac{\partial^4\tilde{u}^2_{n(z\omega)}}{\partial z^4} - \omega^2\rho_s A_w u^2_{n(z,\omega)} = \rho_{liq} i\omega\tilde{\phi}_{(x=L,z,t)} \tag{D.76}$$

With the same following step as the previous equation, the integration and the structural mode shape multiplication would result in the following expression

$$\begin{aligned}\int_0^H \sum_{k=1}^{\infty} \left(\left(\frac{\beta_{wk}}{\beta_w}\right)^4 - 1\right) U_p X^2_{k(z)} \cdot X^2_{j(z)} dz = \\ \int_0^H \sum_{n=1}^{\infty} \left[\left(C_{1(n)} \cosh\left(\frac{n\pi z}{L}\right) + D_{1(n)} \sinh\left(\frac{n\pi z}{L}\right)\right) \cos(n\pi) + \right. \\ \left(A_{2(n)} \cosh\left(\frac{\pi(2n-1)L}{2H}\right) + B_{2(n)} \sinh\left(\frac{\pi(2n-1)L}{2H}\right)\right) \\ \left. \cos\left(\frac{\pi(2n-1)z}{2H}\right)\right] \times \frac{i\omega\rho_l \cdot X^2_{j(z)}}{E_w I_w \beta_w^4} dz\end{aligned} \tag{D.77}$$

PLATE EQUATION OF MOTION

While for the plate the equation of motion can be defined in the following expression

$$E_p \cdot I_p \cdot \frac{\partial^4 \tilde{u}^3_{n(x\omega)}}{\partial x^4} - (\omega^2 \rho_s A_p - k) u^3_{n(x,\omega)} = \rho_{liq} i\omega \tilde{\phi}_{(x,z=0,t)} \tag{D.78}$$

With the same step the equation can be expressed into the following

$$\begin{aligned}\int_0^H \sum_{k=1}^{\infty} \left(\left(\frac{\beta_{pk}}{\beta_p}\right)^4 - 1\right) U_k X^3_{k(z)} \cdot X^3_{j(z)} dx = \\ \int_0^L \sum_{n=1}^{\infty} \left[\left(C_{1(n)} \cosh\left(\frac{n\pi x}{L}\right) + \left(A_{2(n)} \cosh\left(\frac{\pi(2n-1)x}{2H}\right) + \right.\right. \\ \left.\left. B_{2(n)} \sinh\left(\frac{\pi(2n-1)x}{2H}\right)\right)\right] \times \frac{i\omega\rho_l \cdot X^3_{m(x)}}{E_p I_p \beta_p^4} dx\end{aligned} \tag{D.79}$$

Seeing from the equation it can be seen that the the number of unknowns and the the number of equations do not balance each other. The total unknowns are $4\times n+1\times p$ and the number of equations are $4\times n+3\times p$. In order to satisfied the number of unknowns, the expression can be manipulated throgh summation. Through summation the principle of ortogonality can be also applied. The equation that will be sum of : D.79, D.77 , D.75 which will be resulting into the following equation

$$\begin{aligned}\int_0^H \sum_{k=1}^{\infty} \left(\left(\frac{\beta_{wk}}{\beta_w}\right) - 1\right) U_k X^1_{k(z)} \cdot X^1_{j(z)} dz + \\ \int_0^H \sum_{k=1}^{\infty} \left(\left(\frac{\beta_{wk}}{\beta_w}\right)^4 - 1\right) U_p X^2_{k(z)} \cdot X^2_{j(z)} dz + \\ \int_0^H \sum_{k=1}^{\infty} \left(\left(\frac{\beta_{pk}}{\beta_p}\right)^4 - 1\right) U_k X^3_{k(z)} \cdot X^3_{j(z)} dx = \\ \int_{-H}^0 \sum_{n=1}^{\infty} \left[C_{1(n)} \cosh\left(\frac{n\pi z}{L}\right) + D_{1(n)} \sinh\left(\frac{n\pi z}{L}\right) + \right. \\ \left. A_{2(n)} \times \cos\left(\frac{\pi(2n-1)z}{2H}\right)\right] \times \frac{i \cdot X^1_{m(z)} \cdot \omega \cdot \rho_l}{E_W I_w \beta_w^4} dz + \\ \int_0^H \sum_{n=1}^{\infty} \left[\left(C_{1(n)} \cosh\left(\frac{n\pi z}{L}\right) + D_{1(n)} \sinh\left(\frac{n\pi z}{L}\right)\right) \cos(n\pi) + \right. \\ \left(A_{2(n)} \cosh\left(\frac{\pi(2n-1)L}{2H}\right) + B_{2(n)} \sinh\left(\frac{\pi(2n-1)L}{2H}\right)\right) \\ \left. \cos\left(\frac{\pi(2n-1)z}{2H}\right)\right] \times \frac{i\omega\rho_l \cdot X^2_{m(z)}}{E_w I_w \beta_w^4} dz + \\ \int_0^L \sum_{n=1}^{\infty} \left[\left(C_{1(n)} \cosh\left(\frac{n\pi x}{L}\right) + \left(A_{2(n)} \cosh\left(\frac{\pi(2n-1)x}{2H}\right) + \right.\right. \\ \left.\left. B_{2(n)} \sinh\left(\frac{\pi(2n-1)x}{2H}\right)\right)\right] \times \frac{i\omega\rho_l \cdot X^3_{m(x)}}{E_p I_p \beta_p^4} dx\end{aligned} \tag{D.80}$$

From the equation it can be seen that the in the left hand side term the orthogonality principle can be applied here. From the interface boundary conditions between liquid and structure equation of motion, the linear algebra matrix can be derived. The matrix size will be $[4 \cdot n + 1 \cdot k] \times [4 \cdot n + 1 \cdot k]$.

E

THREE DIMENSIONAL DERIVATION

E.1. CYLINDRICAL SHELL DERIVATION

From the Chapter 4.2.3, one can find the main equation of motion of cylindrical shell. However these equation of motions are still incomplete. In order to achieve the the solution just as the two dimensional model, the equation has to decoupled. Meanwhile the equation of motions are totally coupled within the three axis (r,θ,z).

Before decoupling, the forces and the moment have to be in expanded forms first. Each of equation of motion is consisted the three displacement (u_r, u_θ, and u_z). In order to expand the equation of motion in term of displacement, the kinematic component such as strain and stresses should be defined. Substituting the Lame parameter to the equations in the equation B.45, each of the membrane strains for cylindrical shell can be written as:

$$\begin{aligned}
\varepsilon^0_{zz} &= \frac{\partial u_z(z,\theta,t)}{\partial z} \\
\varepsilon^0_{\theta\theta} &= \frac{1}{R}\frac{\partial u_\theta(z,\theta,t)}{\partial \theta} + \frac{u_r(z,\theta,t)}{R} \\
\varepsilon^0_{z\theta} &= \frac{\partial u_\theta(z,\theta,t)}{\partial z} + \frac{1}{R}\frac{\partial u_z(z,\theta,t)}{\partial \theta}
\end{aligned} \tag{E.1}$$

For the membrane strain, the angle has to be calculated first which from the equation B.42, t the angles can be calculate as:

$$\begin{aligned}
\beta_z &= -\frac{\partial u_r(z,\theta,t)}{\partial z} \\
\beta_\theta &= \frac{u_\theta(z,\theta,t)}{R} - \frac{1}{R}\frac{\partial (u_r)(z,\theta,t)}{\partial z}
\end{aligned} \tag{E.2}$$

As from this terms the bending strains in the equation B.46 can be achieved as the following:

$$\begin{aligned}
k_{zz} &= \frac{-\partial^2 u_r(z,\theta,t)}{\partial z^2} \\
k_{\theta\theta} &= \frac{1}{R^2}\left(\frac{\partial u_\theta(z,\theta,t)}{\partial \theta} - \frac{\partial^2 u_r(z,\theta,t)}{\partial \theta^2}\right)
\end{aligned} \tag{E.3}$$

Substituting the Lame parameter to the force, which are in the following equation:

$$\begin{aligned}
N_{zz} &= K\left(\frac{\partial u_z(z,\theta,t)}{\partial z} + \left(\frac{1}{R}\frac{\partial u_\theta(z,\theta,t)}{\partial \theta} + \frac{u_r(z,\theta,t)}{R}\right)\right) \\
N_{z\theta} &= \frac{k(1-\mu)}{2}\left(\frac{\partial u_\theta(z,\theta,t)}{\partial z} + \frac{1}{R}\frac{\partial u_z(z,\theta,t)}{\partial \theta}\right)
\end{aligned} \tag{E.4}$$

Moment force can also be achieved through substitution:

$$\begin{aligned} M_{zz} &= D\left(\frac{\partial^2}{\partial z} + \frac{\mu}{R^2}\left(\frac{\partial u_\theta(z,\theta,t)}{\partial \theta} - \frac{\partial^2 u_r(z,\theta,t)}{\partial \theta^2}\right)\right) \\ M_{\theta\theta} &= D\left(-\mu\left(\frac{\partial^2 u_r(z,\theta,t)}{\partial z^2}\right) + \frac{1}{R^2}\left(\frac{\partial u_\theta(r,z,\theta)}{\partial \theta} - \frac{\partial^2 u_r(z,\theta,t)}{\partial \theta^2}\right)\right) \\ M_{z\theta} &= \frac{D(1-\mu)}{2}\left(\frac{1}{R}\frac{\partial u_\theta(z,\theta,t)}{\partial z} - \frac{2}{R}\frac{\partial^2 u_r(z,\theta,t)}{\partial z \partial \theta}\right) \end{aligned} \tag{E.5}$$

Membrane shear force can also acquired by substituting the equations:

$$\begin{aligned} Q_{zr} &= \frac{\partial M_{zz}(z,\theta,t)}{\partial z} + \frac{1}{R}\frac{\partial M_{z\theta}(z,\theta,t)}{\partial \theta} \\ Q_{\theta r} &= \frac{M_{\theta\theta}(z,\theta,t)}{\partial \theta} + \frac{1}{R}\frac{\partial M_{\theta\theta}(z,\theta,t)}{\partial \theta} \end{aligned} \tag{E.6}$$

Meanwhile for the effective shear force for the first kind can be written in the following form:

$$\begin{aligned} V_{zr} &= D\Big(\frac{\partial^3 u_r(r,z,\theta)}{\partial z^3} + \frac{\mu}{R^2}\Big(\frac{\partial^3 u_r(r,z,\theta)}{\partial z \partial \theta}\Big)\Big) \\ &\quad + \frac{1-\mu^2}{2R^2}D\Big(\frac{\partial^2 u_\theta(r,z,\theta)}{\partial z \partial \theta} - 2\frac{\partial^3 u_r(r,z\theta)}{\partial z \partial \theta^2}\Big) \\ V_{\theta r} &= \frac{D(1-\mu)}{2R}\Big(\frac{\partial^3 u_\theta(z,\theta,t)}{\partial z^2 \partial \theta} - 2\frac{\partial^3 u_r(z,\theta,t)}{\partial z^2 \partial \theta}\Big) \\ &\quad + \frac{D}{R}\Big(-\mu\Big(\frac{\partial^3 u_r(z,\theta,t)}{\partial z^2 \partial \theta}\Big) + \frac{1}{R^2}\frac{\partial^2 u_\theta(z,\theta,t)}{\partial \theta^2} - \frac{1}{R^2}\frac{\partial^3 u_r}{\partial \theta^2}\Big) \end{aligned} \tag{E.7}$$

And for the second kind effective shear can be written in the following form:

$$\begin{aligned} T_{z\theta} &= \frac{K}{2}(1-\mu)\Big(\frac{\partial u_\theta(z,\theta,t)}{\partial z} + \frac{1}{R}\frac{\partial u_z(z,\theta,t)}{\partial \theta}\Big) + \frac{(1-\mu)D}{2R}\Big(\frac{\partial u_\theta(z,\theta,t)}{\partial ; z} - \frac{z}{R}\frac{\partial u_r(z,\theta,t)}{\partial z \partial \theta}\Big) \\ T_{\theta z} &= \frac{K(1-\mu)}{2}\Big(\frac{\partial u_\theta(z,\theta,t)}{\partial z} + \frac{1}{R}\frac{\partial u_z(z,\theta,t)}{\partial \theta}\Big) \end{aligned} \tag{E.8}$$

Substitution the equation of motion with the components above result to the equation of motion:

Equation of motion longitudinal vibration along the axis of revolution:

$$\begin{aligned} &\frac{-2E_w h_w}{R(\mu^2-1)}\Big(\mu\Big(\frac{\partial}{\partial z}u_r(z,\theta,t)\Big) + \Big(\frac{\partial^2}{\partial z^2}u_z(z,\theta,t)\Big)R + \mu\Big(\frac{\partial}{\partial \theta \partial z}u_\theta(z,\theta)\Big)\Big) + \\ &\frac{E_w h_w(1-\mu)}{R(-\mu^2+1)}\Big(\frac{\partial^2}{\partial z \partial \theta}u_\theta(z,\theta,t) + \frac{1}{R}\frac{\partial^2}{\partial \theta^2}u_z(z,\theta,t)\Big) - 2\rho h\frac{\partial^2}{\partial t^2}u_z(z,\theta,t) = 0 \end{aligned} \tag{E.9}$$

Equation of motion longitudinal vibration along the axis of revolution:

$$\begin{aligned} &\frac{h_w E_w}{R(\mu+1)}\Big(\Big(\frac{\partial^2}{\partial z^2}u_\theta(z,\theta,t)\Big)R + \frac{\partial^2}{\partial z \partial \theta}u_z(z,\theta,t)\Big) - \frac{2E_w h_w}{R^2(\mu^2-1)}\Big(\mu\Big(\frac{\partial^2}{\partial z \partial \theta}u_z z,\theta,t\Big)R + \\ &\frac{\partial}{\partial \theta}u_r(z,\theta,t) + \frac{\partial^2}{\partial \theta^2}u_\theta(z,\theta,t)\Big) + \frac{1}{R^4(24\mu^2-24)}\Big(2E\Big(2\Big(\frac{\partial}{\partial z^2 \partial \theta}u_r(z,\theta,t)\Big)R^2 \\ &+R^2(-1+\mu)\Big(\frac{\partial^2}{\partial z^2}u_\theta(z,\theta,t)\Big) - 2\Big(\frac{\partial^2}{\partial \theta^2}u_\theta(z,\theta,t)\Big)\Big)h^3\Big) - 2\rho h\frac{\partial^2}{\partial t^2}u_\theta(z,\theta)u_\theta(z,\theta,t) = 0 \end{aligned} \tag{E.10}$$

Equation of motion transversal vibration along the normal to the surface axis:

$$\begin{aligned}
-\frac{1}{12R^2(\mu^2-1)}\Big(\Big(2\Big(\frac{\partial^4}{\partial z^4}u_r(z,\theta,t)\Big)R^2-\mu\Big(\frac{\partial^3}{\partial z^2\partial\theta}u_\theta(z,\theta,t)\Big)-\\
\Big(\frac{\partial^3}{\partial z^2\partial\theta}u_\theta(z,\theta)\Big)+2\Big(\frac{\partial^4}{\partial z^2\partial\theta^2}u_r(z,\theta,t)\Big)\Big)E_w h_w^3\Big)-\\
\frac{1}{R^4(24\mu^2-24)}\Big(2E_w\Big(2\Big(\frac{\partial^4}{\partial\theta^4}u_r(z,\theta,t)\Big)+\\
2\Big(\frac{\partial^4}{\partial z^2\partial\theta^2}u_r(z,\theta,t)\Big)R^2+R^2(-1+\mu)\Big(\frac{\partial^3}{\partial z^2\partial\theta}u_\theta(z,\theta,t)\Big)-\\
2\Big(\frac{\partial^3}{\partial\theta^3}u_\theta(z,\theta,t)\Big)\Big)h^3\Big)-\frac{2E_w h_w}{(\mu^2-1)R^2}\Big(\mu\Big(\frac{\partial}{\partial z}u_z(z,\theta,t)\Big)R+\\
u_r(z,\theta,t)\frac{\partial}{\partial\theta}u_\theta(z,\theta,t)\Big)+2\rho h\frac{\partial^2}{\partial t^2}u_r(z,\theta,t)=0
\end{aligned} \tag{E.11}$$

These equations can be also written in matrix. The matrix it self consist of mass matrix and stiffness matrix. Overall the equation can be written as the following general form:

$$\underline{\underline{[\mathbf{M}]}}\times\underline{u}+\underline{\underline{[\mathbf{K}]}}\times\underline{u}=\underline{F} \tag{E.12}$$

The matrix **M**, can be written as the following:

$$\underline{\underline{[\mathbf{M}]}}=\begin{bmatrix} m_{11} & 0 & 0\\ 0 & m_{22} & 0\\ 0 & 0 & m_{33}\end{bmatrix} \tag{E.13}$$

Where each of the following component are:

$$\begin{aligned}
m_{11}&=-2\rho h\frac{\partial(\cdot)}{\partial t}\\
m_{22}&=-2\rho h\frac{\partial(\cdot)}{\partial t}\\
m_{33}&=2\rho h\frac{\partial(\cdot)}{\partial t}
\end{aligned} \tag{E.14}$$

Meanwhile for the vector u is written in the following:

$$\underline{u}=\begin{Bmatrix} u_z(z,\theta,t)\\ u_\theta(z,\theta,t)\\ u_r(z,\theta,t)\end{Bmatrix} \tag{E.15}$$

Last but not least, the stiffness matrix (**K**) is:

$$\underline{\underline{[\mathbf{K}]}}=\begin{bmatrix} L_{11} & L_{12} & L_{13}\\ L_{21} & L_{22} & L_{23}\\ L_{31} & L_{32} & L_{33}\end{bmatrix} \tag{E.16}$$

For shell equation of motion, the significant characteristic is the symmetric principle in matrix. Where from the above matrix, one can simply write that $L_{12}=L_{21}$, and $L_{13}=L_{31}$, as well as $L_{23}=L_{32}$. Each of the matrix

component is written as:

$$
\begin{aligned}
L_{11} &= \frac{-h_w E_w}{(\mu^2-1)R^2}\left(2R^2\frac{\partial^2(\cdot)}{\partial z^2} - \frac{\partial^2(\cdot)}{\partial\theta^2}\mu + \frac{\partial^2(\cdot)}{\partial\theta^2}\right)\\
L_{22} &= \frac{12E_w h_w}{(12\mu^2-12)R^4}\left(R^2(-1+\mu)\frac{\partial^2(\cdot)}{\partial z^2} - 2\frac{\partial^2(\cdot)}{\partial\theta^2}\right)\left(R^2+\frac{1}{12}h^2\right)\\
L_{33} &= \frac{E_w h_w}{(6\mu^2-6)R^4}\left(R^4\frac{\partial^4(\cdot)}{\partial z^4}h^2 + \left(\frac{\partial}{\partial^4(\cdot)z^2\partial\theta^2}+12\right)R^2 + \frac{\partial^4}{\partial\theta^4}h^2\right)\\
L_{12} &= L_{21} = -\frac{E_w h_w}{R(-1+\mu)}\frac{\partial^2(\cdot)}{\partial z\partial\theta}\\
L_{13} &= L_{31} = -2\frac{E_w h_w \mu}{R(\mu^2-1)}\frac{\partial(\cdot)}{\partial z}\\
L_{23} &= L_{32} = \frac{E_w h_w^3}{R^2(6\mu^2-6)R^4}\frac{\partial^3(\cdot)}{\partial z^2\partial\theta^2} + \frac{E_w h_w}{(6\mu^2-6)R^4}\left(h_w\frac{\partial^3(\cdot)}{\partial\theta^3} - 12R^2\frac{\partial(\cdot)}{\partial\theta}\right)
\end{aligned}
\tag{E.17}
$$

In the next calculation is how to decouple the equation u_z, u_r, and u_θ. This step, will be discussed in the next section.

E.2. FREQUENCY DOMAIN CALCULATION

In order to solve the analytically more conveniently the calculation continues from the time domain to the frequency domain. Both plate and wall is converted to the frequency domain.

E.2.1. CIRCULAR PLATE

From the equation, one can conclude that the $\tilde{W}$ is dependent on both r,θ. Due to this condition, separation of the variable method is required to be performed to solve a differential equation. Separation of the variable method can be used there is no time-dependent boundary condition. Let introduce the new solution where the r dependency is separated from the θ:

$$\tilde{W}_(r,\theta) = \tilde{W}_r \cdot \tilde{W}_\theta \tag{E.18}$$

Where through substitution to the equation of motion it would result into the following expression: θ.

$$\tilde{W}_\theta \cdot \frac{\partial^2\tilde{W}_r}{\partial r^2} + \frac{\tilde{W}_\theta}{r}\frac{\partial\tilde{W}_r}{\partial r} + \frac{\tilde{W}_r}{r^2}\frac{\partial^2\tilde{W}_\theta}{\partial\theta^2} \pm \beta_p^2\tilde{W}_\theta\tilde{W}_r = 0 \tag{E.19}$$

Afterwards, by multiplying with r^2 and dividing with $(\tilde{W}_\theta \times \tilde{W}_r)$ the expression would result:

$$\left[\left(\frac{\partial^2\tilde{W}_r}{\partial r^2} + \frac{1}{r}\frac{\partial\tilde{W}_r}{\partial r}\right) + \pm\beta_p^2\right]r^2 = -\frac{1}{\tilde{W}_\theta}\frac{\partial^2\tilde{W}_\theta}{\partial\theta^2} \tag{E.20}$$

Subsequently the new separation constant is introduced which is p. The equation would result in the following equation:

$$-\frac{1}{\tilde{W}_\theta}\frac{\partial^2\tilde{W}_\theta}{\partial\theta^2} = p^2 \tag{E.21}$$

From the equation the ordinary differential equation can be solved. However since the load is in the cos form therefore the displacement would also follows the same form with the external load:

$$\tilde{W}_\theta = A_p\cosh(p\cdot\theta) \tag{E.22}$$

From the equation, one must understand a physic behind the value of p. It is unquestionable that at the $\theta = 0$ and $\theta = 2\pi$ must have the same value, which is:

$$
\begin{aligned}
\cosh(p\cdot 2\pi) &= \cosh(0)\\
\cosh(p\cdot 2\pi) &= 1
\end{aligned}
\tag{E.23}
$$

Which from this relation, it only can be satisfied when p is an integer value. For the r, differential equation it can be written as the following equation:

$$r^2\left(\frac{\partial^2 \tilde{W}_r}{\partial r^2} + r\frac{\partial \tilde{W}_r}{\partial r}\right) + (\pm\beta_p^2 r^2 - p^2) \times \tilde{W}_r = 0 \tag{E.24}$$

The equation above its form almost looks like with Besel standard function where for the Bessel function the differential equation is:

$$\begin{aligned} x^2\frac{\partial Y}{\partial x} + x\frac{\partial Y}{\partial x} + (x^2 - a^2)Y = 0 \quad &\text{result to first kind and second kind} \\ x^2\frac{\partial Y}{\partial x} + x\frac{\partial Y}{\partial x} + (-x^2 - a^2)Y = 0 \quad &\text{result to modified first kind and second kind} \end{aligned} \tag{E.25}$$

The Bessel function is highly dependent on the value of x, if the x value is real then it would result to the first and the second kind. Meanwhile if it is imaginary value then it would be the counterpart which is the modified Bessel function. In the following figure will be shown how Bessel function plotted result using Matlab program:

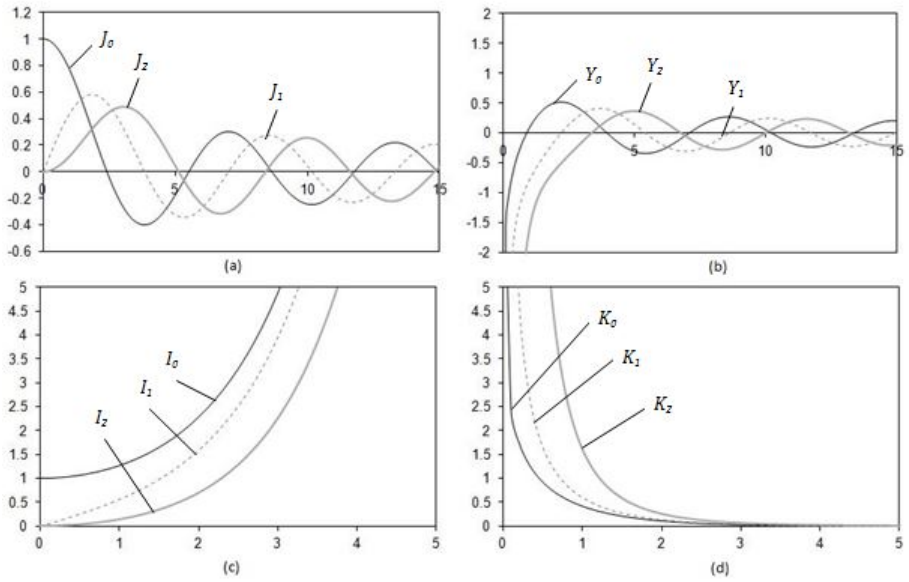

Figure E.1: (a) First Kind Bessel Function ; (b) Second Kind Bessel Function ; (c) First Kind Modified Bessel Function ; (d) Second Kind Modified Bessel Function

In short the bessel function is consisted of J_α, Y_α and the modified Bessel function is I_α, K_α and the value of $\alpha = 0,1,2,3,4...$ The next calculation is how to modified the equation E.24 under the form of the Bessel function. In order to accomplished that new definition is introduced:

$$\begin{aligned} s^2 &= \beta_p^2 \cdot r^2 \\ -s^2 &= (i\beta_p)^2 \cdot r^2 \end{aligned} \tag{E.26}$$

Therefore it can also be written that:

$$\tilde{W}_r(r) = \tilde{W}_r(s(r)) \tag{E.27}$$

Then redefinition of the some terms that are used in the equation can be summarized in the following equation:

First Derivation

$$\begin{aligned}\frac{\partial \tilde{W}_r(r)}{\partial r} &= \frac{\partial \tilde{W}_r(s)}{\partial s} \cdot \frac{\partial s}{\partial r} \\ &= \frac{\partial \tilde{W}_r(s)}{\partial s} \cdot \beta_p\end{aligned} \tag{E.28}$$

Second Derivation

$$\begin{aligned}\frac{\partial^2 \tilde{W}_r(r)}{\partial^2 r} &= \frac{\partial}{\partial r}\Big(\frac{\partial \tilde{W}_r(s)}{\partial s} \cdot \frac{\partial s}{\partial r}\Big) \\ &= \frac{\partial^2 \tilde{W}_r(s)}{\partial s^2} \cdot \beta_p^2\end{aligned} \tag{E.29}$$

Therefore through substitution to the equation E.24 it would result in the following equation:

$$s^2\Big(\frac{\partial^2 \tilde{W}_r(s)}{\partial s^2} + s\frac{\partial \tilde{W}_r(s)}{\partial s}\Big) + (\pm s^2 - p^2) \times \tilde{W}_r(s) = 0 \tag{E.30}$$

From the equation above, one can conclude that it would arrive with two different solution both Bessel function and modified Bessel function, since it is derived that $\pm s^2$. Therefore the solution of the plate equation is:

$$\tilde{W}_r(s) = \sum_{p=0}^{\infty} (L_p \cdot J_p(\beta_p r) + M_p \cdot N_p(\beta_p r) + O_p \cdot I_p(\beta_p r) + D_p \cdot K_p(\beta_p r)) \cos p\theta \tag{E.31}$$

However from the figure E.1, both second kind Bessel function and second kind modified Bessel function at $r = 0$ would result to infinity. This case it is not possible to have such value for a displacement. Therefore the constant multiplier of the two Bessel function must be 0, otherwise the solution will not be a valid solution. Which then it will result the following equation:

$$\tilde{W}_r(s) = \sum_{p=0}^{\infty} (L_p \cdot J_p(\beta_p r) + M_p \cdot I_p(\beta_p r)) \cos(p\theta) \tag{E.32}$$

From the following solution it can be concluded it has two constants which are L_p and M_p.

E.2.2. CYLINDRICAL SHELL

Before decoupling the equation of motions, firstly the solution is assumed in the following forms:

$$\begin{aligned}\tilde{u}_z &= \sum_{j=0}^{\infty} \tilde{U}_z(z) \cos(j\theta) \\ \tilde{u}_\theta &= \sum_{j=0}^{\infty} \tilde{U}_\theta(z) \sin(j\theta) \\ \tilde{u}_r &= \sum_{j=0}^{\infty} \tilde{U}_r(z) \cos(j\theta)\end{aligned} \tag{E.33}$$

This solution is can be fully justified since from both the loading and the plate solution is defined as the cos andsin form. After obtaining the new solutions, through substitution the mass matrix in the equation E.13 would be in the following:

$$\begin{aligned}m_{11} &= 2\omega^2 \rho_w h_w \\ m_{22} &= -2\omega^2 \rho_w h_w \\ m_{33} &= -2\omega^2 \rho_w h_w\end{aligned} \tag{E.34}$$

Meanwhile for the stiffness matrix from the equation E.16, will be in the subsequent expression:

$$\begin{aligned}
L_{11} &= -\frac{h_w E_w}{R^2(\mu^2-1)}\left(2R^2\frac{\partial^2(\cdot)}{\partial z^2} + j^2 mu - j^2\right)\\
L_{22} &= -\frac{E_w h_w (R^2 + 1/12h^2)}{(12\mu^2-12)R^4}\left(2j^2 + (-1+\mu)R^2\frac{\partial^2(\cdot)}{\partial z^2}\right)\\
L_{33} &= -\frac{E_w h_w}{(6\mu^2-6)R^4}\left(R^4 h_w^2\frac{\partial^4}{\partial z^4} + R^2\left(12 - 2h_w^2 j^2\frac{\partial^2(\cdot)}{\partial z^2}\right)\right.\\
L_{12} &= L_{21} = -\frac{E_w h_w j}{(-1+\mu)R}\frac{\partial(\cdot)}{\partial z}\\
L_{13} &= L_{31} = \frac{-2E_w h_w \mu}{R(\mu^2-1)}\frac{\partial(\cdot)}{\partial z}\\
L_{23} &= L_{32} = \frac{E_W j h_w}{(6\mu^2-6)R^4}\left(-h^2 j^2 + R^2\left(-12 + h_w^2\frac{\partial^2(\cdot)}{\partial z^2}\right)\right)
\end{aligned} \tag{E.35}$$

Updating the new equations of motion would turn out in the following expression:

$$\begin{bmatrix} m_{11} & 0 & 0\\ 0 & m_{22} & 0\\ 0 & 0 & m_{33}\end{bmatrix} \times \begin{Bmatrix}\tilde{U}_z\\ \tilde{U}_\theta\\ \tilde{U}_R\end{Bmatrix} + \begin{bmatrix} L_{11} & L_{12} & L_{13}\\ L_{21} & L_{22} & L_{23}\\ L_{31} & L_{32} & L_{33}\end{bmatrix} \times \begin{Bmatrix}\tilde{u}_z\\ \tilde{u}_\theta\\ \tilde{u}_r\end{Bmatrix} = 0 \tag{E.36}$$

In which from this expression summing the mass matrix and the stiffness matrix will not alter the symmetric form of the matrix. Therefore, it can be simply written as the following:

$$\begin{bmatrix} L_{11}+m_{11} & L_{12} & L_{13}\\ L_{21} & L_{22}+m_{22} & L_{23}\\ L_{31} & L_{32} & L_{33}+m_{33}\end{bmatrix} \times \begin{Bmatrix}\tilde{u}_z(z)\\ \tilde{u}_\theta(z)\\ \tilde{u}_r(z)\end{Bmatrix} = 0 \tag{E.37}$$

or just simply written the matrix $\underline{\underline{L}}$ that consist both stiffness matrix and mass matrix in a summation of the two:

$$\begin{bmatrix} L_{11} & L_{12} & L_{13}\\ L_{21} & L_{22} & L_{23}\\ L_{31} & L_{32} & L_{33}\end{bmatrix} \times \begin{Bmatrix}\tilde{u}_z(z)\\ \tilde{u}_\theta(z)\\ \tilde{u}_r(z)\end{Bmatrix} = 0 \tag{E.38}$$

E.2.3. DECOUPLING THE EQUATION OF MOTION

From the previous chapter, it is known that in every equation of motion consist of the three displacements. Meanwhile to solve the differential equation, decoupling into separate equation of motion is need to performed. How to decoupling the equation E.38, elimination will be proceed and result into the following:

$$(L_{11}L_{22}L_{33} - L_{11}L_{32}^2 - L_{21}L_{33} + 2L_{11}L_{31}L_{32} - L_{22}L_{31}^2)\tilde{u}_r(z) = 0 \tag{E.39}$$

From the equation it would result in the following:

$$\left\{F_8\left(\frac{\partial^8(\cdot)}{\partial z^8}\right) + F_6\left(\frac{\partial^6(\cdot)}{\partial z^6}\right) + F_4\left(\frac{\partial^4(\cdot)}{\partial z^4}\right) + F_2\left(\frac{\partial^2(\cdot)}{\partial z^2} + F_0\right)\iota\tilde{u}_r(z) = 0 \tag{E.40}$$

The solution for the ordinary differential equation is:

$$\tilde{U}_r(z) = A\exp\lambda z \tag{E.41}$$

In which from the equation it can be written in the following equation:

$$F_8\lambda^8 + F_6\lambda^6 + F_4\lambda^4 + F_2\lambda^2 + F_0 = 0 \tag{E.42}$$

Where from the polynomials, we can derive the following equation:

$$\tilde{U}_r(z) = \sum_{j=1}^{\infty} A_j \exp\lambda_j z \tag{E.43}$$

As for the other displacements, the other solution would be expressed in term of the relation of $\tilde{U}_r(z)$. In which it will result to the following expressions:

$$\begin{aligned}(L_{11}L_{22}-L_{12}^2)\tilde{U}_\theta(z) &= (L_{12}L_{13}-L_{11}L_{23})\tilde{U}_r(z)\\ (L_{11}L_{22}-L_{12}^2)\tilde{U}_z(z) &= (L_{12}L_{13}-L_{13}L_{22})\tilde{U}_r(z)\end{aligned} \tag{E.44}$$

From the equation above it can be seen the relation between the two displacements. Therefore the result can be expressed with the like of the $\tilde{U}_r(z)$ with multiplier constant:

$$\begin{aligned}\tilde{U}_\theta(z) &= \sum_{j=1}^{8}\delta_j\cdot A_j\exp(\lambda_j z)\tilde{U}_r(z)\\ \tilde{U}_z(z) &= \sum_{j=1}^{8}\gamma_j\cdot A_j\exp(\lambda_j z)\tilde{U}_r(z)\end{aligned} \tag{E.45}$$

Where the δ and γ is already known from relation between the displacement. Where it would result to the 8 constants. Therefore the total 10 constants which are consisted of 8 constants from cylindrical shell and 2 other constants from plate. In which the 10 constants can be fully satisfied 10 boundary conditions.

E.3. LIQUID

The liquid superposition is consisted of three potentials. The first potential considers the shell's wall flexibility in which the liquid velocity will be the same as cylindrical shell. However it considers the plate is rigid and no free surface waves. For the second potential the plate flexibility is regarded where the liquid velocity in z direction will be the same as the plate. But on the contrary, for the second potential the wall flexibility and the free surface waves are disregarded. Lastly for the third potential, it only consist of the free surface waves kinematic boundary condition and consider the whole structure is rigid. In formulation the actual potential will be the linear summation of the three potentials, as for this thesis the liquid is considered linear:

$$\tilde{\phi}(r,z,\theta) = \tilde{\phi}_1(r,z,\theta)+\tilde{\phi}_2(r,z,\theta)+\tilde{\phi}_3(r,z,\theta) \tag{E.46}$$

THE FIRST POTENTIAL ($\tilde{\phi}_1$)

The first potential satisfies the interaction between liquid velocity in x direction with cylindrical shell boundary condition and disregard other components. This condition leads to both homogeneous and non-homogeneous kinematic boundary conditions that consist of the following expression:

1. **Liquid potential velocity in r direction at $r = R$:**

$$\frac{\partial\tilde{\phi}_1(r,z,\theta)}{\partial r}\Big|_{r=R} = -i\cdot\omega\times\tilde{u}_r(z,\theta) \tag{E.47}$$

2. **Liquid potential velocity in z direction at $z = 0$:**

$$\frac{\partial\tilde{\phi}_1(r,z,\theta)}{\partial z}\Big|_{z=0} = 0 \tag{E.48}$$

3. **Free surface waves at $z = H$:**

$$\tilde{\phi}_1(r,z,\theta)\Big|_{z=H} = 0 \tag{E.49}$$

The kinematic boundary condition can also being expressed with the converted axis. On later calculation the final solution can be converted back to the original axis:

1. **Liquid potential velocity in r direction at $\zeta = 1$**

$$\frac{1}{R}\frac{\partial\tilde{\phi}_1(\zeta,\xi,\theta)}{\partial\zeta}\Big|_{\zeta=1} = -i\cdot\omega\times\tilde{u}_r(z,\theta) \tag{E.50}$$

2. **Liquid potential velocity in z direction at** $\xi = 0$

$$\frac{1}{H}\frac{\partial\tilde{\phi}_1(\zeta,\xi,\theta)}{\partial\xi}\Big|_{\xi=0} = 0 \tag{E.51}$$

3. **Free surface waves at** $\xi = 1$

$$\tilde{\phi}_1(\zeta,\xi,\theta)\Big|_{\xi=1} = 0 \tag{E.52}$$

THE SECOND POTENTIAL ($\tilde{\phi}_2$)

Contrary to the first potential velocity, the second potential satisfies the boundary condition for the plate is flexible and consider the shell is rigid and no free surface waves. Therefore on can express the kinematic boundary condition in such manner:

1. **Liquid potential velocity in r direction at** $r = R$

$$\frac{\partial\tilde{\phi}_2(r,z,\theta)}{\partial r}\Big|_{r=R} = 0 \tag{E.53}$$

2. **Liquid potential velocity in z direction at** $z = 0$

$$\frac{\partial\tilde{\phi}_2(r,z,\theta)}{\partial z}\Big|_{z=0} = -i\cdot\omega\times\tilde{w}(z,\theta) \tag{E.54}$$

3. **Free surface waves at** $z = H$

$$\tilde{\phi}_2(r,z,\theta)\Big|_{z=H} = 0 \tag{E.55}$$

The boundary condition can be expressed in the ratio term, which is the product of axis conversion:

1. **Liquid potential velocity in r direction at** $\zeta = 1$

$$\frac{1}{R}\frac{\partial\tilde{\phi}_2(\zeta,\xi,\theta)}{\partial\zeta}\Big|_{\zeta=1} = 0 \tag{E.56}$$

2. **Liquid potential velocity in z direction at** $\xi = 0$

$$\frac{1}{H}\frac{\partial\tilde{\phi}_2(\zeta,\xi,\theta)}{\partial\xi}\Big|_{\xi=0} = -i\cdot\omega\times\tilde{w}(z,\theta) \tag{E.57}$$

3. **Free surface waves at** $\xi = 1$

$$\tilde{\phi}_2(\zeta,\xi,\theta)\Big|_{z=H} = 0 \tag{E.58}$$

THE THIRD POTENTIAL($\tilde{\phi}_3$)

The last potential satisfies the free surface waves and the disregards the other component. Likewise the previous potential, it consists of both homogeneous and non-homogeneous boundary conditions:

1. **Liquid potential velocity in r direction at** $r = R$

$$\frac{\partial\tilde{\phi}_3(r,z,\theta)}{\partial r}\Big|_{r=R} = 0 \tag{E.59}$$

2. **Liquid potential velocity in z direction at** $z = 0$

$$\frac{\partial\tilde{\phi}_3(r,z,\theta)}{\partial z}\Big|_{z=0} = -i\cdot\omega\times\tilde{w}(z,\theta) \tag{E.60}$$

3. **Free surface waves at** $z = H$

$$\begin{aligned}\frac{\omega^2}{g}\tilde{\phi}_{3(r,z,\theta)}\Big|_{z=H} &= \frac{\partial\tilde{\phi}_{(r,z,\theta)}}{\partial z}\Big|_{z=H}\\ \frac{\omega^2}{g}\tilde{\phi}_{1(r,z,\theta)}\Big|_{z=H} &= \frac{\partial(\tilde{\phi}_{1(r,z,\theta)}+\tilde{\phi}_{2(r,z,\theta)}+\tilde{\phi}_{3(r,z,\theta)})}{\partial z}\Big|_{z=H}\end{aligned} \tag{E.61}$$

Likewise the first and the second potential kinematic boundary conditions with converted axis which are:

1. **Liquid potential velocity in r direction at $\zeta = 1$**

$$\frac{1}{R}\frac{\partial\tilde{\phi}_3(\zeta,\xi,\theta)}{\partial\zeta}\Big|_{\zeta=1} = 0 \tag{E.62}$$

2. **Liquid potential velocity in z direction at $\xi = 0$**

$$\frac{\partial\tilde{\phi}_3(\zeta,\xi,\theta)}{\partial\xi}\Big|_{\xi=0} = -i\cdot\omega\times\tilde{w}(z,\theta) \tag{E.63}$$

3. **Free surface waves at $\xi = 1$**

$$\begin{aligned}\frac{\omega^2}{g}\tilde{\phi}_{3(\zeta,\xi,\theta)}\Big|_{z=H} &= \frac{\partial\tilde{\phi}_{(\zeta,\xi,\theta)}}{\partial z}\Big|_{z=H}\\ \frac{\omega^2}{g}\tilde{\phi}_{1(\zeta,\xi,\theta)}\Big|_{z=H} &= \frac{\partial(\tilde{\phi}_{1(\zeta,\xi,\theta)}+\tilde{\phi}_{2(\zeta,\xi,\theta)}+\tilde{\phi}_{3(\zeta,\xi,\theta)})}{\partial z}\Big|_{z=H}\end{aligned} \tag{E.64}$$

E.3.1. SEPARATION OF VARIABLE METHOD

From the potential flow theory it can be seen that the liquid equation of motion is coupled within three axis which are r, θ, and z or in converted axis is coupled in ζ, ξ, and θ

FLUID POTENTIAL FOR ϕ_1

The fluid potential ϕ_1 is dependent on r,z,θ which is also dependent with ζ,ξ,θ. The equation can be expressed in the following:

$$\tilde{\phi}_1(\zeta,\xi,\theta) = \tilde{\phi}_{1\zeta}\cdot\tilde{\phi}_{1\xi}\cdot\tilde{\phi}_{1\theta} \tag{E.65}$$

Through substitution to the equation of motion with the converted axis is written as follows:

$$\begin{aligned}\nabla^2\tilde{\phi}_1 &= 0\\ \Big(\frac{\partial^2(\cdot)}{\partial\zeta^2}+\frac{1}{\zeta}\frac{\partial(\cdot)}{\partial\zeta}+\frac{1}{\zeta^2}\frac{\partial^2(\cdot)}{\partial\theta^2}+\frac{1}{\alpha^2}\frac{\partial(\cdot)}{\partial\xi^2}\Big)\tilde{\phi}_1(\zeta,\xi,t) &= 0\\ \tilde{\phi}_{1\theta}\cdot\tilde{\phi}_{1\xi}\frac{\partial^2\tilde{\phi}_{1\zeta}}{\partial\zeta^2}+\tilde{\phi}_{1\theta}\tilde{\phi}_{1\xi}\frac{\partial\tilde{\phi}_{1\zeta}}{\partial\zeta}+\frac{\tilde{\phi}_{1\zeta}\tilde{\phi}_{1\xi}}{\zeta^2}\frac{\partial^2\tilde{\phi}_{1\theta}}{\partial\theta^2}+\frac{\tilde{\phi}_{1\theta}\tilde{\phi}_{1\zeta}}{\alpha}\frac{\partial^2\tilde{\phi}_{1\xi}}{\partial\xi^2}\end{aligned} \tag{E.66}$$

By dividing the calculation with $\tilde{\phi}_{1\theta}\tilde{\phi}_{1\zeta}\tilde{\phi}_{1\xi}$ the equation would result into the following:

$$\underbrace{\frac{1}{\tilde{\phi}_{1\zeta}}\frac{\partial^2\tilde{\phi}_{1\zeta}}{\partial\zeta^2}+\frac{1}{\zeta\tilde{\phi}_{1\zeta}}\frac{\partial\tilde{\phi}_{1\zeta}}{\partial\zeta}+\frac{1}{\tilde{\phi}_{1\theta}\zeta^2}\frac{\partial^2\tilde{\phi}_{1\theta}}{\partial\theta^2}}_{\text{Second term}}+\underbrace{\frac{1}{\tilde{\phi}_{\xi}\alpha^2}\frac{\partial^2\tilde{\phi}_{1\xi}}{\partial\xi^2}}_{\text{First Term}} = 0 \tag{E.67}$$

By first analyzing the first term, the separation constant (λ) can be introduce to decouple the equation:

$$\begin{aligned}\frac{1}{\tilde{\phi}_{\xi}\alpha^2}\frac{\partial^2\tilde{\phi}_{1\xi}}{\partial\xi^2} &= \lambda^2\\ \frac{\partial^2\tilde{\phi}_{1\xi}}{\partial\xi^2} &= \lambda^2\cdot\tilde{\phi}_{\xi}\alpha^2\end{aligned} \tag{E.68}$$

Solving the ordinary differential equation would result into the following expression:

$$\tilde{\phi}_{1\xi} = A_{1l}\cdot\cosh(\lambda\alpha\xi)+B_{1l}\cdot\sinh(\lambda\alpha\xi) \tag{E.69}$$

As for the second term in the equation E.67 would result into the following calculation:

$$\Big(\underbrace{\frac{1}{\tilde{\phi}_{1\zeta}}\frac{\partial^2\tilde{\phi}_{1\zeta}}{\partial\zeta^2}+\frac{1}{\zeta\tilde{\phi}_{1\zeta}}\frac{\partial\tilde{\phi}_{1\zeta}}{\partial\zeta}}_{2a}+\underbrace{\frac{1}{\tilde{\phi}_{1\theta}\zeta^2}\frac{\partial^2\tilde{\phi}_{1\theta}}{\partial\theta^2}}_{2b} = -\lambda^2\Big)\times\zeta^2 \tag{E.70}$$

The expression of $2b$ can be separated from $2a$ by introducing a new separation constant: (m)

$$\frac{1}{\tilde{\phi}_{1\theta}}\frac{\partial^2\tilde{\phi}_{1\theta}}{\partial\theta^2} = -m^2 \tag{E.71}$$

From this point, in order to calculate the $\tilde{\phi}_{1\theta}$, the ordinary differential equation can be solved in the following expression:

$$\tilde{\phi}_{1\theta} = D_{1l}\cos(m\cdot\theta) \tag{E.72}$$

The value of m will result to an integer value since for multiplication of θ which is an angle. And for the $2a$ the calculation would result into the following:

$$\begin{aligned}\frac{\zeta^2}{\tilde{\phi}_{1\zeta}}\frac{\partial^2\tilde{\phi}_{1\zeta}}{\partial\zeta^2} + \frac{\zeta}{\tilde{\phi}_{1\zeta}}\frac{\partial\tilde{\phi}_{1\zeta}}{\partial\zeta} + \lambda^2\zeta^2 - m^2 = 0\\ \zeta^2\frac{\partial^2\tilde{\phi}_{1\zeta}}{\partial\zeta^2} + \zeta\frac{\partial\tilde{\phi}_{1\zeta}}{\partial\zeta} + (\lambda^2\zeta^2 - m^2)\tilde{\phi}_{1\zeta} = 0\end{aligned} \tag{E.73}$$

Such derivation can be solve by using the Bessel function. It will be depends on the value of λ. If the λ is an imaginary value then it will result to modified Bessel function (I_m and K_m). While for if the λ consist of real value the equation would result to Bessel Function (J_m and Y_m).

Afterwards,the derivation continues by satisfying the homogeneous boundary condition and checking whether the number constants is the same amount as the rest of kinematic boundary condition:

2. **Liquid potential velocity in ξ direction at $\xi = 0$**

$$\begin{aligned}\frac{\partial\tilde{\phi}_1(\zeta,\xi,\theta)}{\partial\xi}\Big|_{\xi=0} = 0\\ \tilde{\phi}_{1\zeta}\tilde{\phi}_{1\theta}\frac{\partial\tilde{\phi}_{1\xi}}{\partial\xi}\Big|_{\xi=0} = 0\end{aligned} \tag{E.74}$$

   As only the non-trivial solution that is considered, the calculation would result into the following:

$$B_{l1} = 0 \tag{E.75}$$

3. **Free surface waves condition at $\xi = 1$**

$$\tilde{\phi}_1(\zeta,\xi,\theta)\Big|_{\xi=1} = 0 \tag{E.76}$$

   By only considering the non-trivial solution, the equation comes to:

$$\begin{aligned}A_{l1}\cosh(\lambda\alpha) = 0 \lambda\alpha = 0\\ \lambda_{nm} = \frac{i\pi(2n-1)}{\alpha}\end{aligned} \tag{E.77}$$

   Since the value of λ is equals to imaginary value, the equation E.73 to a modified Bessel function which is:

$$\tilde{\phi}_{1\zeta} = C^1_{l1}\cdot I_m(\lambda_{mn}\zeta) + C^2_{l1}\cdot K_m(\lambda_{mn}\zeta) \tag{E.78}$$

   The value of modified Bessel function second kind (K_{mn}) is equals to infinity where the $r = 0$, which it is not possible in this case unless C^2_{li} is equals to 0.

Since all the homogeneous boundary condition is already been satisfied the final equation for the liquid first potential would be in the following form:

$$\tilde{\phi}_1 = \sum_{m=0}^{\infty}\sum_{n=1}^{\infty} C_{l1}\cdot I_m(\lambda_{mn}\zeta)\cos(\lambda_{mn}\alpha\xi)\cos(m\theta) \tag{E.79}$$

The n value will starts at 1, since the fundamental waves number is $\pi\cdot(2n-1)/2$ However the m value which is also describe the Bessel function will starts at 0, since the Bessel function starts at 0 ($I_0, I_1, I_2, ..$) The solution above can be written in seperate form, where asymmetric and axisymmetric modes are expanded. From the

bessel function the axisymmetric modes is only where $m = 0$. The axisymmetric and asymmetric is written as follows:

$$\tilde{\phi}_1 = \sum_{n=1}^{\infty} \tilde{\phi}_{10n} + \sum_{n=1}^{\infty}\sum_{m=1}^{\infty} \tilde{\phi}_{1mn} \tag{E.80}$$

where each of the term is under of the expression in the following:

$$\begin{aligned} \tilde{\phi}_{10n} &= C_{l0n} \cdot I_0(\lambda_n \zeta) \cos(\lambda_n \alpha \xi) \\ \tilde{\phi}_{1mn} &= C_{lmn} \cdot I_m(\lambda_n \zeta) \cos(\lambda_n \alpha \xi) \cos(m\theta) \end{aligned} \tag{E.81}$$

It can be seen from the above equation that the number of unknown constant left is only 1 which is C_l and the number of non-homogeneous boundary condition is 1. From such condition, one can conclude that the number of constant and the rest of boundary condition are already balancing each other.

FLUID POTENTIAL FOR ϕ_2

For the second potential, the procedure will follows the first potential from the equation E.65 until equation E.73. However for the separation constant λ will be change into different notation ε, since the calculation will be completely different form the first potential. Therefore the equation E.73 can be rewritten as the following:

$$\zeta^2 \frac{\partial^2 \tilde{\phi}_{2\zeta}}{\partial \zeta^2} + \zeta \frac{\partial \tilde{\phi}_{2\zeta}}{\partial \zeta} + (\varepsilon^2 \zeta^2 - m^2)\tilde{\phi}_{2\zeta} = 0 \tag{E.82}$$

From the equation, the ε can be firstly assume into a real value, then it would result to Bessel function first kind and secondd kind which is expressed in the equation bellow:

$$\tilde{\phi}_{2\zeta} = C^1_{l2} \cdot J_m(\varepsilon\zeta) + C^2_{l2} \cdot Y_m(\varepsilon\zeta) \tag{E.83}$$

Where once again the second kind Bessel function in $r = 0$ will result to infinity and in this case is not possible. Therefore the constant in front of the second kind Bessel Function must be 0. Therefore the solution for the second potentials are:

$$\begin{aligned} \tilde{\phi}_2(\zeta,\xi,\theta) &= \tilde{\phi}_{2\zeta}\tilde{\phi}_{2\xi}\tilde{\phi}_{2\theta} \\ \tilde{\phi}_{2\zeta} &= C_{2l} \cdot J_m(\varepsilon\zeta) \\ \tilde{\phi}_{2\xi} &= A_{2l} \cdot \cosh(\varepsilon\alpha\xi) + B_{2l} \cdot \sinh(\varepsilon\alpha\xi) \\ \tilde{\phi}_{2\theta} &= D_{2l} \cos(m \cdot \theta) \end{aligned} \tag{E.84}$$

From these equation the total solution can be written as:

$$\tilde{\phi}_2(\zeta,\xi,\theta) = \big(A_{2l} \cdot \cosh(\varepsilon\alpha\xi) + B_{2l} \cdot \sinh(\varepsilon\alpha\xi)\big)\cos(m \cdot \theta) J_m(\varepsilon\zeta) \tag{E.85}$$

With the same step as the previous potential velocity, the homogeneous boundary condition has to be satisfied. The kinematic boundary condition which will be satisfied first is the free surface waves boundary condition as it much more simpler compare to the liquid potential velocity in ζ direction at $\zeta = 0$

3. **Free surface waves condition at** $\xi = 1$

$$\tilde{\phi}_1(\zeta,\xi,\theta)\Big|_{\xi=1} = 0 \tag{E.86}$$

Since only the non-trivial solution that is regarded the equation would become:

$$\begin{aligned} A_{2l}\cosh(\varepsilon\alpha) + B_{2l}\sinh(\varepsilon\alpha) &= 0 \\ B_{2l} &= -\frac{A_{2l}}{\tanh(\varepsilon\alpha)} \end{aligned} \tag{E.87}$$

Re-substitution back to the equation would result in the following equation:

$$\tilde{\phi}_{2\xi} = A_{2l} \cdot \left(\cosh(\varepsilon\alpha\xi) + \frac{\sinh(\varepsilon\alpha\xi)}{\tanh(\varepsilon\alpha)}\right) \tag{E.88}$$

1. **Liquid potential velocity in ζ direction at $\zeta = 1$**

$$\frac{1}{R}\frac{\partial \tilde{\phi}_2(\zeta,\xi,\theta)}{\partial \zeta}\Big|_{\zeta=1} = 0 \tag{E.89}$$

As the trivial solution is disregard,

$$\frac{1}{R}\frac{\partial J_m(\varepsilon\zeta)}{\partial \zeta}\Big|_{\zeta=1} = 0 \tag{E.90}$$

This boundary condition would result to variant value of ε. For each value of m, it would result to an infinity value of ε. Or it can be rewritten as the following ε_{mn} in which $m = 0,1,2,3,..$ and $n = 0,1,2,3,..$ which are:

$$\begin{aligned}\epsilon_0 &= 0, 3.8317, 7.0156, 10.1735\\ \epsilon_1 &= 1.8412, 5.3314, 8.5363....\end{aligned} \tag{E.91}$$

The total solution can be rewritten as the following equation:

$$\begin{aligned}\tilde{\phi}_2(\zeta,\xi,\theta) &= \sum_{m=0}^{\infty}\sum_{n=0}^{\infty} A_{2l}\cdot\Big(\cosh(\varepsilon_{mn}\alpha\xi) + \frac{\sinh(\varepsilon_{mn}\alpha\xi)}{\tanh(\varepsilon_{mn}\alpha)}\Big)\cos(m\cdot\theta)J_m(\varepsilon_{mn}\zeta)\\ \tilde{\phi}_2(\zeta,\xi,\theta) &= \sum_{m=0}^{\infty}\sum_{n=0}^{\infty} A_{l}\cdot\Big(\cosh(\varepsilon_{mn}\alpha\xi) + \frac{\sinh(\varepsilon_{mn}\alpha\xi)}{\tanh(\varepsilon_{mn}\alpha)}\Big)\cos(m\cdot\theta)J_m(\varepsilon_{mn}\zeta)\end{aligned} \tag{E.92}$$

Some of the journal separate the axisymmetric solution and asymmetric solution. The axisymmetric solution is represent with the index of 0.

axisymmetric Solution

The axisymmetric modes is described for $m = 0$, however the n can be the value 0 and 1,2,3,..

- **For $m = 0$ and $n = 0$**
  Since the ε_{00} is equals to 0, which result to the following:

$$\tilde{\phi}_{200}(\zeta,\xi,\theta) = A_{l00}\cdot\Big(\cosh(\varepsilon_{00}\alpha\xi) + \frac{\sinh(\varepsilon_{00}\alpha\xi)}{\tanh(\varepsilon_{00}\alpha)}\Big)\cos(0)J_0(\varepsilon_{00}\zeta) \tag{E.93}$$

  From the Bessel function, the value of $J_0(0)$ is equals to 1, However
  $\sinh(0)/\tanh(0) = 0/0$ cannot be solved directly. Therefore limit principle shall be used and resulting the following:

$$\tilde{\phi}_{200}(\zeta,\xi,\theta) = A_{l00}(z-H) \tag{E.94}$$

- **For $m = 0$ and $n = 1,2,3,..$** The value of ε_{0n} is no longer 0, therefore for this term the equation would result in the following:

$$\tilde{\phi}_{20n}(\zeta,\xi,\theta) = A_{l0n}\cdot\Big(\cosh(\varepsilon_{0n}\alpha\xi) + \frac{\sinh(\varepsilon_{0n}\alpha\xi)}{\tanh(\varepsilon_{0n}\alpha)}\Big)J_0(\varepsilon_{0n}\zeta) \tag{E.95}$$

Asymmetric Solution

As for the asymmetric solution the equation index m will be no longer 0.

- **For $m = 1,2,3,4..$ and $n = 0$**
  Since the ε_{m0} is equals to 0, which result to the following:

$$\tilde{\phi}_{2m0}(\zeta,\xi,\theta) = A_{lm0}\cdot\Big(\cosh(\varepsilon_{m0}\alpha\xi) + \frac{\sinh(\varepsilon_{m0}\alpha\xi)}{\tanh(\varepsilon_{m0}\alpha)}\Big)\cos(m\theta)J_m(\varepsilon_{m0}\zeta) \tag{E.96}$$

  Since the Bessel function $J_m(0)$ where $m = 1,2,3,4,..$ is equals to 0:

$$\tilde{\phi}_{2m0}(\zeta,\xi,\theta) = 0 \tag{E.97}$$

- **For $m = 1,2,3,4,..$ and $n = 1,2,3,..$** The equation for this condition would result to the following:

$$\tilde{\phi}_{2mn}(\zeta,\xi,\theta) = A_{lmn}\cdot\Big(\cosh(\varepsilon_{mn}\alpha\xi) + \frac{\sinh(\varepsilon_{mn}\alpha\xi)}{\tanh(\varepsilon_{mn}\alpha)}\Big)\cos(m\cdot\theta)J_m(\varepsilon_{mn}\zeta) \tag{E.98}$$

In short, the solution for the second potential can be rewritten as the following expression:

$$\tilde{\phi}_2(\zeta,\xi,\theta) = \tilde{\phi}_{200} + \sum_{n=1}^{\infty}\tilde{\phi}_{20n} + \sum_{n=1}^{\infty}\sum_{m=1}^{\infty}\tilde{\phi}_{2mn} \tag{E.99}$$

with each of the term result to the following:

$$\begin{aligned}
\tilde{\phi}_{200}(\zeta,\xi,\theta) &= A_{l00}(z-H)\\
\tilde{\phi}_{20n}(\zeta,\xi,\theta) &= A_{l0n}\cdot\Big(\cosh(\varepsilon_{0n}\alpha\xi) + \frac{\sinh(\varepsilon_{0n}\alpha\xi)}{\tanh(\varepsilon_{0n}\alpha)}\Big)J_0(\varepsilon_{0n}\zeta)\\
\tilde{\phi}_{2mn}(\zeta,\xi,\theta) &= A_l\cdot\Big(\cosh(\varepsilon_{mn}\alpha\xi) + \frac{\sinh(\varepsilon_{mn}\alpha\xi)}{\tanh(\varepsilon_{mn}\alpha)}\Big)\cos(m\cdot\theta)J_m(\varepsilon_{mn}\zeta)
\end{aligned} \tag{E.100}$$

Withal the first potential, the solution from the second potential produce only 1 unknown constant A_l which in the later calculation can be satisfied with the only one non-homogeneous boundary condition left.

FLUID POTENTIAL FOR ϕ_3

Similarly with the second potential, the third potential which describe the sloshing motion follows the same procedure in equation E.65 untill E.73. Since the sloshing motion has the same kinematic boundary condition in ζ direction at $\zeta = 1$ with the second potential it will result the same ε_{mn}. The other homogeneous boundary condition (Liquid velocity in ξ direction at $\xi = 0$) will result to $B_{3l} = 0$. Therefore for the total solution for the third potential is:

$$\tilde{\phi}_3(\zeta,\xi,\theta) = \sum_{m=0}^{\infty}\sum_{n=0}^{\infty}A_{3l}\cdot\big(\cosh(\varepsilon_{mn}\alpha\xi)\big)\cos(m\cdot\theta)J_m(\varepsilon_{mn}\zeta) \tag{E.101}$$

In order to avoid mistake, for the third potential new constant is introduced to replace A_{3l} which is B_l. It can be also written in separate formulation (axisymmetric modes and asymmetric modes) similar steps with the second potential:

$$\tilde{\phi}_3(\zeta,\xi,\theta) = \tilde{\phi}_{300} + \sum_{n=1}^{\infty}\tilde{\phi}_{30n} + \sum_{n=1}^{\infty}\sum_{m=1}^{\infty}\tilde{\phi}_{3mn} \tag{E.102}$$

Where each term is in the following expression:

$$\begin{aligned}
\tilde{\phi}_{300}(\zeta,\xi,\theta) &= B_{l00}\\
\tilde{\phi}_{30n}(\zeta,\xi,\theta) &= B_{l0n}\cdot\big(\cosh(\varepsilon_{0n}\alpha\xi)\big)J_0(\varepsilon_{0n}\zeta)\\
\tilde{\phi}_{3mn}(\zeta,\xi,\theta) &= B_{lmn}\cdot\big(\cosh(\varepsilon_{mn}\alpha\xi)\big)\cos(m\cdot\theta)J_m(\varepsilon_{mn}\zeta)
\end{aligned} \tag{E.103}$$

From the final solution it is can be clearly seen that the amount of the unknown constant left which is only B_l, is the same amount as the non-homogeneous boundary condition. Where it can be also concluded that the purpose of superposition in liquid can solve the imbalance number of the unknown constant with the boundary condition. However only when the liquid condition is linear, it can be superimposed linearly.

TOTAL LIQUID POTENTIAL (ϕ)

In a nutshell, the total solution can be written in the following expression:

$$\begin{aligned}
\tilde{\phi}(\zeta,\xi,\theta) &= \tilde{\phi}_1(\zeta,\xi,\theta) + \tilde{\phi}_2(\zeta,\xi,\theta) + \tilde{\phi}_3(\zeta,\xi,\theta)\\
\tilde{\phi}(\zeta,\xi,\theta) &= \sum_{n=1}^{\infty}\tilde{\phi}_{10n} + \sum_{n=1}^{\infty}\sum_{m=1}^{\infty}\tilde{\phi}_{1mn} + \tilde{\phi}_{200} + \sum_{n=1}^{\infty}\tilde{\phi}_{20n} + \sum_{n=1}^{\infty}\sum_{m=1}^{\infty}\tilde{\phi}_{2mn}\\
&\quad + \tilde{\phi}_{300} + \sum_{n=1}^{\infty}\tilde{\phi}_{30n} + \sum_{n=1}^{\infty}\sum_{m=1}^{\infty}\tilde{\phi}_{3mn}
\end{aligned} \tag{E.104}$$

Where each term can be expanded into the following definitions:

$$\begin{aligned}
&\tilde{\phi}_{10n}(\zeta,\xi,\theta) = C_{l0n}\cdot I_0(\lambda_n\zeta)\cosh(\lambda_n\alpha\xi)\\
&\tilde{\phi}_{1mn}(\zeta,\xi,\theta) = C_{lmn}\cdot I_m(\lambda_n\zeta)\cosh(\lambda_n\alpha\xi)\cos(m\theta)\\
&\tilde{\phi}_{200}(\zeta,\xi,\theta) = A_{l00}(z-H)\\
&\tilde{\phi}_{20n}(\zeta,\xi,\theta) = A_{l0n}\cdot\Big(\cosh(\varepsilon_{0n}\alpha\xi)+\frac{\sinh(\varepsilon_{0n}\alpha\xi)}{\tanh(\varepsilon_{0n}\alpha)}\Big)J_0(\varepsilon_{0n}\zeta)\\
&\tilde{\phi}_{2mn}(\zeta,\xi,\theta) = A_l\cdot\Big(\cosh(\varepsilon_{mn}\alpha\xi)+\frac{\sinh(\varepsilon_{mn}\alpha\xi)}{\tanh(\varepsilon_{mn}\alpha)}\Big)\cos(m\cdot\theta)J_m(\varepsilon_{mn}\zeta)\\
&\tilde{\phi}_{300}(\zeta,\xi,\theta) = B_{l00}\\
&\tilde{\phi}_{30n}(\zeta,\xi,\theta) = B_{l0n}\cdot\big(\cosh(\varepsilon_{0n}\alpha\xi)\big)J_0(\varepsilon_{0n}\zeta)\\
&\tilde{\phi}_{3mn}(\zeta,\xi,\theta) = B_{lmn}\cdot\big(\cosh(\varepsilon_{mn}\alpha\xi)\big)\cos(m\cdot\theta)J_m(\varepsilon_{mn}\zeta)
\end{aligned} \tag{E.105}$$

Or the expression can be rewritten back in the original axis which are r,z,θ:

$$\begin{aligned}
&\tilde{\phi}(r,z,\theta) = \tilde{\phi}_1(r,z,\theta)+\tilde{\phi}_2(r,z,\theta)+\tilde{\phi}_3(r,z,\theta)\\
&\tilde{\phi}(r,z,\theta) = \sum_{n=1}^{\infty}\tilde{\phi}_{10n}+\sum_{n=1}^{\infty}\sum_{m=1}^{\infty}\tilde{\phi}_{1mn}+\tilde{\phi}_{200}+\sum_{n=1}^{\infty}\tilde{\phi}_{20n}+\sum_{n=1}^{\infty}\sum_{m=1}^{\infty}\tilde{\phi}_{2mn}\\
&\qquad+\tilde{\phi}_{300}+\sum_{n=1}^{\infty}\tilde{\phi}_{30n}+\sum_{n=1}^{\infty}\sum_{m=1}^{\infty}\tilde{\phi}_{3mn}
\end{aligned} \tag{E.106}$$

Where each term can be also rewritten as:

$$\begin{aligned}
&\tilde{\phi}_{10n}(r,z,\theta) = C_{l0n}\cdot I_0\Big(\frac{\pi(2n-1)r}{2H}\Big)\cos\Big(\frac{\pi(2n-1)z}{2H}\Big)\\
&\tilde{\phi}_{1mn}(r,z,\theta) = C_{lmn}\cdot I_m\Big(\frac{\pi(2n-1)r}{2H}\Big)\cos\Big(\frac{\pi(2n-1)z}{2H}\Big)\cos(m\theta)\\
&\tilde{\phi}_{200}(r,z,\theta) = A_{l00}(z-H)\\
&\tilde{\phi}_{20n}(r,z,\theta) = A_{l0n}\cdot\Big(\cosh(\varepsilon_{0n}z/R)+\frac{\sinh(\varepsilon_{0n}z/R)}{\tanh(\varepsilon_{0n}H/R)}\Big)J_0(\varepsilon_{0n}r/R)\\
&\tilde{\phi}_{2mn}(\zeta,\xi,\theta) = A_{lmn}\cdot\Big(\cosh(\varepsilon_{mn}z/R+\frac{\sinh(\varepsilon_{mn}z/R)}{\tanh(\varepsilon_{mn}H/R)}\Big)\cos(m\cdot\theta)J_m(\varepsilon_{mn}r/R)\\
&\tilde{\phi}_{300}(r,z,\theta) = B_{l00}\\
&\tilde{\phi}_{30n}(r,z,\theta) = B_{l0n}\cdot\big(\cosh(\varepsilon_{0n}z/R)\big)J_0(\varepsilon_{0n}r/R)\\
&\tilde{\phi}_{3mn}(r,z,\theta) = B_{lmn}\cdot\big(\cosh(\varepsilon_{mn}z/R)\big)\cos(m\cdot\theta)J_m(\varepsilon_{mn}r/R)
\end{aligned} \tag{E.107}$$

E.4. MATCHING MODES

The matching modes, are divided into two modes which are the axisymmetric and asymmetric modes. In the following subsections are discussed how the matching modes are performed.

E.4.1. THE AXISYMMETRIC MODE

The matching modes are applied in both the structure equation of motion and kinematic boundary condition. These equations are used in the matching mode process due to the liquid and the structure shape functions are coupled in the equations.

EQUATIONS OF MOTION

The cylindrical shell equation of motion for the axisymmetric mode are written in the following list:

- **Cylindrical shell : longitudinal vibration along the axis of revolution**

$$\frac{E_w h_w}{\mu_w^2-1}\Big(\frac{\mu_w}{R}\frac{d\tilde{u}_{r[0,a]}(z)}{dz}+\frac{d^2\tilde{u}_{z[0,a]}(z)}{dz^2}\Big)-\rho_w h_w\tilde{u}_{z[0,a]}(z)\times\omega^2=0 \tag{E.108}$$

The same principle as the two dimensional model, the differential part of equation E.108 can be expressed as inertia form. This statement can be done since the equation previously define as homogeneous equation of motion as the following:

$$\frac{E_w h_w}{\mu_w^2 - 1}\left(\frac{\mu_w}{R}\frac{d\tilde{u}_{r[0,a]}(z)}{dz} + \frac{d^2\tilde{u}_{z[0,a]}(z)}{dz^2}\right) - \rho_w h_w \tilde{u}_{z[0,a]}(z) \times \omega_{[0,a]}^2 = 0 \tag{E.109}$$

Therefore it can be simply rewritten as:

$$\frac{E_w h_w}{\mu_w^2 - 1}\left(\frac{\mu_w}{R}\frac{d\tilde{u}_{r[0,a]}(z)}{dz} + \frac{d^2\tilde{u}_{z[0,a]}(z)}{dz^2}\right) = \rho_w h_w \tilde{u}_{z[0,a]}(z)\omega_{[0,a]}^2 \tag{E.110}$$

Substituting the equation E.110 to the equation E.108 results in the following:

$$\rho_w h_w \tilde{u}_{z[0,a]}(z) \times (\omega_{[0,a]}^2 - \omega^2) = 0 \tag{E.111}$$

Afterwards, the equation E.111 are substituted with the shape functions that are written in the equation 4.57. This step results in the equation bellow:

$$\rho_w h_w \sum_{a=1}^{\infty} \tilde{U}_{c,[0,a]} \cdot X_{z[0,a]}(z) \cdot (\omega_{[0,a]}^2 - \omega^2) = 0 \tag{E.112}$$

Then the equation is integrated and multiplied by the structure shape function to utilize the orthogonality. This step yields into the expression bellow:

$$\int_0^H \sum_{a=1}^{\infty} \left(\rho_w h_w \tilde{U}_{c,[0,a]} \cdot X_{z[0,a]}(z) \cdot (\omega_{[0,a]}^2 - \omega^2)\right) \cdot X_{z[0,w]}(z) dz = 0 \tag{E.113}$$

- **Cylindrical Shell: Transversal Vibration Along The Normal to The Surface Axis**
  Similiar procedure as the equation Longitudinal vibration along the axis revolution motion, the motion in r direction is written in the inertial form and integrated as the following:

$$\begin{aligned}\int_0^H \sum_{a=1}^{\infty}\left(\rho_w h_w \tilde{U}_{c,[0,a]}\cdot X_{r[0,a]}(z)\cdot(\omega_{[0,a]}^2-\omega^2)\right)\cdot X_{r[0,w]}(z)dz+\\ \int_0^H \sum_{n=1}^{\infty}\rho_{liq}\cdot i\omega\Big\{C_{0n}\cdot J_0\Big(\frac{\pi(2n-1)R}{2H}\Big)\cos\Big(\frac{\pi(2n-1)z}{2H}\Big)+\\ A_{l00}(z-H)+A_{l0n}\Big(\cosh\Big(\frac{\varepsilon_{0n}z}{R}\Big)+\sinh\Big(\frac{\varepsilon_{0n}z}{R}\Big)/\tanh\Big(\frac{\varepsilon_{0n}H}{R}\Big)\Big)J_0(\varepsilon_{0n})+B_{l00}\\ +B_{l0n}\cosh(\varepsilon_{0n}z/R)J_0(\varepsilon_{0n})\Big\}\cdot X_{r[0,w]}(z)dz=0\end{aligned} \tag{E.114}$$

- **Circular Plate**
  The same step as the cylindrical shell, the circular plate equation of motion is written in the inertial form and integrated in the following:

$$\begin{aligned}\int_0^R\Big\{\sum_{a=1}^{\infty}(\beta_p^4-\beta_{p[0,j]^4})\tilde{U}_{c[0,a]}\cdot X_{w[0,a]}(r)+\sum_{n=1}^{\infty}\Big(C_{l0n}I_0\Big(\frac{\pi(2n-1)r}{2H}\Big)-A_{l00}H+A_{l0n}I_0(\varepsilon_{0n}r/R)+\\ B_{l00}+B_{l0n}J_0(\varepsilon_{0n}r/R)\Big)\rho_{liq}\cdot i\omega\Big\}\times X_{w[0,w]}(r)dr=\int_0^R\Big\{-\Big(\frac{\rho\cdot h_p\times\omega^2}{D}\Big)\times w_e\Big\}\times X_{w[0,w]}\Big)(r)dr\end{aligned} \tag{E.115}$$

  Where the variable β_p and $\beta_{p[0,a]}$

$$\begin{aligned}\beta_p&=\Big(\frac{\rho\cdot h_p\times\omega^2-k}{D}\Big)^{\frac{1}{4}}\\ \beta_{p[0,a]}&=\Big(\frac{\rho\cdot h_p\times\omega_{[0,a]}^2-k}{D}\Big)^{\frac{1}{4}}\end{aligned} \tag{E.116}$$

By summing the equation E.113,E.114, and E.116, the orthogonality in the equation 4.59 can be applied in the structure equation of motion.

KINEMATIC BOUNDARY CONDITIONS

Since the calculation has the same procedure for every boundary conditions, only one kinematic boundary conditions are discussed in this subsection. Applying orthogonality in other kinematic boundary conditions follows the same steps. The kinematic boundary condition that is discussed in this section is the wall and the liquid kinematic boundary conditions. By substituting the liquid shape function in equation 4.56 and structure shape function in equation 4.57 to the kinematic boundary condition from the expression 4.32, the expression yields in the following:

$$\begin{aligned}\int_0^H\sum_{n=1}^{\infty}\frac{1}{2H}\Big(C_{l0n}I_1\Big(\frac{\pi(2n-1)R}{2H}\Big)\pi(2n-1)\cos\Big(\frac{\pi(2n-1)z}{2H}\Big)\Big)\cos\Big(\frac{\pi(2f-1)z}{2H}\Big)dz=\\ \int_0^H\sum_{a=1}^{\infty}\tilde{U}c_{[0,a]}\times X_{r[0,a]}(z)\times\cos\Big(\frac{\pi(2f-1)z}{2H}\Big)dz\end{aligned} \tag{E.117}$$

From the equation above it can be seen the orthogonality principle is applied. The left hand-side of the equation above results to 0, when $n\neq f$. If the $n=f$, the equation yields in the following:

$$\Big(C_{l0n}I_1\Big(\frac{\pi(2f-1)R}{2H}\Big)\pi(2f-1)\cos\Big(\frac{\pi(2f-1)z}{2H}\Big)\Big)=i\times\omega int_0^H\sum_{a=1}^{\infty}\tilde{U}c_{[0,a]}\times X_{r[0,a]}(z)\times\cos\Big(\frac{\pi(2f-1)z}{2H}\Big)dz \tag{E.118}$$

The summation in the right handside can be eliminated, since the structure velocity and the liquid velocity is mostly not orthogonal.

E.4.2. THE ASYMMETRIC MODES

Basically, the step in the asymmetric modes are almost the same with the axisymmetric modes. However, there is a fundamental difference between the two. Asymmetric modes are dependent inθ direction while axisymmetric modes do not. The axisymmetric modes have a constant value with respect to the θ axis. Therefore the first summation is eliminated $\sum_{j=1}^{\infty}$. Since, most of the equations repeated the same procedure as the axisymmetric modes, only one example of governing equations that is discussed in this section. The example of the matching modes are performed in the kinematic boundary condition between the cylindrical shell with the liquid, which is written in the following:

$$\int_0^{2\pi}\int_0^{H}\sum_{n=1}^{\infty}\Big[\frac{1}{2H}\Big\{C_{lmn}\cos\left(\pi(2n-1)z/(2H)\right)\Big(I_{m+1}(\pi(2n-1)R/(2H)+\frac{2mHI_m(\pi(2n-1)R/(2H))}{(2n-1)\pi R}\Big)$$
$$(2n-1)\pi\Big\}\cos(m\theta)\Big]\cos\left(\pi(2f-1)z/(2H)\right)\times\cos(e\theta)dzd\theta = i\times\omega\int_0^{2\pi}\int_0^{H}\Big\{\sum_{j=1}^{\infty}\sum_{a=1}^{\infty}\tilde{U}c_{[j,a]}\times X_{r[j,a]}(z)cos(j\theta)\Big\}$$
$$\cos\left(\pi(2f-1)z/(2H)\right)\times\cos(e\theta)dzd\theta + i\times\omega\int_0^{2\pi}\int_0^{H}u_e cos(\theta)\times\cos\left(\pi(2f-1)z/(2H)\right)\times\cos(e\theta)dzd\theta \tag{E.119}$$

From the above equation, one can see that both side of equation only give value if the value m,a, and e are equals. Moreover the earthquake loading are only exist in the equation if the m,a, and e equals to one. These statements are highly important, due to from the equation one can understand that *the most significant contribution of the earthquake are in the fundamental circumferential mode.* This reason is why most of the journals such as the [18] and [5] do not taken into account higher circumferential modes number.